

Enzymatische Oligomerisierung von Alkandiphosphaten

Dissertation

zur Erlangung des akademischen Grades

doctor rerum naturalium (Dr. rer. Nat.)

der

Naturwissenschaftlichen Fakultät II – Chemie und Physik

der Martin-Luther-Universität Halle-Wittenberg

vorgelegt von

Herrn Dipl.-Pharm. Hans Felix Schreckenbach

geboren am 08.04.1985 in Karl-Marx-Stadt (heutigen Chemnitz), Deutschland

Gutachter:

1. Prof. Dr. Ludger A. Wessjohann
2. Prof. Dr. Claus Jacob

22. März 2017

Acknowledgments

Accomplishment of this dissertation has been contributed to some people who supported me. Firstly, I would like to thank my doctoral adviser Prof. Dr. L. A. Wessjohann to welcome me into his laboratory at the Leibniz-Institute, the valuable advice and continuous support, constructive and successful discussions, as well as patience and the availability to attend conferences. Thanks to my committee members for their critical reading and input for this dissertation.

Secondly, I would like to thank the biocatalytic group members for all of their help and support. Special thanks to Dr. Martin Dippe, Dr. Danilo Meyer, Jeanette Keim, Steve Ludwig and Benjamin Weigel for laboratory training, comments and constructive criticism which led to the successful completion of the experiments and studies. Many thanks go to PD Dr. Wolfgang Brandt for the computational models and inspirations, Dr. Andrea Porzel for her efforts to elucidate the prenylated patterns and the qNMR analysis, and Dr. Jürgen Schmidt for high-resolution mass spectrometry analysis. I would like to thank Alexander Otto for the performance of the fungal inhibition assay and following helpful discussions. To Mrs. Ines Stein, Anja Ehrlich, Gudrun Hahn, Martina Lerbs and Katharina Wolf thank you for your advice, patience and humor.

I am deeply indebted to Dr. Felix Stehle for support and mentoring as well as Prof. Dr. Oliver Kayser and his staff at the TU Dortmund for the fruitful stay at the TU Dortmund to perform the THCS experiments. I would especially like to thank Dimitar Vasilev for the design and synthesis of the prenylated (polyoxy)-carboxylates as surrogates of the diphosphates, Amina Msonga for the UbiA results as well as Prof. Dr. Milton Stubbs and Camila Cotrim for providing purified MenA enzyme and I will always appreciate the time we had together during the crystallization and the UbiA-screening projects.

In addition, I would like to thank Angela Schaks, Prof. Dr. Bernhard Westermann, Dr. Devender Singh and the many other friends I have made in Halle for sharing and supporting my life in the past four years. Especially I would like to thank Dr. Thomas Vogt and Christin Naumann for the successful participation at the "Mitteldeutschen Firmmentriathlon".

Last, I would also like to thank my family and my brother for their support along the way.

TABLE OF CONTENTS

| | |
|--|------|
| Acknowledgments..... | ii |
| Table of Contents | viii |
| List of Abbreviations..... | viii |
| 1. General introduction and thesis overview | 1 |
| 1.1. Background and significance of prenyltransferases..... | 1 |
| 1.2. Pathway of the isoprenoid precursors IPP and DMAPP..... | 2 |
| 1.3. Prenyltransferases and the biosynthesis of natural isoprenoid units..... | 3 |
| 1.4. Thesis Overview..... | 5 |
| 2. <i>cis</i> – Prenyltransferases..... | 7 |
| 2.1. Introduction..... | 7 |
| 2.1.1. Structural characteristics and mechanism | 7 |
| 2.1.2. Substrate specificity | 9 |
| 2.1.3. Brief introduction of the selected UPPS..... | 10 |
| 2.1.4. Aim of the project..... | 10 |
| 2.2. Results and discussion..... | 11 |
| 2.2.1. Selection of enzymes..... | 12 |
| 2.2.2. Heterologous expression of cPTases in <i>E. coli</i> and protein purification | 13 |
| 2.2.3. cPTases with homoallylic diphosphates as elongation unit | 14 |
| 2.2.3.1. Methods and procedures | 14 |
| 2.2.3.2. Principle of the P _i -assay | 14 |
| 2.2.3.3. Principle of the fluorescence labeled HPLC-assay..... | 15 |
| 2.2.4. Catalytic parameters of UPPS with homoallylic diphosphates as elongation unit..... | 15 |
| 2.2.4.1. Results of the natural allylic substrate IPP | 15 |
| 2.2.4.2. Results of the non-natural allylic substrate BPP..... | 17 |
| 2.2.4.3. Results of the non-natural allylic substrate Cl-BPP | 18 |
| 2.3. Conclusion and Summary..... | 19 |
| 2.3.1. Assay..... | 19 |
| 2.3.2. Results..... | 19 |
| 2.3.3. Discussion..... | 19 |
| 2.3.4. Outlook..... | 20 |
| 3. Aromatic prenyltransferase NphB..... | 21 |
| 3.1. Background and significance..... | 21 |
| 3.1.1. Brief introduction to the aromatic prenyltransferase NphB..... | 22 |

| | | |
|----------|---|----|
| 3.1.2. | Structure of the aromatic prenyltransferase NphB..... | 23 |
| 3.1.3. | Mechanistic studies of prenyltransferases..... | 24 |
| 3.1.4. | Thesis overview | 25 |
| 3.2. | Results and discussion..... | 25 |
| 3.2.1. | Optimization of expression and purification of NphB..... | 25 |
| 3.2.2. | Identification of the 1,6-DHN products..... | 27 |
| 3.3. | Aromatic substrate promiscuity of NphB..... | 28 |
| 3.3.1. | Prenylation of dihydroxynaphthalenes and aromatic polyphenols | 28 |
| 3.3.2. | Naphthalene, Hydroxynaphthalenes (HN) and Dihydroxynaphthalenes (DHN)..... | 28 |
| 3.3.2.1. | Results and discussion of (di)hydroxynaphthalenes | 28 |
| 3.3.2.2. | Pharmacophore model of (di)hydroxynaphthalenes | 29 |
| 3.3.3. | Flavone derivatives and phenol-derivatives..... | 31 |
| 3.3.3.1. | Results and discussion of polyphenols | 31 |
| 3.3.3.2. | Pharmacophore model of polyphenols | 31 |
| 3.3.4. | Coumarin-derivatives | 35 |
| 3.3.5. | Conclusions..... | 36 |
| 3.4. | Prenyl acceptor promiscuity of NphB | 36 |
| 3.4.1. | Results and discussion of the conversion of artificial prenyl diphosphate derivatives. 36 | |
| 3.5. | Mutagenesis and mechanistic studies of NphB | 39 |
| 3.5.1. | Structure-function analyzes of NphB | 39 |
| 3.5.2. | Magnesium binding site and screening of bivalent metal ions..... | 40 |
| 3.5.3. | Results of the site-directed mutagenizes in the 1,6-DHN binding site | 42 |
| 3.5.4. | Results of the site-directed mutations in the GPP-binding motif | 45 |
| 3.5.5. | Abstraction of the proton | 49 |
| 3.5.6. | Mutations with different regio-specificity | 52 |
| 3.6. | Conclusion and proposed catalytic mechanism based on the mutation-results | 53 |
| 4. | Applications of prenylated compounds | 56 |
| 4.1. | Attempt to cyclize geranylated 1,6-DHN with THCA-synthase | 56 |
| 4.1.1. | Introduction of THCA-synthases..... | 56 |
| 4.1.2. | Aim of the cyclisation attempt | 58 |
| 4.1.3. | Results and discussion | 58 |
| 4.1.3.1. | Selection of the substrates | 58 |
| 4.1.3.2. | Results of the LC-MC analyzes | 59 |
| 4.1.3.3. | Structural explanation for the non-acceptance of the alternative substrates..... | 60 |
| 4.1.4. | Conclusion and future work | 61 |

| | | |
|----------|---|----|
| 4.2. | Anti-fungal effects of aromatic compounds and their prenylated analogues | 62 |
| 4.2.1. | Introduction | 62 |
| 4.2.2. | Results and discussion..... | 62 |
| 5. | Development and validation of the quantitative NMR method without internal standards...65 | |
| 5.1.1. | Abstract | 65 |
| 5.1.2. | Background and Significance..... | 65 |
| 5.1.3. | Results and discussion | 67 |
| 5.1.3.1. | T1 measurements | 67 |
| 5.1.3.2. | Measuring Conditions..... | 67 |
| 5.1.3.3. | Determination of the concentration | 68 |
| 5.1.4. | Conclusion | 70 |
| 5.2. | Development and validation of an UV/Vis procedure for the quantification of geranylated 1,6-dihydroxy naphthalene catalyzed by NphB | 71 |
| 5.2.1. | Introduction | 71 |
| 5.2.2. | Results and Discussion..... | 71 |
| 5.2.2.1. | Separation and detection of 1,6-DHN and geranylated 1,6-DHN by HPLC..... | 71 |
| 5.2.2.2. | Method validation | 73 |
| 5.2.2.3. | Proof of method..... | 74 |
| 5.2.3. | Summary..... | 75 |
| 6. | Prenylated (polyoxy)-carboxylates as surrogates of prenyl diphosphates and their potential as prenyltransferase inhibitors..... | 77 |
| 6.1. | Abstract | 77 |
| 6.2. | Introduction | 77 |
| 6.3. | Results and Discussion | 80 |
| 6.3.1. | Chemical selection of mimics..... | 80 |
| 6.3.2. | Aromatic prenyltransferase inhibition | 80 |
| 6.3.3. | Dependency on the chain length | 82 |
| 6.3.4. | Dependency of the head group..... | 83 |
| 6.3.5. | Dependency of the chain linker atom (C versus O)..... | 84 |
| 6.4. | Summary | 85 |
| 7. | Methods | 86 |
| 7.1. | General methods used for cPTases | 86 |
| 7.1.1. | Protein expression and purification | 86 |
| 7.1.2. | HPLC analyzis | 87 |
| 7.1.3. | Enzyme assay..... | 87 |

| | | |
|----------|---|-----|
| 7.1.4. | Diphosphate assay (PPi-Assay) | 88 |
| 7.2. | Methods used to handle the aromatic PTases NphB | 89 |
| 7.2.1. | Protein expression and purification | 89 |
| 7.2.2. | Enzyme assay | 90 |
| 7.2.3. | HPLC measurements | 90 |
| 7.2.4. | Mutagenesis of NphB gene | 90 |
| 7.2.5. | Protein-MS-analyzis | 92 |
| 7.3. | Methods used for the cyclisation attempt | 93 |
| 7.3.1. | Expression, purification and enzyme assay of THCA synthase (THCA-S) | 93 |
| 7.3.2. | Analysis of the THCA synthase product by HPLC | 93 |
| 7.4. | Material and Methods for the antifungal tests | 94 |
| 7.4.1. | Material | 94 |
| 7.4.2. | Bioactivity tests | 94 |
| 7.5. | Development and validation of the qNMR-method | 95 |
| 7.5.1. | Sample preparation | 95 |
| 7.5.2. | NMR spectra | 95 |
| 7.5.3. | Determination of the concentration | 95 |
| 7.6. | Method used to establish the UV/Vis-assay | 96 |
| 7.6.1. | Enzyme assay | 96 |
| 7.6.2. | HPLC | 96 |
| 7.6.3. | UV/Vis spectra of the geranylated 1,6-DHNS | 96 |
| 7.7. | Methods used for the inhibition test of PTases MenA, NphB and UbiA | 97 |
| 7.7.1. | Chemical synthesis | 97 |
| 7.7.2. | Aromatic prenyltransferase UbiA | 97 |
| 7.7.2.1. | UbiA enzyme expression and membrane fraction preparation | 97 |
| 7.7.2.2. | UbiA enzyme inhibition assay | 97 |
| 7.7.2.3. | IC ₅₀ values | 98 |
| 7.7.2.4. | HPLC conditions | 98 |
| 7.7.3. | Aromatic prenyltransferase NphB | 98 |
| 7.7.3.1. | NphB expression and purification | 98 |
| 7.7.3.2. | NphB enzyme inhibition assay | 98 |
| 7.7.4. | Aromatic prenyltransferase MenA | 99 |
| 7.7.4.1. | MenA enzyme inhibition assay | 99 |
| 7.7.4.2. | MenA enzyme expression and membrane fraction preparation | 99 |
| 7.7.4.3. | Analytical HPLC separation | 100 |

| | | |
|----------|---|-----|
| 7.7.4.4. | Product elucidation | 100 |
| 8. | Zusammenfassung..... | 102 |
| 9. | References..... | 104 |
| 10. | Appendix | 114 |
| 10.1. | ¹ H-NMR-Data of aromatic prenylated products mediated by NphB..... | 114 |
| 10.2. | ¹ H-NMR-spectra of geranylated NphB-enzyme-products | 120 |
| 10.3. | Supplementary figures | 135 |
| 10.3.1. | Protein expression and purification of the NphB mutants | 135 |
| 10.3.2. | NphB UV/Vis-assay validation..... | 136 |
| 10.3.3. | MenA – assay conditions | 137 |
| 10.4. | Material and equipment | 138 |
| 10.5. | Nucleotide sequence of the use enzymes (5'-3') | 141 |
| 10.5.1. | Ec_UPPS..... | 141 |
| 10.5.2. | Hb_UPPS..... | 141 |
| 10.5.3. | Hp_UPPS | 142 |
| 10.5.4. | MI_UPPS | 142 |
| 10.5.5. | Mt_UPPS..... | 142 |
| 10.5.6. | NphB with Trx-Tag..... | 143 |
| 11. | Tables..... | 144 |
| 11.1. | Table of figures..... | 144 |
| 11.2. | Table of tables | 147 |
| 11.3. | Table of equations..... | 148 |
| 11.4. | Table of supplementary figures..... | 148 |
| | Eidesstattliche Erklärung..... | 148 |
| | Lebenslauf | 148 |
| | Publikationsliste | 150 |

List of Abbreviations

| | |
|----------------------------------|--|
| Δ^1-THC | Δ^1 -tetrahydrocannabinol |
| 1,6-DHN | 1,6-dihydroxynaphthalene |
| ACN | acetonitrile |
| ARTSI | amplitude-corrected Referencing Through Signal Injection |
| ATP | adenosine triphosphate |
| AUC | area under the curve |
| AUS | area under the signal |
| Br-IPP | 3-bromo-3-butenyl diphosphate |
| CBGA | cannabigerolic acid |
| CDP-MEP | 4-diphosphocytidyl-2-methyl-D-erythritol 2-phosphate |
| Cl-BPP | 3-chloro-3-butenyl-diphosphat |
| cPTases | <i>cis</i> -prenyltransferases |
| DAD | diode array detector |
| DMAPP | dimethylallyl diphosphate |
| DMATS | dimethylallyltryptophan synthases |
| DMSO | dimethyl sulfoxide |
| DOXP | 1-deoxy-D-xylulose-5-phosphate |
| DTT | dithiothreitol |
| Ec_UPPS | <i>Escherichia coli</i> undecaprenyl diphosphate synthase |
| ePTases | chain elongation prenyltransferases |
| ERETIC | electronic referencing to access <i>in vivo</i> concentrations |
| ESI | electrospray ionization |
| FAD | flavin adenine dinucleotide |
| FOH | farnesol |
| FPP | farnesyl diphosphate |
| FPPase | farnesyl diphosphate synthases |
| G | geranyl-moiety |
| GC | gas chromatography |
| GHB | geranyl hydroxybenzoate |
| GPP | geranyl diphosphate |
| GPPase | geranyl diphosphate synthase |
| GGPP | geranylgeranyl diphosphate |
| Hb_PPS | <i>Hevea brasiliensis</i> polyprenyl diphosphate synthase |
| HMBPP | (<i>E</i>)-4-hydroxy-3-methyl-but-2-enyl pyrophosphate |
| HepPPS | heptaprenyl diphosphate synthase |
| HMBC | heteronuclear multiple bond correlation |
| HMG-CoA | 3-hydroxy-3-methylglutaryl-coenzyme A |
| HN | hydroxynaphthalenes |
| Hs_DHDDS | <i>Homo sapiens</i> dehydrodolichyl diphosphate synthase |
| HPLC | high performance liquid chromatography |
| Hp_UPPS | <i>Helicobacter pylori</i> undecaprenyl diphosphate synthase |
| HSQC | heteronuclear single-quantum correlation |
| IC₅₀ values | concentration where the enzyme activity is inhibited by 50% |
| IDI | isopentenyl diphosphate isomerase |
| IMAC | immobilized metal ion affinity chromatography |

| | |
|---|---|
| IPP | isopentenyl diphosphate |
| IPTG | isopropyl-1-thio- β -D-galactopyranoside |
| LC | liquide chromatography |
| MAPP | methylallyl diphosphate |
| MALDI-TOF | matrix-assisted laser desorption/ionization-time of flight |
| MEP | methylerythritol phosphate pathway |
| MI_UPPS | <i>Micrococcus luteus</i> undecaprenyl diphosphate synthase |
| MS | mass spectrometry |
| Mt_UPPS | <i>Mycobacterium tuberculosis</i> undecaprenyl diphosphate synthase |
| MVA | mevalonate pathway |
| NADPH | nicotinamide adenine dinucleotide phosphate |
| NphB | assumed abbreviation for “Naphterpin Biosynthesis” |
| NMR | nuclear magnetic resonance |
| Orf2 | open reading frame 2 |
| PAGE | polyacrylamide gel electrophoresis |
| PFTases | protein farnesyl transferases |
| PIG | pulse into gradient |
| P_i | inorganic monophosphate |
| PP_i | inorganic diphosphate |
| PHB | 4-hydroxybenzoic acid |
| Ps_PPS | <i>Periploca sepium</i> polyprenyl diphosphate synthase |
| qNMR | quantitative NMR |
| QUANTAS | quantification by Artificial Signal |
| R, R¹, R², ... | organic residues |
| REF | rubber elongation factor |
| RP-HPLC | reverse phase high performance liquid chromatography |
| rt | room temperature |
| SDS | sodium dodecyl sulfate |
| S_N1 | unimolecular nucleophilic substitution |
| S_N2 | bimolecular nucleophilic substitution |
| SRPP | small rubber particle protein |
| T₁ | longitudinal relaxation time |
| THC | tetrahydrocannabinolic |
| THCA | tetrahydrocannabinolic acid |
| THCA-S | tetrahydrocannabinolic acid synthase |
| tPTases | <i>trans</i> -prenyltransferases |
| Trx | thioredoxin |
| UPP | undecaprenyl diphosphate |
| UPPS | undecaprenyl diphosphate synthase |
| UV/Vis | ultraviolet–visible |
| WT | wild-type |

1.0. General introduction and thesis overview

1.1. Background and significance of prenyltransferases

“Isoprenoid, any of a class of organic compounds composed of two or more units of hydrocarbons, with each unit consisting of five carbon atoms arranged in a specific pattern.”

Encyclopaedia Britannica

Isoprenoids are composed of two or more units of five carbon atoms^[1] and in nature they encompass an enormous and structurally diverse family of natural compounds. Therefore, isoprenoids are important for various biological functions; for example cholesterol, which is required for cell membrane stability^[2], or carotenoids (i.e. lutein) as natural pigments in bacteria, fungi, algae, and plants^[3] and also they can be found in photosynthetic organisms.^[3] One of well-known pharmaceutical drug from this family of compounds is Taxol, used as a cytostatic agent in a cancer treatment (Figure 1).^[4]

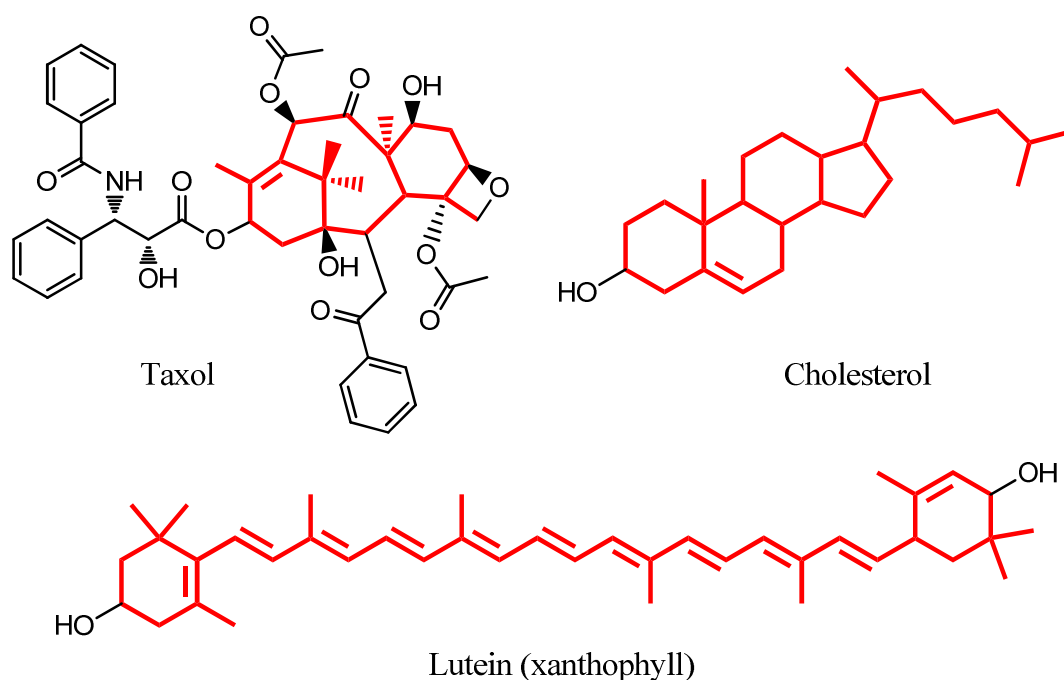


Figure 1. Selected isoprenoids, the isoprene-scaffold is marked in red.

In the last years, several enzymes involved in isoprenoid biosynthesis became attractive targets for drug research and development. The most prominent and profitable example are the statins which lower the cholesterol level in the blood by inhibiting enzyme HMG-CoA reductase.^{[5][6][7]} Other promising targets of intense research are the protein farnesyl

transferases (PFTases) which are known to be involved in cancer development (see chapter 6).^{[8][9]}

1.2. Pathway of the isoprenoid precursors IPP and DMAPP

The enormous structural and functional diversity found within the isoprenoids is derived from two C₅-isomers, dimethylallyl diphosphate (DMAPP) and its allylic isomer isopentenyl diphosphate (IPP) (Figure 2). DMAPP and IPP are produced by one of two following pathways. The mevalonate pathway (MVA) is predominately found in Eukarya, Archaea and some Eubacteria and is described shortly.^{[10][11]} The biological synthesis of prenyl diphosphate starts from the central metabolite acetyl-CoA.^[12] Three molecules of acetyl-CoA are condensed to 3-hydroxy-3-methylglutaryl-CoA (HMG-CoA). In the cytosol, HMG-CoA is reduced in a NADPH-dependent process to mevalonic acid and further converted to 5-pyrophosphomevalonate by ATP dependent phosphorylations. In the last step, CO₂ is released by the ATP-dependent decarboxylation forming IPP. The second building block of the isoprenoid biosynthetic pathway (DMAPP) is formed by isomerization of IPP by enzyme isopentenyl diphosphate isomerase (IDI) (Figure 2).^{[12][13]}

A second option to build the isoprenyl building blocks is the methylerythritol phosphate pathway (MEP) which was discovered approximately 40 years later by Rohmer and coworkers and appears in bacteria, algae, and plant chloroplasts.^[14] In contrast to the classic MVA, the MEP pathway forms IPP and DMAPP. All plants, apicomplexan protozoa (i.e. malaria parasites) and bacteria which include most pathogens (i.e. *Mycobacterium tuberculosis*) have the ability to produce IPP and DMAPP starting from glyceraldehyde-3-phosphate and pyruvate to form 1-deoxy-D-xylulose-5-phosphate (DOXP). The reduction of DOXP to 2-methyl-D-erythritol 4-phosphate in an NADPH dependent process is followed by a cytidyltransferase and a phosphorylation to the intermediate 4-diphosphocytidyl-2-methyl-D-erythritol 2-phosphate (CDP-MEP). In the final steps, the compound is converted to a cyclic diphosphate and transformed into (*E*)-4-hydroxy-3-methyl-but-2-enyl pyrophosphate (HMBPP). Contrarily to the MVA, in MEP pathway HMBPP can be reduced into both IPP and DMAPP.^{[13][14]} In contrast to the cytosolic mevalonate pathway, the MEP-pathway in plants is localized in the plastids.^[15]

1.3. Prenyltransferases and the biosynthesis of natural isoprenoid units

The two basic C₅-isoprene units are the building blocks for a huge variety of different biological active compounds in living organisms.^[16] DMAPP serves as starter unit and condenses with one IPP molecule to geranyl diphosphate (GPP) in the presence of the short-chain prenyltransferases GPP synthase (GPPase).^[17] The C₁₀-product is a substrate for several aromatic prenyl transferases such as NphB (Chapter 3). By addition of two molecules of IPP to the allylic substrate DMAPP, farnesyl diphosphate (FPP) is formed by farnesyl diphosphate synthase (FPPase).^[18] FPP is a precursor for a numerous different natural products such as *epi*-aristolochene (the cyclization product of the 5-*epi*-aristolochene synthase)^[19] or the squalene synthase (uses two FPP molecules to produce squalene, the precursor of cholesterol and other mammalian hormones).^{[20][21]} In addition, FPP can react as starter unit with further IPP units to generate geranylgeranyl diphosphate (GGPP) used in protein signaling on a conserved cysteine,^[22] as precursor in the taxadiene^[23] or carotenoids biosynthesis.^[24] Furthermore, FPP can also serve as allylic starter substrate for medium- and long-chain PTases to prolong the prenyl diphosphate up to C₅₅ (Chapter 2) or even longer chain elongation products like natural rubber.^[25] Among these highly unsaturated structures two stereochemical products are synthesized by medium- and/or long-chain PTases based on the double bond configuration formation during the condensation step. According to the stereochemistry of the prenyl chain units, chain elongation prenyltransferases (ePTases) are divided into two major groups, *trans*- and *cis*-ePTases and secondly subgrouped after the preferred product chain lengths.^{[26][27]} The *trans*-ePTases range from C₁₀ (geranyl diphosphate) to C₅₀ product (solanesol diphosphate)^[28] and *cis*-prenyltransferases produce larger polymers including C₅₅ product (undecaprenyl diphosphate) but also up to C₃₀₀₀₋₅₀₀₀, known as natural rubber.^{[29][30]} An almost unlimited chain elongation is found in *Hevea brasiliensis* and requires additional enzymes like the small rubber particle protein (SRPP) or rubber elongation factor (REF).^[25] Both ePTase families do not share sequence or structural homology(Figure 3).^[31] A summary of the described PTases and their products is given in Figure 2.

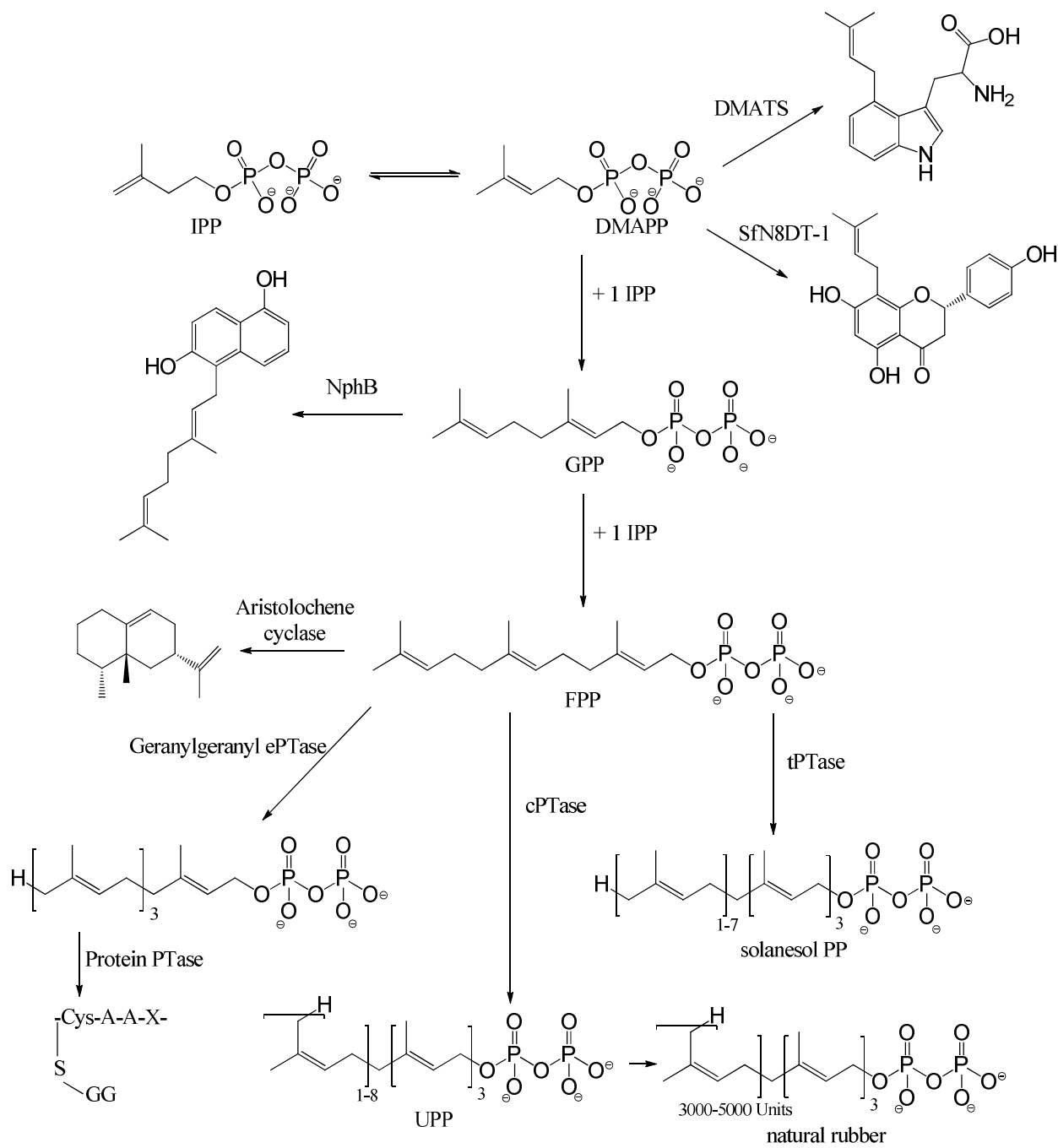


Figure 2. Prenyltransferases discussed in the text including their biosynthetic products, the natural isoprenoids.

1.4. Thesis Overview

The chemical synthesis of C–C-bond formations is difficult, unselective and requires often increased financial and time-effort.^[32] Therefore, enzymatic attended syntheses of C–C coupling in non-aromatic and aromatic systems became more important in fine-chemical application like in case of food and fragrance industries or in research and development.^[32] Alkylating enzymes are such a group which catalyzes C–C-bond formations.

Chapter 1 presents a general overview that combines application of prenylated compounds, short pathway descriptions of isoprenoid precursors IPP and DMAPP as well as the introduction of the enzyme family PTases and the aromatic PTase NphB.

Chapter 2 is focused on linear prenylation emanated from FPP to UPP. The aim was to identify an enzyme which is able to prolong FPP with alternative IPP-substrates. Therefore, an extensive work has been carried out to purify various *cis*-prenyltransferases from different organisms and to assay them for their ability to use alternative IPP-substrates as prenyl-elongation unit(s).

Chapter 3 describes the aromatic prenyltransferase NphB which catalysis the geranylation of polyphenols. Following questions were addressed: How are substrates (aromatic substrate, geranyl diphosphate and Mg^{2+} -ion) bound to the enzyme pocket? In which way does the enzyme catalyze the attachment of a prenyl residue to the aromatic core? And how does the catalytic cascade take place? Furthermore, the application of NphB in chemo enzymatic synthesis has been performed. Thus, a series of artificial GPP analogues were used for production of prenylated compounds as well as aromatic substrates. Subsequently, site-directed mutagenesis was carried out for regio-selective prenylation using 1,6-dihydroxynaphthalene (1,6-DHN) as model substrate.

Chapter 4 shows the application of prenylated aromatic products mediated by NphB. Several attempts to cyclize geranylated 1,6-DHN with THCA-synthase were unsuccessful. However, anti-fungal effects were observed for prenylated 1,6-DHN compared to its non-prenylated counterpart.

Chapter 5 describes the development and validation of an UV/Vis procedure to quantify the formation of geranylated 1,6-DHN. Explicitly, this includes the determination of the turnover number and thus, the kinetic value as well as characterization of mutants. Furthermore, NphB-inhibition with (polyoxy)-carboxylates as mimics of geranyl diphosphates was assessed. The second part of chapter 5 describes the method to establish quantitative

NMR without internal standard. With this tool, the exact amount of geranylated 1,6-DHN products was determined to perform the anti-fungal test and the attempts to cyclize geranylated products.

Finally, chapter 6 focuses on the inhibition of aromatic prenyltransferases with prenylated (polyoxy)-carboxylates as surrogates of prenyl diphosphates. The enzyme NphB and MenA were compared to the aromatic prenyltransferases UbiA.

Chapter 7 summarizes the methods used in this thesis.

2.0. *cis* – Prenyltransferases

2.1. Introduction

2.1.1. Structural characteristics and mechanism

The first *cis*-prenyltransferases (cPTases) were identified in *Micrococcus luteus* B-P 26 as undecaprenyl diphosphate synthase (UPPS) in 1998.^[33] Interestingly, the primary and tertiary structure of UPPS is totally different from those of the outlier known *trans*-prenyltransferases (tPTases). The tPTase share the common protein fold named “isoprenoids synthase fold”^[34] which contains 10-12 antiparallel α -helices and exists in GGPP synthases,^[35] sesquiterpene cyclases,^[36] protein farnesyl transferases^[37] and squalene synthase.^[20] Instead, cPTases consist of seven α -helices and a core formed of six parallel β -sheets (Figure 3).

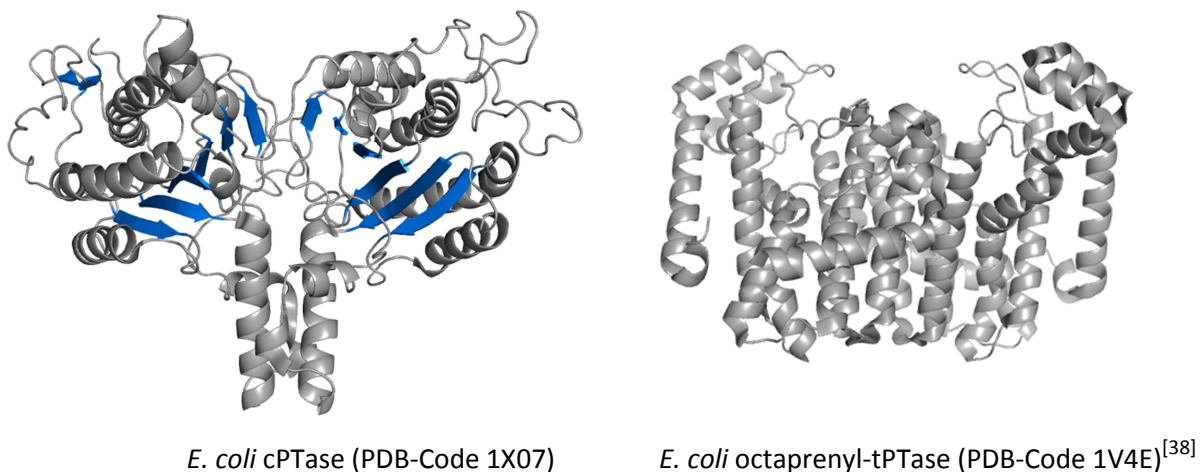


Figure 3. Comparison of tertiary structures of *cis*- and *trans*- prenyltransferase. View of structural elements without substrate. The α -helices or the loops are in darker grey and the β -sheets are in navy blue colored.

Furthermore, the cPTases miss the common substrate binding motif with the two functionally important Asp-rich motifs (Dx(x)D).^{[29][39][40]} Therefore, another reaction mechanism was postulated and up to now two possible mechanisms are described in literature.^{[31][41]} On the one hand, the ionization–condensation–elimination mechanism where the FPP or longer intermediate substrate cleaves the Mg^{2+} -activated diphosphate. The formed carbocation attacks the double bond of the homoallylic IPP and results in a second carbocation intermediate. In the last step, the *cis* standing proton of the C2 position of the IPP moiety gets eliminated (Figure 4). The result is a prolonged allylic substrate. On the other hand, the concerted condensation–elimination mechanism is proposed whereby the allylic

substrate is ionized and simultaneously condensed with the IPP. Even though, *cis*- and *trans*-PTases are structural different, they still share the same substrates FPP and IPP. Therefore, it is most likely that both enzymes may utilize different mechanisms.^{[31][41]}

For UPPS family, a conformational change during the reaction is discussed.^{[42][43]} Herein, a flexible loop called “P-loop” forms the entrance to the hydrophobic cleft and consists of the amino acids phenylalanine and serine (FS-motif)^[44] which might function as holder, coordinator and stabilizer of the hydrocarbon moiety of the homoallylic substrate IPP. The loop is connected to the α -helix 3. Comparing the crystal structure of UPPS in the apo-form and in the substrate-bound-closed form, it can be observed that the α -3 helix is kinked and therefore closer to the allylic substrate. It is proposed that these conformational changes regulate the catalytic activity by closing and opening the hydrophilic cleft.^{[41][43][44][45][46]} In the crystal structure of UPPS obtained from *Escherichia coli*, the FPP diphosphate is coordinated to octahedral Mg^{2+} . The coordination sphere of Mg^{2+} is completed with an aspartate (Asp 26) and an arginine (Arg 30) residue as well as three water molecules.

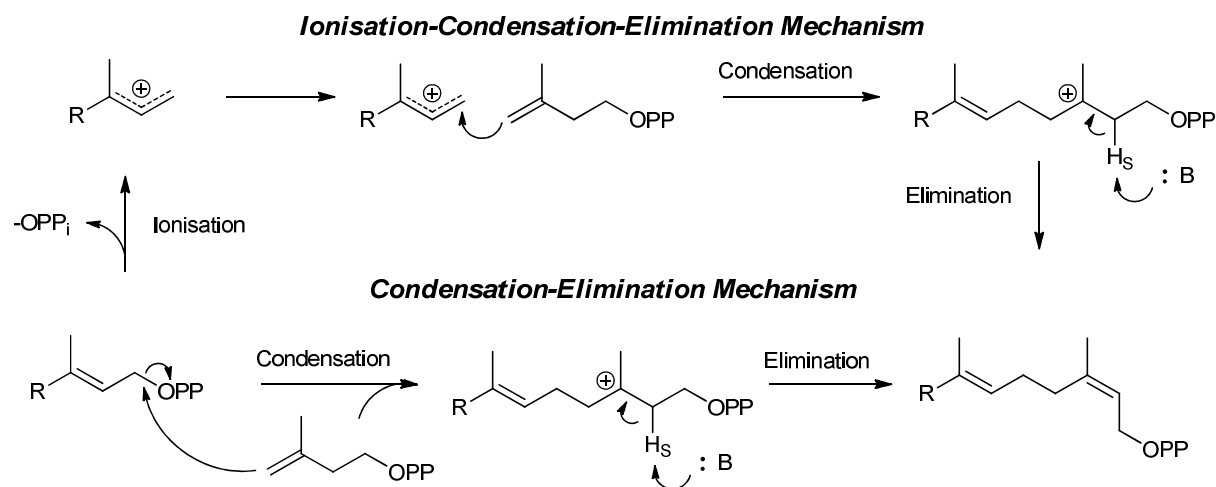


Figure 4. Two alternative mechanisms of FPP or intermediate substrate condensate with IPP forming the final product UPP catalyzed by UPPS. (R = C₅-unit; PP = diphosphate)

After the condensation reaction by ionization of the diphosphate moiety from FPP or the intermediate substrate, the Mg^{2+} ion seems to migrate from the IPP binding pocket to the FPP pocket. The next condensation step can occur until it reaches the chain length of 11 prenyl units.^[41] One of the most interesting questions is how the enzyme recognizes the prenyl chain length of the allylic substrates and the final product. Site-directed mutagenesis study reported the replacement of Leu137 against alanine in *E. coli* UPPS. This specific amino

acid is located at the bottom of the hydrophobic cleft and seems to trigger the enzyme to release the product. This variant exhibits a prolonged product chain length up to C₇₀₋₇₅ compared to C₅₅₋₆₀ in the wild-type.^[47]

2.1.2. Substrate specificity

In general, the universal elongation unit IPP seems to be highly restricted to the binding pocket of PTases from all types. For the homo allylic substrate BPP (Figure 5), only one condensation step could be observed for the tPTases heptaprenyl diphosphate synthases (HepPPS) from *M. luteus* and *Bacillus subtilis*^{[48][49]} as well as FPPase from *Bacillus stearothermophilus*^[50] and the cPTases UPPS from *M. luteus*.^{[51][52]} Exchanging the methyl for an ethyl or propyl group leads to a simple prolongation for HepPPS from *B. subtilis* and *M. luteus*. The increase of the chain-length on the C-3 atom (3-methyl-BPP = IPP to 3-ethyl-BPP or 3-propyl-BPP) reduces the enzyme activity.^[53] The data show also that the tPTases seem more tolerant toward the IPP as substrate compared to cPTases.

The reaction product nor-GPP (DMAPP condensate with BPP) does not serve as starter unit for *B. stearothermophilus* FPPase in the presence of IPP or BPP as allylic substrate.^[50] On the contrary, two-times condensation with FPP and 3-bromo-3-butenyl diphosphate (Br-IPP) could be confirmed in the presence of Ec_UPPS.^{[54][55]}

Substrate analogues of IPP and FPP are mainly applied in mechanistic studies of cPTases and the involved catalytic amino acids. 3-Bromo-3-butenyl diphosphate (Br-IPP),^[55] a substrate analog for IPP with an electron-withdrawing effect due to the present bromide, was tested as substrate for UPPS. The replaced methyl group should destabilize the second carbocation intermediate. This leads to a decreased condensation reaction and results in a detectable amount of farnesol (FOH) if an ionization-elimination mechanism underlies the prenyl attachment. In case of tPTases, FOH could be detected but not for the UPPS-family.^[55] Moreover, 2-fluoro-FPP and [1,1-2H₂]FPP as FPP analogues were used to explain the mechanism. The strong electron-withdrawing fluorinated substituent was introduced at the C2-carbon to form the carbocation and to destabilize the intermediate. The deuterium FPP substrate was used to illustrate the change of hybridization at the C1-carbon.^{[55][56]} The authors interpreted the findings as supportive for the condensation–elimination mechanism for UPPS.

However, cPTases (e.g. *E. coli* UPPS) catalyze the alkylation of a variety of artificial FPP substrates,^[54] but they are more conservative toward modifications of the homoallylic substrate IPP which restricts their application as biocatalysts in industry.

2.1.3. Brief introduction of the selected UPPS

The products of these cPTases are extremely diverse regarding the chain lengths which range from C₁₅ up to several thousand for natural rubber. cPTases are therefore classified into three groups.

1. The short-chain cPTases like Z,Z-FPP synthases (FPPS from *Solanum habrochaites*)^[57] utilize the precursor DMAPP and catalyze the consecutive addition of two IPP in *cis*-position.
2. The medium-chain cPTases like UPPS are more common in all organisms. These enzymes carry out the more or less precise addition of eight IPP to the allylic starter unit *E,E*-FPP to the *E,Z*-form 55-carbon undecaprenyl diphosphate (UPP) which is usually found to be associated with bacterial cell membranes.^[58] Herein, UPP plays a major role in the glycan lipid carrier trafficked across the plasma membrane^[59] and in constructing the bacterial peptidoglycan cell wall.^[60] Thus, the UPPS is an attractive potential drug target for new antibiotics.^[61]
3. The long-chain cPTases are able to produce unlimited additions of IPP units to the allylic starter unit *E,E*-FPP. The most famous cPTase is found in *H. brasiliensis* and is capable to produce products of C₃₀₀₀₋₅₀₀₀ known as latex, the basic of natural rubber. Therefore, it requires additional enzymes like the small rubber particle protein (SRPP) or rubber elongation factor (REF).^{[25][31]}

A selection of enzymes containing four medium-chain cPTases and one long-chain cPTase have been chosen for initial screening to find a candidate which prolongs the starter unit with non-natural IPP analogs. All proteins were soluble and condensed the IPP unit to the allylic starter unit or to one intermediate. The summary of the enzymes is given in Table 1.

2.1.4. Aim of the project

The aim of the project was to screen different cPTases for their ability to prolong the starter unit FPP with two and more non-natural allylic substrates. The findings were published as a patent (number: WO2015036335 A1 und EP2848693A1).

Table 1. Overview about the selected cPTases.

| | <i>E. coli</i> | <i>H. pylori</i> | <i>M. luteus</i> | <i>M. tuberculosis</i> | <i>H. brasiliensis</i> |
|--|--|--|--|--|--|
| | UPPS | UPPS | UPPS | UPPS | PPS |
| original organism | <i>E. coli</i> | <i>H. pylori</i> | <i>M. luteus</i> | <i>M. tuberculosis</i> | <i>H. brasiliensis</i> |
| protein molecular weight (kDa) | 28.4 | 27.5 | 28.9 | 33.8 | 32.7 |
| product chain length | C ₅₅ | C ₅₅ | C ₅₅ | C ₅₅ | C ₃₀₀₀₋₅₀₀₀ |
| starter substrate + prolongation unit | <i>E,E</i> -FPP + IPP | <i>E,E</i> -FPP + IPP | <i>E,E</i> -FPP + IPP | <i>E,E</i> -FPP or <i>Z,E</i> -FPP or <i>E</i> -GPP+ IPP | <i>E,E</i> -FPP + IPP |
| crystal structure with PDB-code | available i.e. 4H2J, 1X09 | available i.e. 2DTN, 2D2R | available 1F75 | available i.e. 2VG4, 2VG2 | not available |
| reason for selection | reference to previous work ^[54] | 38.34% Identity toward <i>E. coli</i> UPPS | numerous site-directed mutagenesis studies | accept various starter units | capability to form C ₃₀₀₀₋₅₀₀₀ products |
| Reference | [61][62][63] | [61] | [64] | [65] | [66] |

2.2. Results and discussion

Various cPTase from different organisms were purified: *M. luteus* UPPS (MI_UPPS), *M. tuberculosis* UPPS (Mt_UPPS), *H. pylori* UPPS (Hp_UPPS), human dehydrodolichyl diphosphate synthase, and the rubber synthase from *H. brasiliensis* (Hb_PPS) (Table 1). The enzymes were assayed for their ability to use alternative IPP-substrates as prenyl-elongation unit(s) (Figure 5) in order to produce novel linear polyisoprenoid compounds containing modifiable functional groups.

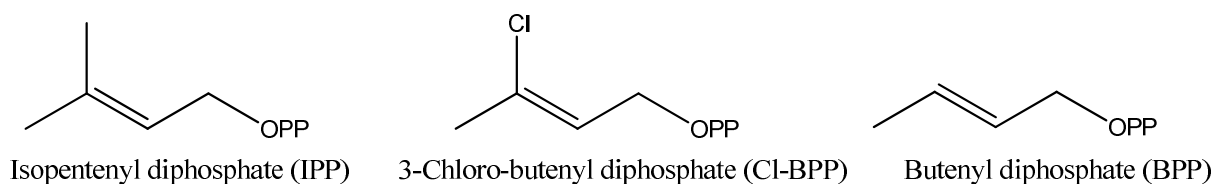


Figure 5. Biocatalytic converted non-natural IPP analogs by UPPSs

In continuation of this work, the most promising candidate(s) would be further modified by site-directed mutagenesis with the aim to enhance activity, yield and unlimited elongation.

2.2.1. Selection of enzymes

All genes of the following cPTases from the linear type were *codon-usage* optimized, synthesized (by MWG-Biotech AG, Ebersberg, Germany) and cloned into the pET28a(+) vector. The selection covers bacterial UPPS from *M. luteus* (MI_UPPS), *M. tuberculosis* Rv2361c (Mt_UPPS) and *H. pylori* (Hp_UPPS), as well as polyprenyltransferases (PPS) from the rubber tree *H. brasiliensis* (Hb_PPS) and the dehydrodolichyl diphosphate synthase (DHDDS) from *Homo sapiens* (Hs_DHDDS). Furthermore, the plant cPTase of the Chinese climber *Periploca sepium* (Ps_PPS) was used.^[67] The cladogram in Figure 6 shows the synthesized genes of cPTases and Ec_UPPS (marked in green) among the literature described cPTases. A clear division into prokaryotic and eukaryotic groups is not observed. However, the bacterial UPPS sub-group (Mt_UPPS, MI_UPPS, Ec_UPPS and Hp_UPPS) as well as the plant cPTases from *Arabidopsis lyrata* and the natural rubber producer TkCPT1 (cPTase from *Taraxacum kok-saghyis*), *H. brasiliensis* (Hb_PPS) and the Ps_PT seem to build cluster.

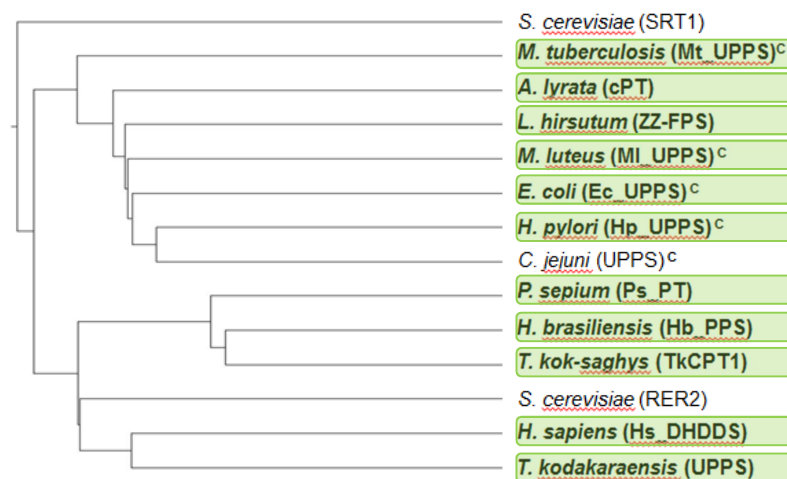


Figure 6. Cladogram of the protein sequence of cPTases from the linear type described in literature.

The investigated enzymes are marked in green; PTases marked with (c) are crystalized and available as PDB-file. SRT1, *C. jejuni* UPPS and RER2 are included to the list of known cPTase. (Accession files: *Saccharomyces cerevisiae* (SRT1): Q03175; Mt_UPPS: P60479; *Arabidopsis lyrata* cPT: D7LFB0; *Lycopersicon hirsutum* (Z,Z-FPS): B8XA40; MI_UPPS: O82827; Ec_UPPS: P60472; Hp_UPPS: P55984; *Campylobacter jejuni* UPPS: Q9PP99; *Periploca sepium* (Ps_PT): Q8H984; Hb_PPS: Q8W3U4; *Taraxacum kok-saghyis*: (TkCPT1)^[68]; *S. cerevisiae* (RER2): P35196; Hs_DHDDS: Q86SQ9; *Thermococcus kodakaraensis* UPPS: Q5JGE1)

2.2.2. Heterologous expression of cPTases in *E. coli* and protein purification

Expression of each construct in different media, at different expression temperatures and in different expression strains was checked by SDS-PAGE (data not shown). Optimum expression of soluble prenyltransferase was observed in BL21(DE3) harboring pET28a(+) at 25°C and after 16 h of induction with 1 mM IPTG. The His₆-tagged proteins MI_UPPS, Mt_UPPS, Hp_UPPS and Hb_PPS were purified by Ni²⁺-affinity chromatography. Figure 7 shows the SDS-PAGE gel of the purified enzyme. The purity was estimated to be over 90 % except of Hb_UPPS due the poor yield. Using the established purification protocols, 300–1500 µg × ml⁻¹ pure protein could be achieved. Under this condition, the eukaryotic PTase Hb_PPS exhibited the weakest yield which might be explained by the hydrophobic parts of the enzyme and the high tendency to aggregate (inclusion bodies). The enzyme of Hs_DHDDS and Ps_PPS could not be expressed or purified (method 7.1.1.).

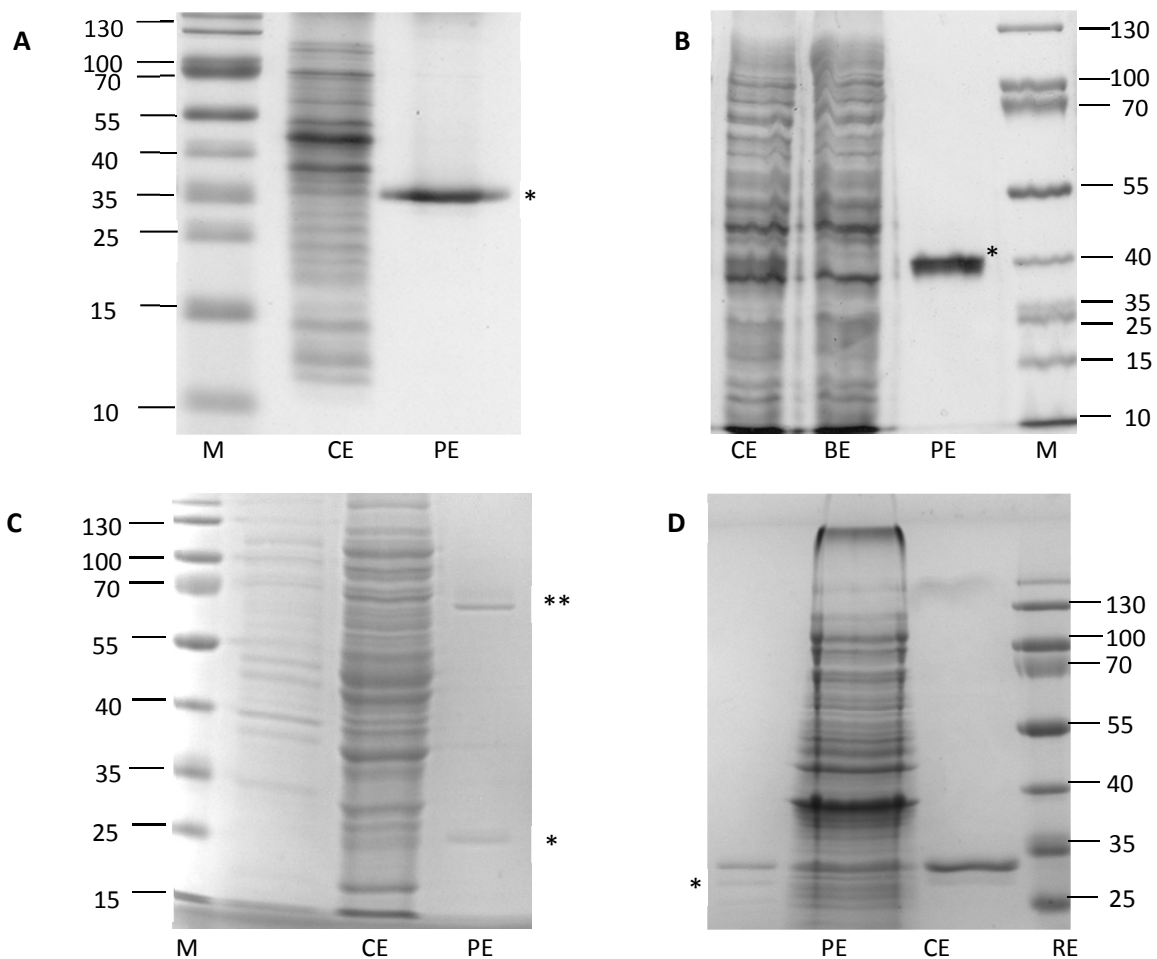


Figure 7. Expression and purification of MI_UPPS (A), Mt_UPPS (B), Hp_UPPS (C) and Hb_UPPS (D). CE = crude extract after protein expression, PE = purified protein after separation by IMAC and desalting, M = molecular marker, RE = Reference Enzyme (in comparison Mt_UPPS with a

concentration of 27.2 mg ml⁻¹ determined by Bradford) and BE = before induction with IPTG.
 * = purified enzyme, ** = *E. coli* chaperon.^[69]

2.2.3. cPTases with homoallylic diphosphates as elongation unit

2.2.3.1. Methods and procedures

To characterize the cPTases regarding the substrate conversion, two assay systems were established (method 7.1.3.). The catalytic parameters were determined by a phosphate detection assay (P_i-assay) which is based on side-product inorganic diphosphate (Figure 8). The advantage is the conversion of non-radio labeled substrates which are the different starter units ((*E,E*)-FPP or Mant-O-GPP) or elongation units (IPP, BPP or Cl-BPP).

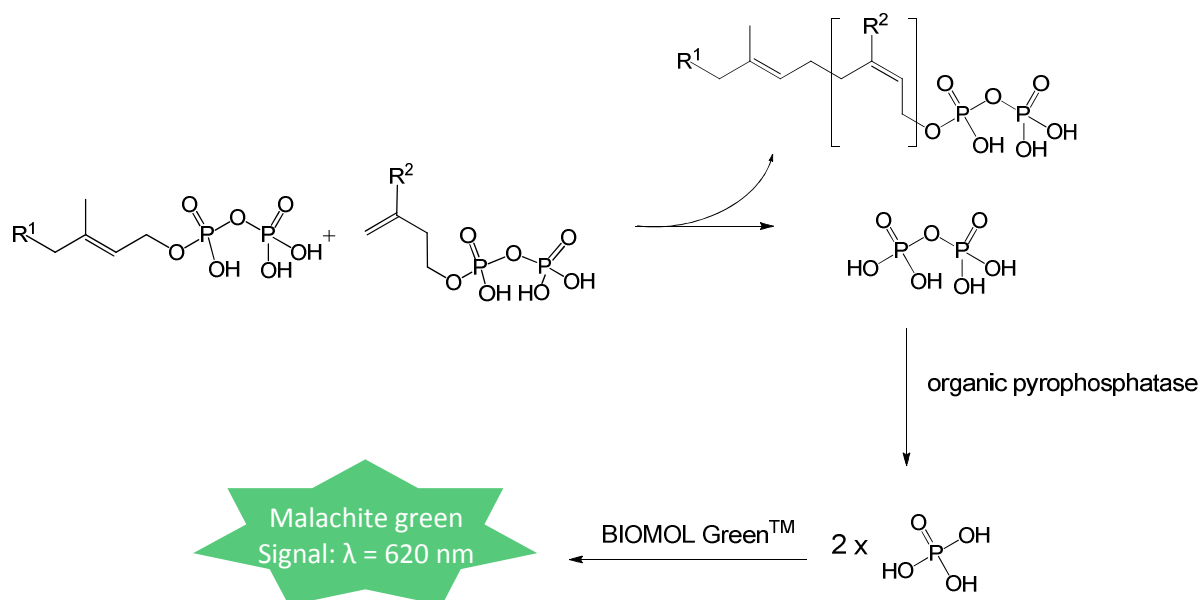


Figure 8. Principle of the P_i-assay.^{[70][71]} cPTases conjugates one prenyl unit (i.e. IPP) to the allylic substrate (i.e. FPP).

2.2.3.2. Principle of the P_i-assay

cPTases catalyze the conjugates of one prenyl elongation unit (i.e. IPP) with one allylic substrate (i.e. FPP) to form the product and one organic diphosphate as side-product. Then, the enzyme "inorganic pyrophosphatase" cleaves the inorganic diphosphate (PP_i) into two inorganic monophosphates (P_i). By adding BIOMOL Green™, only the liberated monophosphate forms a colored complex with molybdate/malachite green under acidic conditions. Thereby, the yellow solution changes the color to green which was quantified by measuring the absorbance at 620 nm (Figure 8) (method 7.1.4.).

2.2.3.3. Principle of the fluorescence labeled HPLC-assay

To investigate the product chain length and the product distribution, the enzyme was incubated with the fluorescence labeled starter unit Mant-O-GPP (instead of *E,E*-FPP) and ten units of IPP or analogues (Figure 9). This labeled substrate is poorly accepted, but due to the fluorescence the detection limit is increased and sometimes even a weak product formation could be measured.^[54] To monitor the biocatalytic activity, aliquots of the enzyme mixture were taken and the substrate conversion was measured by P_i -assays. The product formation was analyzed by HPLC (method 7.1.2.).

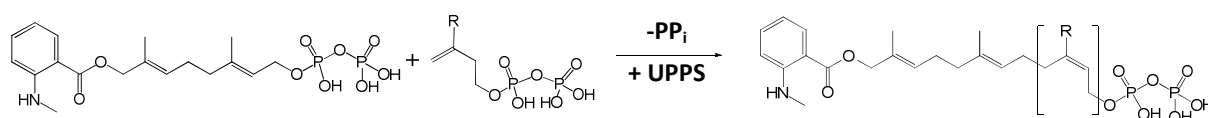


Figure 9. Principle of the HPLC assay. Mixtures were incubated with the fluorescence labeled allylic starter unit (Mant-O-GPP) and the elongation substrates (R = H: BPP; R = Cl: Cl-BPP; R = CH₃: IPP) with recombinant MI_UPPS and Mt_UPPS at rt for 16 h. Detection was carried out with a fluorescence detector ($\lambda_{Ex} = 352 \text{ nm} / \lambda_{Em} = 420 \text{ nm}$).

2.2.4. Catalytic parameters of UPPS with homoallylic diphosphates as elongation unit

2.2.4.1. Results of the natural allylic substrate IPP

Based on the UV data, the purified cPTases exhibit a product formation with the natural substrates *E,E*-FPP and IPP (Figure 9). The most active enzymes which catalyze the elongation were found to be Ec_UPPS, MI_UPPS, Hb_UPPS, Hp_PPS and Mt_UPPS. Enzyme assays with *E. coli* UPPS were described previously^[54] and were used in this study as positive controls. Comparing the cleavage of the diphosphate group from MI_UPPS and Mt_UPPS, it is remarkable that MI_UPPS catalyzes elongation continuously and after 30 min, the enzyme cleaved off 25% of the possible diphosphate. Otherwise, Mt_UPPS shows the weakest specific activity. The reason for this is that in Mt_UPPS utilizes the diastereomer *Z,E*-FPP as starter unit.^[72]

Product formation was analyzed by HPLC with MI_UPPS and Mt_UPPS in the presences of Mant-O-GPP and IPP. The final product length was C₅₀₋₅₅ which is the common chain length for UPPSs. MI_UPPS and Mt_UPPS show a different product distribution. Furthermore, the biocatalytic conversion is in the steady state range for the first 30 min.

A Summary table of the catalytic activity.

| Catalytic activity ($\text{pmol}_{\text{PPi}} \times \text{min} \times \text{pmol}_{\text{Enzyme}}^{-1}$) | | | | |
|---|------------------|----------------|------------------|------------------------|
| | <i>H. pylori</i> | <i>E. coli</i> | <i>M. luteus</i> | <i>M. tuberculosis</i> |
| IPP | 2.550 | 4.901 | 1.210 | 0.295 |
| BPP | 0.084 | 0.125 | 0.127 | 0.263 |
| CI-BPP | 0.062 | 0.101 | 0.078 | 0.133 |

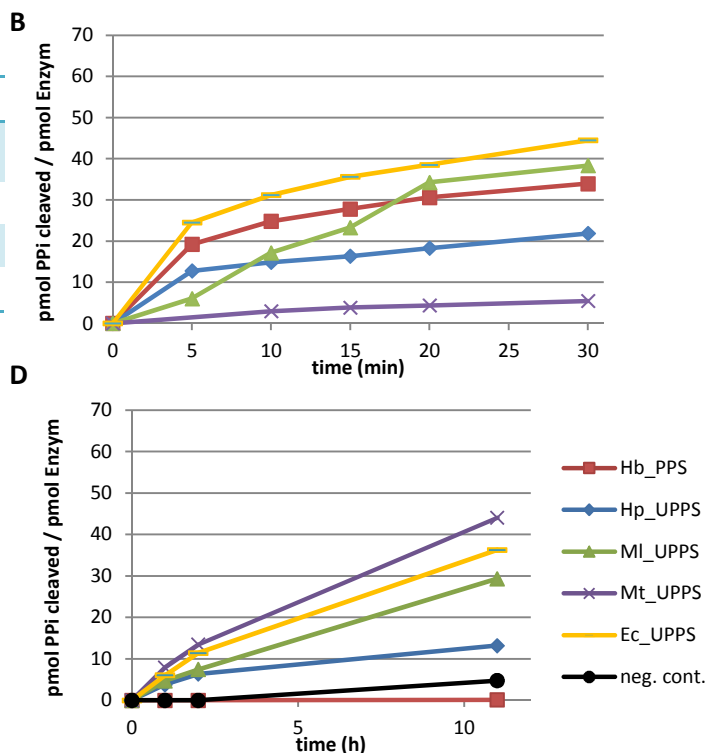


Figure 10. Biocatalytic activity of cPTases with allylic prolongation unit. Measured with the Pi-assay, (A) shows the summary table. *E,E*-FPP is the starter unit with IPP (B), BPP (C) and CI-BPP (D) as prolongation unit.

Mt_UPPS seems to preferentially produce elongation until C₃₅ intermediate and mainly C₄₅₋₅₀ as final products. MI_UPPS catalyzes exclusively the chain length of C₅₀₋₅₅ with rarely liberated intermediates (Figure 11).

Based on the UV data, the purified cPTases exhibit a product formation with the natural substrates *E,E*-FPP and BPP (Figure 10). Interestingly, Mt_UPPS catalyzed diphosphate cleavage of but-3-enyl diphosphate (BPP) which is easily misinterpreted as product formation. After 11 h, a PP_i release of approximately 60% was detected in the P_i-assay. From the first impression, the substrate acceptance of the alternative elongation unit was in the same range as the natural substrate IPP. Instead, MI_UPPS and Hp_UPPS showed a weak activity with *E,E*-FPP and BPP. In contrast, Hb_PPS reveals as non-active at all. The HPLC results with Mant-O-GPP could not confirm the product formation (Figure 12).

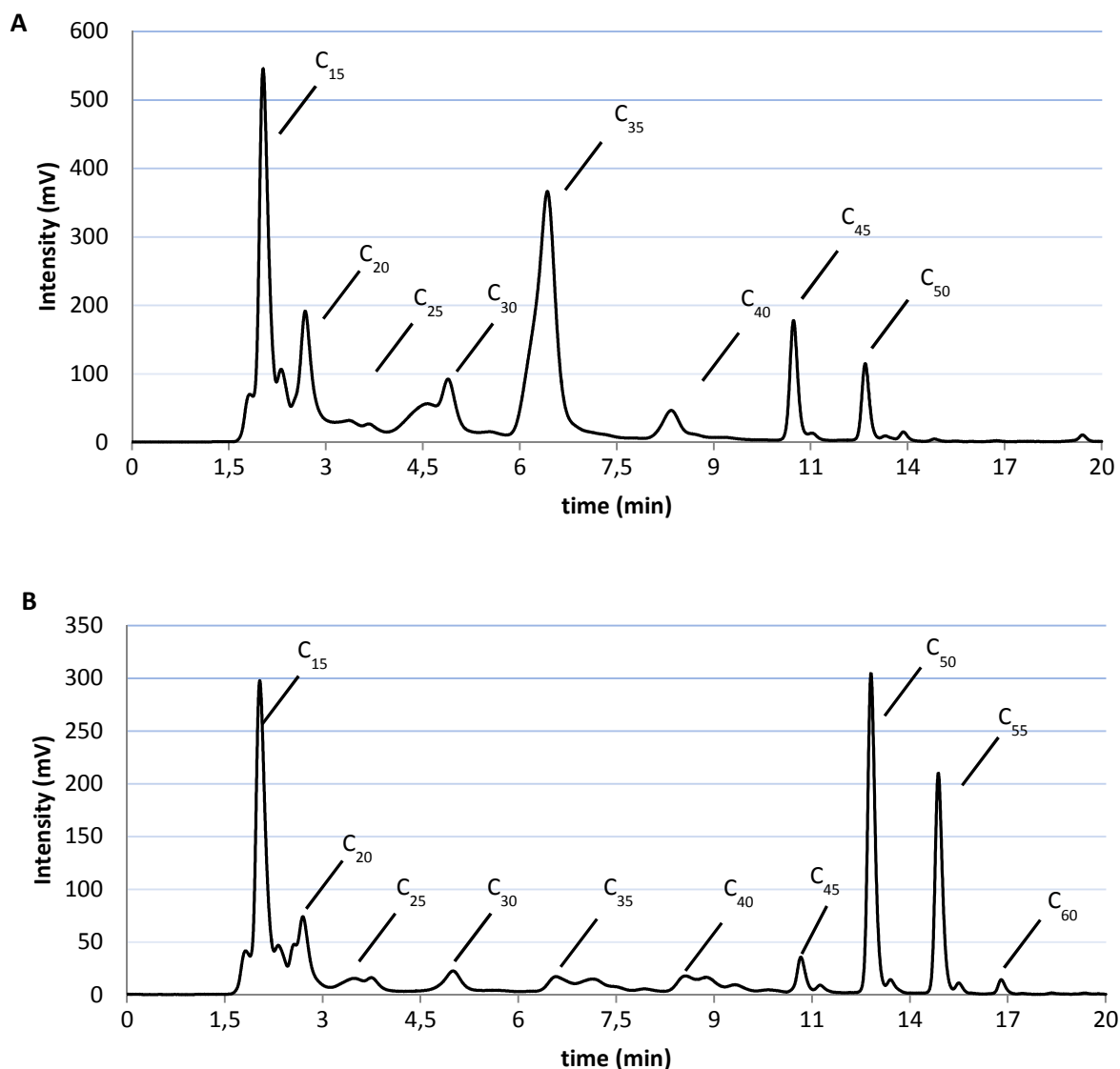


Figure 11. HPLC chromatogram of the MI_UPPS and Mt_UPPS product formation. Mt_UPPS (A) and MI_UPPS (B) incubated with Mant-O-GPP and IPP at rt for 16 h. The fluorescence was detected at $\lambda_{\text{Ex}} = 352 \text{ nm}$ and $\lambda_{\text{Em}} = 420 \text{ nm}$.

2.2.4.2. Results of the non-natural allylic substrate BPP

In the present of BPP, no additional peak could be observed. This finding may be explained by the poor acceptance of Mant-O-GPP. Therefore, the level of all elongated products is under the detection limit. However, this seems unlikely especially considering the results from the IPP conversion and the excellent detection limits of fluorescence labeled compounds. Another reason might be that the enzymes cleave off the diphosphate moiety which gives a false signal in the P_i -assay. Calculating the liberated PP_i -concentration and comparing to the amount of enzyme, it seems plausible that one Mt_UPPS cleave 2 molecules of allylic substrate. The questions arise which diphosphate residue (FPP or BPP) is cleaved.

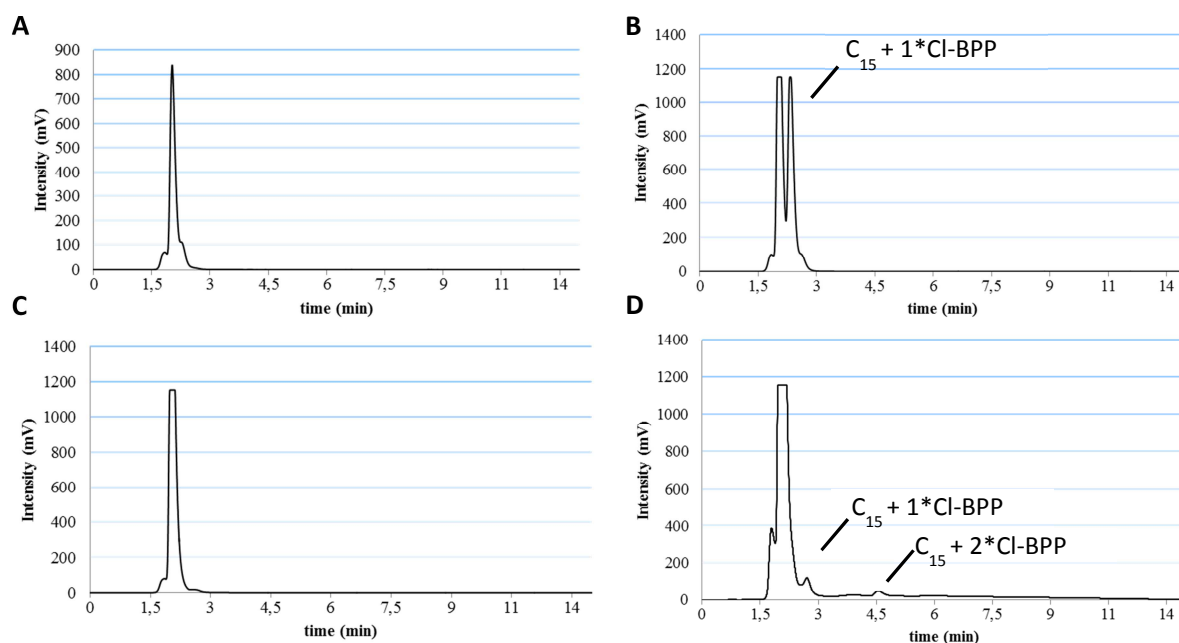


Figure 12. HPLC chromatograms of artificial substrates. (A) MI_UPPS with BPP and (B) CI-BPP or (C) Mt_UPPS with BPP and (D) CI-BPP incubated at rt for 16 h with Mant-O-GPP as starter unit. Detection was carried with a fluorescence detector ($\lambda_{\text{Ex}} = 352 \text{ nm} / \lambda_{\text{Em}} = 420 \text{ nm}$).

2.2.4.3. Results of the non-natural allylic substrate CI-BPP

UV data for MI_UPPS and Mt_UPPS in the P_i -assay indicate a product formation with the natural substrates *E,E*-FPP and CI-BPP (Figure 10). After 11 h, a PP_i release of approximately 20–30% was detected. In comparison, no product formation could be seen for Hb_PPS.

Interestingly, HPLC confirmed the product formation with the prolongation unit CI-BPP with Mant-O-GPP as starter unit instead of the natural *E,E*-FPP (Figure 12). In the presence of MI_UPPS, the addition of one CI-BPP unit was achieved. In the presence of Mt_UPPS, the addition of one and two CI-BPP building blocks was obtained. Analyzing HPLC results revealed that the enzyme products of Mant-O-GPP with the CI-BPP eluted at the same retention time as IPP-conjugated products (Mant-O-GPP with IPP: C_{20} -product eluted at $R_t=2.8 \text{ min}$ or the C_{25} -product $R_t=4.5 \text{ min}$). This could be an indication for the possible product chain length.

However, the conversion rate was found to be significantly lower in comparison to the natural substrate. In conclusion, these results demonstrate the acceptance of preferentially IPP as prolongation unit to form the natural chain length of C_{55} . No alternative substrate was accepted with equal efficiency.

2.3. Conclusion and Summary

2.3.1. Assay

The prenyltransferase activity was screened and quantitatively determined using the byproduct diphosphate (PPi). The diphosphate was cleaved off to liberate monophosphate which forms a green colored complex with molybdate/malachite green. Then, the malachite green complex was quantified by reading the absorbance at 620 nm (method 7.1.4.).

The chain length of the enzymatic product was routinely estimated by HPLC-measurements using the fluorescence detectible FPP-analogous Mant-O-GPP instead of *E,E*-FPP (method 7.1.2.).

2.3.2. Results

The microbial UPPS from *M. luteus*, *M. tuberculosis*, *H. pylori* and the rubber synthase from *H. brasiliensis* could be expressed and purified (method 7.1.1.). The activities of the four heterologously expressed proteins (method 7.1.3.) were determined in the presence of *E,E*-FPP and IPP or BPP or Cl-BPP using the P_i-assay. The precise elongation count of the product chain was analyzed by HPLC using the fluorescence labeled FPP-analogous Mant-O-GPP with IPP or BPP or Cl-BPP in the presence of MI_UPPS and Mt_UPPS. The product formation was observed with both enzymes but only in the presence of the elongation unit Cl-BPP. In contrast, BPP was not accepted by any of these tested enzymes.

2.3.3. Discussion

But-3-enyl diphosphate (BPP) and chloro-but-3-enyl diphosphate (Cl-BPP) have been chosen for the following reasons (Figure 5). The chloride moiety in Cl-BPP is a mimic group for the methyl in sense of molecular volume ($\text{CH}_3 = 22.9 \text{ \AA}^3$ / $\text{Cl} = 19.9 \text{ \AA}^3$) and the hydrophobicity, but with the opposite inductive and an additional mesomeric effect. Characteristic for the heteroatom group (Cl-BPP) is also the weak inductive electron withdrawing-effect (-I) and the mesomeric releasing-effect (+M)^[73] which is predominate regarding the conjugated double bond. This accounts for the stabilization of delocalization of charge like it occurs during the condensation steps (Figure 4). The same effect is taken by the alkyl group (IPP) with the electron-releasing effect (+I). This results in a slight positive charge of the C3-atom of the butene backbone. Exchanging the methyl-group against a hydrogen atom (BPP) leads to a loss of the inductive effect and therefore, the loss of stabilization of the carbenium ion.

However, an electron rich C3-C4 double bond is required for the diphosphate activation which explains the non-acceptance of BPP as allylic substrate.

It is clear that very small changes in the IPP-analogue structure affect the ability to catalyze the prolongation (see chapter 2.2.), but it is not clear how these differences relate to the protein structure. Although, it surprised that all enzymes seem to catalyze the condensation step of BPP and Cl-BPP starting from FPP (Figure 10) which was detected in the UV/Vis assay. Selecting the two active MI_UPPS and Mt_UPPS, and using the fluorescence-active Mant-O-GPP as starter unit, no conversion could be observed for BPP and a weak conversion for Cl-BPP (Figure 12). Mt_UPPS seems to condensate one unit and MI_UPPS may condensate up to two units. These HPLC analyzes with Mant-O-GPP are a selective method but the product retention times are different to regular enzyme products (means FPP + IPP). The reason to use Mant-O-GPP instead of FPP was to enhance the detection. It is known that this substrate is a weaker one for UPPS,^{[54][74]} but the increased detection overcompensates the poor acceptance. For IPP, the enzymes showed a regular product pattern of 7-9 prolongation units (Figure 11).

The reason for the poor acceptance of Cl-BPP may be the electron withdrawing properties of the substituents based on the inductive or mesomeric effects. Further, during evolution, it is thought that the binding pocket of the allylic substrate was adapted to the IPP: to bind, activate and release the prolonged allylic compound.

2.3.4. Outlook

In the future, the interest of artificial rubber might be probably increase due to the altered properties like for Cl-BPP results in polychloroprene known as neoprene or BPP results in polybutadiene available under "synthetic rubber". The demonstrated observations herein suggest the screen of other UPPS enzymes from other organisms which might have the ability to condensate non-natural allylic substrates. These experiments are seen as starting point for mutational high-through-put studies and as basic science to understand the conversion of artificial substrates.

3.0. Aromatic prenyltransferase NphB

3.1. Background and significance

Prenylated polyphenol compounds are omnipresent across all organisms like archaea, eubacteria, plants, fungi and animals.^{[75][76]} Recent discoveries indicate distinct pharmaceutical characteristics like anti-microbial, anti-oxidant, anti-inflammatory, anti-viral and anti-cancer activity.^{[77][78][79]} Prenylation takes place in the later biosynthetic steps^[80] and often occurs in the common “regular” sense where the primary allylic C-1 carbon atom is added to the aromatic ring system as in the case of 8-prenyl-naringenin (Figure 13). This is in contrast to the “reverse” sense where the tertiary C-3 carbon atom is added to the aromatic core under allylic rearrangement. One example for the “reverse” prenylation is the indole prenyltransferase AnaPT involved in the biosynthesis of aszonalenin (Figure 13).^{[81][82]}

The aromatic core is typically an electron rich benzene residue (i.e. 8-dimethylallylnaringenin). In most cases, the prenyl donor is a five-carbon (dimethylallyl) or a ten-carbon (geranyl) unit which is attached to an activated position on the aromatic ring. Relevant examples are the addition of a dimethylallyl moiety to naringenin resulting in the strongest phytoestrogen 8-prenylnaringenin.^{[83][84][85]} The attachment of a geranyl-residue to a tryptophan leads to ergotamine^[86] which is medicinally used to treat acute migraine attacks,^[87] or another pathway leads to Δ^1 -tetrahydrocannabinolic (Δ^1 -THC) which is an important representative among the cannabinoids.^[88] Noteworthy for Δ^1 -THC is the cyclization of the geranyl residue within the *ortho*-hydroxy group of the core mediated by an enzyme called cyclase (chapter 4.1). More rarely and hard to identify is the attachment of a twenty-carbon (geranylgeranyl) group as shown in the biosynthesis of paxilline.^[89] Pharmaceutically important examples are summarized in Figure 13. The isolation of such compounds from natural sources is challenging because they occur mostly in traces and are often tissue or organ specific. One alternative possibility is the chemical synthesis of aromatic, prenylated compounds. Depending on the target structure, this can be time consuming and suffer from high costs due to multi step reaction procedures.^{[90][91]} An alternative approach could be the introduction of a prenyl group to an aromatic core mediated by engineered prenyltransferases.^[32] For a wide application in biocatalytic synthesis, soluble enzymes with a broad substrate spectrum and distinct regio-specificity are required. One example for such an aromatic prenyltransferase could be NphB.

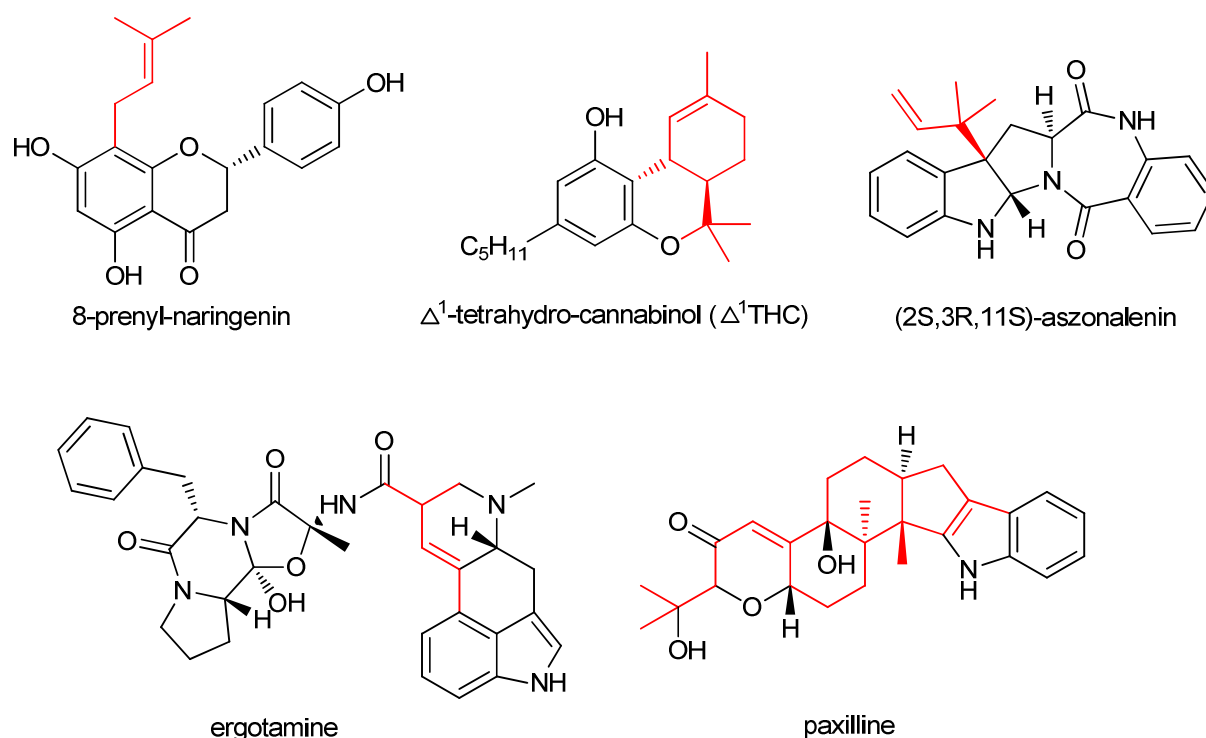


Figure 13. Representative structures of prenylated aromatic ring systems.

3.1.1. Brief introduction to the aromatic prenyltransferase NphB

NphB is a well-characterized promiscuous prenyltransferase (assumed abbreviation for **Naphterpin Biosynthesis**). This enzyme originates from *Streptomyces* sp. strain CL190, and has been described earlier as Orf2.^[92] This prenyltransferase is part of the gene cluster for naphterpin biosynthesis. The indispensable prenylation step, i.e. the attachment of a geranyl (C_{10}) moiety to the intermediate flaviolin,^[77] is assumed to be catalyzed by NphB (Figure 14).^{[79][92][93][94]}

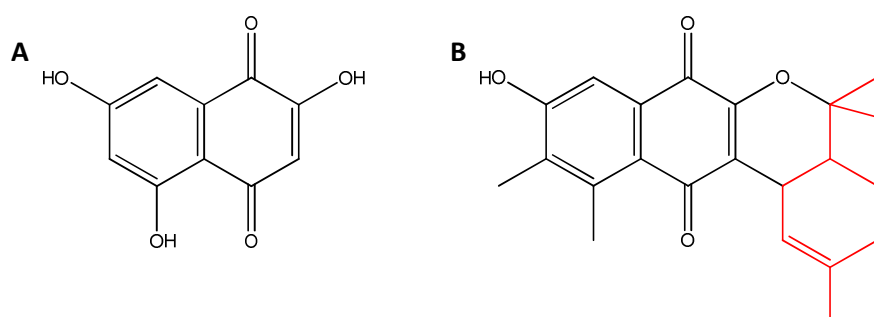


Figure 14. The biosynthesis of naphterpin involves prenylation of flaviolin (A). The geranyl moiety is depicted in red (B).

A significant advancement in the understanding of prenyltransferases to the aromatic core was described in 2005 when the first structure of a microbial aromatic prenyltransferase was

described.^[92] Later, in 2008, Kuzuyama *et al.* demonstrated that a series of non-natural polyphenolic aromatic compounds is also accepted by NphB.^[93] For example, the flavonoid naringenin was geranylated, resulted in the formation of both, 7*O*-geranyl-naringenin and 6-geranyl naringenin (bonannione A), a compound with cytotoxic activity against human tumor cell lines.^{[95][93][96]} Another example was the geranylation of the simple phenol, olivetol, to form a prenylated intermediate. This is also known in the biosynthetic pathway of Δ^1 -tetrahydrocannabinol and of great interested in pharmaceutical applications.^[97]

3.1.2. Structure of the aromatic prenyltransferase NphB

NphB belongs to the ABBA superfamily of prenyltransferases which are structurally characterized by α - β - β - α repeating elements (called PT barrel).^{[98][99]} This structural motif forms the active site accommodating the aromatic substrate, the prenyl donor GPP and a tightly bound Mg^{2+} ion (Figure 15), which seems to be required for acquisition of the diphosphate moiety of the co-substrate. Many aromatic prenyltransferases shares this structural motif and are evolutionarily related. Interestingly, the superfamily includes metal-dependent as well as metal-independent members. NphB is Mg^{2+} -dependent. Usually, enzymes which require an Mg^{2+} -ion to catalyze biochemical reaction have two aspartates in the active centrum. These amino acids coordinate the metal ion and are known as “DxxD-motif”.^{[29][39][100]} Interestingly, NphB is missing this structural scaffold.

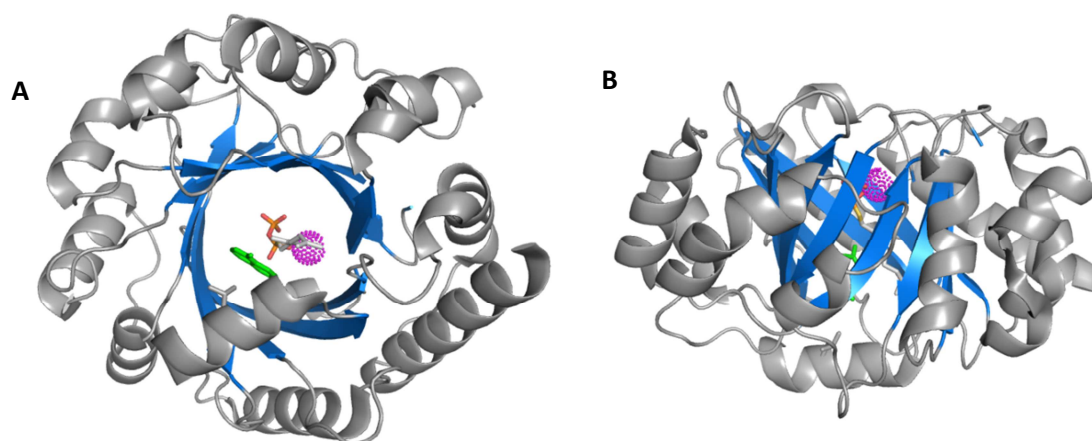


Figure 15. Structure of the aromatic prenyltransferase NphB (PDB-Code 1ZB6). (A) Top view of structural elements and (B) surface representation of the protein with bound aromatic substrate 1,6-DHN (green), the co-substrate analogue geranyl-S-thiolodiphosphate (orange = thiolodiphosphate; grey = allylic residue) and the catalytic Mg^{2+} ion (violet spherical dots). The α -helices and loops are depicted in darker grey and the β -sheets are in navy blue.

3.1.3. Mechanistic studies of prenyltransferases

The reactions catalyzed by PTases are often compared with the chemical Friedel-Crafts-alkylation (S_N1 -like) of nucleophilic aromatic systems such as flavonoids, indoles, naphthalenes, or phenylpropanoids (Figure 16 A). In the first step, the prenyl diphosphate may bind to the enzyme with the aid of Mg^{2+} as well as the prenyl donor. Subsequently, under the influence of the enzyme and the acceptor substrate, the diphosphate is cleaved. An electrophilic enzyme-stabilized carbocation is generated. In the next “step”, the electrophile attacks the nucleophilic ring system and forms a Wheland-intermediate and finally, the complex releases a proton to form the product. Such a “Friedel Crafts alkylation-like” reaction was initially proposed for UbiA and can be transferred to other PTases.^{[101][102][93][103]}

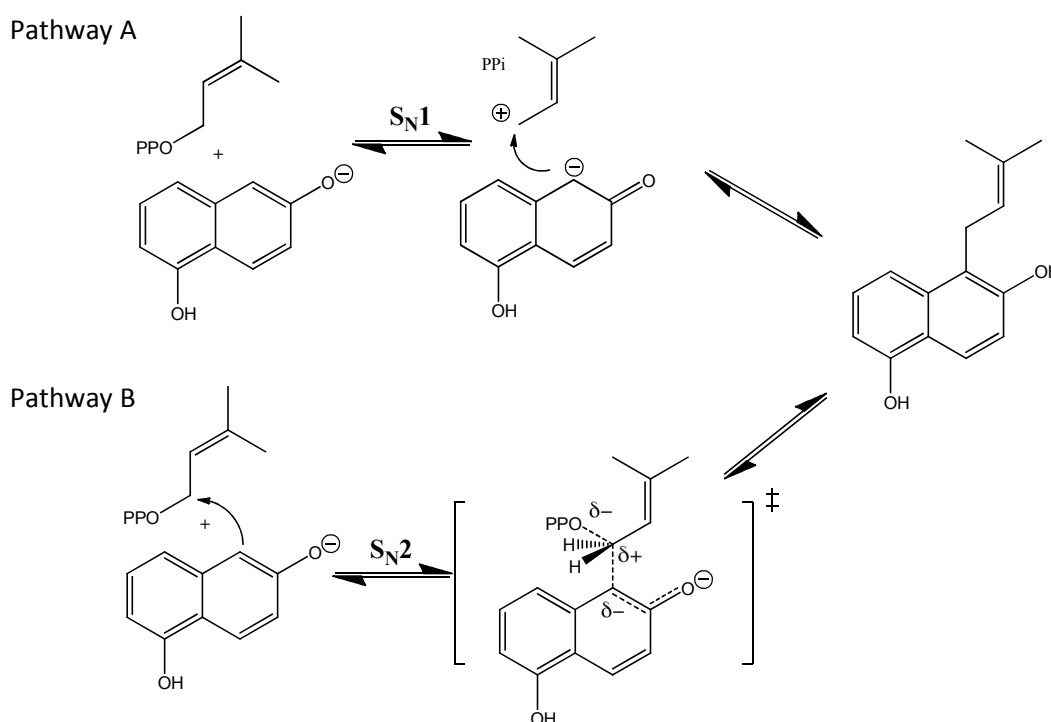


Figure 16. General steps of the “regular” prenylation of aromatic compounds. (A) S_N1 – like pathway and (B) S_N2 – like pathway proposed mechanisms for the reaction mediated by NphB . PP represent a diphosphate residue.

Among the dissociative S_N1 -like pathway (A), a so-called associative S_N2 -like mechanism (B) cannot be excluded. The nucleophile attacks the aromatic substrate directly (S_N2 -like) and forms the arenium ion intermediate. The diphosphate leaving group gets separated and the aromatic core prenylated in a single step (Figure 16). This is known for farnesyltransferases and is currently discussed for dimethylallyltryptophan synthases (DMATS).^{[104][105]}

3.1.4. Thesis overview

In the recent years, most studies have been focused on the identification of NphB gene,^[92] the substrate promiscuity^{[92][93]} and computational mechanistic studies.^{[106][104]} From these works it is clear that NphB accepts a variety of alternate phenol-containing substrates which come along with a carbon- and oxygen-prenylation at expected position on the aromatic core.^{[92][93]} Only computational studies have focused on the catalytic mechanism without any site-directed mutations for experimental validation. Therefore, this chapter will firstly focus on the elucidation of the allylic and aromatic substrate binding pocket as well as the investigation of the enzyme promiscuity (chapter 3.3. and 3.4.). The following chapter will throw light on the prenylation mechanism using site-directed mutations on NphB (chapter 3.5.) with the aim to answer the following three questions:

1. How do the substrates bind into the catalytic pocket?
2. How does NphB catalyze the attachment of a prenyl residue to the aromatic core?
3. How can the catalytic activity be increased and regio-specificity influenced?

3.2. Results and discussion

3.2.1. Optimization of expression and purification of NphB

Expression of the construct pET28a(+)_NphB in different media, at different expression temperatures and in different expression strains was checked by SDS-PAGE (Figure 17). Unfortunately, no soluble protein was obtained under all the conditions tested. Therefore, the NphB gene was introduced into the vectors pET32a. Optimum expression of soluble aromatic prenyltransferase was observed in *BL21* (DE3) harboring pET32a_NphB at 25°C and after 16 hours of induction with 1 mM IPTG (Figure 17). The fusion protein thioredoxin (Trx)-NphB was purified to homogeneity by Ni²⁺-affinity chromatography. For subsequent cleavage of the fusion partner Trx, human thrombin was used. To separate the fusion partner containing the N-terminal His₆-tag from NphB, the reaction mixture was applied to a Ni²⁺- agarose matrix. The different purification steps and proteolysis are shown on the SDS-PAGE (Figure 18). The enzyme purity after removal of the fusion partner was estimated to be over 90% (by Bradford). To monitor the biocatalytic activity during purification, aliquots

were taken at each step and the substrate conversion was measured by HPLC. The specific activity increased by a factor of 5.35 compared to the crude extract (Table 2).

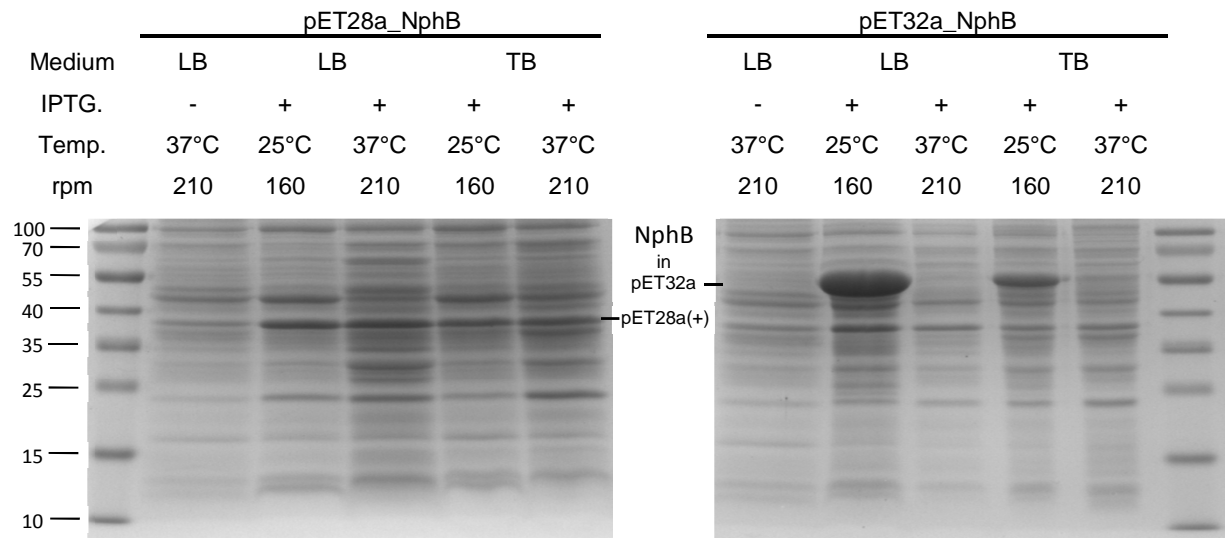


Figure 17. Expression of different NphB constructs. Lanes of the SDS-PAGE (10 % crosslinking) represent the molecular markers (M), before and after induction of gene expression in different medium, under different conditions and in different vector constructs.

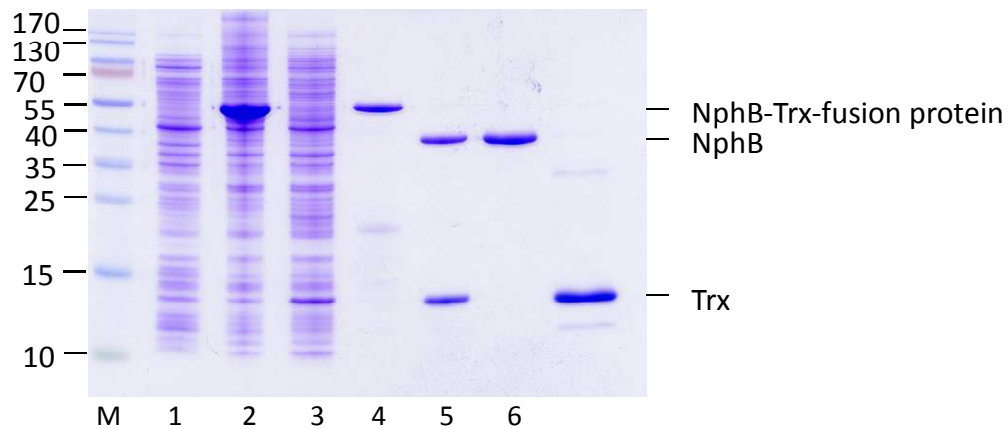


Figure 18. Purification of NphB. Lanes of the SDS-PAGE (16 % crosslinking) represent the molecular markers (M), the crude extracts of cells before (1) and after (2) induction of gene expression, flow through of the IMAC (3), Trx-NphB purified by metal ion affinity chromatography (4), a sample after proteolytic cleavage of Trx-NphB (5), and NphB (6) and Trx (7) after separation by metal ion affinity chromatography.

Table 2. Biocatalytic activity during the purification of NphB. Lanes present the crude extracts of cells after induction of gene expression in *E. coli*, Trx-NphB purified by metal ion affinity chromatography and after proteolytic cleavage of Trx-NphB and separation by metal ion affinity chromatography. Samples were incubated for 24 h at 25 °C and analyzed by HPLC.

| Purification step | Vol. Activity (pkat ml ⁻¹) | Volume (ml) | Protein (mg ml ⁻¹) | Spec. Activity (pkat mg ⁻¹) | Total Yield (%) |
|---------------------------------|--|-------------|--------------------------------|---|-----------------|
| crude extracts | 25.0 | 40.0 | 10.3 | 2.43 | 100.0 |
| NphB with Trx-Fusion Protein | 20.0 | 18.5 | 2.5 | 8.00 | 37.0 |
| NphB without Trx-Fusion Protein | 15.0 | 24.0 | 1.2 | 12.50 | 36.0 |

3.2.2. Identification of the 1,6-DHN products

LC-ESI-MS data for geranylated 1,6-DHN are in line with the literature data.^{[92][107]} To confirm the structure, peak 3, 5-geranyl-1,6-DHN, was exemplarily isolated by semi-preparative HPLC. The solvent was exchanged against deuterated methanol for NMR measurements (Appendix 10.1. and 10.2.). The ¹H-NMR-spectrum showed a similar aromatic ring pattern of 1,6-DHN without the proton signal in position 5 which indicates the prenylation on this aromatic carbon. The remaining signals stand in-line with the geranyl-group signals obtained from pure geraniol. Consequently, the aromatic carbon atom C-5 was linked to the geranyl chain carbon atom in position 1' which finally confirms the presence of 5-geranylated-1,6-DHN and is consistent with the literature.^{[92][107]}

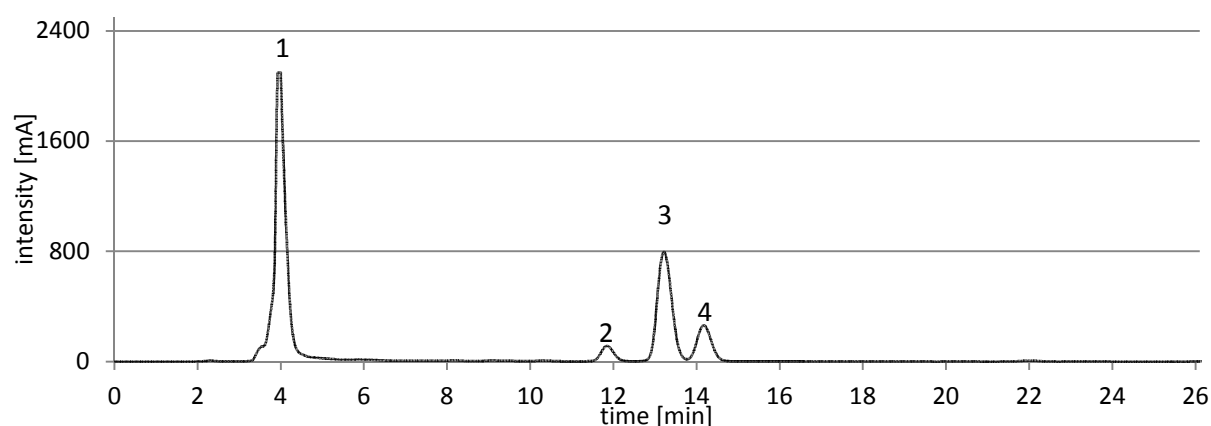


Figure 19. HPLC-chromatogram. UV-Vis-Spectra coupled with ESI-MS spectra to confirm the conversion of 1,6-DHN and GPP by NphB. Peak 1: 1,6-DHN (MW 159,04); Peak 2: 4-geranyl-1,6-DHN; Peak 3: 5-geranyl-1,6-DHN, Peak 4: 2-geranyl-1,6-DHN (for all products: MW 295,17).

3.3. Aromatic substrate promiscuity of NphB

3.3.1. Prenylation of dihydroxynaphthalenes and aromatic polyphenols

The aromatic prenyltransferase NphB has been reported to catalyze the prenylation of different aromatic substrates. For testing the biocatalytic activity of NphB, geranyl diphosphate was chosen as standard prenyl donor and 1,6-dihydroxynaphthalenes as prenyl acceptor to compare among them. In total, 24 compounds were screened including the three sub-classes: 1. naphthalenes, hydroxynaphthalenes (HN) and dihydroxynaphthalenes (DHN) (chapter 3.3.1.), 2. flavone derivatives and phenol-derivatives (chapter 3.3.2.) and 3. coumarin derivatives (chapter 3.3.3.).

3.3.2. Naphthalene, Hydroxynaphthalenes (HN) and Dihydroxynaphthalenes (DHN)

3.3.2.1. Results and discussion of (di)hydroxynaphthalenes

Naphthalene, two hydroxynaphthalenes (1-HN and 2-HN) and seven dihydroxynaphthalenes were screened (1,3-DHN, 1,4-DHN, 1,5-DHN, 1,7-DHN, 2,3-DHN, 2,6-DHN and 2,7-DHN). Whereby all NphB products underwent a mono-prenylation except the model substrate 1,6-DHN which formed three products 2-geranyl-, 4-geranyl-, 5-geranyl-1,6-DHN with a respective yield of 10.8, 5.4 and 37.8% (conversion after 16 h and product structure: Figure 20). The compounds were confirmed by LC-MS and NMR spectroscopy (Appendix: 10.1. and 10.2.) and exhibit a new C-C bond formation. Among all DHN derivatives, no O-prenylation was observed. The geranylation occurred mainly in *ortho* position with respect to the neighboring hydroxyl group. One explanation for the prenylation pattern of 1,6-DHN might be the orientations into the aromatic active-binding site. The activated geranyl is stoichiometrically close to one of the geranylation positions to the aromatic C-atoms 2, 4 and 5. The aromatic C5 atom seems to be the closest to the geranyl C1-position which leads to the preferred product 5-geranyl-1,6-DHN. Furthermore, the weak 4-geranyl-1,6-DHN formation may be a consequence of the electronic effects (+M-effect) of the hydroxyl-group which activates the ring in the favored *ortho* position (C2 or C5) and the less favorable *para* position (C4), and none in the disfavored *meta* position. However, one interesting result is the geranylation of 1,5-DHN which only occurs in the rare *para* position.

For the other DHN derivatives, the conversion yields were 17.3%, 10.9%, 9.7% and 0.4% after 16 hours for 2,7-DHN, 1,5-DHN, 2,6-DHN and 2,3-DHN, respectively. The

geranylation position of the 2,6-DHN and 2,7-DHN products was *ortho* with respect to a neighboring hydroxy group. Only the 1,5-DHN product showed the prenylation pattern in the *para* position. For 2,3-DHN, the product could only be confirmed by LC-MS. Unfortunately, no NMR-spectra could be obtained. Testing the hydroxynaphthalenes, the 2-naphthol was prenylated to 1-geranyl-2-naphthol and no product was obtained for naphthalene and 1-naphthol. These findings may support the assumption that the aromatic ring needs to be activated by a hydroxy-group which seems to be in C-2 position of the aromatic core (chapter 3.5.4.). Figure 20 summaries the findings and the elucidated structures.

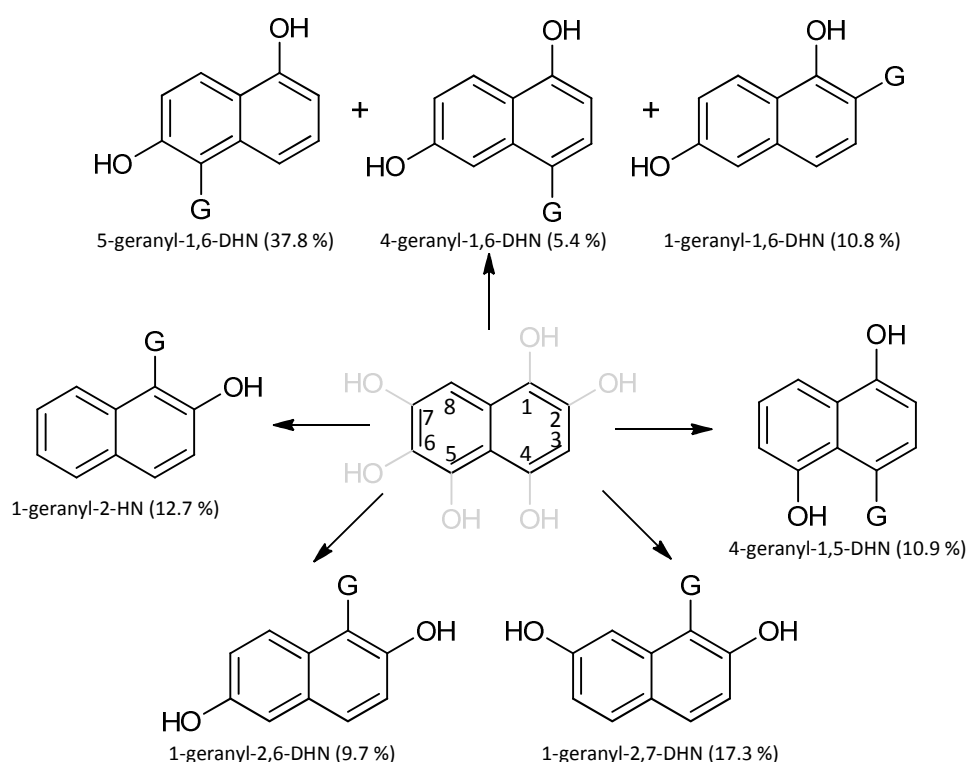


Figure 20. Prenylation reaction of different naphthols catalyzed by NphB. The structural scaffold is displaced in the center and in braces the yield. (G = geranyl moiety)

3.3.2.2. Pharmacophore model of (di)hydroxynaphthalenes

For further investigations, a pharmacophore was established to describe steric and electronic features required for interaction with the NphB enzyme and to explain catalytically conversion (Figure 21). The best substrate, 1,6-DHN, exemplarily shows how ligands bind into the aromatic ligand site. These following properties are interesting:

- 1. Hydrogen bond donor or acceptor:** The hydroxy group acts as hydrogen bond donor as well as hydrogen bond acceptor.
- 2. π -orbitals:** The aromatic ring π -system is sp^2 -hybridized and allows π - π - and π -cation- interaction.
- 3. Lipophilicity:** The aromatic ring structure is the lipophilic part and tends to enter the binding pocket driven by entropy of water displacement and van der Waal interaction.
- 4. Size:** From the geometric point of view, the ring structure is rigid and planar as well as the oxygen in the hydroxy group. Therefore, the substrate allows a unique binding position in the catalytic center.
- 5. Positive/negative charge:** The hydroxy groups strongly coordinate the location of aromatic core in the binding pocket due to the hydrophilic interaction with amino acids like Ser51. In dependence of the pK_a , a hydroxy group can be deprotonated under certain physiological conditions. Thus, the aromatic π -system will be activated and the prenylation can take place in appropriate *ortho* or *para*-position.

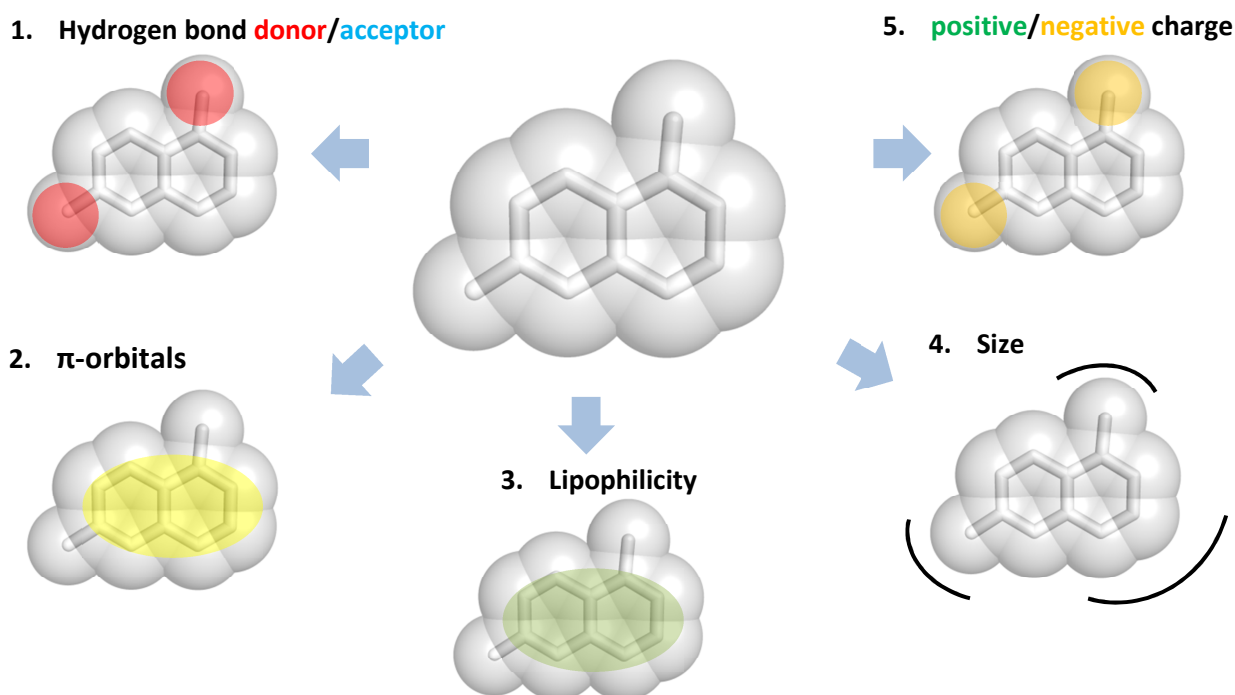


Figure 21. Pharmacophore model of 1,6-DHN. The properties include: hydrogen bond donors/acceptors, π -orbitals, lipophilicity, size, positivity/negativity charge(s).

3.3.3. Flavone derivatives and phenol-derivatives

3.3.3.1. Results and discussion of polyphenols

Probing the substrate requirements of the aromatic prenyltransferase NphB, the following flavones and polyphenols were tested: eriodictyol, luteolin, naringenin, 2-(3-hydroxy,4-ethoxy)-phenyl)-5,7-dihydroxy-4-chromanone (4'-O-ethyl-eriodictyol), quercetin as well as *p*-coumaric acid, caffeic acid and olivetolic acid (Table 3). All substrates, except for *p*-coumaric acid, caffeic acid and quercetin, underwent monogeranylation yielding one or two products. The most efficient conversion occurs for 4'-O-ethyl-eriodictyol (53.7%) which yielded in an O-alkylation. Instead, naringenin (34.6%) and eriodictyol (28.2%) formed the 6- and 7O-geranylated product(s) at the A-ring. The structures were elucidated by 2D-NMR and stay in line with the results from Takuto Kumano *et. al.*^[107]. However, luteolin shows only a weak substrate conversion rate (9.6%) as well as olivetolic acid which products could only be detected by LC-MS. The prenyl-patterns are summarized in Figure 22.

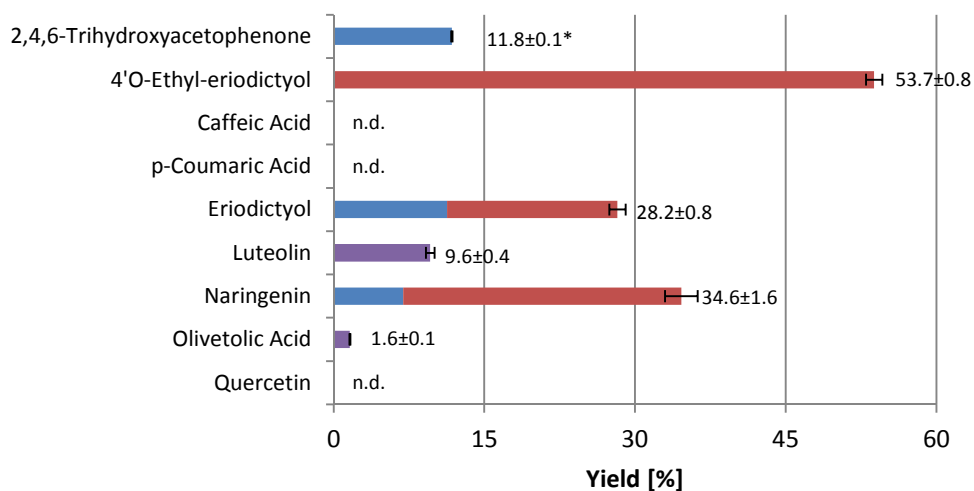


Figure 22. Biocatalytic geranylation of flavones and polyphenols by NphB. Samples were incubated for 16 h, analyzed by HPLC and structurally elucidated by NMR. (n.d. = not detectible or product yield $\leq 0.1\%$; * = multi-geranylated products (only obtained by MS); Blue = C-prenylation; Red = O-prenylation and in violet geranylated products of unknown constitution are presented.

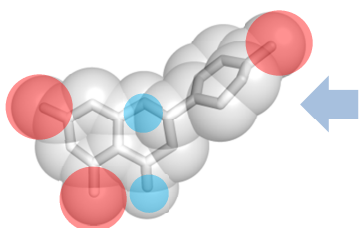
3.3.3.2. Pharmacophore model of polyphenols

To gain insight into the substrate preference, a pharmacophore model was used to explain the binding mode of the putative substrates, to describe steric and electronic features and to ensure catalytical conversion. Naringenin was used as an example to explain common features of an aromatic ligand (Figure 23). The following properties are interesting:

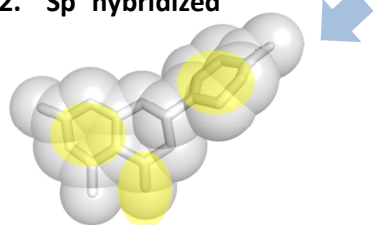
1. **Hydrogen bond donor or acceptor:** The hydroxyl in position 6 and 8 are hydrogen bond donors and acceptors whereas the ether-oxygen and the keto-oxygen are hydrogen bond acceptors only. The hydroxy groups on the B-ring may not be of great interest for the catalytic process but seem to be of importance for the substrate orientation. Best example is 4'-O-ethyl-eriodictyol and eriodictyol. Although both compounds share the same backbone, 4'-O-ethyl-eriodictyol underwent only an O-geranylation on the 7-OH group and eriodictyol forms the C- and O-geranylation products with slight preference towards 7O-geranyleriodictyol (11.3% and 16.9%).
2. **sp² hybridization:** The aromatic π -system is sp²-hybridized and explains the planar molecular geometry. With respect to the C-ring, NphB appended one geranyl group on luteolin at a relative low yield (9.6%) and did not accept quercetin. One reason could be the steric inflexibility of the compound due to the additional double bond in the C-ring. In quercetin, the extra hydroxy group seems unfavorable.
3. **Lipophilicity:** The aromatic A-ring and B-ring are the lipophilic parts. It seems likely that the B-ring plays an important role in the orientation of the substrate into the binding site. Eriodictyol (28.2%) has an additional hydroxy group in 3'-position compared to naringenin (34.6%) and 4'-O-ethyl-eriodictyol (53.7%) a lipophilic ethoxy-group in this position. On one hand, the lipophilicity of the B-ring may enhance the entrance into the hydrophobic entrance-cave of the geranyl-pocket and pushes the water out of the binding pocket which results in a better product yield. On the other hand, steric arguments maybe of importance to place the aromatic substrate in the right position and therefore cannot be dismissed.
4. **Possible charged position:** The 5 and 7-hydroxy groups are phenylogous acids that easily form a negative charge by deprotonation. Thus, the aromatic A-ring will be activated and the prenylation can take place in appropriate *ortho* position of the neighboring hydroxyl moiety or at the deprotonated oxygen of the phenolate. It depends on the orientation in the aromatic binding pocket, if NphB forms O-geranylation linkage like for 4'-O-eriodictyol, luteolin or the synthetic flavone precursor 2,4,6-trihydroxyacetophenone, or C-geranylation in case of eriodictyol and naringenin.

5. **Positive/negative partial charges:** The hydroxy group in position C5 and the keto-group (vinylogous carboxylic acid) may strongly coordinate the location of the aromatic core in the binding pocket due to the hydrophilic interaction with amino acids like Ser51.

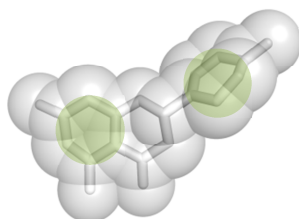
1. **Hydrogen bond donor/acceptor**



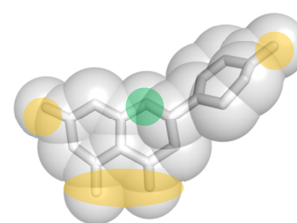
2. **Sp² hybridized**



3. **Lipophilicity**



5. **Positive/negative partial charges**



4. **Possible charged position**

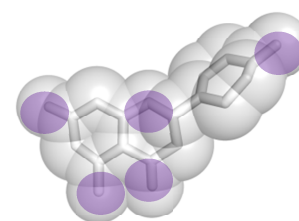
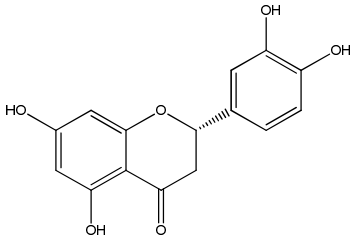
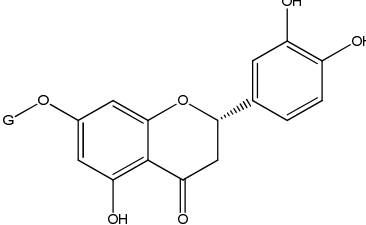
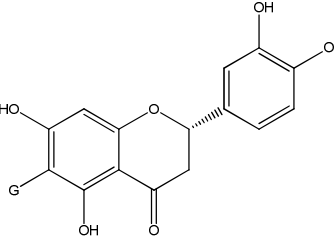
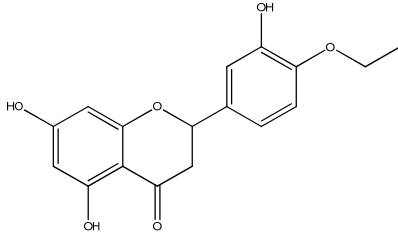
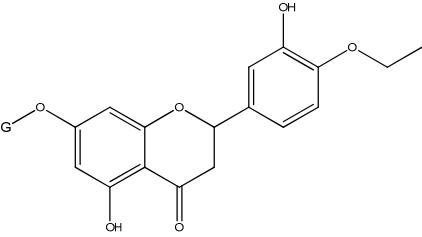
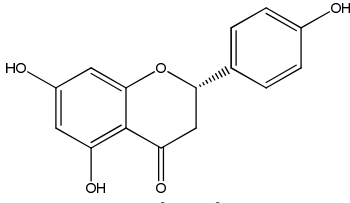
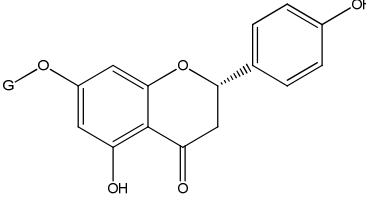
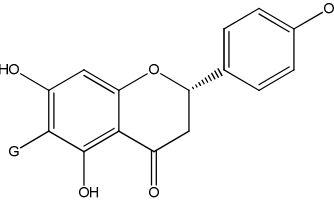
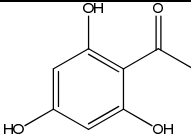
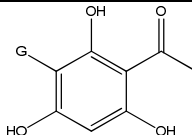


Figure 23. Pharmacophore model of the flavone naringenin. The properties include: hydrogen bond donors/acceptors, sp² hybridization, lipophilicity, size, electro positivity/negativity and charge(s).

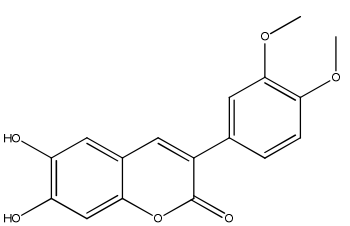
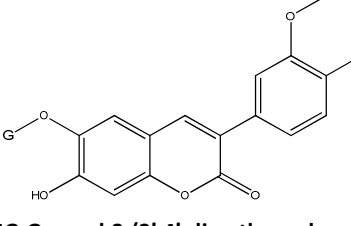
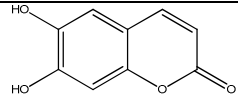
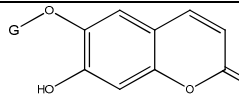
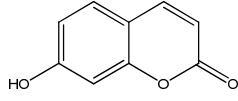
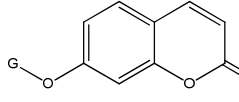
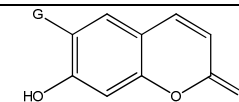
Table 3. NphB catalyzed geranylation of flavones and polyphenols. The yield was calculated from the AUC of the product divided by the overall yield (substrate plus product) measured by HPLC after 16 h incubation at room temperatur.

| Substrate | Product | Overall yield [%] |
|--|---|-------------------|
|  <p>Eriodictyol</p> |  <p>7O-Geranyl-eriodictyol</p> | 16.9 |
| |  <p>6-Geranyl-eriodictyol</p> | 11.3 |
|  <p>4'O-Ethyl-eriodictyol</p> |  <p>7O-Geranyl-ethyl-eriodictyol</p> | 53.7 |
|  <p>Naringenin</p> |  <p>7O-Geranyl-naringenin</p> | 27.7 |
| |  <p>6-Geranyl-naringenin</p> | 6.9 |
|  <p>2,4,6-Trihydroxyacetophenone</p> |  <p>3-Gernaly-2,4,6-trihydroxyacetophenone</p> | 11.8 |

3.3.4. Coumarin-derivatives

3-(3,4-Dimethoxyphenyl)-coumarin, 3-(3,4-dimethoxyphenyl)-esculetin, esculetin and umbelliferone were tested. 3-(3,4-Methoxyphenyl)-coumarin showed no product with NphB in the presence of GPP whereas 3-(3,4-methoxyphenyl)-esculetin underwent a regio-selective geranylation to 6*O*-geranyl-esculetin (7.1%) as well as esculetin to 6*O*-geranyl-esculetin (4.4%). Surprisingly, NphB catalyzed a carbon and an interesting oxygen geranyl attachment to umbelliferone in a 1:12 ratio (Table 4). The main NphB mediated products contain the geranyl moiety in the *ortho*-position to the neighboring hydroxy group. Therefore, the prenylation of the possible activated hydroxy-group is an unexpected finding. Interestingly, the phenyl-residue of 3-(3,4-dimethoxyphenyl)-esculetin had no essential steric influence except for the yield reduction. With 3-(3,4-dimethoxyphenyl)-coumarin, no product was obtained which was predicted due to the missing hydroxy groups on the coumarin scaffold and therefore, the activation of the ring could not occur.

Table 4. Geranylated coumarin derivatives by NphB. The yield was calculated from the AUC of the product divided by the overall yield (substrate plus product) measured by HPLC after 16 h incubation at room temperature.

| Substrate | Product | Overall yield [%] |
|---|--|-------------------|
|  <p>3-(3',4'-Dimethoxyphenyl)-esculetin</p> |  <p>7<i>O</i>-Geranyl-3-(3',4'-dimethoxyphenyl)-esculetin</p> | 4.4 |
|  <p>Esculetin</p> |  <p>6<i>O</i>-Geranyl-esculetin</p> | 7.1 |
|  <p>Umbelliferone</p> |  <p>7<i>O</i>-Geranyl-umbelliferone</p> | 3.7 |
| |  <p>6-Geranyl-umbelliferone</p> | 0.3 |

3.3.5. Conclusions

In conclusion, 24 different aromatic substrates were successfully tested, 11 (di)hydroxynaphthalenes and naphthalene as well as 9 flavonoids and polyphenols, and 4 coumarin derivatives. Among them, nine compounds underwent no prenylation. This shows the high acceptance and promiscuity of NphB for aromatic compounds. Two properties seem to be important for an aromatic prenyl acceptor. On the one hand, the hydroxy groups on the aromatic ring (phenol) whereby the geranylation occurred at the *ortho*-position. Using naringenin as example, the substitution occurred at carbon to form 6-geranyl-naringenin, or on the hydroxy group in *meta*-hydroxyl which leads to 7*O*-geranyl-naringenin. On the other hand, the substrate need to be small (naphthalene derivateves) or structurally flexible to fit into the pocket why Quercetin was a poor substrate. No attempt was made to probe tri-cyclic (Table 4).

3.4. Prenyl acceptor promiscuity of NphB

3.4.1. Results and discussion of the conversion of artificial prenyl diphosphate derivatives

Prenyltransferases of the aromatic PTase NphB catalyze Friedel-Crafts alkylation with high promiscuity toward the aromatic prenyl acceptors, but with high specificity for GPP.^[92] Herein, the acceptance of 14 different prenyl donors was screened toward natural and non-natural prenyl diphosphates. The prenyl donors were synthesized by Dr. Roman Weber.^[108] A summary of all tested compounds is given in Figure 24. The analogues of GPP were used as prenyl donors and 1,6-DHN as prenyl acceptor for the enzyme assay with NphB. GPP served as positive control. The turnover-number was determined by UV/Vis-assay described in Chapter 5.2. The same mixtures were analyzed by HPLC after 16 h of incubation. Product formation was observed for compound **1**, **2**, **3**, **4**, GPP and *E,E*-FPP in the UV/Vis assay and confirmed by LC-MS. Whereas, **5**, **6** and Mant-O-GPP products were measured by LCMS. All NphB reaction products contain a geranyl-like group with a chain length between C₉- to C₁₅. The alkyl acceptors containing C₁₄-atoms were preferred. In particular the non-flexible compound **1** with a triple bond between C₆-C₇ was the best substrate among the prenyl donors. Shifting the chain-length from C₈ to C₉ or even C₁₀, as in the case of **3** < **4** < **5**, strongly increases the activity of NphB. It seems that terminal di-methyl groups like in the

natural substrate GPP or a longer chain length are required for stabilization and to better position the allylic moiety in the binding site. The twist of the terminal methyl-group results from the inserted sulfur and could be one reason. This indicates also the importance of the terminal di-methyl-moiety and corresponds well to the reduced activity of compounds **2**, **3** and **4** which do not have this structural feature. No product formation was detected for prenyl donors with shorter chain length like DMAPP (C₅) or long chain-length like FPP or GGPP. Furthermore, switching the conformation of the first C₅-unit from the *E* to *Z* conformation like in *Z,E*-FPP or neryldiphosphate does not lead to product formation. The same was observed for nor-GPP with the missing methyl-group in C-3 position. This proves that the protein structure of NphB is adapted to *trans*-substrates with a methyl-group in C-3 position. The allylic binding pocket consists of several amino acid residues involved in the activation due to a catalytic base i.e. an amino acid like asparagine^[54] and lysine,^{[105][109][110]} or the possibility to activate itself due to the diphosphate oxygen.^[111] The carbocation must also be stabilized which occurs mainly by tyrosine or tryptophane in combination with the aromatic ring systems of the substrate. Thus, the system protects itself also against undesired nucleophilic attacks.^[112]

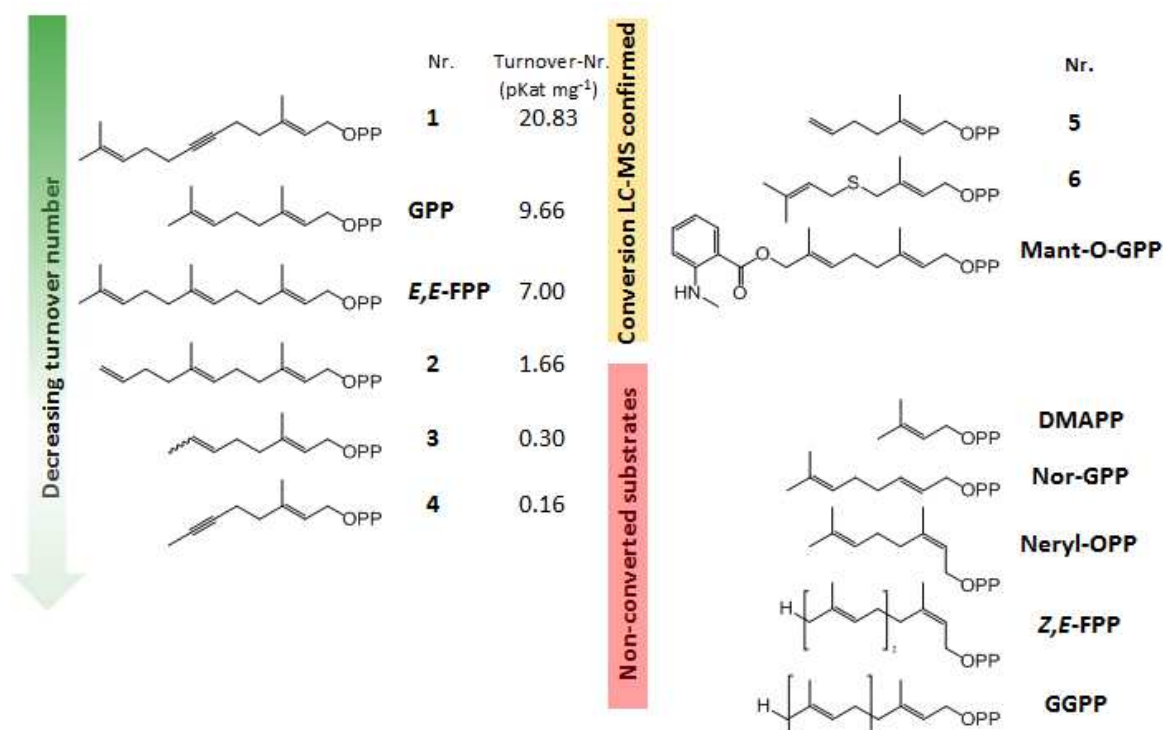


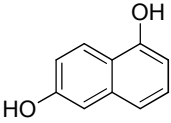
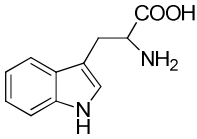
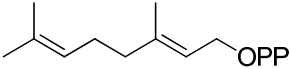
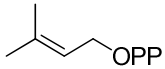
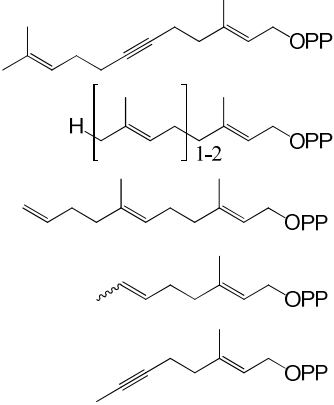
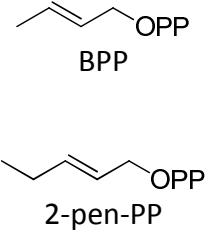
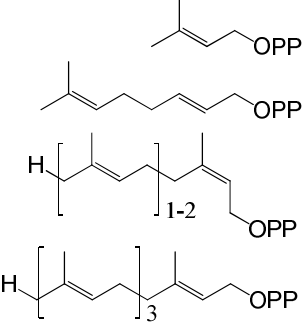
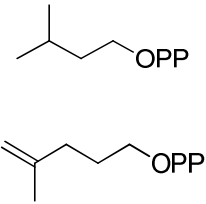
Figure 24. Natural and artificial prenyl-donors for NphB. The outcome is divided in converted (green), conversion only LC-MS confirmed (yellow) and non-converted substrates (red). Kinetics were analyzed during the first hour in the presences of 5 mM 1,6-DHN and 5 mM GPP or its analogues.

3.4.2. Discussion and comparison among PTases

NphBs catalytic promiscuity is the key for a powerful synthetic tool to expand the diversity of natural compounds. The prenylation of the aromatic cores seems to be preferred for prenyl-donors which fulfill three requirements: they should have a backbone of C₈-C₁₅, they should have a terminal di-methyl moiety as well as a methyl-group in position C3 and they should have a rigid structure in all-*trans* conformation.

The chemical properties of the allylic substrates were compared among the aromatic prenyltransferases NphB and FgaPT2.^[103] FgaPT2 is a dimethylallyl transferase (DMATS) from *Aspergillus clavatus* which catalyzes the prenylation of L-tryptophan at C7 with DMAPP.^[113] The HPLC analyzes of both enzymes are highly specific toward their natural substrates. It is no surprise that Liebhold *et al.* found less than 3% rest activity for FgtPT2 toward unnatural alkyl diphosphates (turnover number in comparison to the DMAPP) (Table 5).^[103] Interestingly, FgaPT2 accepted the but-3-enyl diphosphate (BPP) as substrate. The missing methyl of C-3 position seems not required for the conversion and consequentially, the authors proposed a S_N1 – like pathway (Figure 16). In contrast, NphB showed no product formation with nor-GPP and therefore it can be assumed that the missing methyl group in C3-position stabilizes the activated carbocation intermediate in the binding site. Further, a S_N2-like mechanism might take place at C1 of GPP which for that has to be in a certain three-dimensional position towards the aromatic substrate and the catalytically involved amino acids (see chapter 3.5.4.).^[92] However, in summary for FgaPT2, the chain length or the methyl group in DMAPP can be eliminated or shifted as shown for (*E*)-2-pentene diphosphate (2-pen-PP), but the double bond at the β-position is essential for the stability of the formed allylcation intermediate. In contrast, NphB accepts to a certain degree the prolongation up to the chain length of FPP, but not the omission of the 3-methyl groups.

Table 5. Comparison of the aromatic PTases NphB and FgaPT2 regarding the allylic donor.

| | NphB | FgaPT2 |
|-----------------|---|---|
| Prenyl acceptor | | |
| |  |  |
| Prenyl donor | | |
| Natural |  |  |
| Converted |  |  |
| Non-converted |  |  |

3.5. Mutagenesis and mechanistic studies of NphB

3.5.1. Structure-function analyzes of NphB

The 3D structure of NphB consists of a 10 antiparallel β -strands surrounded by a ring of solvent-exposed α -helices which form a central barrel (Figure 15). This common protein fold is also found among other aromatic prenyltransferases like FgaPT2 from a fungus.^[87] The structure of NphB can be described as five structurally similar repeating units (α - β - β - α) where the α -helices mainly function as loop regions and are surrounded by β -strand units which form a hydrophobic core. The hydrophobic residues stabilize the protein framework also known as barrel fold. Substrate binding and catalysis takes place in the center of this

barrel (Figure 15) and nearly all involved amino acids were part of the β -strands. To explore the binding pocket, most amino acids interacting with the substrates were mutated. Two strategies were carried out. First, key amino acids were exchanged against alanine (alanine scan) or other amino acids with different functional groups to identify their functional role in substrate binding and catalysis. Secondly, mutations of aspartic acid (D) or glutamic acid (E) were done with the objective to increase the turnover number. The aim was to increase the polarization by deprotonating the aromatic hydroxy group. Thus, the neighboring position may be activated and the C-C-prenylation occurs more often which results in increased turnover number. Furthermore, the substrate coordination is imperative in determining the precise nature of the catalytic mechanism and to influence the regio-selectivity. This subchapter focuses on the identification of the relevant amino acids for binding Mg^{2+} -ion (3.5.1.), GPP (3.5.2.) and the aromatic substrate 1,6-DHN (3.5.3.). In the last part, the regio-selectivity and the proposed mechanism are discussed.

3.5.2. Magnesium binding site and screening of bivalent metal ions

The aromatic prenyltransferases share the structural α - β - β - α motif, but not the common Mg^{2+} -binding DxxD-motif.^{[99][111]} NphB is found to be Mg^{2+} -dependent but without the DxxD-motif. It seems reasonable that the divalent metal ion is coordinated by the amino acids S51, D62, D110, K118 and four water molecules (known as SxxDxxDxxK – motif^[114]) whereas each amino acid is provided by one β -sheet (Figure 25). Eventually, the magnesium triggers a protein-conformation change by coordinating and bringing together the β -sheets. To confirm this hypothesis, the metal ion-binding site was mutated. As a result, S51A and D110A mutants lead to almost undetectable catalytic activity (turnover number under 1% relative to the WT). From this results, it seems that the divalent metal ion is coordinated by the hydroxyl residue of Ser51, carboxylic acid residues of Asp62, Asp110, and the amino-group of Lys118 (SxxDxxDxxK – motif), water molecules as well as by the α -phosphate of the diphosphate substrate. Furthermore, the bivalent metal ion is surrounded by water molecules which also have contact with the α - and β -phosphates.

Different metal-ion were studied for effect on the regio-specific geranylation of the model substrate 1,6-DHN. So far, Mg^{2+} exhibit the best activity and yield after 16 hour incubation followed by Mn^{2+} , Ca^{2+} , Co^{2+} , Ba^{2+} and Ni^{2+} in decreasing order. No activity could be observed

in the presence of Zn^{2+} . Interestingly, the prenylated product pattern changed remarkable in the presences of Ni^{2+} and Zn^{2+} ions. It seems to be that the product 2-geranyl and 5-geranyl-1,6 DHN are formed in more equal amounts. In the presences of the common divalent ions of Co, Mg and Mn, NphB prenylates the aromatic compound mainly in C5 position (69-83%) or in C2 position (10-20%). In the absence of added metal ions and in the presences of EDTA, no enzyme activity could be observed (Figure 26).

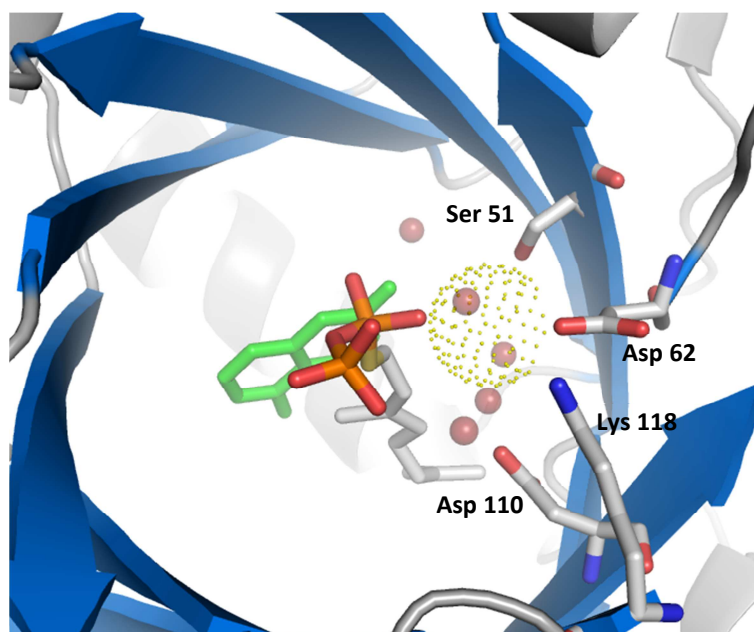


Figure 25. Binding mode of the Mg^{2+} -ion (yellow spherical arranged dots) coordinated by the amino acids Ser51, Asp62, Asp110 and Lys118 and water molecules (Bordeaux red spherical arranged dots) in the commonly found octahedral magnesium cluster in the active site. 1,6 DHN is colored in green, the diphosphate motif is held in orange (phosphate)/light red (oxygen) and the allylic carbons are grey. (PDB-code: 1ZB6)

To summarize and discuss, the product formation patterns were consistent except for Ni^{2+} and Zn^{2+} which forms more equal amount of all 2- and 5-geranyl-1,6-DHN. No activity could be observed in the absence of metal ions. This suggests that the regio-selectivity, at least in part, is governed by the property of the metal ion in comparison with the enzyme. The ability to catalyze different stereochemical outcomes seems to be determined by different metal ions. It is well-recognized that prenyltransferase enzymes require bivalent metal ion such as Mg^{2+} to catalyze biochemical reactions.^[115] Mg^{2+} is thought to bind in the active center with the prenyl-donor to accelerate the cation-formation step.^{[92][104]} Previous results from Frick *et al.*^[116] and Ohnuma *et al.*^[117] have shown that the chain length distributions of linear polyprenyl diphosphates are effected by different metal ions and can be altered and

manipulated. These experiments have suggested that the size of the active center determines the product chain length. The steric effects of the metal ions due to the “crystal” radii (ionic radii determined from crystal structures^{[118][119]}) of Mg²⁺ (0.86 Å), Mn²⁺ (0.81 Å) and Ni²⁺ (0.70 Å) may lead to slight changes in the protein conformation or rearrangements of the allylic substrate position.^[116] This influences the decreased activity toward Mg²⁺ as cofactor and toward the outcome of the altered product pattern. Furthermore, Zn²⁺ is a well-known cofactor for enzymes containing the “zinc-finger” moiety (Cys₄ or Cys₂His₂).^[120] The domain is typically found in clusters which do not exist in aromatic prenyltransferases. Therefore, Zn²⁺ plays no role as a cofactor in a number of PTases like the ones studied here and the catalytic activity is weak, or absent.

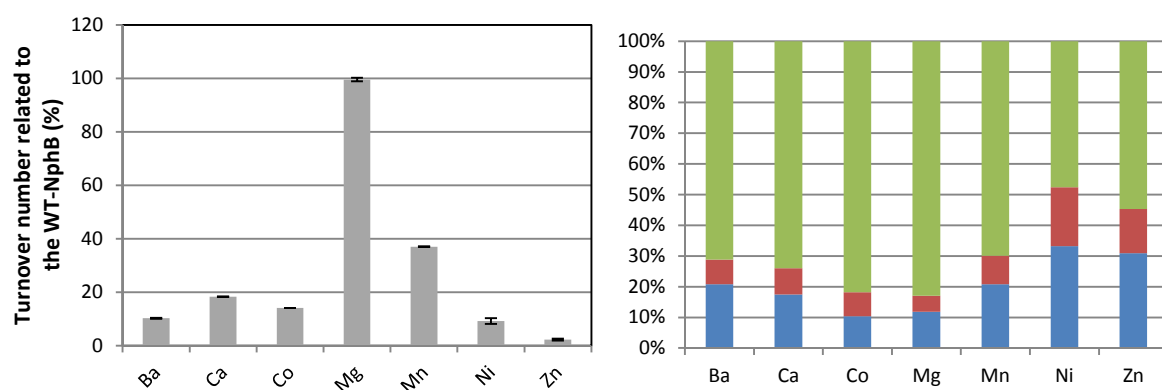


Figure 26. HPLC analysis of the reaction mixture containing different metal ions. The most active one was Mg²⁺ followed by Mn²⁺, Ca²⁺, Co²⁺, Ba²⁺ and Ni²⁺ with respectively decreases. Less activity could be observed in the presences of Zn²⁺. (Right) part shows the distribution of the products (n. D. = not detected; blue = 2-geranyl-1,6-DHN; red = 4-geranyl-1,6-DHN; green = 5-geranyl-1,6-DHN) and (left) part shows the activity among the different metal-ions relative to the WT-enzyme (9.50 pKat mg⁻¹) determined by UV-Vis assay.

3.5.3. Results of the site-directed mutagenizes in the 1,6-DHN binding site

The crystal structure of NphB provides an insight into the binding pocket of the aromatic substrate (Figure 27). Today, two out of four crystal structures are available with bound aromatic substrate; one with 1,6-DHN (PDB-code 1ZB6) and the other one with flaviolin (PBD-code 1ZDW). Flaviolin is not accepted as a substrate for NphB from the crystal structure point of view. The other crystal structures show NphB with N-tris(hydroxymethyl)methyl-3-aminopropanesulfonic acid (PDB-code 1ZDY) or complexed with GPP and Mg²⁺(PDB-code 1ZCW). The arrangement of the amino acid residues overlaps in all crystal structures and therefore, it gives no arguments regarding the structural changes

during substrate binding. However, 1ZB6 is used as standard to illustrate the residues involved in binding, interaction and activation of the aromatic substrate as well as the influence on the regio-selective prenylation of the aromatic core (Figure 27). Kinetic parameters, turnover numbers, and the product ratio were used to compare the mutants among each other. A summary of the results is given in Figure 29.

General overview of the involved amino acids; all mutants showed a reduced activity except V49E and V294A which increased the catalytic efficiency by 34.2% (chapter 3.5.4) and 23.1%, respectively, in comparison to the wild-type. No activity or less than 5% rest activity were obtained for the amino acids exchanges: Ser51, Aps110, Tyr216, Phe213 and Leu298 to alanine, Val271 to aspartic or glutamic acid as well as Ser51 and Tyr216 to aspartic acid. For Tyr216 to alanine remained a rest activity of 57.6%.

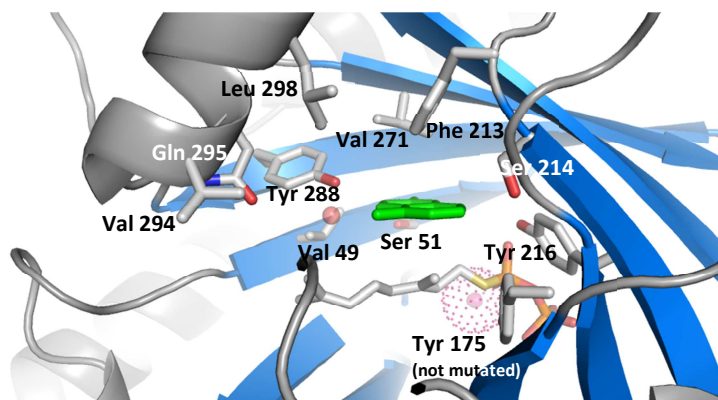


Figure 27. Binding of the aromatic substrate 1,6-DHN in the active side with the amino acids involved (labeled). 1,6 DHN is colored in green and the diphosphate motif is held in orange (phosphate)/light red (oxygen); the allylic carbons are grey. Mg²⁺-ion (shown as pink spherically arranged dots) and blue represents the β -sheets.

Role of the FS-Motif; the amino acids Phe213 and Ser214 are located in the loop. Combining their position in the crystal structure and the observation from previous studies on UPPS,^[121] this FS-motif is thought to “catch” the aromatic substrate due a π - π interaction between the aromatic core of the phenyl-moieties of Phe213 (4.0 Å) and 1,6-DHN as well as the weak interaction between the phenolic hydroxide and the Ser214 hydroxide (6.0 Å). Like in the UPPS enzyme, this moiety connects the α -helix with the β -sheet and therefore leads to a conformational change during its reaction.^[41] Comparing the crystal structure of UPPS in the apo-form and in the substrate-bound-closed form, it can be observed that the α -3 helix is kinked and closer to the allylic substrate. It is proposed that these conformational changes regulate the catalytic activity by closing and opening the hydrophilic cleft.^{[41][43][44][45][46]}

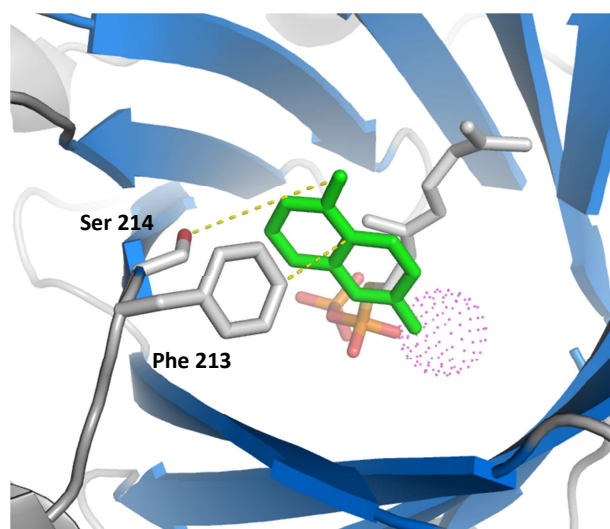


Figure 28. FS-motif with interaction to the aromatic substrate. Eliminating the serine hydroxy group (Ser214Ala) leads to a slight decrease activity of 13.0%. In contrast, alteration of the Phe213 moiety to lipophilic side chain goes along with the bioactivity of the chain length: Leu > Val > Ala with 82.7%, 15.9% and 0.1% remaining activity, respectively.

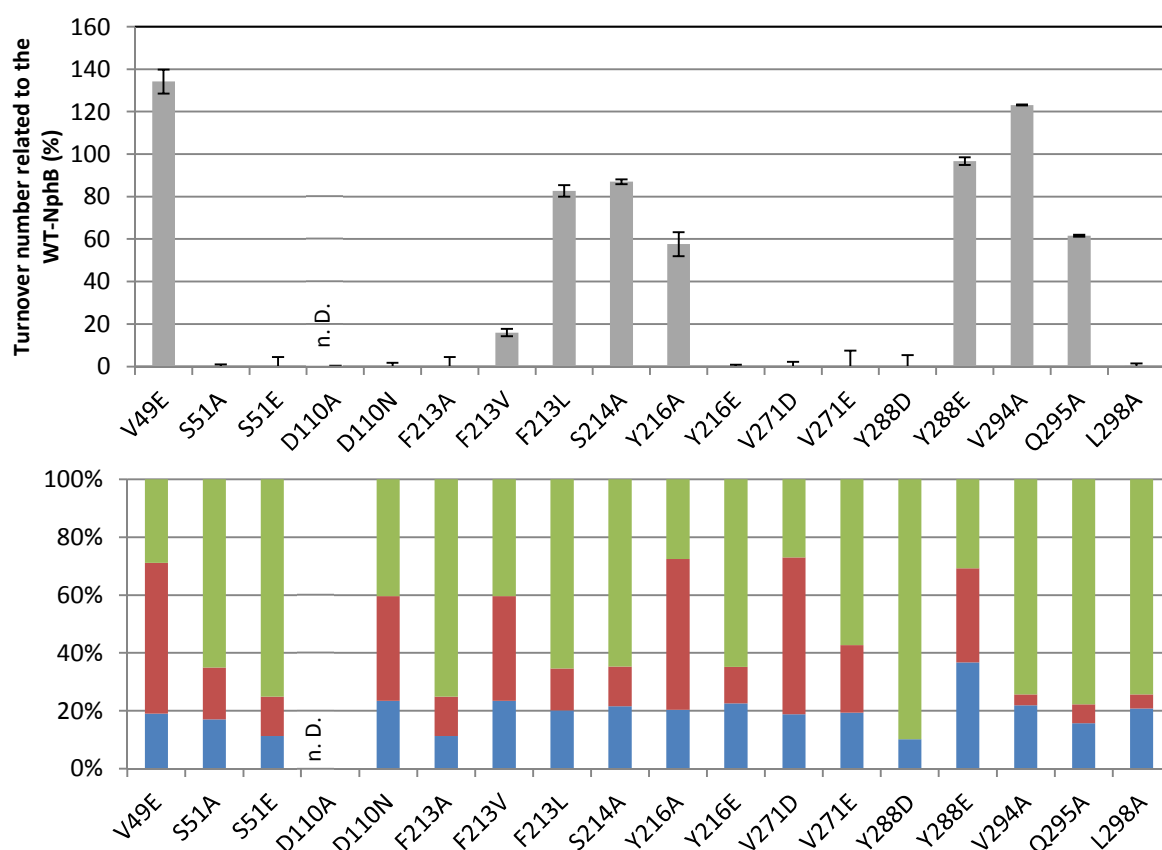


Figure 29. Mutagenesis of the 1,6-DHN binding pockets. (Top) Turnover number of the mutants relative to the WT-enzyme ($9.50 \text{ pKat mg}^{-1}$) determined by UV-Vis assay. (Bottom) Product ratio after additional incubation of 16 h analyzed by HPLC. (n. D. = not detected; blue = 2-geranyl-1,6-DHN; red = 4-geranyl-1,6-DHN; green = 5-geranyl-1,6-DHN)

Unfortunately, the crystal structures of NphB are equal and therefore, the evidences are missing to prove this hypothesis. However, the flexibility of the loop through “down” and “up” conformational changes escorts the aromatic substrate into the binding pocket. The FS-moiety may further be involved in stabilization of the intermediates and release of the product (Figure 28). To summarize, 17 amino acid residues involved in the aromatic substrate binding were successfully exchanged. Enzymatic studies of these mutations with GPP and 1,6-DHN were discussed and evaluated. All mutants exhibited a reduced activity except V49E and V294A which increased the catalytic efficiency by 34.2% and 23.1%, respectively, in comparison to the wild-type.

3.5.4. Results of the site-directed mutations in the GPP-binding motif

NphB prefers GPP as prenyl-donor. This binding site (diphosphate motif in orange, the sulfide group in yellow and the allylic residue in grey) is surrounded by the key amino acid residues (Figure 30). To identify the residues involved in the GPP-binding and to determine their catalytic role, 11 mutants were made. The summary of the kinetic parameters and the product distribution is given in Figure 31. Among the magnesium-dependent aromatic PTases, a motif of three basic amino acids could be identified. These residues are involved in the binding of the phosphate group and contain two conserved lysines, Lys 119 and Lys 284, as well as arginine, Arg 228 (Figure 30). Interestingly, this moiety is found in the structure of FgaPT2 (Arg 292, Lys 211 and Lys 283)^[110] or other indole PTases from fungi (i.e. cyclic dipeptide N-prenyltransferase *Aspergillus fumigatus*)^[82] and in the structure of a UbiA homolog from *Aeropyrum pernix* (Lys 119 and Arg 67).^[122] Model studies of the Mg²⁺-independent PTases CloQ and Fqn26 from the same protein family of NphB propose a direct involvement of these basic amino acid residues in the prenyl diphosphate binding.^[98] Site-directed mutagenesis experiments were performed on the FPPases indicated the importance of this region for the catalytic activity.^[123] This may explain why these essential amino acids are conserved among the PTases.^{[82][110][122]}

Regarding the P-O-C bond formation, the three involved tyrosines are also highly conserved among PTases. The role of these amino acid residues is described later (Figure 32).

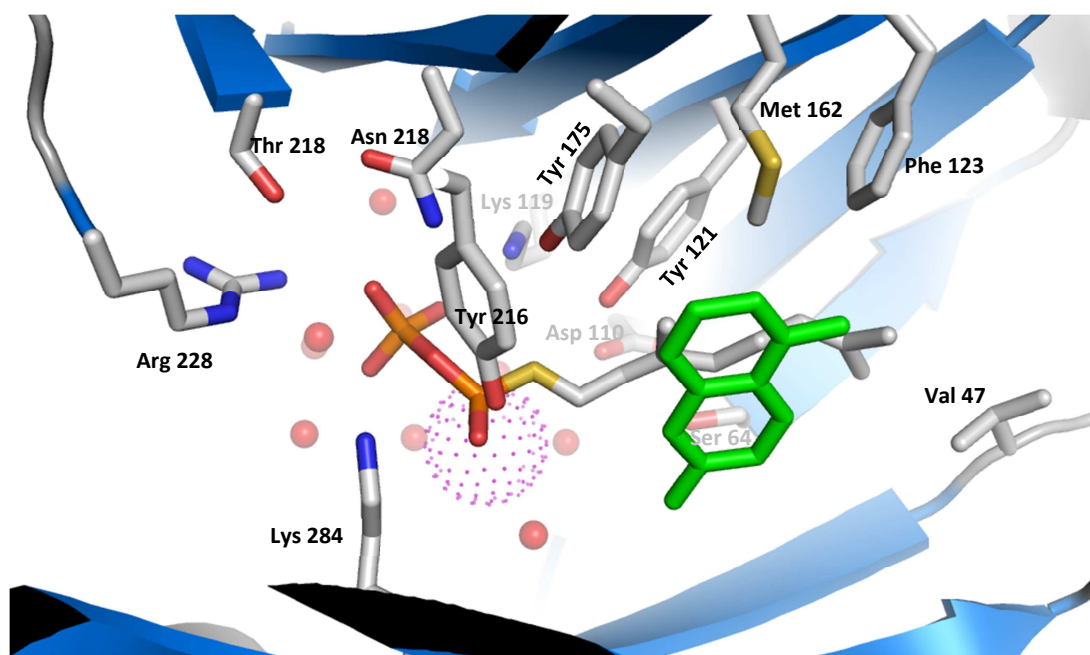


Figure 30. The binding site of GPP (diphosphate motif in orange, the sulfide group in yellow and the allylic residue in grey) is shown with the key amino acids residues in the center. In green the aromatic substrate 1,6-DHN, in magenta the Mg^{2+} -ion and the water molecules are in red dots.

Is there a catalytic role for Met 162? Originally, the electron orbitals of the sulfur of Met 162 were thought to interact with the carbocation intermediate. This idea was first described for the prenyltransferase UbiA from *E. coli* where it seems to play an essential role in the catalytic cascade (Kufka *et al.* unpublished results). The allyl group of GPP and the free electron pair of the Met 162 sulfur were thought to interact and thus, to allow the ionization and stabilization before undergoing the ring attachment (Kufka and Brandt *et al.* unpublished results). To probe this assumption, the amino acid was exchanged against aromatic residues which allow π -cation interactions. When mutated to the amino acids tryptophan or phenylalanine, the value of the turnover number was decreased by 79.7 and 73.8% and the product pattern consisted of >95% 5-geranyl-1,6-DHN and <5% 4-geranyl-1,6-DHN. In contrast, amino acids with lipophilic allylic side chains (alanine and leucine) which have no free electron pair of the side chain decreased the ability to stabilize the carbocation intermediate. In case of leucine, the activity decreased by 79.6% and for alanine by 94.8%. Interestingly, the resulting product pattern does not greatly differ from the wild-type which indicates that the allylic side chain of alanine or leucine may have little influence on coordinating, neither of the cation intermediate nor of the aromatic ring. To investigate the key role of Met 162 and to confirm the requirement as prenyl-donor intermediate,

Met 162 was mutated to cysteine. The aim was that the cysteine binds the prenyl-residue and hopefully, the amino residue eliminates the hydrogen of the cysteine to build a covalent bond (in a suicide inhibition fashion). Thus, the protein may be geranylated which would demonstrate the functional role of the sulfur in the catalytic sequence.

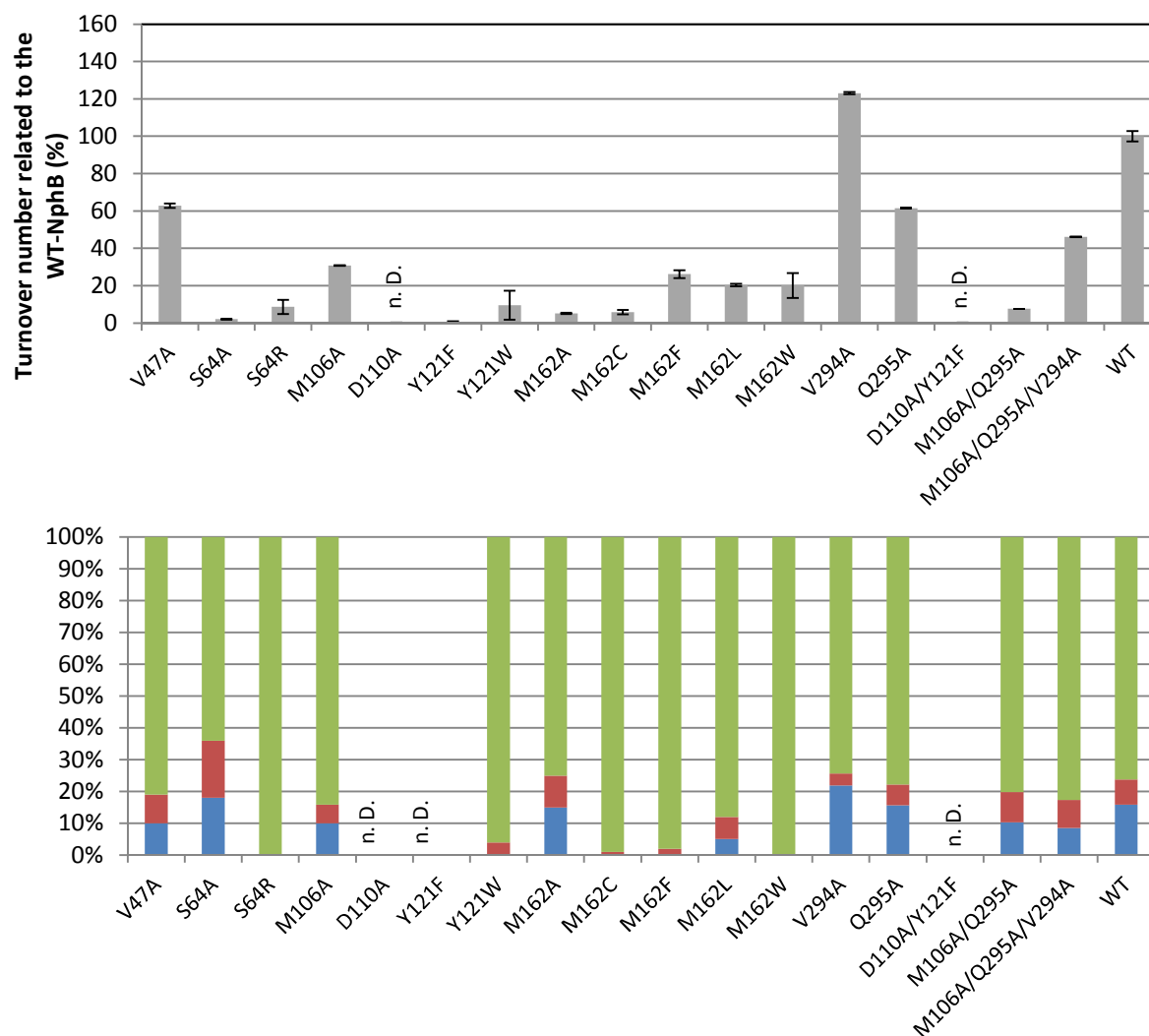


Figure 31. Mutagenesis of the GPP binding pockets. (Top) Turnover number of the mutants relative to the wild-type (WT)-enzyme (9.50 pKat mg⁻¹) determined by UV-Vis assay. (Bottom) Product ratio after additional incubation of 16 h analyzed by HPLC. (n. D. = not detected; violate = product proportion not determined; blue = 2-geranyl-1,6-DHN; red = 4-geranyl-1,6-DHN; green = 5-geranyl-1,6-DHN)

Stabilization of the intermediate by three tyrosines. The prenyl group of GPP is coplanar with the aromatic ring system of 1,6-DHN. The phenol hydroxy groups of the three tyrosines (tyrosine 121, 175 and 216) are located 3.8 – 4.22 Å away from the C-1 atom of GPP (Figure 32). These interactions may trigger the ionization step to form the carbocation, to stabilize

the positively charge at the allylic C-1 atom via π -cation interactions and most important, the reactive carbocation is prevented from reacting with water or other nucleophiles. The three tyrosine side chains shield the reactive carbocation from the surroundings. Furthermore, Tyr 121 may also be deprotonated by the neighboring carboxylate moiety of Asp 110. This activated hydroxy group could play an essential role in the activation of the prenyl-moiety before transferred to the aromatic core like discussed in Figure 34. When Tyr 121 was mutated to phenylalanine which lacks the hydroxy group no activity was observed. In contrast, Tyr 216 Ala mutation showed a rest activity of 57.6%. Instead, the exchange of the Tyr 216 against glutamic acid results in a catalytic activity of <0.1%. The interaction of the anionic residue of glutamate and the allylic cation might explain this observation.

Comparison of the “three tyrosine” motif between NphB and FgaPT2; NphB exhibits 13% sequence identity to the DMATs FgaPT2 from *A. fumigatus* (alignment by CLUSTALO). Both enzymes catalyze the prenylation of an aromatic substrate. In the catalytic center of both enzymes, nearly all involved amino acids are tyrosines which coordinate the C-1 position of the allylic substrate. These three phenolic residues are responsible for the shielding of the allylic cation, binding of the aromatic substrate, and proposed deprotonation from the Wheland intermediate (σ -complex). Therefore, the reaction mechanism is likely to be identical in both aromatic PTases.

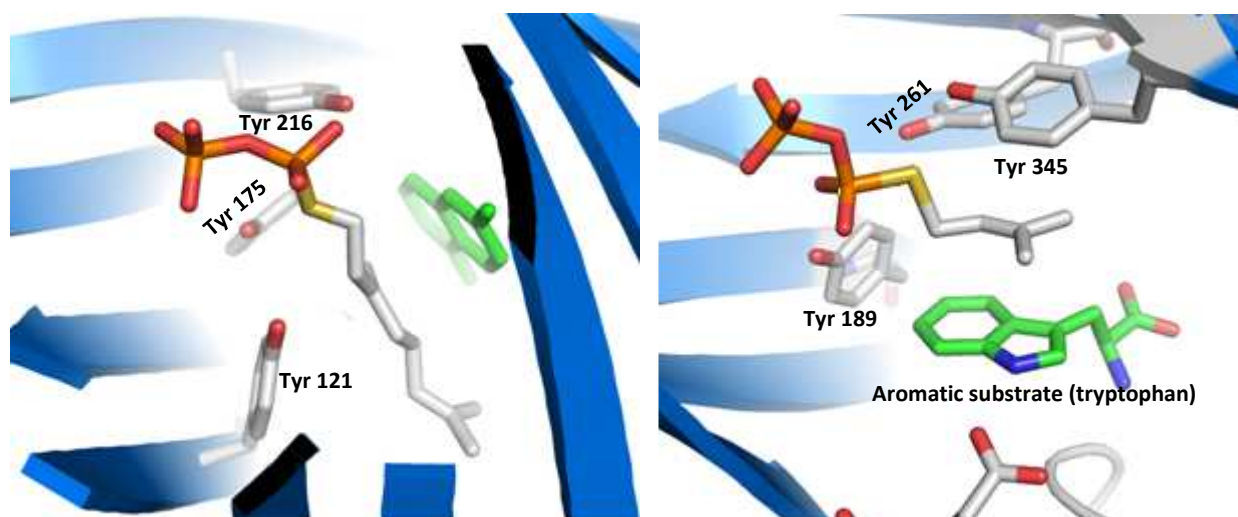


Figure 32. Stabilization of the intermediate by three tyrosines. (Left)Active center of NphB (PDB-code 1ZB6) with aromatic substrate 1,6-DHN (green) and GSPP in comparison **(Right)** to FgaPT2 with tryptophan and dimethylallyl-S-thiolodiphosphate in the center (PDB-code 3I4X). Tryptophan side chains stabilize the allylic cation by cation- π interactions with the aromatic ring.

Hydrophobic binding pocket for prenyl-residues. The isoprenyl chain is bound in a mainly hydrophobic pocket and faces the aromatic substrate on one side and aromatic (i.e. Phe 123) or allylic amino acids (i.e. Val 47, Val 294, Leu 298) on the other side (Figure 27). The surrounding also protects the highly reactive carbocation intermediate from water. The terminal amino acids Met 106, Gln 295 and V294 were mutated to explore, firstly, if they are required to stabilize the chain length and secondly, if this side can be opened due to the exchange against amino acids with a small residue like alanine. The advantage could be the faster immigration of the prenyl substrate into the pocket or the release of the product. In case of V294A, this idea was successfully proven. A decrease of the activity was observed for all the other mutations including the double and triple mutants (Figure 31).

In summary, 14 amino acid residues involved in the GPP substrate binding pocket were successfully exchanged. Enzymatic studies of these mutations with GPP and 1,6-DHN were discussed and evaluated. All mutants exhibited a reduced activity except V294A which increased the catalytic efficiency by 23.1%. Furthermore, the proposed essential role of Met 162 was elucidated and may not involve a putative covalent geranyl-protein-complex formation as previously assumed. The summary of the turnover numbers and the product ratio is presented in Figure 31.

3.5.5. Abstraction of the proton

Figure 34 shows the Friedel-Crafts-alkylation-like reaction. The geranyl group is coplanar with the naphthalene ring and the C-5 is 4.16 Å away from the C-1 of the GSPP (Figure 34 (Right)). Two ways are postulated to abstract the proton and form the product. Firstly, the aromatic ring gets activated due to deprotonation of the hydroxy group by carboxylate groups like aspartate or glutamate. The mesomeric effect of the phenolate causes electron density shift and activation the *ortho*- and *para*-position in the aromatic substrate for nucleophilic attacks to C-1 of GPP. Exchange of V49E results in an enzyme that has 134.2% of its WT-activity (Figure 33). Secondly, after cleaving the diphosphate moiety, the C_{G(S)PP-1} atom interacts with the aromatic ring to form a positively charged intermediate. To abstract the proton from the aromatic substrate, the hydroxy residue of the Tyr 121 is deprotonated due to the carboxylic acid substituent of Asp 110.

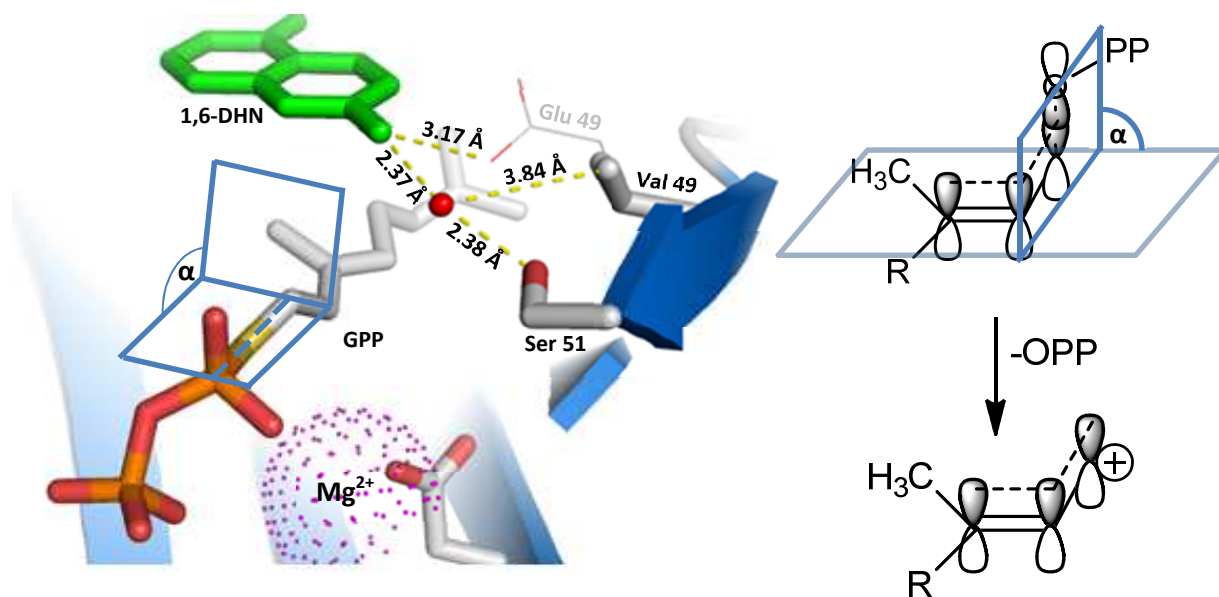


Figure 33. Mutation of Val 49 into glutamic acid. (Left) The torsion angle is drawn the crystal structure. (Right) The torsion angle (α) of the allylic substrate is $\alpha = 80^\circ$ in the original enzyme and $\alpha = 89^\circ$ in the V49E mutant (calculation MOE version 2014.9). The π -bond interacts with the d_{sp^2} -C-O orbital and forms the delocalization of the allylic cation. Thus, the energy effort is reduced for the cleavage of the C-O-bond and the cation formation.

Role of Asp 110; Asp 110 is involved in the binding of the allylic diphosphate of GPP directly (4.7Å) or through the magnesium ion. To prove if the role of the amino acid is to complex the magnesium or if the amino acid is otherwise involved in the catalytic cascade, a mutation towards alanine (D110A) was done (Figure 34). The residue of the carboxylic acid group was exchanged against the primary amide (D110N). The amide should not sufficiently alter the metal binding properties to complex divalent ions and furthermore, the length of the amino acid residue is similar which reduces the possibility of structural conformation changes. The experimental data showed no product formation. This observation prompted the notion that a proton withdrawing effect plays a role in the catalytic sequence. This possibility is missing in both mutations (D110A/N). The deprotonation is based on the low pKa-value ($pK_{a\text{-carboxylic acid}} \sim 4.6$) of the carboxylic acid and abstracts the hydrogen of the neighboring amino acid as in the case of Tyr 121. In the mutant D110N, the functional group was exchanged against a weak base (such as asparagine $pK_{a\text{-amide}} \sim 15$) which did not show a deprotonation effect under experimental conditions (pH 7.4). As clearly shown, the carboxylate has a base effect (Figure 34). It should also be noted that the diphosphate moiety can also act as proton acceptor due to the acidic function.^[111] As expected for the proposed mechanism, site directed mutations of Tyr 121 to phenylalanine lacks the hydroxy

group and leads to inactive enzyme like the mutations of D110A or D110N (no proton acceptor effect). Less activity could be observed for the Y121W mutant which can be explained by the weak base function of the secondary amine in the indole ring. The nitrogen acts also as a nucleophile via deprotonation or as assistance to form a charged H-bond.^[124] However, the allyl residue of GSPP is sandwiched between the prenyl acceptor (1,6-DHN) and π -ring system achieved by electrostatic interactions with three Tyr residues phenolic ring (Figure 32). This interaction triggers the ionization step, stabilize the carbocation intermediate via π -cation and/or deprotonates hydroxide interactions and further shields the activated intermediates against water molecules. Asp 110 and Tyr 121 presumably function as key acid–base residues due to their appropriate position in the active site. The activation of the aromatic ring of the substrate may occur by the amino acids Ser 51, Gln 295 and Tyr 288 whereas typical “activators” like Asp or Glu are missing in the area surrounding the aromatic substrate 1,6-DHN (Figure 35). This may explain the poor activity of NphB among PTs. Of particular relevance to the V49E mutation and catalytic cascade is the mechanism proposed for FgaPT2. It invokes an S_N2 -like attack in which Glu89 and Lys 174 act as key acid–base residues. In case of FgaPT2, the glutamate serves as a nucleophile and is likely to assist the deprotonation of the NH of the aromatic substrate (in NphB, this key role belongs to the mutated Glu 49). The lysine is positioned to play the role of a weak base (in the NphB it is the hydroxy-group of the tyrosine) to abstracted the remaining proton in the final step (Figure 34).

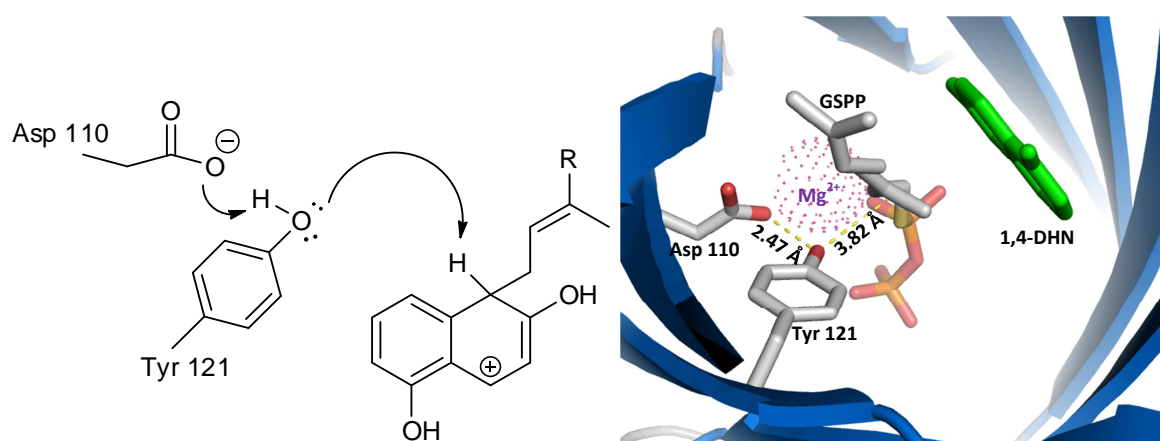


Figure 34. A S_N2 - or Friedel-Crafts-alkylation-like reaction mechanism.^[92] (Left) Presentation of the catalytic sequence in NphB with the putative roles of Asp 110 and Tyr 121. (Right) The position of the amino acids in the active site. Tyr 121 appears to be in the perfect place to deprotonate the σ -complex.

3.5.6. Mutations with different regio-specificity

Herein, 32 amino acids were mutated and the prenylation pattern of 1,6-DHN was studied to further illustrate the influence on the regio-specificity. The mutants can be classified according to the significant change in the product pattern compared to the WT enzyme and they are highlighted in this chapter (only enzymes with a remaining activity of over 5% are considered).

The first group includes mutations with not significantly altered product formation compared to the WT enzyme which means a product distribution of approximately 3:1:7 of the three products 2-, 4-, and 5-geranyl-1,6-DHN. This is the major group with V47A, F213L, S124A, V294A or Q295A. It is remarkable that all variants consist of an aliphatic side chain and are mainly located on the entrance of the binding pocket.

The second group consists of mutants with only one product (M162W and S64R) or two products whereby the by-product is formed in less than 5% yield (Y121W, M162F). In common, all these exchanges are made in the GPP binding area and are close to the first double bond of the prenyl residue (distances are between 3.3 – 3.7 Å). Furthermore, the exchanged amino acids consist of a more bulky side-chain than the previous ones. This means that the size of the binding pocket is reduced and that the allylic side-chain is more fixed. A result of this fixation could be the lower residual activity of 8-25%.

The third group includes a significant pattern change leading to a product distribution of approximately 1:1:1 of the three products (V49E, F213V, Y216A and Y288E). Y288E and V49E are located on neighboring β -sheets and seem to coordinate or activate the ring system by their carboxylate. For V49E, activation of the 6-hydroxy-group from 1,6-DHN is postulated (Figure 33). The exchange of a phenol side chain against a carboxylate may result into an increased polarity which could alter the coordination of the aromatic substrate in the binding pocket. The aromatic amino acids Phe 213 and Try 216 belong to another β -sheet and it seems likely that they interact with the hydrophobic part of the aromatic substrate. The evidence for this hypothesis could be that Y216E showed no activity. For all four mutants, the significant shift of the prenylation position from C-5 to C-4 of the aromatic core indicates an altered positioning of the ring substrate in the active site. A crystal structure

would be required to proof these conformational changes of the prenyl acceptor. However, the summary of the turnover numbers and the product ratio are presented in Figure 29.

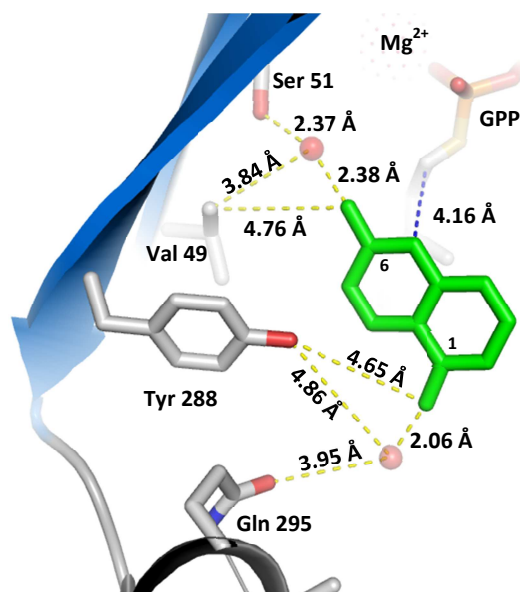


Figure 35. H-Bond formation with the aromatic substrate and the surrounded residues. In green 1,6-DHN is shown, the blue dashed line indicates the distance to the second substrate GPP, and red the corresponding water molecules.

3.6. Conclusion and proposed catalytic mechanism based on the mutation-results

The reactions catalyzed by PTases are often compared with the chemical Friedel-Crafts-alkylation of nucleophilic aromatic systems such as flavonoids, indoles, naphthalenes, or phenylpropanoids (Figure 36). Here, a more S_N2-like catalytic mechanism is proposed based on the site-directed mutation studies. The overall structure of NphB contains eight β-sheets (Figure 15) surround the catalytic center. Further, it contains the SxxDxxDxxK – motif to bind the required Mg²⁺-ion for its enzymatic activity (Figure 25) and the “three tyrosine” motif (Tyr 121, 175 and 216 shown in Figure 32). The cap over the active center is shielded by α-helix/loop regions containing the FS motif (Figure 28). In the first step, the prenyl diphosphate is captured by the FS-motif and accommodates through a conserved cluster of hydrophilic residues into the cave. To date, it is not confirmed if the Mg²⁺-ion binds first in the PTase followed by GPP or if the Mg²⁺ complexes GPP are formed outside the enzyme, before entering the central cavity. The entrance might be formed by the residues Val294, Gln295, Leu298 or Met106. In fact, the Mg²⁺-ion is recognized by the Asp-rich motif and the

diphosphate whereby the amino acids of the SxxDxxDxxK – motif are arranged among the four β -sheet (Figure 25). The binding of Mg^{2+} is assumed to trigger a conformational structure-change. One strong evidence for this hypothesis could be the failure of NphB crystallization without the ion.^{[92][94]} However, in the next step, the aromatic substrate seem to bind and to induce local changes in the surrounded amino acid residues like Ser 51, Aps 110, Tyr 216, Phe 213, Val 271 and Leu 298. Under the influence of the amino acids Asp 110 and Tyr 121, the diphosphate is cleaved (explained in chapter 3.5.5) and an electrophilic enzyme–stabilized carbocation is generated. The residues of Tyr 121, 175 and 216 are close to C1 of the GSPP. Therefore, they are candidates to shield water molecules and to stabilize the reactive intermediate. Of particular relevance is the mechanistic study of FgaPT2 which contains the responsible tyrosine phenols in the position and therefore provides a strong support for this mechanism-theory (Figure 32). In this way, NphB holds the geranyl group in a position that the C-1 allylic carbon reside directly above the C-2, C-4 or C-5 carbons of the naphthalene ring. In the same moment, the aromatic hydroxyl group is deprotonated by the weak base Ser 51 or V49E and subsequently, the electrophile attacks the nucleophilic ring system and forms a Wheland-intermediate (Figure 33). Mutated residues involved in this cascade generate a dramatic decrease of activity up to non-activity as seen for D110A, Y121F, S51A or F213A. In the final step, the product is neutralized and released. After the reaction, the enzyme releases the product as well as the cleaved diphosphate as Mg^{2+} -complex. The cycle starts again (Figure 36).

Regarding the Friedel Crafts alkylation-like reaction, this catalytic mechanism was firstly proposed for all members of the PTases and described initially for UbiA.^{[101][102][93][103]} UbiA also belongs to the aromatic PTases but shares no sequence similarity with soluble aromatic PTases like NphB or FgaPT2. Instead, it consists of nine transmembrane α -helixes and might be evolutionarily related to trans-PTases (tPTases). tPTases are built up of α -helixes (Figure 3) and catalyze the elongation of isoprenyl chains in the stereochemical *trans*-formation (see chapter 1.3.).^[125] As it is typical for tPTases, the Mg^{2+} ions seems to trigger the cleavage of the diphosphate group from the GPP substrate and generates the carbocation which reacts with the *ortho*-position of the phenolic substrate.^{[111][125]} This substrate specificity and selectivity could be explained by a S_N1 -like Friedel-Crafts mechanism.^{[102][126]}

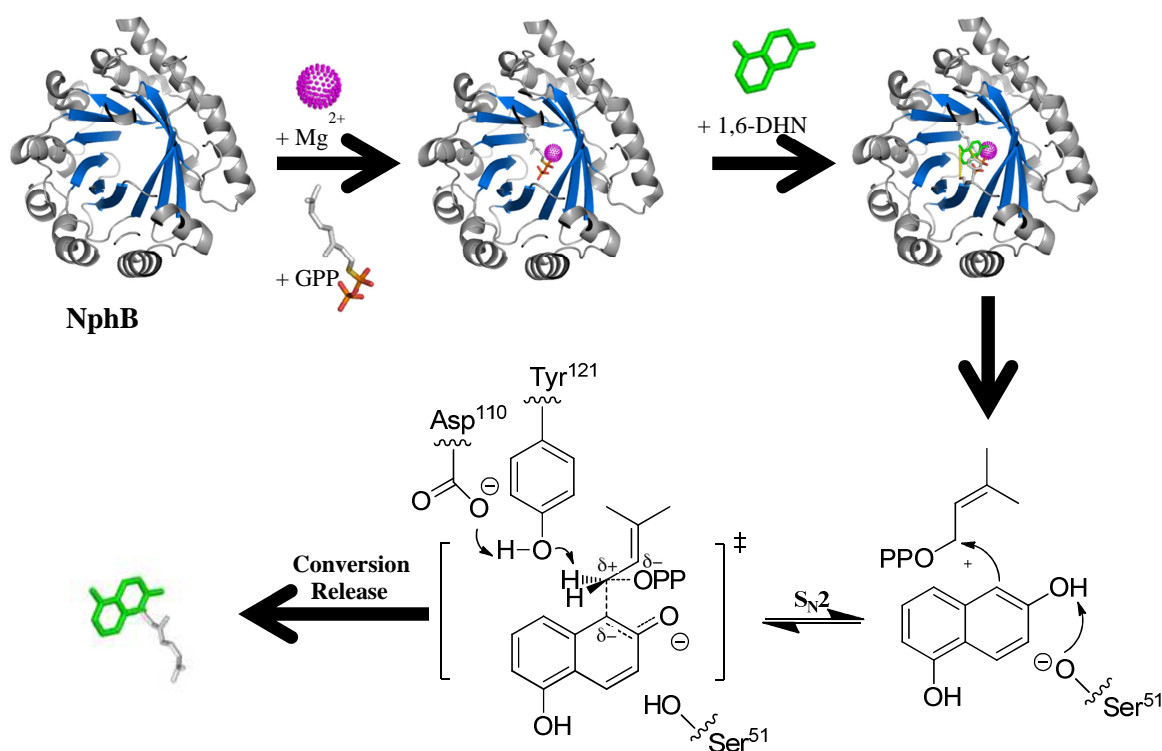


Figure 36. Proposed biocatalytic geranylation of 1,6-DHN catalyzed by the aromatic PTase NphB. 1,6 DHN is colored in green and the diphasphate motif is held in orange (phosphate)/light red (oxygen); the allylic carbons are grey. Mg²⁺-ion (pink spherical arranged dots) and blue represents the β -sheets.

It could be shown in chapter 3 that mutations of NphB lower the enzymatic activity if they are located in the active site or in the substrate binding site. Only two mutations induce an increased activity. One of them was thought to increase the cap size in the cavity center (V294A) and the other one was supposed to be involved in the activation of the aromatic substrate (V49E). The mutations of the soluble PTase reveal a likely more S_N2-like catalytic mechanism that might be commonly applicable to other soluble PTase with this structural characteristic. This study may serve as framework to understand other PTases and to use NphB in the future for rational design in chemoenzymatic synthesis of new aromatic compounds in a more “green” chemistry.

The next chapter presents the use of the gained products. Chapter 4.1. demonstrates the attempts to cyclize the geranylated bis-aromatics to create new tricyclic compounds and chapter 4.2. points out the advantage of prenylated compounds in plant protection against fungi.

4.0. Applications of prenylated compounds

4.1. Attempt to cyclize geranylated 1,6-DHN with THCA-synthase

4.1.1. Introduction of THCA-synthases

Among the over 60 cannabinoids which are found in *Cannabis sativa*, tetrahydrocannabinol (THC) is a well-known psychoactive cannabinoid.^[127] Its pharmacological properties are used in medicine to treat pain or as additive in the pain therapy and as suppressor of spasticity associated in multiple sclerosis patients.^[128] Thus, the demand of THC has increased. Currently, the drug is legalized for private consumption in parts of the US, which promotes its use as an alternative medicine. Chemically, the synthesis of THC is quite difficult due to the two chiral centers in position 3 and 4 of Δ^1 -THC acid (THCA).^[129]

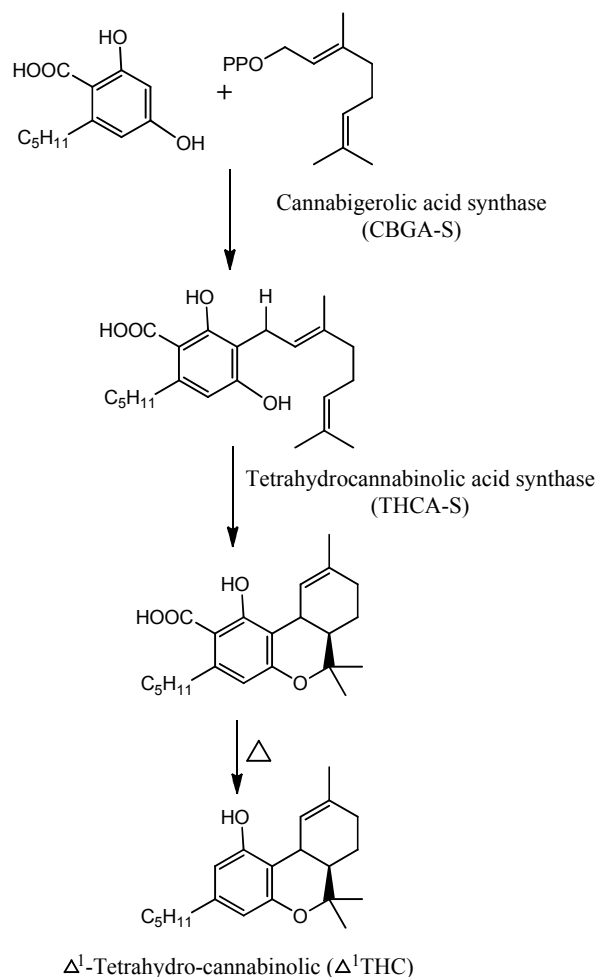


Figure 37. Biosynthetic pathway of Δ^1 -tetrahydrocannabinolic starts with cannabigerolic acid (CBGA) and geranyl diphosphate (GPP). The decarboxylation is a non-enzymatic reaction during the storage or induced by heat.

In Germany, synthetic cannabinoids are available as prescription drugs under the name Marinol® (dronabinol). The extraction out of fresh *Cannabis sativa* plant material is not easy due to the low level of the pharmacological relevant compounds.^{[130][131]} Thus, the discovery of the biosynthetic pathway of THC has attracted attention particular for the isolation of the involved enzymes and their optimization. Figure 37 illustrates the pathway starting with cannabigerolic acid (CBGA) to the final product Δ^1 -THC. The conversion of CBGA into THCA is catalyzed by THCA-synthase (THCA-S). This cyclase belongs to the family of the oxidoreductases containing a flavin binding site and the characteristic isoprene moiety. In the presence of flavin adenine dinucleotide (FAD), the THCA-S synthesizes the CBGA to THCA (Figure 38).^{[131][132]}

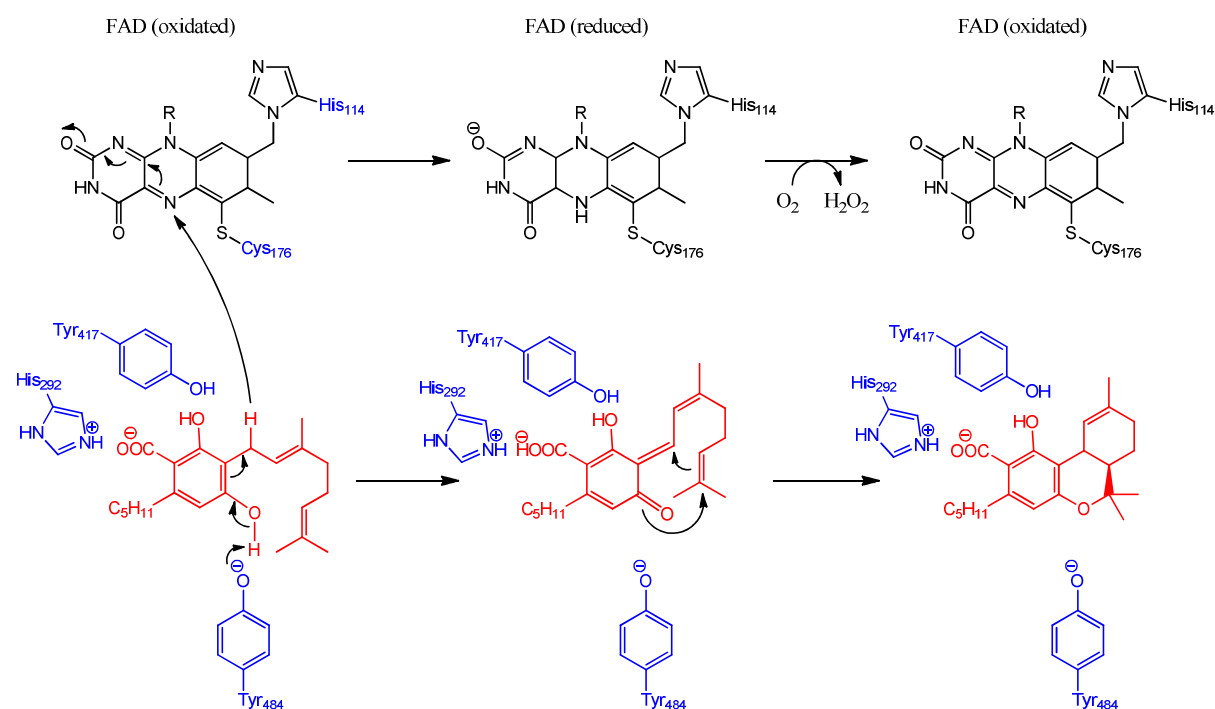


Figure 38. Proposed catalytic cascade of THCA synthesis beginning with CBGA to THCA. FAD is colored in black, substrates in red and the enzymatic involved key amino acids in blue. Figure modified according to Yoshinari Shoyama et. al.^[132]

The enzyme structure was elucidated by X-ray^[127] and site-directed mutations suggested a key role of the amino acids His 292, Tyr 417 and Tyr 484 (Figure 38) in the catalytic cascade.^[132]

4.1.2. Aim of the cyclisation attempt

Nature presents a diversity of cyclic compounds like the vitamin E complex with tocopherol and tocotrienol,^[133] Δ^1 -tetrahydrocannabinolic^[132] or ergotamine.^{[134][135]} Interestingly, the products often exhibit a different spectrum of efficacy than the educts. Chemical cyclisation reactions are often far more challenging than expected. Therefore, enzymes of suitable selectivity and reactivity might be a tool for natural product chemists.

To date, no alternative substrates were tested for acceptance by THCA-S. The aim was to screen a selection of geranylated products mediated by NphB (Chapter 3) for their ability to cyclize new products, to understand better the property of the THCA-product spectrum and the catalytic center which could serve as starting point for potentially manipulate.

4.1.3. Results and discussion

4.1.3.1. Selection of the substrates

Possible candidates to mimic the cannabigerolic acid should fulfill the following three requirements:

1. contain a geranyl moiety
2. presence of an hydroxyl group in *ortho*-position of the geranyl residue for the cyclization
3. presence of an aromatic ring system to enhance the affinity to the binding pocket of the THCA-synthase.

With these three requirements in mind, three compounds were selected for the first approach (Figure 39).

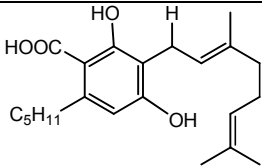
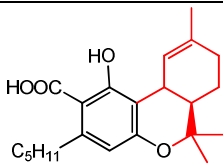
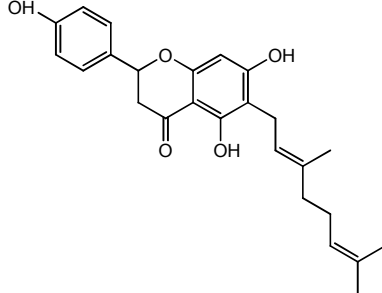
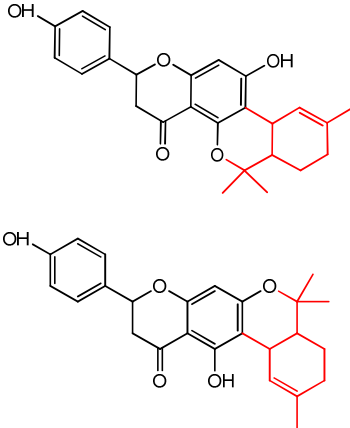
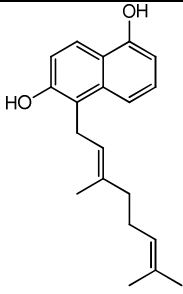
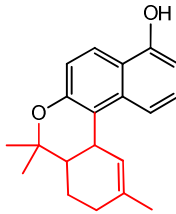
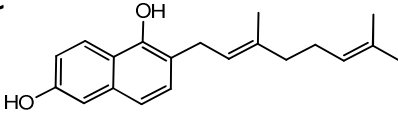
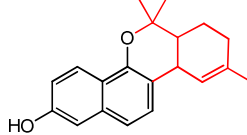
| Substrate | Possible product |
|---|--|
| <p>Natural substrate</p>  | <p>Natural product</p>  |
| <p>A</p>  |  |
| <p>B</p>  |  |
| <p>C</p>  |  |

Figure 39. Possible non-natural substrates for THCAS and their assumed products: (A) 6-geranyl naringenin, (B) 2-geranyl-1,6-DHN and (C) 5-geranyl 1,6-DHN.

4.1.3.2. Results of the LC-MC analyzes

The enzymatic conversion of CBGA to THCA was confirmed using the described assay condition with an activity of $5224 \text{ pkat ml}^{-1}$. The natural substrate CBGA was already converted to approximately 66% THCA after 10 min (data not shown). For the alternative substrates 6-geranyl-naringenin, 2-geranyl-1,6-DHN and 5-geranyl-1,6-DHN an incubation time of 60 min was selected. To avoid non-enzymatic product formation or the appearance of a non-expected compound with the desired mass, controls were performed. As negative control, the substrate was incubated with the assay buffer in the absence of the enzyme as well as the enzyme was incubated with 1% (v/v) DMSO, respectively. Unfortunately, no

product formation for all three substrates was observed. The HPLC-chromatogram shows the UV/Vis trace on the y-axis and the time on the x-axis (Figure 40). Furthermore, the expected molecular mass of the possible cyclized product was recorded. The negative control and the experiment were compared for all three possible substrates. The internal standards were used to examine the retention time (R_t) and the corresponding MS-spectra (latter ones are not shown).

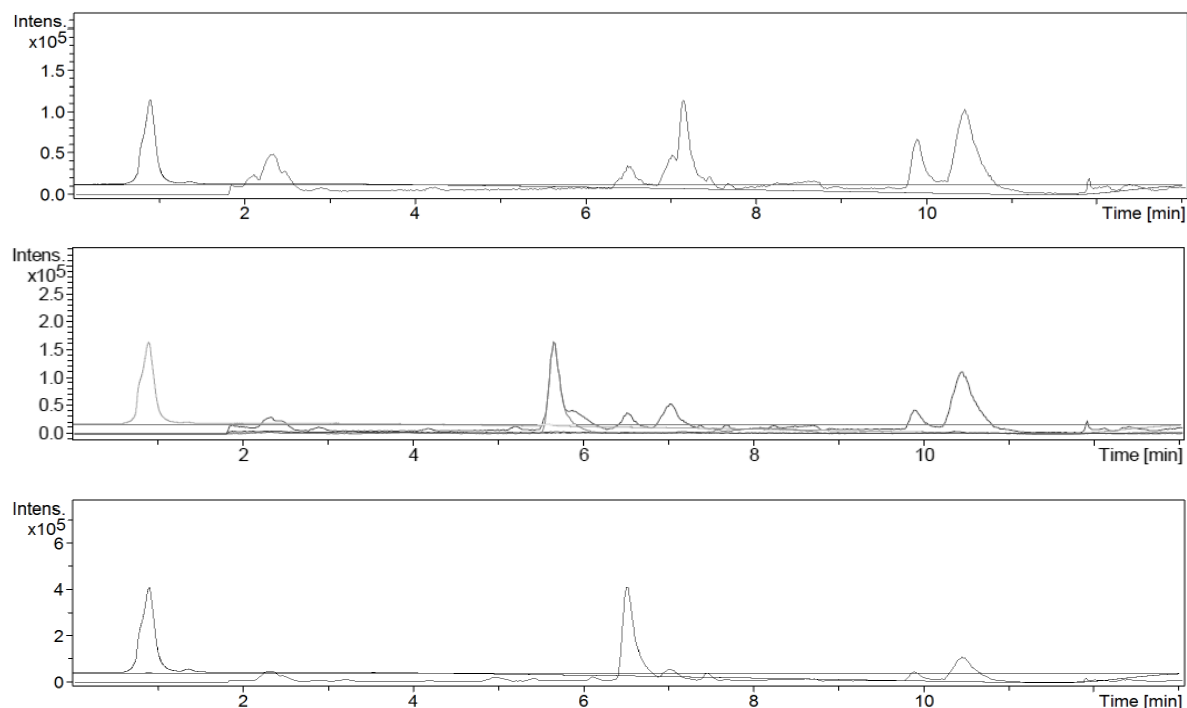


Figure 40. HPLC chromatograph of the enzyme-conversion. Assay with (A) 2-geranyl-1,6-dihydroxynaphthalene and THCA-synthase ($R_{t-Educt} = 7.1$ min); (B) 5-geranyl-1,6-dihydroxynaphthalene ($R_{t-Educt} = 5.7$ min) and (C) 6-geranyl-naringenin ($R_{t-Educt} = 6.5$ min) in the presences of THCA-synthase. No signals or corresponding m/z of the cyclic product could be observed which lead to the assumption that this product was not formed.

4.1.3.3. Structural explanation for the non-acceptance of the alternative substrates

Regarding the THCA-synthase binding pocket for the aromatic substrate, the pre-docking showed the acceptance of 2-geranyl-1,6-DHN (Figure 41). However, the experimental data could not confirm this hypothesis. One explanation could be the lower polarity of the naphthalene derivatives and the missing second hydroxyl group to form the catechol moiety in comparison to CBGA. This hydroxyl group might serve as activator. Mutation experiments exchanging the Tyr 417 and Tyr 484 against alanine show an decrease in activity of 58% and 100% relative to the wild-type enzyme, respectively.^[132] Also the His 292 binds tightly the

carboxylic group and seems to fix the substrate in the right coordination.^[132] Even the substrate cannabigerol (CBGA without carboxyl group) which fulfills all structural requirements did not react. This finding confirmed the importance of the carboxylate.^[136] In case of the DHN-derivatives, the carboxylate is missing. Furthermore, the second aromatic ring enhanced the lipophilicity and might also excellently mimic the “*new forming ring*”. These assumptions may explain that no cyclisation occurred. In case of the 6-geranylated-naringenin, this substrate is speculated to be too bulky and too inflexible to fit into the binding pocket.

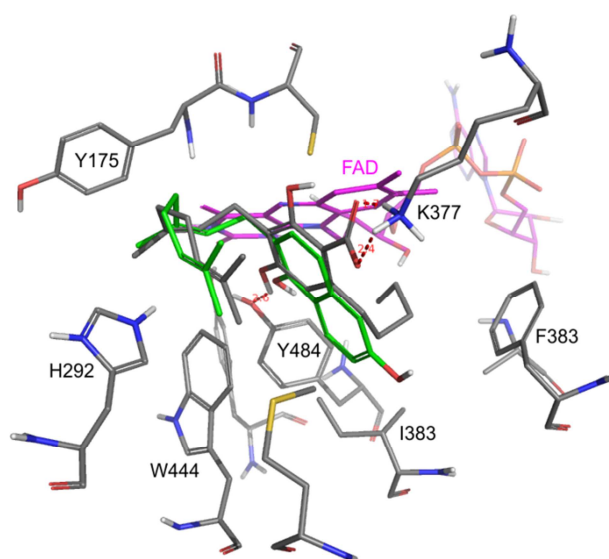


Figure 41. View into the active center of THCA Synthase. The natural substrate CBGA (grey) and the proposed alternative substrate 2-geranyl-1,6-DHN (green) are docked in the active center with the co-substrate FAD (violet). The docking was performed by PD Dr. Wolfgang Brandt with MOE (2014).

4.1.4. Conclusion and future work

Herein, the enzyme THCA-S was tested with three non-natural substrates: 6-geranyl-naringenin, 2-geranyl-1,6-DHN and 5-geranyl-1,6-DHN (method chapter 7.3). Unfortunately, no desired product was formed. The enzyme seems to be highly selective for the natural substrate and it could be interesting to study why this is the case. This work could serve as a starting point to elucidate the binding pocket and to observe possible new structures with novel bi-cyclic structures containing oxygen or even other heteroatoms in one or several aromatic rings. This enzyme could be part in a multi-step-enzyme assay to (re)build complex natural compounds like ergotamine or naphterpin.

4.2. Anti-fungal effects of aromatic compounds and their prenylated analogues

Annotation: In the field of agriculture, all data are represented in [$\mu\text{g ml}^{-1}$] which is different to the common unit [μM] used in molecular biology and pharmaceutical publications. To compare the values with literature, all units are given in [$\mu\text{g ml}^{-1}$].

4.2.1. Introduction

Phytopathogenic fungi and oomycetes are two types of major parasitic organisms inducing serious diseases such as septoria leaf blotch^[137] or “potato blight”^[138] and yield losses in crops.^[139] In general, infections on plants are treated with synthetic fungicides such as Pyraclostrobin or Captan.^[140] Currently, the synthetic fungicides are efficient and widely spread. Although, these substances started to show a decrease in inhibition activity and increase in resistance or environmental problems.^{[141][142]}

Prenylated compounds are known to exhibit enhanced effects, e.g. cytotoxins^[143] or antimicrobials^[144] or on pharmacological interesting targets like prostaglandin E2 synthesis^[145] or cholinesterases.^{[146][147]} To evaluate the antifungal activity of the geranylated diaromatic compounds, 1,5-DHN (**1**) and 5-geranyl-1,6-DHN (**2**) (Figure 20) were tested on fungi and oomycete organisms.

Firstly, bioactivity assays were performed using the three model organisms: (I) *P. infestans* (oomycete) that causes the potato disease known as “late blight” or “potato blight”,^[138] (II) *B. cinerea* (fungi) which most notable hosts are the wine grapes^[148] and (III) *S. tritici* (fungi) which is a wheat plant pathogen and responsible for the septoria leaf blotch.^[137] The geranylated substituted naphthyl compound inhibits the growth of all model organisms. For the phytopathogenic fungus *B. cinerea* and *S. tritici*, only the presence of the prenyl moiety was relevant for an active compound. The oomycete ambassador *P. infestans* were inhibited by the **1** and **2** in the same way.

4.2.2. Results and discussion

To evaluate the antifungal activity of **1** and **2**, the growth of the pathogens *B. cinerea*, *S. tritici* and *P. infestans* were determined by using a growth inhibition assay. The results are

expressed as percentage of inhibition which was measured 5-7 days after inoculation of the growth. The ratio was calculated at $OD_{405\text{ nm}}$ in the absence and presence of the substances. Furthermore, the geranylated bicyclic aromatic nucleus was compared to the precursor **1** to show the effect of the attached geranyl residue. At an initial screening concentration of $42\ \mu\text{g ml}^{-1}$ among these pathogens, the fungi were sensitive to the **2** with a growth inhibition for *S. tritici* and *B. cinerea*. Instead, the compounds **1** and **2** showed strong inhibition activity against *P. infestans* of 98.4 ± 3.6 and $99.6 \pm 1.0\%$, respectively (summarized in Figure 42).

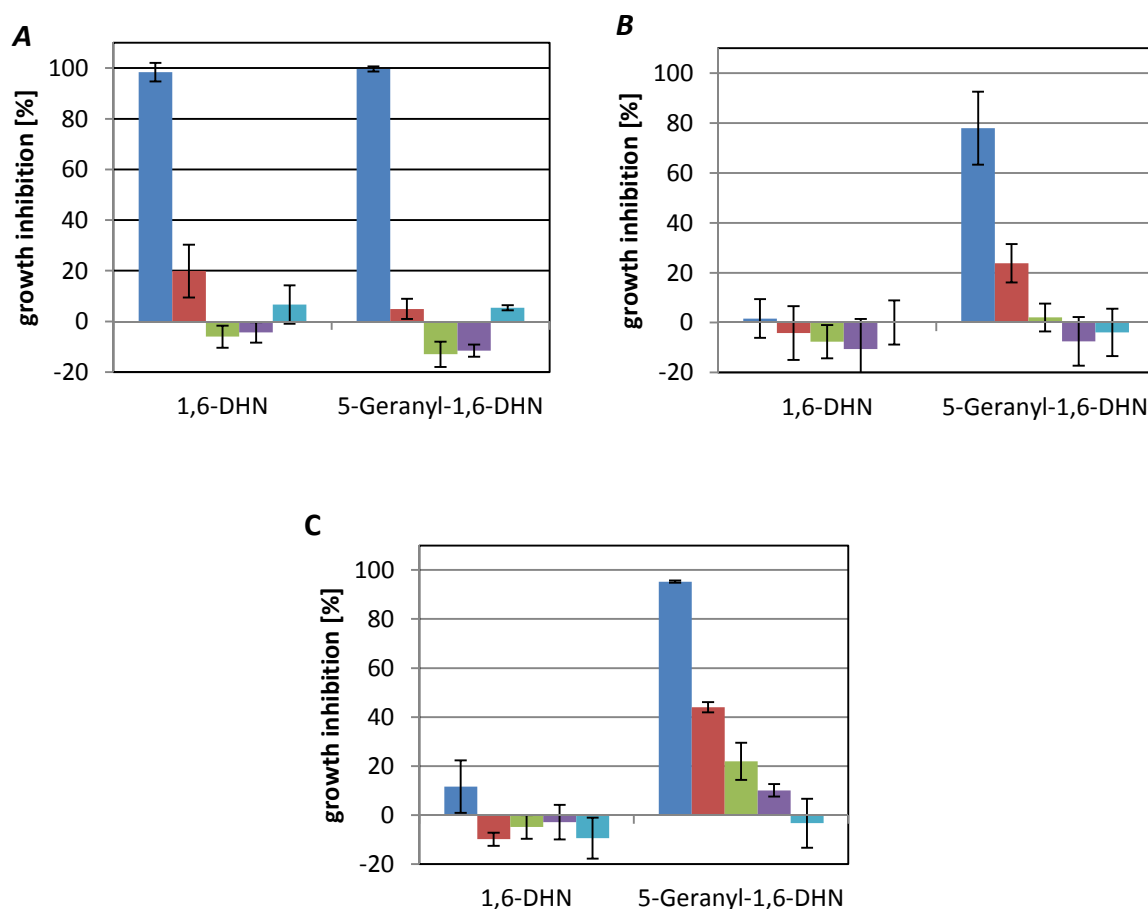


Figure 42. Growth inhibition action on fungi. (A) *Phytophthora infestans* (B) *Septoria tritici* (C) *Botrytis cinerea* were measured in the presences of 42 (blue), 14 (red), 4.7 (green), 1.6 (purple), and $0.52\ \mu\text{g ml}^{-1}$ (light blue) of 1,6-DHN (left) and 5-geranyl-1,6-DHN (right). DMSO served as control and as positive control Pyraclostrobin (data not shown). Furthermore, every value was corrected with the negative control and the difference was represented in [%].

The data indicate that the antifungal activity strongly depends on the geranyl moiety. Thus, the prenyl-moiety attached to the aromatic substrate increases the growth inhibition of *S. tritici* and *B. cinerea* at a concentration of $42\ \mu\text{g ml}^{-1}$. The exact mechanism by which the higher prenylated 1,6-DHN exert antimicrobial activity is unknown. One explanation could be

the composition of the cell wall. The cell walls of oomycetes are generally composed of cellulose rather than chitin.^[149] In contrast, fungal cell walls mainly contain chitin and glucans.^[150] Based on observations of other authors, many fungicides utilize the cell membrane to inhibit the growth by altering their permeability.^[141] One example is boron which exhibited antifungal activity by affecting the cell membrane.^[151] A more speculative explanation was given by Gong *et al.* who assumed that the toxicity is correlated by blockage of the respiratory pathway.^[152] This has been demonstrated for bacterial enzymes like UbiA or MenA (see chapter 6) and could explain why the geranyl chain is required for inhibition. These results are the interference with the growth of the pathogens *B. cinerea*, *S. tritici* and *P. infestans*. Although, this preliminary study can still be seen as a test to illustrate the consequences of a prenyl moiety on a bioactive substance demonstrated on the growth of fungus.

In summary, the present study focused on geranylated diaromatic compounds and their growth inhibition effect on the pathogens *B. cinerea*, *S. tritici* and *P. infestans*. The prenylated substance was compared to the precursor 1,6-DHN to show the effect of the attached geranyl residue (tested according to method described in chapter 7.4.). Among these pathogens, the fungi were sensitive to the 5-geranylated-1,6-DHN with a growth inhibition of 77.9 ± 14.7 % for *S. tritici* and 95.2 ± 0.4 % against *B. cinerea* at $42 \mu\text{g ml}^{-1}$ but not to the precursor 1,6-DHN. Instead, the geranylated and non-geranylated substances showed inhibitory activity against *P. infestans* of 98.4 ± 3.6 and 99.6 ± 1.0 %, respectively (Figure 42).

5. Development and validation of the quantitative NMR method without internal standards

5.1.1. Abstract

The aim of this study was to measure the exact amount of prenylated 1,6-DHN without using a balance. This was required because of the small available amount and the exact weight for the test against the phytopathogenic fungus *B. cinerea* and *S. tritici* and the oomycete *P. infestans*. Furthermore, the method was used to determine the product formation of dihydroxynaphthalenes tested as substrate for THCA-S.

5.1.2. Background and Significance

In 1963, the first study on quantitative NMR (qNMR) was introduced in the field of pharmaceuticals^[153] and since then the scientific publications continued to rise. qNMR has been established as a powerful tool to quantify small amounts of substance present in a sample. The area under the given resonance signals (AUS) is proportional to the amount of nuclei responsible for the given signal. To quantify the areas and to correlate them with the accurate concentration requires additional efforts. In the beginning, the quantitative samples were spiked with an internal standard of known concentration. Examples of compounds were used as quantitative standards i.e. 1,4-dinitrobenzene, maleic acid or dimethyl formamide.^[154] Such an application has been widespread in areas of biology, chemistry, medicine and pharmacy. The accuracy of this approach is very good but it also has drawbacks.^[154] Firstly, the sample is contaminated with an additional substance which induces recovery-steps. Secondly, the preparation requires additional steps i.e. weighting the internal standard for quantification. Thirdly, a number of restrictions concerning the reference compound has to be taken into account. For example the (a) longitudinal relaxation time (T_1) of the internal standard must be known; (b) no chemical interactions with the sample, (c) as well as solubility and stability issues or (d) even the resonance overlap with the signals of the compound of interest have to be considered. These methods might be inapplicable in case of more complex measurement for example in metabolomics studies, quality and quantitative analysis of complex natural samples in the food and flavor industry or even in plants and herbal extraction mixtures.^[155] Therefore, in the recent year, several novel electronic referencing approaches find their way into the accurate and precise

qNMR. Prominent examples are ERETIC (Electronic Referencing to access in vivo Concentrations),^[156] PIG (Pulse Into Gradient), ARTSI (Amplitude-corrected Referencing Through Signal Injection) and QUANTAS (Quantification by Artificial Signal). These qNMR approaches are confined in scope and are inherently error-prone.^{[154][157][158][159]}

An alternative technique is provided by qNMR tools in VnmrJ software (Agilent Technologies, USA), which only uses a 1D spectrum and an external concentration standard to calibrate the method for accurate and precise quantitative measurements.

The direct signal digitization occurs in the receiver path and the calibration can be done using any sample of known concentration. The requirements are a reasonably separated sharply assigned resonances or a group of resonances (“signal” referees later to this term). A single 1D spectrum is then collected using a 90° excitation degree pulse as well as an adjusted spectrum width. Sequentially, the signal is baseline corrected, integrated and correlated with the concentration of the reference signal. This integral once calibrated against an external standard provides a method to accurately determine the unknown sample concentration.

Equation 1. Equation for accurate determination of unknown sample concentration.^[160]

$$m_T = M_T \times \frac{I_T}{I_{St}} \times \frac{x_{St}}{x_T} \times c_{St} \times v_{St} \times \frac{P_{St}}{100}$$

| | |
|----------|--|
| M_T | molecular weight of target compound [g/mol] |
| I_T | relative integral value of ^1H NMR signal of the target compound |
| I_{St} | relative integral value of ^1H NMR signal of the standard compound |
| x_{St} | number of protons belonging to the ^1H NMR signal of the standard compound |
| x_T | number of protons belonging to the ^1H NMR signal of the target compound |
| c_{St} | concentration of standard compound in the solution used for ^1H NMR measurement [mmol l ⁻¹] |
| v_{St} | volume of solution used for ^1H NMR measurement [ml] |
| P_{St} | certified value of the purity of standard compound [%] |

The immediate advantages are the prevented addition of an internal standard. The experiment is less time-consuming and no longer dependent on any relaxation times of the reference signal. The approach is applicable to ^1H and other nuclei. The only two drawbacks

of this approach are the regular calibration of the equipment and the contamination of the samples regarding signals close to the threshold (low signal-to-noise-ratio). In this chapter, quantitative measurements of the geranylated 1,6-DHN products are reported.

5.1.3. Results and discussion

5.1.3.1. T1 measurements

¹H spin-lattice relaxation, T1, is the time that the nucleus needs to equilibrate in the direction of the z-axis. For quantitative experiment, T1 must be determined to setup the correct measurements. One popular method is the inversion-recovery method in which the magnetisation is inverted and the time τ is determined to allow the full relaxation in the direction of the z-axis. T1 was calculated using the aromatic protons of the external standard 1,6-DHN, the time τ at the node (τ_n) reasonably estimated from Figure 43 and the Equation 2.

Equation 2. T1 calculation to correctly setup the quantitative experiment.

$$T1 \approx \tau_n / \ln 2$$

Time τ was measured in steps from 0.1 – 20.0 s and the values were found for the exemplary proton of the aromatic ring T1_{7.0 ppm} was 5.8. Consequently, the repetition time was set at 30 s to ensure the complete relaxation of the aromatic proton.

5.1.3.2. Measuring Conditions

Cookson and Smith^[161] have shown that the optimal signal-to-noise ratio was achieved by a pulse angle of 70-90°. Sequentially, the measuring conditions were: flip angle 90°, spectra width 7183.9 Hz, data points 32k. These parameters were suitable for quantitative analysis and to avoid truncation of the signal. All parameters were optimised for 1,6-DHN as model substrate.

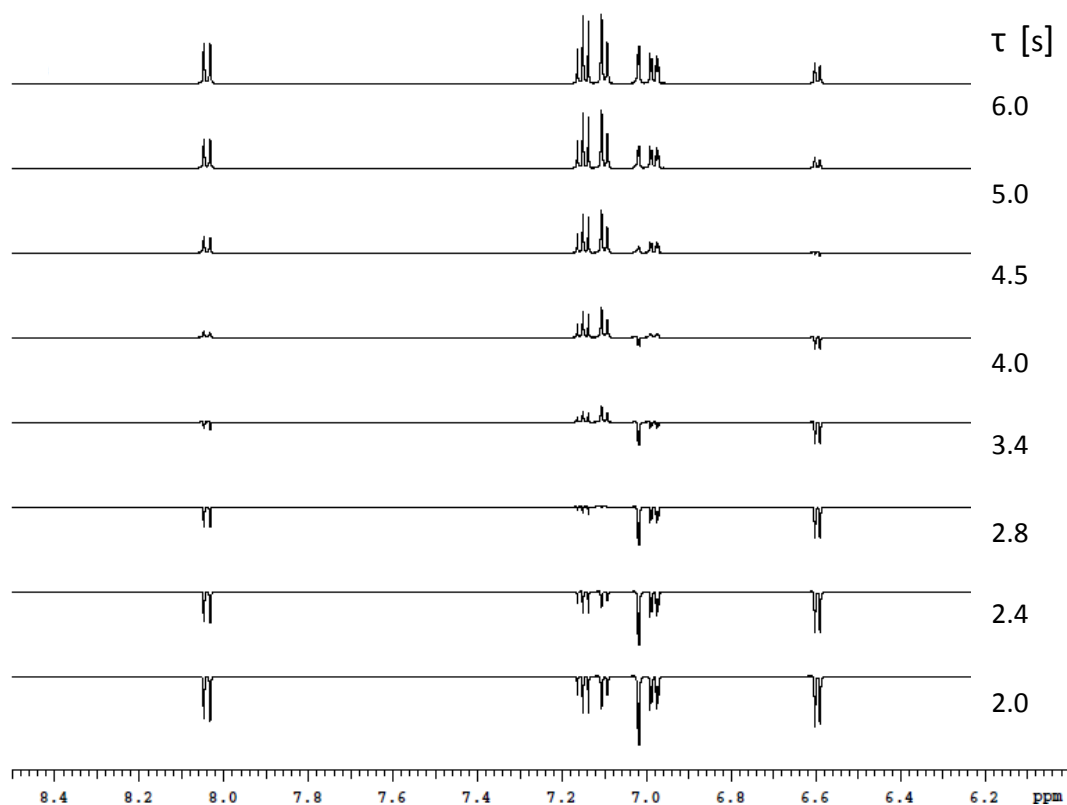


Figure 43. Estimation of T1 of the external standard 1,6-DHN by an inversion recovery

5.1.3.3. Determination of the concentration

Dihydroxynaphthalene derivatives and the concentration of geranylated-1,6-DHN were determined by the “Agilent qNMR tool using a single-point calibration” method using 1,6-DHN as external standard. The calibration of the signal was achieved with 1,6-DHN in the concentration of 0.0, 0.635, 0.865 and 1.212 mg in 660 μ l CD₃OD solution (Figure 44). For accurate and time-independent measurements, the samples were analysed in one concentration (technical replication marked in green diamond) as well as at different time points within 72 hours (value consistent with the technical replication – data not shown). Furthermore, the DHN-derivatives 1,7- and 2,3-DHN with known concentration were analysed. The results clearly demonstrate that 1,7-DHN and 2,3-DHN fit well into the graph. To evaluate and proof the concept, 13.64 mg of 5-geranyl-1,6-DHN were weighed, solved in CD₃OD (stock solution) and three samples out of the stock solution were diluted to be in the range of the calibration curve and were finally measured. The area of the signal was fitted to the calibration curve and the mass was calculated according to Equation 1.

The proof of concept was to compare the balanced mass (13.64 mg) of 5-geranyl-1,6-DHN with the qNMR calculated mass (13.41 mg). With an accuracy of 98.3%, the method reveals to be a quantified procedure.

In literature,^[162] an uncertainty of 0.10-3.0 % is reported for this qNMR method. The quantification limit comes along with the concentration. In the range of 0.0-0.2 mg per 660 μ l of solvent, the signal-to-noise ratio is bad for a reliable integration of the NMR signals which results in a high standard deviation among the triplicates. On the other side, with the increase of the concentration, the T1 decreases^{[156][163]} as well as solubility starts to play a role (particular for geranylated 1,6-DHN which in higher amounts is not fully soluble in methanol).

With reference to the balance, the uncertainty increases with the decrease of the weighted amount. With respect to this standard deviation, the value of 98.3% accuracy is a good value for the quantification of the sample.

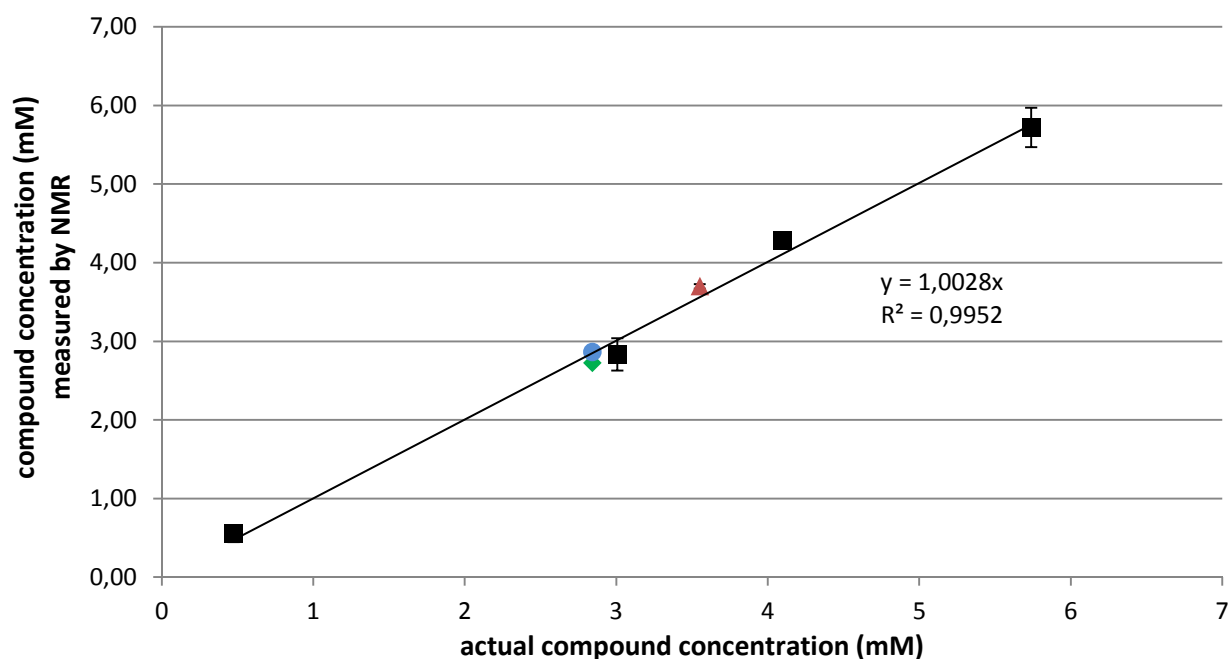


Figure 44. Calibration curve for qNMR using 1,6-DHN as standard (black-squares). The method was validated with the dihydroxynaphthalene analogues 1,7-DHN (± 0.01 mM) and 2,3-DHN (± 0.05 mM) marked as blue-circles and red-triangle, respectively. The technical replicate 1,6-DHN (± 0.01 mM) confirms the accuracy and is coloured as green-diamond.

5.1.4. Conclusion

The demonstrated results of the *“Agilent qNMR tool using a single-point calibration”* – method in case of geranyl-1,6 DHN show an accuracy and precision in the explored concentration range which is better or the same than those obtained under the same conditions by weighing the probes (method chapter 7.5.). This accuracy is achieved without adding additional reference substance and overlap of signals. Furthermore, this method is time-saving due the elimination of the weighing step and might be a useful tool to measure the concentration of geranylated and non-geranylated dihydroxynaphthalenes in one probe without further purification steps.

5.2. Development and validation of an UV/Vis procedure for the quantification of geranylated 1,6-dihydroxy naphthalene catalyzed by NphB

5.2.1. Introduction

A reliable analytical method was required for screening and evaluation of new potential diphosphate mimics which competitive inhibits the NphB-mediated catalyzation of a prenyl residue (geranyl) to an aromatic core (1,6-DHN). To date, several approaches for quantification of product formation have been described; among them are methods such as unselective thin layer chromatography, time-consuming gas chromatography–mass spectrometry (GC–MS) or wide spread usage of HPLC. Here, the first fully validated UV/Vis method is presented for reliable quantification of the geranylated product formation. The poor HPLC approach was overcome by the powerful novel UV/Vis procedure to screen rapidly and routinely the inhibitor with the aim to find a new pharmacophore for NphB based on the diphosphate mimic.

5.2.2. Results and Discussion

5.2.2.1. Separation and detection of 1,6-DHN and geranylated 1,6-DHN by HPLC

An isocratic gradient was used to separate the components (chapter 7.2.3. method part). The three geranyl-1,6-DHN products were isolated from NphB reaction mixture by liquid–liquid extraction in order to obtain pure products and to reduce the risk to contamination the column. A diode array detector-spectrum (DAD-spectrum) was recorded whereas the respective geranylated products resulted in a local maximum at 336 nm (in the range from 320 till 360 nm). Instead, the spectrum of 1,6-DHN showed a local absorption maximum at 332 nm which is a difference of 4 nm. This shift results from the prenylation and can be taken as evidence for product formation (Figure 45). By subtraction of the substrate spectra from the product spectra, the highest amplitude was obtained at the wavelength of 340 nm (Figure 45) whereas the enzymatic conversation reaches the optical density of 1.2 (seen as limit) after 40 min enzyme reaction time. To prolong the experimental time, $\lambda=345$ nm was chosen because of the similar amplitude (Figure 46). Furthermore, a “baseline” was defined by measuring at 600 nm to identify precipitation and micelle formation of the inhibitors

which may occur due to the surfactant-like character. All values are given as difference between the wavelengths:

Equation 3.

$$y = \lambda_{345 \text{ nm}} - \lambda_{600 \text{ nm}}$$

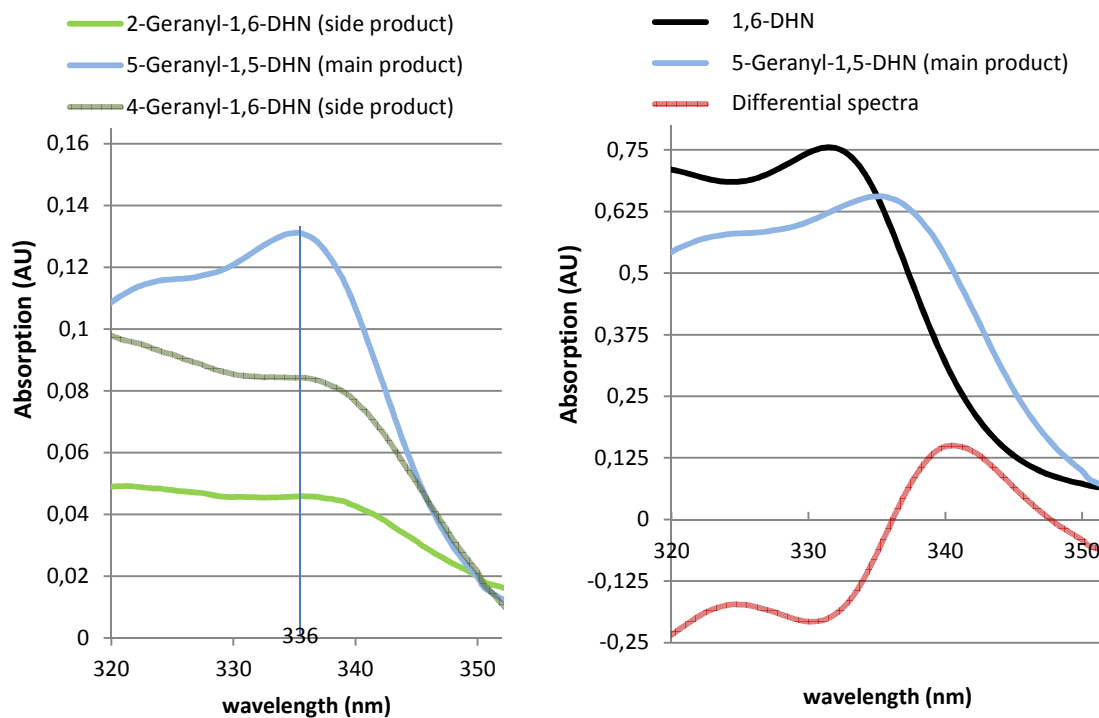


Figure 45. Spectra of the non- and geranylated 1,6-DHNs to illustrate the wavelength shift. (Left) Spectra of the three geranylated 1,6-DHN separated by chromatography and measured by UV/Vis spectrometry. The local maxima of all three geranylated products is at 336 nm (Blue = main product 5-geranyl-1,6-DHN; grey = 4-geranyl-1,6-DHN; green = 2-geranyl-1,6-DHN). **(Right)** Spectra of 1,6-DHN and 5-geranylated-1,6-DHN. UV/Vis spectra shows the local maxima shift of the substrate (1,6-DHN) and the product (exemplarily 5-geranylated 1,6-DHN) (Black = 1,6-DHN; Blue = 5-geranylated-1,6-DHN; red = differential spectra between the geranylated and non-geranylated 1,6-DHN).

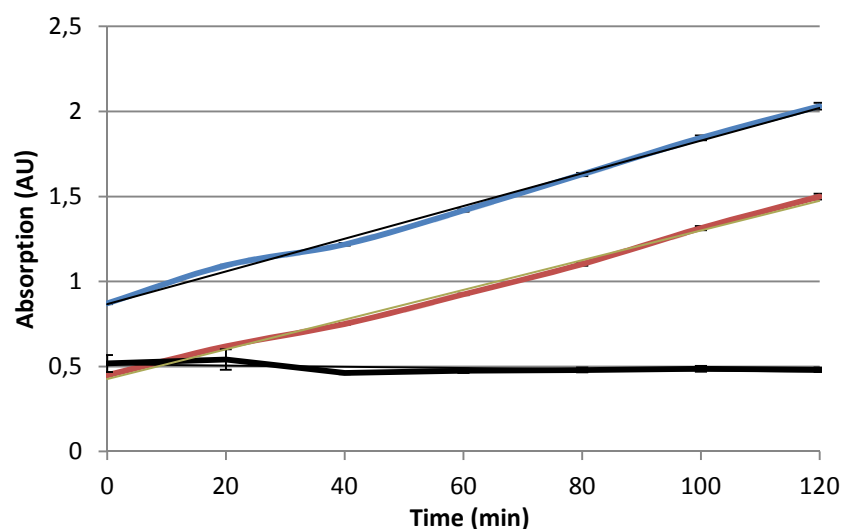


Figure 46. UV/Vis spectra indicate the time dependent product formation of geranylated 1,6-DHN at 340 nm (dark blue) and 345 nm (Bordeaux red). Samples of the enzymatic reaction were incubated for 0-2 h at 28°C, measuring the UV/Vis absorption at 340 nm ($R^2=0.997$) and 345 nm ($R^2=0.996$). The enzyme reaction without GPP is represented in black. No product formation is observed during this time.

5.2.2.2. Method validation

In order to simplify the model and to further validate the method, 5-geranyl-1,6-DHN was chosen as test substance. The reasons for this decision were the highest purity (a quantitative NMR provided the correct mass compared with the 99% pure 1,6-DHN achieved from Sigma Aldrich), and that this prenylated product is the main product with approximately 80% relative conversion to the other products.

Furthermore, all three geranylated products are identical concerning the local maxima at 336 nm and the composition of all three products does not change during the reaction time between 20 and 120 minute (Figure 47). To validate the UV/Vis assay, the product formation was followed by the UV/Vis approach and confirmed by HPLC. Firstly, a calibration curve was recorded by measuring the UV/Vis absorption at 345 nm (and 600 nm) and the same samples were later quantitatively analyzed by HPLC. The total concentration was 5.0 mM of aromatic compound consisting of 5-geranyl-1,6-DHN which represents the three prenylated products and 1,6-DHN. Starting from 0.0 mM to 0.4 mM 5-geranyl-1,6-DHN and the 1,6-DHN concentration dropped down from 5.0 mM to 4.6 mM to achieve the final concentration of 5.0 mM. The calibration curve was at first measured by UV-Vis and then by HPLC. The m-value stands for the absorption change of 1.38 AU per 1 mg product formation

(Supplementary Figure 3). In conclusion, this experiment gives the absorption coefficients different of 1,6-DHN and the product 5-geranyl-1,6-DHN and reflexes the enzymatic activity due to the product formation.

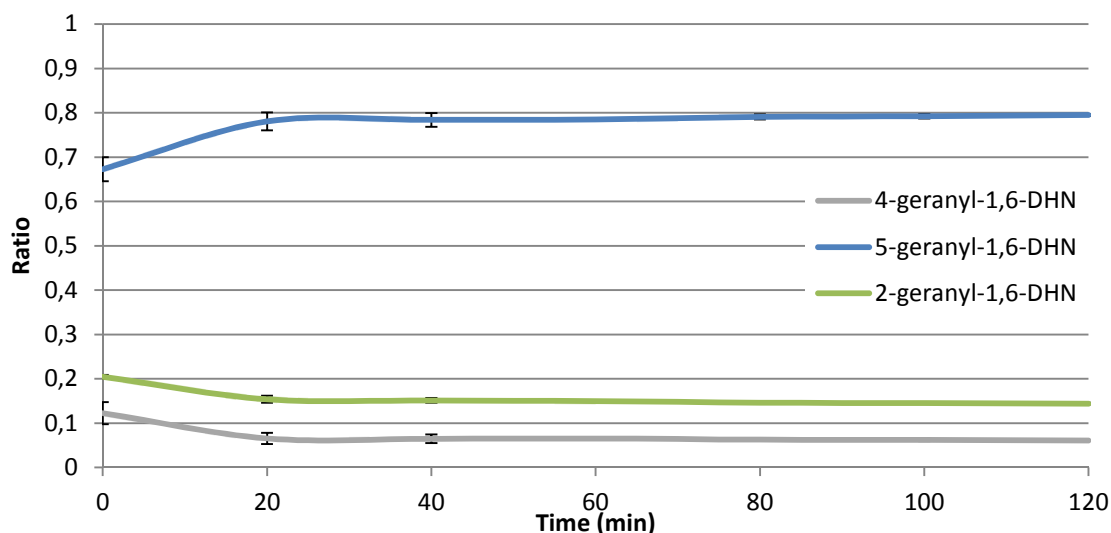


Figure 47. Ratio between the biocatalytic conversions of 1,6-DHN with GPP by NphB. (Blue = 5-geranyl-1,6-DHN; grey = 4-geranyl-1,6-DHN; green = 2-geranyl-1,6-DHN).

For the HPLC measurements, the slope was calculated to be 14.217.000 absorption units under the curve (AUC) and represents 1 mg of the product. Both curves taken together and applied to the enzymatic conversion, a specific activity of 8.60 pKat mg⁻¹ (based on HPLC measurements) and 7.95 pKat mg⁻¹ (based on UV/Vis-measurements) could be obtained.

5.2.2.3. Proof of method

The new method was tested for applicability by analyzing NphB-mediated product formation by seven concentration levels with two replicates. Each value was constructed to evaluate the procedure and to consider a calibration range from 0.0 – 0.5 mg geranylated product. Thus, reliable quantification of low geranylated 1,6-DHN levels was achieved with the aim to identify strong inhibition. Nevertheless, the time dependent enzymatic conversion was analyzed using HPLC and UV/Vis. Then, the activity was calculated according to the calibration curve and both graphs showing the product formations vs. time were plotted in Figure 48. This allows the validation of the new method. Until now, one problem occurs after 120 min which has to be solved before testing the inhibitor. The enzyme preparation shows a white cloud. It is assumed, that the lipophilic product(s) fell out due to the low solubility. This phenomenon could not be prevented even in the presence of different surfactants. To

overcome the problem, the screening time limit was set up to 40 min and a second absorption at 600 nm was included. The difference between the value at $\lambda_{345\text{nm}}$ and $\lambda_{600\text{nm}}$ was calculated for additional assessment in accuracy and precision (Figure 48).

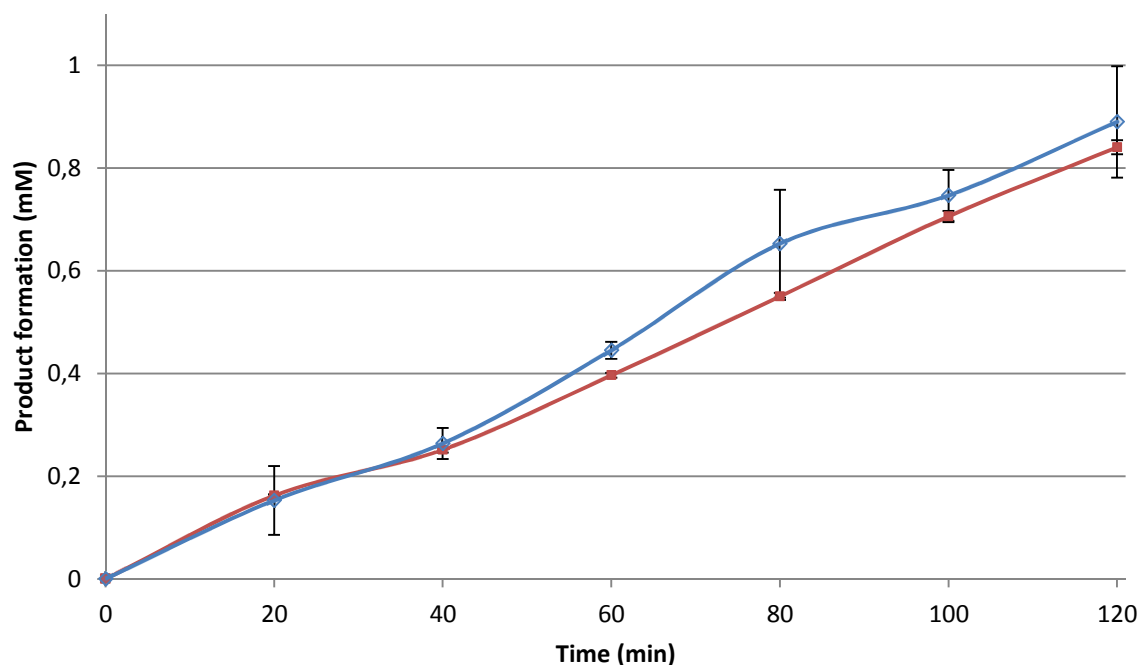


Figure 48. Comparison of enzyme activity using the two different approaches. Samples of the enzymatic reaction were incubated for 2 h and afterwards analyzed by HPLC (blue line; $y = 0.0075$; $R^2=0.99$) and by UV/Vis (red line; $y = 0.0069$; $R^2=0.99$). The specific enzyme activity based on HPLC-data was calculated to be $8.60 \text{ pKat mg}^{-1}$ and based on UV/Vis, $7.95 \text{ pKat mg}^{-1}$ which is an accuracy of 92.6%.

5.2.3. Summary

High throughput measurements of enzyme catalyzed product formation require novel strategies. In the past, one common approach was the reverse phase-HPLC particular in the field of prenylated aromatic products. The advantage of the HPLC method is the easy separation of products and substrate(s). The disadvantages are the time consuming procedure, the cost of the solvents as well as the reproducibility concerning the integration of the peaks. This might be overcome using internal standards (chapter 5.1.). The goal of the present study was the development and validation of an easy, rapid, reproducible and robust quantification method to determine the prenylated product. The poor chromatographic method reported by others could be overcome by fast microtiter-plate-assisted UV/Vis assay that fulfilled all requirements of common validation guidelines. The

slope response was linear within the concentration range of 0.0-1.0 mM ($R^2=0.99$) and the sensitivity of the method could be provided until the optical density reaches 1.2. Its applicability was successfully proven in testing of inhibition (chapter 6), calculating the turnover number for mutants of NphB (chapter 3) and of geranyl diphosphate mimics and analogues (i.e. farnesyl diphosphate, nor-geranyl diphosphate) (chapter 3.4) as well as for different divalent metal ions (chapter 3.5.2).

In summary, the method provides a useful tool for the rapid screening of new geranyl diphosphate mimics, diphosphate analogues.

6. Prenylated (polyoxy)-carboxylates as surrogates of prenyl diphosphates and their potential as prenyltransferase inhibitors

6.1. Abstract

A compound library of 20 diphosphate mimics was synthesized by Dimitar Vasilev^[164] whereby the diphosphate moiety was substituted by various functional groups such as carboxylic acids or esters, hydroxyl group(s) and/or thiol(s) containing a geranyl side chain as well as larger aliphatic side chains (farnesyl) or shorter side chains (dimethylallyl). All compounds were screened *in vitro* against the aromatic prenyltransferases MenA and NphB and compared to UbiA (UbiA – experiments are done by Amina Msonga (PhD-thesis in press)) at 1 mM concentration. The most potent candidates were used for IC₅₀ determination (inhibitory concentration 50 which is the compound dose required to inhibit 50% enzyme activity). The aim of the study was to explore the unique diphosphate binding pocket of the model enzyme, of aromatic prenyltransferases MenA, NphB and of UbiA. The results are discussed regarding the structure-activity relationship of the head-group mimic and chain length of the tail group. In general, all inhibitors with basic farnesyl aliphatic side chain are shown to be better inhibitors than those with shorter hydrophobic aliphatic residue. Furthermore, the head groups containing the monocarboxylic acid/ester and β-hydroxyl group(s) were the most effective ones among the screened compounds.

6.2. Introduction

Nature provides alkylating enzymes that selectively transfer prenyl groups to an aromatic carbon atom in excellent chemo- and regio-selectivity. This enzymatic C-alkylation of aromatic compounds are essential in all organisms for example during the biosynthesis of vitamin K, of the respiratory quinones, or of vitamin E.^{[32][166]} In humans, for instance, the UBIAD1 (aka TERE1) is a prenylation enzyme in the menaquinone-4 biosynthetic pathway. A reasonable assumption is that a single mutation in the enzyme with either decrease or loss of function contributes to an elevated cholesterol level. Sequentially, cholesterol accumulates in the cornea and leads to opacity (Schnyder corneal dystrophy disease).^{[167][168][169]}

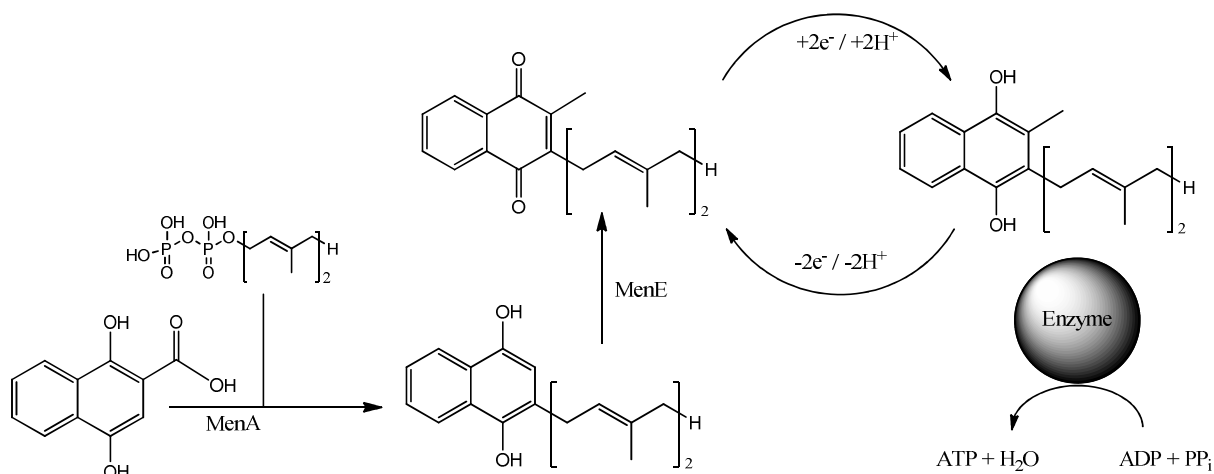


Figure 49. Prenylation of 1,4-Dihydroxy-2-naphthoic acid and geranyl diphosphate catalyzed by MenA to menaquinone and their role in the electron flow system mediate the energy pathway.

Other prenylating enzymes such as the representative UBIAD1 in *E. coli*, UbiA, is required in the prenylation step in the ubiquinone biosynthesis (i.e. CoQ10).^{[170][171]} The prenylated product plays a unique role in a majority of gram-negative organisms where it is essentially required for electron transport chain under aerobic conditions.^[172] In gram-positive bacteria (i.e. *M. tuberculosis*), the prenylation of 1,4-dihydroxy-2-naphthoic acid (menaquinone; prenylating enzyme is named MenA) serves as electron transfer systems in their electron transport systems under anaerobic conditions (Figure 49).^{[173][174]} The function of both products is crucial for generating energy (ATP). Inhibition of these enzymes could therefore lead to cell death. Thus, potential inhibitors may be developed as antibiotics interrupting the respiratory chain. However, *in vivo*, the UbiA transfers geranyl diphosphate to the *meta*-position of 4-hydroxybenzoic acid (PHB).^{[170][171]}

The complex role of the enzyme in the prenylation step makes it an excellent target to develop inhibitors.^[175] Several classes of compounds that inhibit UbiA activity have been discovered in our group (Figure 50).^[176] Among the tested compounds, only candidates bearing a carboxylic acid showed inhibitory activity against UbiA. The β -hydroxyl carboxylic acids showed an IC_{50} value of 0.36 mM and the β -keto carboxylic acids an IC_{50} value of 0.58 mM (Figure 50). Therefore, a number of diphosphate mimics were designed to replace bioisosteric phosphates with carboxylic acids, hydroxyl- or thiol- group(s). Furthermore, all possible candidates for surrogates of geranyl diphosphate should meet the following three

requirements: (1) affinity to prenyl diphosphate transferases, (2) stability under investigated conditions (especially hydrolysis), and (3) simple synthetic preparation.



Figure 50. The most potent inhibitors for the UbiA-transferases. (Left) β -keto carboxylic acids with an IC_{50} value of 0.36 mM and the (right) β -hydroxy carboxylic acids with a IC_{50} value of 0.58 mM.^[176]

To test their potential inhibition, three enzymes among the family of the aromatic prenyltransferases were chosen which catalyze the transfer of a geranyl residue to the aromatic substrate 1,6-DHN (for NphB), PHB (for UbiA) and 1,4-dihydroxy-2-naphthoic acid (for MenA).^{[99][98][75]} The difference between MenA, NphB and UbiA is in the protein structure. MenA and UbiA are found in nature anchored to the cell membrane and contain the common (N/D)Dx(x)D Mg^{2+} -diphosphate binding motif which is involved in the binding of the allylic diphosphate.^{[170][171][177]} They possess a diverse substrate spectrum. Diversely, UbiA attaches a geranyl residue to mono cyclic aromatic ring systems and MenA a geranyl residue to the bicyclic 1,4-dihydroxy-2-naphthoic acid under *in vitro* conditions.^{[178][179]} The genes coding for UbiA and MenA are from *E. coli* and exhibit an 19.2% identity in the sequence alignment. Instead, NphB from *Streptomyces* sp. strain CL190 is a soluble enzyme which requires Mg^{2+} but without Dx(x)D motif.^{[92][107][104]}

In the present chapter, the 20 different diphosphates possessing head-group-mimics such as carboxylic acids/esters, hydroxyl group(s) or thiol(s) and side chains, are presented: dimethylallyl, geranyl or farnesyl are reported. All compounds were tested in a competitive enzyme assay with the model enzymes MenA, NphB and UbiA. For NphB, a new, rapid and robust assay was established to quantify the prenylated product formation and to determine the conversion online by using UV/Vis spectrometry (Chapter 5.2). The enzymes MenA and UbiA were analyzed by an HPLC based approach. All compounds were screened at a 1 mM concentration. For the most potent compounds the IC_{50} value was determined. The methods used here are described in chapter 7.7.

6.3. Results and Discussion

6.3.1. Chemical selection of mimics

All 12 different diphosphates head-group mimics with geranyl as prenyl chain unit are presented in Figure 51. The head-groups **3-5** and **7** were synthesized by Dimitar Vasilev^[164] with different prenyl chains and **3** and **5** were also tested before the protecting step.

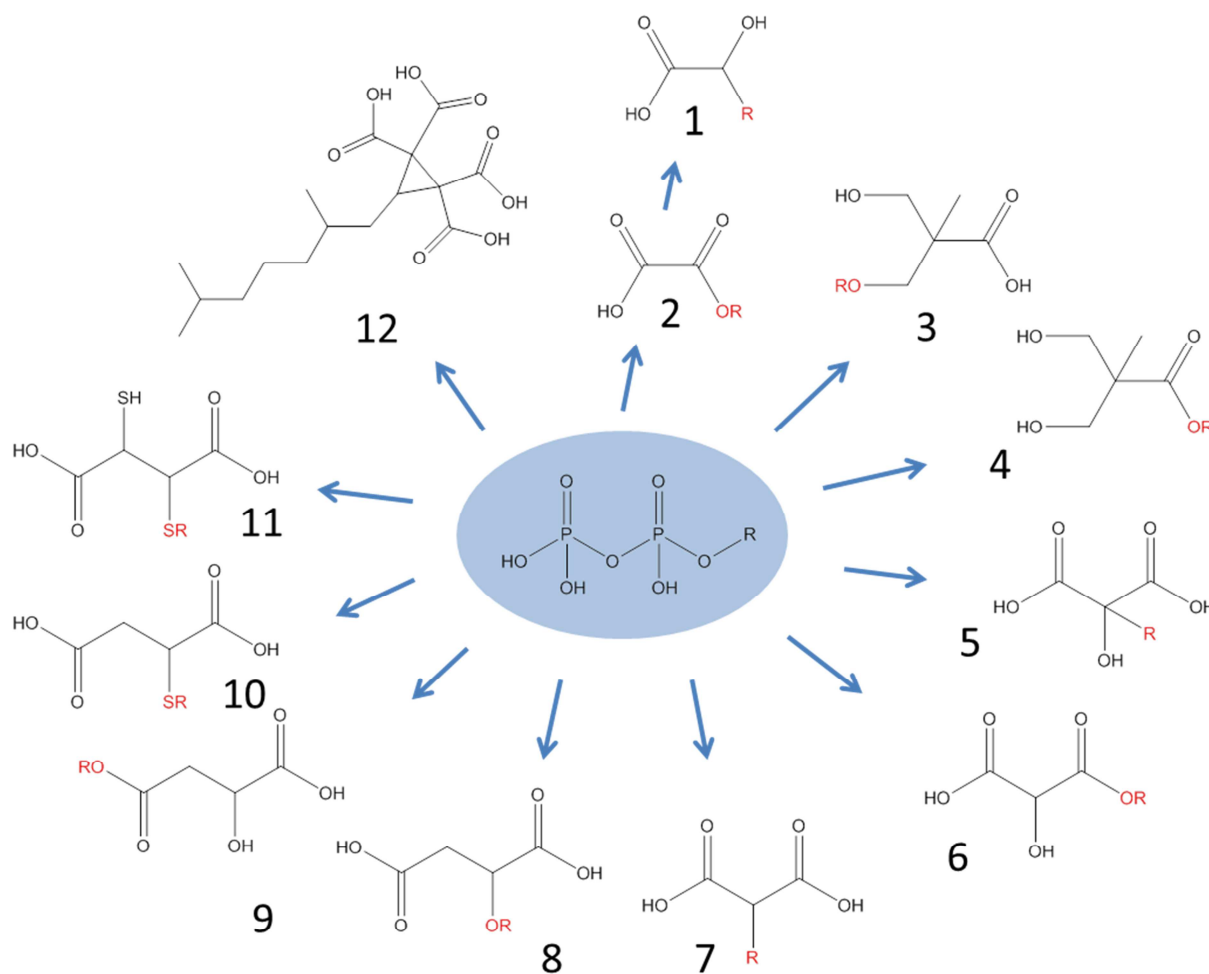


Figure 51. Overview of the different head groups designed for mimicking the diphosphate group (R = geranyl residue; **4** and **5**: R = dimethylallyl (**4a**, **5a**), geranyl (**4b**, **5b**), farnesyl (**4c**, **5c**); **3**: R = geranyl (**3b**), farnesyl (**3c**); **7**: R = dimethylallyl (**7a**), geranyl (**7b**)).

6.3.2. Aromatic prenyltransferase inhibition

The compounds described in Figure 51 were tested for their ability to inhibit the PTases catalyzed by MenA, NphB and UbiA and the results are presented in Figure 52. For MenA-mediated transfer, the membrane fraction of disrupted *E. coli* K12 was used and assayed in

competition to 5 mM GPP and 5 mM 1,4-dihydroxy-2-naphthoic acid. The product and an internal standard were extracted and assayed by using HPLC. For UbiA-mediated transfer, the membrane fractions of disrupted *E. coli* K12 were used in a competition assay containing 2.5 mM GPP and 2 mM hydroxylbenzoate. The results were analyzed by HPLC and represent the geranyl hydroxylbenzoate (GHB) formation. For NphB-mediated transfer, the soluble proteins were immobilized on an IMAC column and purified before testing in competition to 5 mM GPP and 5 mM 1,6-DHN. Product formation was kinetically determined using UV/Vis spectrometry. All results are expressed as relative conversions which mean the ratio of the product formation in the presence of the product formation and in the absence of the inhibitor. For MenA, the monocarboxylic acid/ester **3** and **4**, respectively, with β -hydroxyl group(s) inhibits as well as the dicarboxylic acid **5** and **7** act as inhibitors. Among **3**, **4** and **5** compounds, the dimethylallyl (**4a** and **5a**) and geranyl derivatives (**3b** and **4b**) exhibit the most significant inhibition with relative conversions degrees of $89.9 \pm 3.5\%$, $78.3 \pm 11.5\%$, and $71.9 \pm 2.6\%$, $89.9 \pm 2.1\%$, respectively (Table 6). For UbiA, only the monocarboxylic acid/ester **3** and **4**, respectively, with β -hydroxyl group(s) exhibited strong inhibition whereas the dicarboxylic acid **5** showed less inhibition. Among these compounds, the farnesyl derivatives (**3c**, **4c** and **5c**) exhibit the most significant inhibition with relative conversions degrees of $20.87 \pm 1.59\%$, $31.73 \pm 4.78\%$, and $42.00 \pm 1.68\%$, respectively (Table 6). For NphB, only the **4c** ester with β -hydroxyl groups, shows inhibition of the product formation of $54.00 \pm 0.49\%$. The dimethylolpropionic acid-derivatives (**3** and **4**) are structurally more related to the diphosphate moiety in context of steric effects and protonation state (for the ether-derivative **3**).

The findings suggest that the inhibition strongly depends on the chain length as well as on the head group whereas the linkage of the prenyl group carbon acid moiety is redundant.

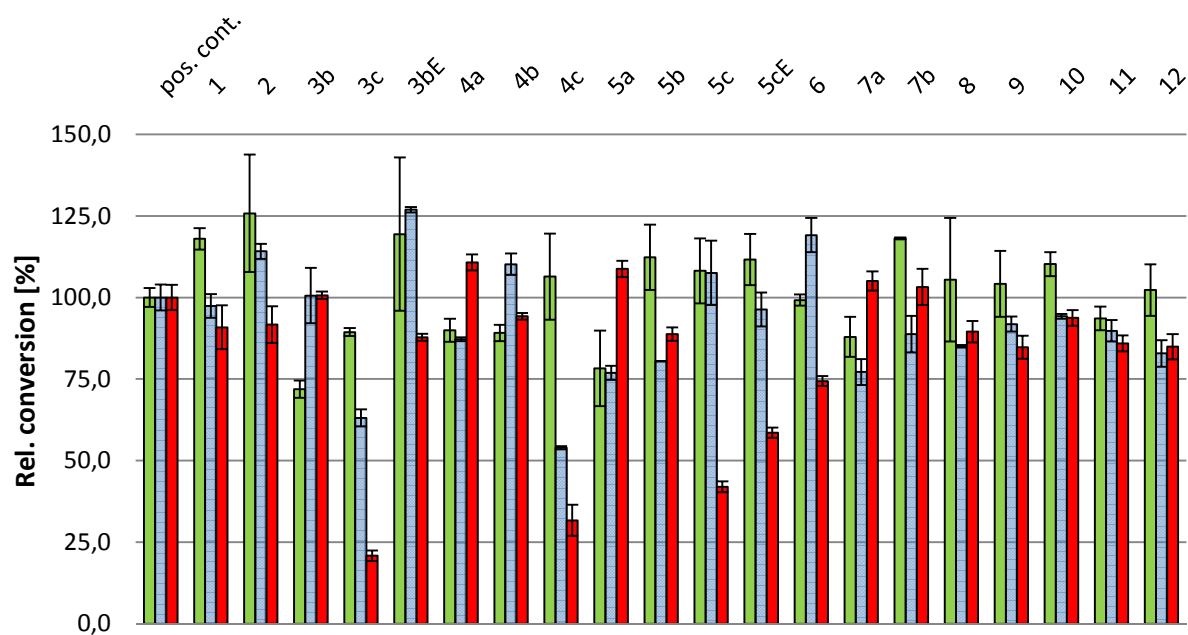


Figure 52. Inhibition of the three prenyltransferases: MenA (green column), NphB (blue column) and UbiA (red column). Pos. cont. = positive control without any inhibitor. E = with the methyl-ester protection group.

6.3.3. Dependency on the chain length

The molecules possessing the same head group display a clear dependency on the chain length to the enzyme inhibition. For MenA, dimethylallyl moieties **4a** and **5a** exhibit no significant inhibitory activities compared to the derivatives with farnesyl residues **4c** and **5c**. It seems likely that the long chain might sterically block the binding pocket and consequentially the substrate cannot enter. In contrast, the diphosphate mimics containing the shorter chain length maybe more stable in the binding pocket of the Mg^{2+} -ion (**3b**, **4a**, **4b** and **5a**). However, dimethylallyl moieties (**4a** and **5a**) did not show significant inhibition for UbiA, but the analogue with farnesyl residues (**4c** and **5c**) was performing better. As expected, the inhibition potential of geranyl derivatives such as **4b** and **5b** in comparison to dimethylallyl and farnesyl analogues was moderate (Table 6). This phenomenon might be explained by the interaction between the hydrophobic pocket and the substrate which is in the case of longer chain more favorable and may explain the stronger inhibition of inhibitors with farnesyl residues.^[180] Kinetic data for UbiA showed that geranyl diphosphate is converted 3.5 times faster than farnesyl diphosphate. A farnesyl chain might block the hydrophilic pocket and lead so to an occlusion in the GPP binding channel and sequentially

lowers the entering of GPP and the turnover. The more hydrophobic the prenyl chain is the more stable is the binding to the tunnel amino acids Leu141 and Leu256.^[177] In contrast, NphB prefers GPP as substrate and therefore, the shorter chain length was more active concerning the inhibition of the product formation than the farnesyl moieties.^[92] However, the farnesyl moiety is the most hydrophobic ones among the prenyl residues. Regarding the assumption that the increased chain length has a higher affinity to the enzyme in a competitive way, it might also bind into the aromatic substrate pocket. Furthermore, prenyl diphosphate with long chain length may form micelles and reduce the reaction velocity (Figure 52).^{[171][177][181]}

Table 6. Inhibition in percent (in comparison to the positive control without inhibition) for the compound **4** and **5** with focus on the chain length dependency at 1 mM concentration.

| Compound | MenA | NphB | UbiA |
|----------------------------------|-------------|------------|-------------|
| 4a (dimethylallyl-moiety) | 28.1 ± 2.6 | 12.8 ± 0.5 | -10.7 ± 2.4 |
| 4b (geranyl-moiety) | 10.6 ± 1.2 | 10.2 ± 0.5 | 5.8 ± 1.0 |
| 4c (farnesyl-moiety) | 10.1 ± 3.5 | 46.0 ± 0.5 | 68.3 ± 4.8 |
| 5a (dimethylallyl-moiety) | 10.1 ± 2.0 | 23.1 ± 2.2 | -8.7 ± 2.5 |
| 5b (geranyl-moiety) | -6.3 ± 13.1 | 19.5 ± 0.1 | 11.2 ± 2.1 |
| 5c (farnesyl-moiety) | 21.7 ± 11.5 | -7.5 ± 9.8 | 58.0 ± 1.7 |

[a] C₅-moiety. [b] C₁₀-moiety. [c] C₁₅-moiety.

6.3.4. Dependency of the head group

The phosphate mimics were classified according to the head groups. The most active ones are the mono-carboxylic acids/esters which are in particular the surrogates of dimethylolpropionic acid with **3b-c** and **4a-c**. Later on, **4c** was the only compound which showed inhibition for NphB. Furthermore, the malonic acid surrogates **5a-b** showed less inhibition for UbiA. The other surrogates exhibit no inhibition or even slight activation was observed. In contrast, MenA activity was mostly inhibited by the acidic surrogates **3a** and **5a** and the mono-carboxylic esters **4**. No inhibition could be obtained for the geranyl analogous

of the head group **1**, **2**, **5**, **6-12**. For NphB and UbiA, the thiol- as well as the tetracarboxylic acid-head groups showed low or no inhibition at all. One reason for such behavior of **8-11** might be the structural difference compared to the mimicked diphosphate group. For example, for compound **9** the distance between the linking hydroxide and the ending hydroxyl-group is one atom longer and might not fit into the Mg^{2+} -binding pocket of MenA, UbiA (Dx(x)xD motif) or NphB. The dicarboxylic acids **8**, **10** and **11** showed weak inhibition for all enzymes. It could be assumed that this mimics will represent the bisphosphonate (a well-known drug which mimics the pyrophosphate structure and thereby, the activity of enzymes that utilize diphosphate is inhibited). The reason for the low inhibition of **8** and **9** could be the sulfur atom which is less common in nature. Normally, atoms like sulfur (C-S-P) are used predominately as a geranyl thiodiphosphate (GSPP) which is a very poor substrate or even an inhibitor of prenyltransferase and therefore relevant for crystallization purposes.^[182] An interesting pattern was observed for compound **5c**. It slightly activates both prenyltransferases MenA and NphB by approximately 10%. This phenomenon was already described previously by our group. The Mg^{2+} concentration strongly affects the enzyme activity (in this case for UbiA).^[176] Instead, **5c** was the third most potent inhibitor for UbiA. Earlier studies^{[101][183]} have shown that even a small reduction of the Mg^{2+} -concentration resulted in an increased product formation. The authors speculated about enhanced enzyme stability due complexing of magnesium with the allylic diphosphate. Thus, the lower magnesium level decelerates protein denaturation. The inhibitors are mimics of the allyl and particularly of the diphosphate group and therefore are responsible for complexing the Mg^{2+} -ions (like the well-known chelate - complexer EDTA).

6.3.5. Dependency of the chain linker atom (C versus O)

For UbiA, the most active compounds were the dimethylolpropionic acid analogues **3b-c** and **4a-c** whereas the linkage to the prenyl chain through an ether bond is more efficient for **4a-c** compared to the ester bond linkage of the prenyl chain. However, the determinations of the IC_{50} -values for the potential inhibitors were performed for the most prominent inhibitors **3c** and **4c** with the model enzyme UbiA. The surrogates of dimethylolpropionic acid exhibit an IC_{50} -value of 0.69 ± 0.03 mM for **3c** and 0.75 ± 0.02 mM for **4c** (Figure 53). Both compounds were tested in the range of 0.01-10 mM for the enzyme UbiA and the results were determined by HPLC analysis. For MenA and NphB, no IC_{50} values were measured due to the

fact that no inhibition reduced the remaining activity by $\geq 50\%$. As stated above, MenA and UbiA are involved in menadione and ubiquinone biosynthesis, respectively. Thus, potential inhibitors may be developed as antibiotics interrupting the respiratory chain.

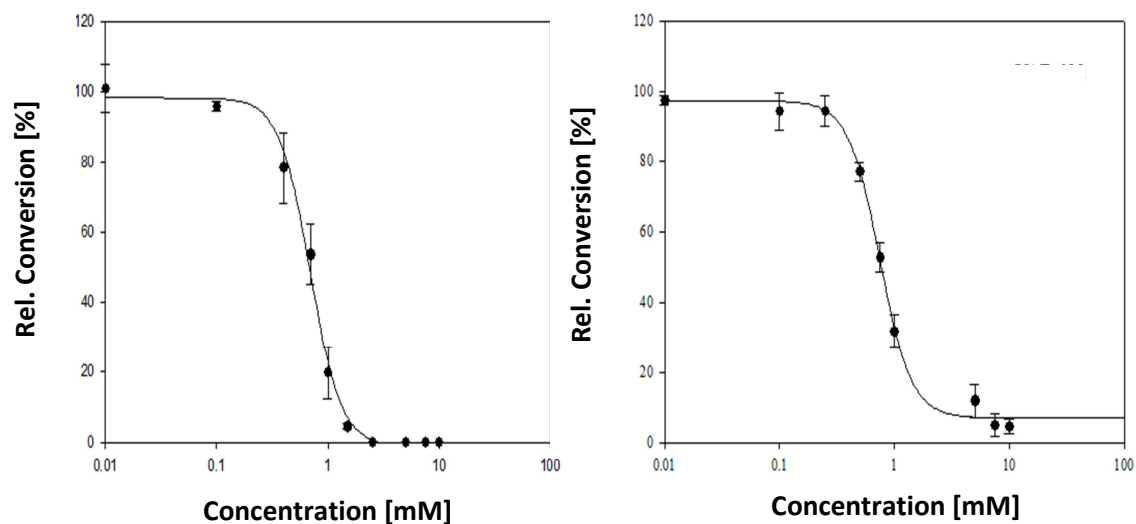


Figure 53. IC_{50} -values of the compound **3c** and **4c** for UbiA. (Left) **3c** showed an IC_{50} -value of 0.69 ± 0.03 mM and (right) **4c** with on value of 0.75 ± 0.02 mM (data out of Msonga PhD thesis).

6.4. Summary

A series of 20 prenylated (polyoxy)-carboxylates were presented as surrogates of the diphosphates. All diphosphate-mimics were assayed as competitive inhibitors for the aromatic prenyltransferases Mena, NphB and UbiA. The results indicated that compounds containing a monocarboxylic acids/ester coupled with β -hydroxyl groups (**3b-c** and **4a-c**) or α -coupled dicarboxylic acids (**5b-c**) were the most effective ones among the investigated compounds. This investigation supports subsequent analysis of the role of the diphosphate moiety. In this first attempt to find a new pharmacophore for MenA, NphB and UbiA inhibition, an overall structural ensemble of carboxylic acids/esters, hydroxyl group(s) and/or thiol(s) was synthesized as “first-generation” and used for the development of novel diphosphate mimics which are more potent and selective towards inhibition. The involvement of MenA and UbiA in the respiratory chain makes them potent targets. Therefore, the development of selective inhibitors could lead to a new class of antibiotics which interrupts the menadione or ubiquinone biosynthesis and thus the ATP regeneration.

7. Methods

7.1. General methods used for cPTases

7.1.1. Protein expression and purification

The cDNAs from the UPPS of *M. tuberculosis* (Mt_UPPS) (UniProt-Code P60479), *M. luteus* (Ml_UPPS) (UniProt-Code O82827), *H. pylori* (Hp_UPPS) (UniProt-Code P55984) and *H. brasiliensis* (Hb_PPS) (UniProt-Code Q8W3U4) were synthesized and optimized with respect to codon usage by MWG Eurofins (MWG-Biotech AG, Ebersberg, Germany) and introduced into the *E. coli* expression vectors pET28a(+) (Merck KGaA, Darmstadt, Germany) via the *Xho*I and *Nde*I restriction sites. All constructs were transformed into chemically competent *E. coli* (DE3) expression strains. Transformed cells were selected on lysogeny broth (LB) agar plates containing the required antibiotics (50 μ l ml⁻¹ kanamycin). For gene expression, the cells were grown in Erlenmeyer flasks containing 350 ml LB medium with the required antibiotics. Gene expression was induced by addition of 1 mM isopropyl-1-thio- β -D-galactopyranoside (IPTG) from a 1 M stock solution at an OD₅₉₅ of 0.6 - 0.8. The cultures were incubated at 23 °C and 210 rpm for 16 h.

For protein purification, the *E. coli* BL21 (DE3) cells containing the particular construct in pET28a(+) were harvested by centrifugation (8000 x *g*, 10 min) and resuspended in extraction buffer (50 mM Tris/HCl, 500 mM NaCl, 40 mM imidazole, 1 mM DTT, 0.15% Triton-X 100, pH 7.5). The suspension was homogenized by high-pressure dispersion (Constant Systems Ltd., Northants, UK) at 1000 bar. The crude extract was applied to a Ni²⁺-loaded immobilized metal ion affinity chromatography (IMAC) column (HisTrap HP, 1 ml, Qiagen, Hilden, Germany) on a ÄKTA FPLC system (GE Healthcare, Little Chalfont, UK). The recombinant His₆-tagged fusion protein was eluted by a linear gradient of elution buffer (50 mM Tris/HCl, 500 mM NaCl, 500 mM imidazole, pH 7.5). Fractions containing UPPS were scanned for content according to Bradford^[184] and were checked for homogeneity by polyacrylamide gel electrophoresis (PAGE). Fractions containing homogeneous protein were desalted on a PD-10 column (GE Healthcare, Little Chalfont, UK) or by dialysis and were stored in assay buffer (50 mM Tris/HCl, 100 mM NaCl, pH 7.5) containing additionally 10 % (v/v) glycerol at -80 °C.

7.1.2. HPLC analysis

Analytical HPLC separation was performed on a Merck Hitachi HPLC system (Merck HITACHI D-7000) equipped with a UV-Vis detector L-7420 (Hitachi, Ltd., Tokyo, Japan) and an auto sampler (Merck HITACHI L-7250). Samples (5 μ l) were applied to a C18 column (YMC-ODS AQ 150 x 4 mm, 5 μ m, YMC Europe GmbH, Dinslaken, Germany), and the substrate and/or the prenylated products were eluted by a linear gradient which started from 100 % A (H_2O /methanol/isopropanol 1:12:8 (v/v/v)) and increased up to 45 % B (*n*-hexane/isopropanol 3:7 (v/v)) in 30 min, then up to 70 % B in 5 min and within 1 min up to 100 % B. The flow-rate was 1 ml min⁻¹.

All solvents were filtered and degassed before usage and samples (see section 2.12.3.) were filtered and redissolved in methanol. The column was maintained at 23 °C. The chromatographic process was recorded at 210 nm (for UV-Vis). For calculation, the integrated area under the peak (AUC) of the interested product was taken and divided by the total AUC. All values are given in percent.

To analyze small amount of prenylated products with non-natural prolongation units (Cl-BPP or BPP), the starter unit FPP was exchanged against the fluorescence labeled substrate Mant-O-GPP (Figure 9). The fluorescence detection sensitivity at 10 μ M Mant-O-GPP was 10-1000 times higher than that of the UV detection with excitation and emission wavelengths of 352 nm and 420 nm, respectively.

7.1.3. Enzyme assay

General procedure, Enzyme reactions (50 μ l) contained 1.0 mM MgCl_2 , 5 μ M FPP, 50 μ M IPP or Cl-BPP or BPP and 10 μ M purified UPPS dissolved in assay buffer (50 mM Tris/HCl, 100 mM NaCl, 0.1 % Triton X-100 (v/v), pH 7.5). Reactions, which were initiated by the addition of the enzyme, were incubated at 25°C for 0 - 24 h. Products were extracted twice with 500 μ l of 1-butanol. The solvent was evaporated under N_2 stream. For the hydrolysis of the diphosphate to the responding polyprenols, the residual was re-dissolved in 200 μ l of hydrolysis puffer containing 20 % isopropanol (v/v), 4.4 units/ml acidic phosphatase from potato (Sigma-Aldrich, St. Louis, USA), 0.1 % Triton X-100 and 50 mM sodium acetate pH 4.7. The reaction was incubated at 37°C overnight. Afterwards, the products were extracted with 500 μ l *n*-hexane, evaporated, resolved in methanol and prepared for the high performance liquid chromatography (HPLC) analysis (see section 2.12.2.).

7.1.4. Diphosphate assay (PPi-Assay)

The diphosphate assay was performed according to the procedure of Lee *et al.*^[185] and modified according to Jeanette Keim.^[54]

The enzymatic reactions were carried out in 50 µl volume (96-well microtiter plate) containing 1.0 mM MgCl₂, 5 µM farnesyl diphosphate, 50 µM IPP or Cl-BPP or BPP and 10 µM purified UPPS dissolved in assay buffer (50 mM Tris/HCl, 100 mM NaCl, 0.1% Triton X-100 (v/v), pH 7.5) with additional 4 U mL⁻¹ of inorganic pyrophosphatase from *S. cerevisiae* (Sigma-Aldrich, St. Louis, USA). Reactions, which were initiated by the addition of the enzyme, were incubated at 25°C for 0 - 24 h. All reactions were performed in triplets and the background hydrolysis of PPi to Pi was compensated by a control reaction with denatured enzyme (30 min boiled at 95°C). After certain time points, the enzyme reaction was stopped with 100 µl BIOMOL Green™ detection reagent (ENZO LIFE SCIENCES GmbH, Lorrach, Germany) and incubated for 15 min before measuring the absorbance at 620 nm. Released phosphate was determined using a phosphate calibration curve starting from 0-160 µM P_i (diluting a stock solution delivered by ENZO LIFE SCIENCES GmbH, Lorrach, Germany). The quantification experiments were performed in the linear range of Pi calibration curve and the enzyme activity was calculated according to equation 1.

Equation 1:

$$V_0 = \frac{(A_{\text{Enzyme}} - A_{\text{Blank}}) \times 1000}{2 \times m \times t \times [E]}$$

| | |
|---------------------|---|
| V ₀ | initial rate of the PPi hydrolysis (nkat mg ⁻¹) |
| A _{Enzyme} | absorption at 620 nm of the enzyme activity |
| A _{Blank} | absorption at 620 nm of the negative control |
| m | slope of the Pi curve (µM ⁻¹) |
| t | time of the enzyme reaction (s) |
| [E] | Enzyme concentration (mg L ⁻¹) |

In order to define the quantitative enzymatic conversion, the unit katal was used. One katal expresses the conversion of 1 mol substrate per second from an exact determined amount of enzyme. In this specific case, one katal (kat) corresponds to the (indirect) release of P_i generated from the PP_i elimination during product formation (Equation 1).

7.2. Methods used to handle the aromatic PTases NphB

7.2.1. Protein expression and purification

The *NphB* gene from *Streptomyces* sp. strain CL190 (GenBank accession AB187169) was synthesized with optimized codon usage by MWG Eurofins (Germany) and introduced into the bacterial *E. coli* expression vector pET32a (Merck KGaA, Darmstadt, Germany) via the *SacI* and *BamHI* restriction sites. The construct was transformed into chemically competent strains and transformed cells were selected on LB agar plates containing the required antibiotic (100 $\mu\text{g ml}^{-1}$ ampicillin). For gene expression, the cells were grown in Erlenmeyer flasks with LB medium (350 ml containing 100 $\mu\text{g ml}^{-1}$ ampicillin) at 37°C. To induce gene expression, 1 mM IPTG was added to the solution at an OD_{595} of 0.6 - 0.8 and further incubated at 25°C and 160 rpm for 16 h. The cells were harvested by centrifugation (8000 x *g*, 10 min) and resuspended into extraction buffer (50 mM Tris/HCl, 500 mM NaCl, 40 mM imidazole, pH 7.5). The suspension was homogenized and cells were disrupted by high-pressure dispersion (Constant Systems Ltd., Northants, UK) at 1000 bar. The crude extract was again centrifuged (16000 x *g*, 20 min), incubated with 25 $\mu\text{g ml}^{-1}$ DNase I (3000 U mg^{-1} , Rinderpankreas, AppliChem, Darmstadt, Germany) on ice for 20 min, before it was applied to a Ni^{2+} - loaded IMAC column (HisTrap HP, 1 ml, Qiagen, Hilden, Germany) on an ÄKTA FPLC system (GE Healthcare, Little Chalfont, UK). The recombinant His₆-tagged fusion protein was eluted by a linear gradient of elution buffer (50 mM Tris/HCl, 500 mM NaCl, 500 mM imidazole, pH 7.5). Fractions containing NphB were identified by protein determination according to Bradford^[184] and were checked for purity by polyacrylamide gel electrophoresis (PAGE). Fractions containing homogeneous protein were desalted via dialysis overnight at 6°C. To obtain untagged protein, the fusion protein was further treated with human thrombin (Sigma, St. Louis, USA) (3 units per mg of recombinant protein) at 10°C for 3 h. The Trx-tag containing the N-terminal His-tag was removed by chromatography on Ni^{2+} - loaded HisTrap highly cross-linked with spherical agarose (6 %) (GE Healthcare, Little Chalfont, UK). The cleaved protein was stored in assay buffer (50 mM Tris/HCl, 100 mM NaCl, pH 7.5) at -80 °C. Yield was 1.2 g l^{-1} WT-NphB without Trx-Fusion Protein (Biocatalytic activity and yield during the purification of NphB is shown in Table 2). The purity of the mutations is shown in Supplementary Figure 1 and Supplementary Figure 2.

7.2.2. Enzyme assay

Enzyme reactions (100 μ l) contained 5 mM $MgCl_2$, 5 mM 1,6-DHN, 5 mM geranyl diphosphate (GPP) and 10 μ M of purified NphB dissolved in assay buffer (50 mM Tris/HCl, 100 mM NaCl, pH 7.4) All concentrations are final concentrations. The reactions, which were initiated by the addition of the enzyme, were incubated at 27°C up to 1 h. The product formation (calculation of the turnover number) was followed via UV-Vis- spectroscopy at wavelengths of 345 nm and 600 nm, respectively (chapter 5.2.). After the final measurement, the reaction was incubated at 25°C for 16 h, stopped by adding 150 μ l of ethyl acetate. The products were extracted twice with 150 μ l of ethyl acetate. The solvent was evaporated under N_2 stream. The residue was re-dissolved in 300 μ l of acetonitrile, and the products were analyzed by HPLC to determine the product ratio.

7.2.3. HPLC measurements

Analytical HPLC separation was performed on a Merck Hitachi HPLC system (Interface D-7000) equipped with the UV-Vis detector L-7420, auto sampler L-7200 and pump L-7100 (Hitachi, Ltd., Tokyo, Japan). Samples (20 μ l) were applied to a C18 column (YMC-Pack, R-ODS-5-A, 250 x 4.6 mm I.D., S-5 μ m, 120 A, YMC Co., Ltd., Kyoto, Japan). The prenylated products were eluted starting with 95% water for 4 min followed by an acetonitrile gradient up to 100% over 20 min and 4 min at 100% acetonitrile. Both solvents contained 0.2 % formic acid and the flow rate was 0.8 ml min^{-1} . HPLC was monitored at 280 nm. For calculation, the total AUC (absorbance area under the curve) was taken and divided by the integrated peak area of the interested product. All values were given in percent.

7.2.4. Mutagenesis of NphB gene

For site-directed mutagenesis, the pET32a - plasmid containing the wild type NphB prenyltransferase gene was transformed in *E. coli* DH5 α . The transformed cells were grown over night at 37°C in 5 ml LB medium supplemented with ampicillin (100 μ g ml^{-1}). Then, the plasmids were purified using the Qiagen miniprep kit as described by the manufacturer. 50 ng isolated purified DNA was used as template for all single mutations. For the double mutation, the D110A-plasmid served as template. All site-directed mutagenesis experiments were carried out by PCR with AccuPrime Pfx Supermix (Invitrogen AG, Kalifornien, USA)

following the recommended manual conditions. Briefly, the reaction was performed in 50 μ l reaction tube containing 10 μ l reaction mixture of 2 U Pfu-DNA-polymerase, reaction puffer, 0.2 mM dNTP-Mix, 10 pmol of the required primer pair and 700-900 ng DNA. The amplification was initiated by denaturation (2 min 95 °C) and 35 cycles (1 min 95°C, 30 s 57°C, 6 min 72°C). The mutagenic oligonucleotides designed to produce the desired point mutations are listed in Table 7. After PCR reaction, the 10 μ l samples were treated for 1 hour

Table 7. Oligonucleotides for site-directed mutagenesis.

| Mutated position | Forward 5'-3' | Reverse 3'-5' |
|------------------|-------------------------------------|-------------------------------------|
| V47A | GTGGAAGGTGGTCCGCGGTAGTGTCTCAATG | CATTGAGAACACTACCGCGGAACCACCTCCAC |
| V49E | GGTCCGTGGTAGAGTTCTCAATGGCATCC | GGATGCCATTGAGAACTCTACCACGGAACC |
| S51A | GGTAGTGTTCCGAATGGCATCCGG | CCGGATGCCATTGCGAACACTACC |
| S51E | CCGTGGTAGTGTTCGAAATGGCATCCGG | CCGGATGCCATTTGGAACACTACCACGG |
| S64A | GAACTGGACTTCGCCATTTCACTCC | GGACTGAAATGGCGAAGTCCAGTTC |
| S64R | CCGAACTGGACTTCGCATTTCACTCCGG | CGGGACTGAAATGGCGAAGTCCAGTTCGG |
| M106A | CCCAGTAAGCGCGTTTGCCATTG | CAATGGCAAACGCGCTTACTGGG |
| D110A | GTTTGCCATTGCCGCGAAGTGAC | GTCACCTCGCCGCAATGGCAAAC |
| D110N | CATGTTTGCCATTAACGGCGAAGTGACTG | CAGTCACTTCGCCGTTAATGGCAAACATG |
| Y121F | CAAGAAAACCTTCGCGTTCTTTCC | GGAAAGAACGCGAAGGTTTTCTTG |
| Y121W | CTTCAAGAAAACCTGGGCGTTCTTTCCG | CGGAAAGAACGCCAGGTTTTCTTGAAG |
| M162A | CAAAGTCCAGGCGACGAGTATGG | CCATACTCGTCGCTGGACTTTG |
| M162C | GGACAAAGTCCAGTGCACGAGTATGGAC | GTCCATACTCGTGCCTGGACTTTGTCC |
| M162F | GGACAAAGTCCAGTTCACGAGTATGGAC | GTCCATACTCGTGAAGTGGACTTTGTCC |
| M162L | CAAAGTCCAGCTGACGAGTATGG | CCATACTCGTCAGCTGGACTTTG |
| M162W | GGACAAAGTCCAGTGGACGAGTATGGAC | GTCCATACTCGTCCACTGGACTTTGTCC |
| F213A | GCAAACGGAGCGCTTCGGTGTATCCCACGCTG | CAGCGTGGGATACACCGAAGCGCTCCGTTTGC |
| F213V | CAGCGTGGGATACACCGAAACGCTCCGTTTGC | GCAAACGGAGCGTTTCGGTGTATCCCACGCTG |
| F213L | GCAAACGGAGCTTGTGCGTGTATCCCACGCTG | CAGCGTGGGATACACCGACAAGCTCCGTTTGC |
| S214A | GCAAACGGAGCTTGTGCGTGTATCCCACGCTG | CAGCGTGGGATACACCGCAAAGCTCCGTTTGC |
| Y216A | GGAGCTTTTCGGTGGCTCCCACGCTGAATTG | CAATTCAGCGTGGGAGCCACCGAAAAGCTCC |
| Y216E | GGAGCTTTTCGGTGGAGCCACGCTGAATTG | CAATTCAGCGTGGGCTCCACCGAAAAGCTCC |
| V271D | GAAAAGCGCACGTTAGACTACGGCCTTACGCTC | GAGCGTAAGGCCGTAGTCTAACGTGCGCTTTTC |
| V271E | GAAAAGCGCACGTTAGAGTACGGCCTTACGCTC | GAGCGTAAGGCCGTACTCTAACGTGCGCTTTTC |
| Y288D | CTACAAACTGGGTGCGGATTACCACATTACCGATG | CATCGGTAATGTGGTAATCCGCACCCAGTTTGTAG |
| Y288E | CTACAAACTGGGTGCGGAGTACCACATTACCGATG | CATCGGTAATGTGGTACTCCGCACCCAGTTTGTAG |
| V294A | CATTACCGATGCCAACGCGGGTTAC | GTAACCCGCGTTGGGCATCGGTAATG |
| Q295A | CATTACCGATGTCGCACGCGGGTTAC | GTAACCCGCGTGCACATCGGTAATG |
| L298A | CCAACGCGGGGCACTGAAAGCCTTTG | CAAAGGCTTTCAGTGCCCCGCGTTGG |
| TrippleMut. | CATTACCGATGCCGCACGCGGGTTAC | GTAACCCGCGTGCAGCATCGGTAATG |

with 1 μl FastDigest[®] Dnpi (Fermentas, Waltham, USA) and finally 5 μl of the mixture were transformed into chemo-competent *E. coli* DH5 α cells. Transfected cells were grown on LB agar plates containing 100 $\mu\text{g ml}^{-1}$ ampicillin and incubated overnight at 37°C. One single colony was selected for plasmid purification. After growing overnight, the plasmids were purified using Qiagen miniprep kit and the mutated construct was confirmed by DNA sequencing using the T7 and T7 term sequencing primers from Eurofins (Eurofins MWG Operon, Ebersberg Germany).

7.2.5. Protein-MS-analyzis

MALDI-TOF Mass Spectrometry; after the enzyme reaction carried out as previously described, the samples were desalted and concentrated by C18 ZipTip[®] (Millipore). The peptides of interest were eluted with 70% (v/v) acetonitrile, 0.1% (v/v) trifluoroacetic acid in water and 1 μl of the sample was added to 1 μl of sinapic acid in the same solvent composition. 1 μl of the mixture was deposited onto a stainless steel target. Mass spectra were recorded on an Ultraflex-II TOF/TOF mass spectrometer (Bruker Daltonik, Bremen, Germany) equipped with a MALDI source, nitrogen laser, LIFT cell for fragment ion postacceleration and gridless ion reflector. Data acquisition, data evaluation and instrument operation were carried out with Flex Analysis 3.0 and Biotoools 3.0 and FlexControl software (Bruker Daltonik, Bremen, Germany).

ESI-QTOF-MS/MS-Analyzis. The in-gel trypsin digestion was performed by cutting out the protein bands of the SDS-Page-gels and incubated with 10 mM dithiothreitol (Sigma) in 100 mM ammonium bicarbonate for 45 min at 50°C. Afterwards, the solvent was removed and a mixture of 55 mM iodoacetamide (Sigma) in 100 mM ammonium bicarbonate was added to modify cysteine residues. The reaction occurred in dark for 45 min. Then, the solution was removed, the gel containing the modified protein was washed three times with water, two times with 100 mM ammonium bicarbonate and then with 100 mM ammonium bicarbonate in 50 % (v/v) acetonitrile. The gel was dried under N₂-stream, reswollen in 20 μl of 50 mM ammonium bicarbonate (pH 8.0) and digested with trypsin (Promega, Madison, WI, USA) overnight at 37°C.

Proteolysis products were injected into a nano ACQUITY UPLC system (Waters Corporation, Eschborn, Germany) including a binary solvent manager, a sample manager

with integrated heating system and trapping module. 2 μl were injected via “microliter pickup” mode, desalted on-line through a symmetric C18 180 μm \times 20 mm pre-column. Finally, the peptides were separated on a 100 μm \times 100mm analytical RP column (1.7 μm BEH 130 C18, Waters Corporation, Massachusetts, USA). The gradient for separation was 3.0-33.0% (0.1% formic acid in water and 0.1% formic acid in acetonitrile) in 15 min. Online-MS was performed on an SYNAPT G2 HDMS which is a hybrid quadrupole tandem time-of-flight (Q-TOF) mass spectrometer equipped with Tri-wave ion guides (Waters Corporation, Massachusetts, USA). The data were recorded in LC/MSE by switching between low and elevated energy on alternated scans. Sequentially, the correlation of precursor and product ions can be achieved by using the correlation of the retention and drift time and their alignment. All mass spectra recorded during the elution of the C-terminal Lys-C fragment of NphB and the C₁₆₂-mutant were analyzed and deconvoluted using the BiopharmaLynx (1.3.2, Waters Corporation, Eschborn, Germany).

7.3. Methods used for the cyclisation attempt

7.3.1. Expression, purification and enzyme assay of THCA synthase (THCA-S)

THCA-S was expressed in yeast *Pichia pastoris*, purified and tested for its activity according to a established method in Prof. Oliver Kayser laboratory (TU Dortmund, Germany). To proof the enzyme activity, the enzyme fractions were used for the activity measurements of the natural and the three non-natural substrates. Briefly, 99 μl of the enzyme stock solution were added to 1 μl of a 10 mM substrate stock solution solved in DMSO. Finally, the total volume was 100 μl containing 100 μM substrate, 1% (v/v) DMSO and 100 mM sodium citrate (pH 5.5). After 1 hour at 37 °C, the reaction was stopped by adding 30 μl formic acid. The enzymatic product and the remaining substrate were extracted three-times with 400 μl ethyl acetate. The extract was evaporated and the residue redissolved in 300 μl acetonitrile. 10 μl of the acetonitrile solution was analyzed by HPLC-MS. For the activity measurements, the THCA was also quantified by reverse phase HPLC. THCA-S activity was measured at least twice for the aromatic substrate.

7.3.2. Analysis of the THCA synthase product by HPLC

To measure the enzyme activity with the natural substrate CBGA, 10 μl of the reaction mixture were injected. The cyclized product was quantified by HPLC coupled with mass

spectra provided by Agilent Technologies (HPLC-MS equipment: 1260 Infinity), the column (Poroshell 120, EC-C18, particle size: 2,7 μm) and the pre-column (UHPLC-Guard Poroshell 120 EC-C18h PEGASIL ODS). CBGA and THCA were eluted using an isocratic system containing 25 % water and 75 % acetonitrile (ACN) added with 0.1 % FA, monitored at 225 nm, at a flow rate of 0.7 ml x min⁻¹ and quantified according to a calibration curve (method established in the laboratory of Prof. O. Kayser, TU Dortmund, Germany).

The separation of the non-natural geranylated substrates were carried out on the Agilent-1260 Infinity HPLC system (Agilent Technologies, Santa Clara, USA) coupled to a Bruker compact ESI-qTOF mass spectrometer (positive charged mode ranged from 90-700 m/z; Set Capillary 3800 V; Set End Plate Offset -500 V; Set Charging Voltage 2000 V; Set Dry Heater 220 °C). The analysis via HPLC was carried out by a linear gradient starting with 50 % : 50 % (H₂O/ACN) up to 100 % ACN added with 0.1 % FA in 10 min and additional 4 min for recalibration of the column at a flow rate of 0.4 ml x min⁻¹.

7.4. Material and Methods for the antifungal tests

7.4.1. Material

The chemical 1,6-DHN (**1**) was purchased by Sigma-Aldrich (St. Louis, MO, USA) and the 5-geranyl-1,6-DHN (**2**) was biochemically obtained using the aromatic prenyl-transferase NphB in the presence of GPP and 1,6-DHN. The enzyme product was purified using HPLC and the structure was confirmed using NMR and high resolution MS (see chapter 7.2.).

7.4.2. Bioactivity tests

In this study, the strains of the fungus *B. cinerea*, *P. infestans* and *S. tritici* were a gift from BASF. The inoculation and the assay were performed according to the methods described by Alexander Otto (unpublished dissertation, IPB (Halle), NWC, 2016). Briefly, the non- and geranylated-1,6-DHN were dissolved in DMSO diluted (42, 14, 4.7, 1.6, 0.52 $\mu\text{g ml}^{-1}$) and incubated with the organisms in 96-well microtiter plates. Pyraclostrobin served as positive control (C+) and DMSO as negative control (C-). The mixture was incubated for seven days for the fungus *B. cinerea* and *S. tritici* and five days for the oomycete *P. infestans* at 18°C in darkness. The growth was measured at OD_{405 nm} and analyzed by Excel 2010® (Microsoft). For each compound and fungicide concentration, three replicate wells were measured.

7.5. Development and validation of the qNMR-method

7.5.1. Sample preparation

NMR tubes (bore 5 mm, length 8 inch) were filled with 660 μl CD_3OD solution containing the probe and tetramethylsilane (TMS). For calibration, the final concentration was set 0.0, 0.635, 0.865 and 1.212 mg of 1,6-DHN in 660 μl CD_3OD . All samples were measured in triplets and the average as well as the standard deviation was taken for the calibration line.

7.5.2. NMR spectra

The establishment and optimization of the method was performed on a 600 MHz NMR spectrometer (Agilent VNMRS 600) whereas the routine measurements were recorded on a 400 MHz NMR spectrometer (Agilent DD2 400). The proton channel was used for transmitting and receiving RF pulses. The fully relaxed spectra were obtained by: flip angle 90° , spectra width 7183.9 Hz, data points 32k, and pulse repetition time 30s. These parameters were suitable for quantitative analysis and to avoid truncation of the signal. All parameters were optimised for 1,6-DHN as model substrate. The T_1 values of 1,6-DHN was experimentally determined (Figure 43) and $T_{17.0 \text{ ppm}}$ was 5.8 and set to a repetition time of 30 s.

7.5.3. Determination of the concentration

Calibration of the *“Agilent qNMR tool using a single-point calibration”* –method was performed according to equation 1. In order to confirm the accuracy of the method, all samples were performed as triplicates. One sample was performed as technical triplicate subsequent by a long-time measurement of 72h. The probe was kept during this time at $2-6^\circ\text{C}$ to avoid evaporation of the solvent. When the probes exceeded the mass limit of 1.2 mg per 660 μl the solution were diluted to a final concentration of 0.2 till 1.2 mg per 660 μl solvents to ensure measurements in the accurate range of the calibration line because the T_1 value can changes with increasing concentration.^[156]

7.6. Method used to establish the UV/Vis-assay

7.6.1. Enzyme assay

Enzyme reactions (100 μ l) contained as final concentration 5 mM $MgCl_2$, 5 mM aromatic substrate, 5 mM GPP and 40 μ M of purified NphB dissolved in assay buffer (50 mM Tris/HCl, 100 mM NaCl, pH 7.5). The reactions, which were initiated by the addition of the enzyme, were incubated at 27 $^{\circ}$ C for 0 - 2 h. The product formation was followed via UV/Vis-spectroscopy (Spectra Max M5, Molecular Devices LLC., California, USA) at a wavelength of 340 nm and/or 345 nm. After measuring the absorption, the reaction was quenched with ethyl acetate and products were extracted twice with 150 μ l of ethyl acetate. The solvent was evaporated under N_2 stream. The residual was re-dissolved in 300 μ l of methanol, and the products were analyzed by HPLC.

7.6.2. HPLC

Analytical HPLC separation was performed as described in chapter 7.2.3.

7.6.3. UV/Vis spectra of the geranylated 1,6-DHNs

Semi-preparative approach was used to obtain pure 5-geranyl-1,6-DHN. Enzymatic conversions were performed similar to chapter 3 but in larger scales (6 ml). The extraction procedure was carried out under the same conditions as described above using 3 ml of ethyl acetate. The products were separated by HPLC (see chapter 3). Fractions containing the product were collected and the solvent was evaporated under N_2 stream and finally the weight was determined. The UV-Vis spectra were measured in assay buffer containing additional 12% DMSO and 0.25 mM of 1,6-DHN or the received geranylated 1,6-DHN products. The UV/Vis data were acquired using a Lambda 900 UV spectrometer (Waltham, Massachusetts, USA). Briefly, the absorption spectra were recorded from 300 to 400 nm using a quartz cuvette (Suprasil[®], Hellma Analytics, Müllheim, Germany) diameter of 10 mm, a bandwidth of 1.0 nm and a scan speed of 100 nm min^{-1} . The spectra were determined by adding 2 μ l of the substance of interest 500 μ l of assay buffer and referenced to 500 μ L of pure assay buffer.

7.7. Methods used for the inhibition test of PTases MenA, NphB and UbiA

7.7.1. Chemical synthesis

The chemical synthesis was performed by the Dimitar Vasilev^[164] for the design and syntheses of 20 prenylated (polyoxy)-carboxylates as surrogates of the diphosphates.

7.7.2. Aromatic prenyltransferase UbiA

7.7.2.1. UbiA enzyme expression and membrane fraction preparation

The UbiA wild-type originates from *E. coli* K12, was cloned in the pALMU3 vector and expressed in *E. coli* C41 (DE3) cells. A pre-culture (50 ml) of LB medium with 100 µg ml⁻¹ ampicillin and 0.2 % glucose was incubated at 37 °C and shook 250 rpm overnight. The pre-culture was added to LB medium containing 100 µg ml⁻¹ ampicillin (1L) and then, incubated at 37 °C until an OD₆₀₀ of 0.8 was reached. The expression was induced by adding 1 ml of 1 M IPTG and further incubated for 8 h at 37 °C with shaking at 250 rpm. Cell were harvested by centrifugation at 10000 rpm for 10 min at 4 °C and the pellet resuspended in 50 mM Tris/HCl (pH 7.8) containing 10 mM 1,4-DTT (20 ml). The homogenized suspension was disrupted twice by high-pressure dispersion (Constant Systems Ltd., Northants, UK) at 1000 bar. The crude extract was centrifuged at 15000 rpm at 4 °C for 15 min and the supernatant was ultra-centrifuged at 40000 rpm at 4 °C for additional 75 min. The pellets with the membrane bound enzyme were resuspended in assay-buffer containing 50 mM Tris/HCl (pH 7.8), 2 mM 1,4 DTT (40 ml) and an aliquot of 500 µL were stored at -20 °C.

7.7.2.2. UbiA enzyme inhibition assay

Enzyme reactions (100 µL) contained 10% DMSO with a final concentration of 10 mM inhibitor, 2 mM p-hydroxybenzoic acid, 2.5 mM geranyl diphosphate (GPP), 5 mM MgCl₂ dissolved in assay buffer 45 mM Tris/HCl (pH 7.8), and 25 µl of UbiA membrane fraction in 50 mM Tris/HCl (pH 7.8) containing 2 mM DTT. The reaction was initiated by the addition of the enzyme (25 µL) and incubated for 10 min at 37°C and 250 rpm. Reaction products were extracted with ethyl acetate (500 µL). A portion of this ethyl acetate (450 µL) was taken and evaporated under N₂ stream. The residue was re-dissolved in methanol (100 µL), containing

100 μM p-hydroxybiphenyl as HPLC internal standard. The product formation of GHB was then analyzed by HPLC, quantified using the AUC (area under the curve) and standardized using the AUC of the internal standard.

7.7.2.3. IC₅₀ values

IC₅₀ values (concentration where the enzyme activity is reduced down to 50%) were calculated with SigmaPlot graphing software (version 12.0) using the four-parameter logistic equation.

7.7.2.4. HPLC conditions

Analytical HPLC separation was performed on an Agilent 1100 HPLC system (Agilent, USA) equipped with an Agilent 1100 multi wavelength detector. Samples (0.2 μl) were applied to a C18 column (Ascentis Express C18 2.7 μm , 5 cm x 1 mm I.D., Supelco (Sigma-Aldrich), Pennsylvania, USA), and prenylated products was eluted isocratically with methanol/H₂O (50:50, v/v) containing 0.1% aqueous formic acid at a flow rate of 50 $\mu\text{l min}^{-1}$. The chromatographic process was recorded at 260 nm. All results are expressed as relative conversion which means the ratio of the product formation in the presence to the product formation in the absence of the inhibitor

All experiments for UbiA were performed according to Julia Kufka (PhD thesis, IPB-Halle, Prof. Wessjohann) and the inhibition was calculated by Amina Msonga (PhD thesis, IPB-Halle, Prof. Wessjohann).

7.7.3. Aromatic prenyltransferase NphB

7.7.3.1. NphB expression and purification

Expression and purification is described in chapter 7.2.

7.7.3.2. NphB enzyme inhibition assay

Enzyme reactions (100 μl) contained 5 mM MgCl₂, 5 mM 1,6-DHN, 5 mM GPP and 20 nM purified NphB dissolved in assay buffer (50 mM Tris/HCl, 100 mM NaCl, pH 7.4). The reactions, which were initiated by the addition of the enzyme, were measured at 25°C for 1

h using an UV/Vis-spectrometer. The product formation was followed at a $\lambda=345$ nm minus $\lambda=600$ nm. The UV/Vis approach is described in chapter 5.2.

7.7.4. Aromatic prenyltransferase MenA

7.7.4.1. MenA enzyme inhibition assay

Enzyme reactions (100 μ L) contained 12% DMSO without inhibitor, 5 mM 1,4-dihydroxy-2-naphthoic acid (1,4-DHN-2A), 5 mM GPP, 5 mM $MgCl_2$ dissolved in assay buffer 50 mM Tris/100 mM NaCl (pH 7.5), and 5 μ L of MenA membrane fraction in 50 mM Tris/HCl (pH 7.8). The reaction was initiated by the addition of the enzyme and incubated for 10 min at 37°C and 350 rpm (linear product formation (Supplementary Figure 4)). Reaction products were extracted with *n*-hexane (300 μ L) containing 100 μ M *p*-hydroxybiphenyl as HPLC internal standard. *n*-Hexane (250 μ L) were taken and evaporated under N.stream. The residue was re-dissolved in methanol (200 μ L). The product formation of 2-geranyl-naphthalene-1,4-dione was then analyzed and quantified by HPLC.

7.7.4.2. MenA enzyme expression and membrane fraction preparation

The MenA wild-type (originally derived from an *E. coli* K12 construct) was cloned in the pET15b-TEV vector and expressed in Rosetta gami (DE3) pLysS $\Delta menA$ cells. A pre-culture (50 ml) of LB medium with 100 μ g ml^{-1} ampicillin was incubated at 37 °C under agitation overnight. The pre-culture was added to LB medium (1L) containing 100 μ g ml^{-1} ampicillin and then incubated at 37 °C until an OD_{600} of 0.8 was reached. The expression was induced by adding 300 μ L of 1 M IPTG and further overnight incubation at 30 °C. Cells were harvested by centrifugation at 4200 rpm for 25 min at 4 °C and the pellet was resuspended 50 mM Tris/HCl pH 8.5. For membrane fraction preparation, the cells were disrupted by a high-pressure homogenizer (1200 bar) and the debris cells were separated by centrifugation at 10.000 g for 12 minutes at 4 °C. The pellet was discharged and supernatant was centrifuged at 100.000 g for 2 h at 4 °C. The resulting pellet was resuspended in homogenization buffer (50 mM Tris/HCl pH 8.5, 0.15 M KCl) using a Potter/Elvehjem PTFE pestle and glass tube. The membrane fraction was frozen with liquid nitrogen and stored at -20 °C.

7.7.4.3. Analytical HPLC separation

Analytical HPLC separation was performed on an Agilent 1100 HPLC system (Agilent, USA) equipped with an Agilent 1100 multi wavelength detector. Samples (0.2 μl) were applied to a C18 column (YMC-Pack, R-ODS-5-A, 250 x 4.6 mm I.D., S-5 μm , 120 A, YMC Co., Ltd., Kyoto, Japan), and prenylated products were eluted starting with 95% water for 4 min followed by an acetonitrile increase up to 100% over 15 min and 5 min at 100% acetonitrile. Both solvents contained 0.2 % formic acid. The flow rate was 0.8 ml min⁻¹. The chromatographically process was recorded at 254 nm. For calculation, the total AUC (integration of the area under the curve) was taken and divided by the integrated peak area of the interested product. All values were expressed as relative conversion which means the ratio of the product formation among the time.

7.7.4.4. Product elucidation

Enzymatic conversions were performed as previously described and scaled up to 6 ml. The extraction procedure was carried out with *n*-hexane without internal standard and the solvent was evaporated under an N₂ stream. The extract was re-dissolved in CD₃OD. The ¹H-NMR spectra were recorded on a 400 MHz NMR spectrometer (Agilent DD2 400, USA). Chemical shifts were referenced to internal tetramethylsilane at 0 ppm. The product was confirmed (Figure 54).

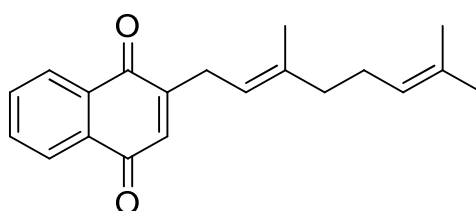


Figure 54. Biocatalytic conversion to 2-geranyl-naphthalene-1,4-dione starting with 1,4-dihydroxy-2-naphthoic acid (1,4-DHN-2A) and GPP in the presence of purified *E. coli* MenA. This product gets auto-decarboxylation and oxidation to 2-geranyl-naphthalene-1,4-dione under this condition. The structure was confirmed by ¹H-NMR, IR and HRMS.

¹H-NMR of 2-geranyl-naphthalene-1,4-dione (product was synthesized biocatalytically from 1,4-dihydroxy-2-naphthoic acid and GPP by MenA)

MS (ESI) calculation for C₂₀H₂₂O₂ (M), 294,16198; found 295.2; ¹H-NMR (CD₃OD) δ = 1.52 (d, J = 0.7 Hz, 3H, H-10'), 1.56 (d, J = 1.0 Hz, 3H, H-8'), 1.86 (d, J = 1.0 Hz, 3H, H-9'), 1.96 (m, J = 15.5 Hz, 2H,

H-4'), 2.04 (*m*, $J = 15.0$ Hz, 2H, *H-5'*), 3.69 (*d*, $J = 6.2$ Hz, 2H, *H-1'*), 5.03 (*m*, $J = 14.0$ Hz, 1H, *H-6'*), 5.17 (*m*, $J = 12.0$ Hz, 1H, *H-2'*), 6.60 (*dd*, $J = 0.8, 7.4$ Hz, 1H, *H-2*); 7.01 (*d*, $J = 9.0$ Hz, 1H, *H-7*); 7.17 (*dd*, $J = 7.4, 8.6$ Hz, 1H, *H-3*); 7.29 (*dt*, $J = 0.6, 0.8, 8.6$ Hz, 1H, *H-4*); 7.94 (*dd*, $J = 0.6, 9.0$ Hz, 1H, *H-8*) ppm.

IR-spectrum confirmed the absence of the hydroxy group due the missing band in the range of 3600 till 3200 nm. Instead, the $\lambda_{C=O} = 1760-1720$ nm confirms the presences of the 1,4-dione motif.

8. Zusammenfassung

Selektive C-C Verknüpfungen gehören zu den schwierigsten Reaktionen in der Biologie und Chemie. Die vorliegende Arbeit befasst sich speziell mit einer Gruppe der alkylierenden Enzyme, die solche C-C-Verknüpfungen ermöglichen.

Kapitel 1 gibt einen allgemeinen Überblick über die Anwendung prenylierter Verbindungen, eine kurze Beschreibung der Isoprenoid-Vorläufer IPP und DMAPP und deren biologischen Ursprung. Es gibt eine Einführung in die Enzymfamilie elongierender Prenyltransferasen und der aromatischen Prenyltransferase NphB.

Das zweite Kapitel beginnt mit einer Einführung zu linearen Prenyltransferasen. Diese Enzym-Familie katalysiert konsekutiv die Kondensation von Isopentenyl-diphosphat (IPP) an ein allylisches Prenyldiphosphat und verlängert auf diese Weise die Startereinheit. Das industriell forcierte Ziel bestand im Screening verschiedener Enzyme, um einen Kandidaten zu finden, der Farnesyl-diphosphate mit alternativen Isopentenyl-diphosphat-Substraten verlängert. Die *cis*-Prenyltransferasen von *H. pylori*, *M. luteus* und *M. tuberculosis* und die poly-Prenyltransferase von *H. brasiliensis* wurden zu diesem Zweck aufgereinigt und auf die Umsetzung artifiziellen homoallylischen Substraten (BPP und Cl-BPP) getestet. *M. luteus* und *M. tuberculosis* katalysierten erfolgreich die Kondensation von Cl-BPP, jedoch nicht die Konjugation von BPP an das allylischen Substrat. Diese Resultate wurden letztendlich mit jenen von Dr. Jeanette Keim, Dr. Steve Ludwig, Prof. Dr. Wessjohann und der Firma Lanxess in einem Patent verwertet.

Das dritte Kapitel befasst sich mit den Studien zur aromatischen Prenyltransferase NphB. Dieses Enzym katalysiert die Geranylierung von Polyphenolen bevorzugt am Kohlenstoff in *ortho*-Stellung zur Hydroxy-Gruppe. Zielgerichtete Mutagenese-Studien erfolgten, um die katalytischen Kaskade und die molekularen Abläufe der Kondensationsreaktion besser zu verstehen. Anhand dieser Daten wurde eine katalytische Diade postuliert. Es scheint, dass die Tyrosine 121, 175 und 216 eine entscheidend Rolle bei der Aktivierung und Stabilisierung des Produktintermediates spielen. Interessanterweise zeigten die Mutation V49E und V294A eine Aktivitätssteigerung um etwa 30% gegenüber dem Wildtyp. Computergestützte Modelle verdeutlichen, dass die Glutaminsäure den aromatischen Ring aktiviert und zudem dessen Lage gegenüber dem Geranylrest verändert. Die unübliche Geranylierung in *para*-Position bestätigt diese Arbeitstheorie. Die Mutation des Valins (V294A) bewirkt hingegen

eine Öffnung der Bindetasche und damit ein schnelleres Binden/Freilassen des Substrates/Produktes. Besonders hervorzuheben sind die Mutanten Y288E, welche eine unveränderte enzymatische Aktivität aufweisen und dabei ein ausgewogenes Produktverhältnis von 1:1:1 (2-Geranyl-1,6-DHN, 4-Geranyl-1,6-DHN und 5-Geranyl-1,6-DHN) aufweist. Die Mutation M162W ist interessant, da sie eine 25% Restaktivität hat und ausschließlich das Produkt 5-Geranyl-1,6-DHN bildet. Neben den Mutationsstudien wurde die Umsetzung von 14 synthetischen allylischen Prenyldonoren und 24 aromatischen Substraten (Prenylakzeptoren) getestet und die Produkte strukturell aufgeklärt mit NMR-Spektroskopie und HRMS. Die von NphB umgesetzten artifiziellen Prenyldiphosphate zeichneten sich vor allem dadurch aus, dass sie eine längerer Kettenlänge als GPP aufweisen dürfen (**1**, *E,E*-FPP, **2**). Nicht akzeptiert wurden kürzeren Kettenlängen als C₁₀, intramolekulare Heteroatome oder *cis*-konjugierte Prenyleinheiten. Bei den aromatischen Substraten ist besonders hervorzuheben, dass Naringenin, 4'-O-Ethylerydiol und 1,6-DHN umgesetzt werden. Interessanterweise kam es bei den Flavonen häufig zur Sauerstoff-Prenylierung an Position 7 des A-Ringes.

Kapitel 4 enthält Anwendungsbeispiele der NphB-Produkte. Besonders hervorzuheben ist die antimykotische Wirkung des prenylierten gegenüber dem nicht-prenylierten 1,6-DHN. Des Weiteren wurde getestet, ob eine Zyklisierung der Geranyl-Gruppe mit der *ortho*-ständigen Hydroxy-Gruppe möglich ist, jedoch konnte das Ziel mit der Tetrahydrocannabinol-Zyklase aus *Cannabis sativa* nicht erreicht werden.

Kapitel 5 beschreibt die Methodenentwicklung eines UV/Vis-Assays zur Bestimmung enzymkinetischer Parameter. Auf diese Weise konnte die Umsetzung der verschiedenen Prenyl-Donoren, die Charakterisierung von Mutanten und in einem kompetitiven Inhibitionsassay, der hemmende Einfluss von Geranyldiphosphat-Mimetika untersucht werden. Des Weiteren wurde ein quantitatives NMR Verfahren validiert, um auch kleine Mengen der NphB-Produkte zu bestimmen und für die in Kapitel 2 beschriebenen Anwendungen bereit zu stellen.

Die Ergebnisse des kompetitiven Inhibitionsassay sind in Kapitel 6 beschrieben. Zudem wurden die NphB-Resultate mit denen der aromatische Prenyltransferase MenA und UbiA verglichen.

9. References

- [1] *ENCYCLOPEDIA BRITANNICA*, Focus Multimedia Ltd, **2014**.
- [2] H. Ohvo-Rekil??, B. Ramstedt, P. Leppim??ki, J. Peter Slotte, *Progress in Lipid Research* **2002**, *41*, 66–97.
- [3] G. A. Armstrong, J. E. Hearst, *The FASEB journal : official publication of the Federation of American Societies for Experimental Biology* **1996**, *10*, 228–237.
- [4] M. L. Miller, I. Ojima, *Chem. Rec.* **2001**, *1*, 195–211.
- [5] R. MULLIN, *Chemical & Engineering News Archive* **2011**, *89*, 12–18.
- [6] E. E. Slater, J. S. MacDonald, *Drugs* **1988**, *36 Suppl 3*, 72–82.
- [7] D. W. Russell, *Cardiovascular drugs and therapy / sponsored by the International Society of Cardiovascular Pharmacotherapy* **1992**, *6*, 103–110.
- [8] C. J. Dinsmore, I. M. Bell, *Current topics in medicinal chemistry* **2003**, *3*, 1075–1093.
- [9] Y. Qiao, J. Gao, Y. Qiu, L. Wu, F. Guo, K. Kam-Wing Lo, D. Li, *European Journal of Medicinal Chemistry* **2011**, *46*, 2264–2273.
- [10] T. Kuzuyama, *Bioscience, biotechnology, and biochemistry* **2002**, *66*, 1619–1627.
- [11] T. Kuzuyama, H. Seto, *Proceedings of the Japan Academy. Series B, Physical and biological sciences* **2012**, *88*, 41–52.
- [12] J. L. Goldstein, M. S. Brown, *Nature* **1990**, *343*, 425–430.
- [13] T. Kuzuyama, H. Seto, *Natural product reports* **2003**, *20*, 171–183.
- [14] M. Rohmer, *Nat Prod Rep* **1999**, *16*, 565–574.
- [15] M. Sapir-Mir, A. Mett, E. Belausov, S. Tal-Meshulam, A. Frydman, D. Gidoni, Y. Eyal, *Plant Physiology* **2008**, *148*, 1219–1228.
- [16] F. Lynen, H. Eggerer, U. Henning, I. Kessel, *Angewandte Chemie* **1958**, *70*, 738–742.
- [17] B. A. Kellogg, C. D. Poulter, *Current opinion in chemical biology* **1997**, *1*, 570–578.
- [18] M. K. Dhar, A. Koul, S. Kaul, *New Biotechnology* **2013**, *30*, 114–123.
- [19] C. M. Starks, K. Back, J. Chappell, J. P. Noel, *Science (New York, N.Y.)* **1997**, *277*, 1815–1820.
- [20] J. Pandit, D. E. Danley, G. K. Schulte, S. Mazzalupo, T. A. Pauly, C. M. Hayward, E. S. Hamanaka, J. F. Thompson, H. J. Harwood, *The Journal of biological chemistry* **2000**, *275*, 30610–30617.

- [21] R. Do, R. S. Kiss, D. Gaudet, J. C. Engert, *Clinical Genetics* **2009**, *75*, 19–29.
- [22] A. Rak, O. Pylypenko, A. Niculae, K. Pyatkov, R. S. Goody, K. Alexandrov, *Cell* **2004**, *117*, 749–760.
- [23] M. C. Chang, J. D. Keasling, *Nat Chem Biol* **2006**, *2*, 674–681.
- [24] J. C. Verdoes, G. Sandmann, H. Visser, M. Diaz, M. van Mossel, A. J. van Ooyen, *Appl Environ Microbiol* **2003**, *69*, 3728–3738.
- [25] K. Cornish, *Nat Prod Rep* **2001**, *18*, 182–189.
- [26] Y. Kharel, T. Koyama, *Nat Prod Rep* **2003**, *20*, 111–118.
- [27] T. Koyama, *Biosci Biotechnol Biochem* **1999**, *63*, 1671–1676.
- [28] D. Sasaki, M. Fujihashi, N. Okuyama, Y. Kobayashi, M. Noike, T. Koyama, K. Miki, *J Biol Chem* **2011**, *286*, 3729–3740.
- [29] K. Ohtake, N. Saito, S. Shibuya, W. Kobayashi, R. Amano, T. Hirai, S. Sasaki, C. Nakano, T. Hoshino, *FEBS J* **2014**, *281*, 5479–5497.
- [30] M. Nagaki, T. Ichijo, R. Kobashi, Y. Yagihashi, T. Musashi, J. Kawakami, N. Ohya, T. Gotoh, H. Sagami, *Journal of Molecular Catalysis B: Enzymatic* **2012**, *80*, 1–6.
- [31] S. Takahashi, T. Koyama, *Chem Rec* **2006**, *6*, 194–205.
- [32] L. A. Wessjohann, H. F. & K. Schreckenbach G. N., in *Biocatalysis in Organic Synthesis, Vol. 2 (Science of Synthesis)*. (Ed.: K. & F. Faber W.-D.), **2015**, pp. 177–211.
- [33] N. Shimizu, T. Koyama, K. Ogura, *Journal of Biological Chemistry* **1998**, *273*, 19476–19481.
- [34] J. C. Sacchettini, C. D. Poulter, *Science* **1997**, *277*, 1788–1789.
- [35] R. Cao, C. K.-M. Chen, R.-T. Guo, A. H.-J. Wang, E. Oldfield, *Proteins: Structure, Function, and Bioinformatics* **2008**, *73*, 431–439.
- [36] P. Baer, P. Rabe, K. Fischer, C. A. Citron, T. A. Klapschinski, M. Groll, J. S. Dickschat, *Angewandte Chemie International Edition* **2014**, n/a–n/a.
- [37] M. F. Mabanglo, M. A. Hast, N. B. Lubock, H. W. Hellinga, L. S. Beese, *Protein Sci* **2014**, *23*, 289–301.
- [38] X. Han, C. C. Chen, C. J. Kuo, C. H. Huang, Y. Zheng, T. P. Ko, Z. Zhu, X. Feng, K. Wang, E. Oldfield, et al., *Proteins* **2015**, *83*, 37–45.
- [39] O. Saleh, Y. Haagen, K. Seeger, L. Heide, *Phytochemistry* **2009**, *70*, 1728–1738.
- [40] K. Sasaki, K. Mito, K. Ohara, H. Yamamoto, K. Yazaki, *Plant Physiol* **2008**, *146*, 1075–1084.

- [41] K.-H. Teng, P.-H. Liang, *Bioorganic Chemistry* **2012**, *43*, 51–57.
- [42] K. Kinoshita, K. Sadanami, A. Kidera, N. Go, *Protein Engineering* **1999**, *12*, 11–14.
- [43] S.-Y. Chang, T.-P. Ko, A. P.-C. Chen, A. H.-J. Wang, P.-H. Liang, *Protein Science* **2004**, *13*, 971–978.
- [44] S.-Y. Chang, T.-P. Ko, P.-H. Liang, A. H.-J. Wang, *Journal of Biological Chemistry* **2003**, *278*, 29298–29307.
- [45] Y.-H. Chen, A. P.-C. Chen, C.-T. Chen, A. H.-J. Wang, P.-H. Liang, *Journal of Biological Chemistry* **2002**, *277*, 7369–7376.
- [46] S.-Y. Chang, Y.-K. Chen, A. H.-J. Wang, P.-H. Liang, *Biochemistry* **2003**, *42*, 14452–14459.
- [47] T.-P. Ko, Y.-K. Chen, H. Robinson, P.-C. Tsai, Y.-G. Gao, A. P.-C. Chen, A. H.-J. Wang, P.-H. Liang, *Journal of Biological Chemistry* **2001**, *276*, 47474–47482.
- [48] M. Nagaki, K. Kimura, H. Kimura, Y. Maki, E. Goto, T. Nishino, T. Koyama, *Bioorganic & medicinal chemistry letters* **2001**, *11*, 2157–9.
- [49] M. Nagaki, K. Kuwahara, K. Kimura, J. Kawakami, Y. Maki, S. Ito, N. Morita, T. Nishino, T. Koyama, *Journal of Molecular Catalysis B: Enzymatic* **2003**, *22*, 97–103.
- [50] M. Nagaki, M. Nakada, T. Musashi, J. Kawakami, T. Endo, Y. Maki, T. Koyama, *Journal of Molecular Catalysis B: Enzymatic* **2009**, *59*, 225–230.
- [51] M. Nagaki, S. Sato, Y. Maki, T. Nishino, T. Koyama, *Journal of Molecular Catalysis - B Enzymatic* **2000**, *9*, 33–38.
- [52] K. Fujikura, Y. Maki, N. Ohya, M. Satoh, T. Koyama, *Bioscience, biotechnology, and biochemistry* **2008**, *72*, 851–855.
- [53] M. Nagaki, H. Yamamoto, A. Takahashi, Y. Maki, J. Ishibashi, T. Nishino, T. Koyama, *Journal of Molecular Catalysis - B Enzymatic* **2002**, *17*, 81–89.
- [54] J. Keim, Biokatalytische Umsetzung von Natürlichen Und Artifiziiellen Prenyldiphosphaten, Halle, Univ., Naturwissenschaftliche Fakultät I., **2014**.
- [55] Y.-P. Lu, H.-G. Liu, P.-H. Liang, *Biochemical and Biophysical Research Communications* **2009**, *379*, 351–355.
- [56] Y.-P. Lu, H.-G. Liu, K.-H. Teng, P.-H. Liang, *Biochemical and Biophysical Research Communications* **2010**, *400*, 758–762.
- [57] C. Sallaud, D. Rontein, S. Onillon, F. Jabes, P. Duffe, C. Giacalone, S. Thoraval, C. Escoffier, G. Herbette, N. Leonhardt, et al., *The Plant cell* **2009**, *21*, 301–317.
- [58] H. Hashizume, R. Sawa, S. Harada, M. Igarashi, H. Adachi, Y. Nishimura, A. Nomoto, *Antimicrobial agents and chemotherapy* **2011**, *55*, 3821–3828.

- [59] G. Manat, S. Roure, R. Auger, A. Bouhss, H. Barreteau, D. Mengin-Lecreulx, T. Touze, *Microbial drug resistance (Larchmont, N.Y.)* **2014**, *20*, 199–214.
- [60] M. Sato, K. Sato, S. Nishikawa, A. Hirata, J. Kato, A. Nakano, *Molecular and cellular biology* **1999**, *19*, 471–483.
- [61] C.-J. Kuo, R.-T. Guo, I.-L. Lu, H.-G. Liu, S.-Y. Wu, T.-P. Ko, A. H.-J. Wang, P.-H. Liang, *Journal of biomedicine & biotechnology* **2008**, *2008*, 841312.
- [62] W. Zhu, Y. Zhang, W. Sinko, M. E. Hensler, J. Olson, K. J. Molohon, S. Lindert, R. Cao, K. Li, K. Wang, et al., *Proceedings of the National Academy of Sciences of the United States of America* **2013**, *110*, 123–128.
- [63] R.-T. Guo, T.-P. Ko, A. P.-C. Chen, C.-J. Kuo, A. H.-J. Wang, P.-H. Liang, *The Journal of biological chemistry* **2005**, *280*, 20762–20774.
- [64] M. Fujihashi, Y. W. Zhang, Y. Higuchi, X. Y. Li, T. Koyama, K. Miki, *Proceedings of the National Academy of Sciences of the United States of America* **2001**, *98*, 4337–4342.
- [65] W. Wang, C. Dong, M. McNeil, D. Kaur, S. Mahapatra, D. C. Crick, J. H. Naismith, *Journal of molecular biology* **2008**, *381*, 129–140.
- [66] K. Asawatreratanakul, Y.-W. Zhang, D. Wititsuwannakul, R. Wititsuwannakul, S. Takahashi, A. Rattanapittayaporn, T. Koyama, *European journal of biochemistry / FEBS* **2003**, *270*, 4671–4680.
- [67] T. Bamba, T. Sando, A. Miyabashira, K. Gyokusen, Y. Nakazawa, Y. Su, E. Fukusaki, A. Kobayashi, *Z Naturforsch C* **2007**, *62*, 579–582.
- [68] T. Schmidt, A. Hillebrand, D. Wurbs, D. Wahler, M. Lenders, C. Schulze Gronover, D. Prüfer, *Plant Molecular Biology Reporter* **2010**, *28*, 277–284.
- [69] B. Bukau, A. L. Horwich, *Cell* **1998**, *92*, 351–366.
- [70] A. A. Baykov, O. A. Evtushenko, S. M. Avaeva, *Analytical biochemistry* **1988**, *171*, 266–270.
- [71] T. P. Geladopoulos, T. G. Sotiroidis, A. E. Evangelopoulos, *Analytical biochemistry* **1991**, *192*, 112–116.
- [72] D. Kaur, P. J. Brennan, D. C. Crick, *Journal of bacteriology* **2004**, *186*, 7564–7570.
- [73] N. E. Vollhardt, K. Peter C. / Schore, *Organische Chemie*, Wiley-VCH, Weinheim, **2011**.
- [74] S. Dodbele, C. D. Martinez, J. M. Troutman, *Biochemistry* **2014**, *53*, 5042–5050.
- [75] L. Heide, *Curr Opin Chem Biol* **2009**, *13*, 171–179.
- [76] T. Bonitz, V. Alva, O. Saleh, A. N. Lupas, L. Heide, *PLoS One* **2011**, *6*, e27336.

- [77] K. Yazaki, K. Sasaki, Y. Tsurumaru, *Phytochemistry* **2009**, *70*, 1739–1745.
- [78] A. Di Pietro, G. Conseil, J. M. Perez-Victoria, G. Dayan, H. Baubichon-Cortay, D. Trompier, E. Steinfels, J. M. Jault, H. de Wet, M. Maitrejean, et al., *Cell Mol Life Sci* **2002**, *59*, 307–322.
- [79] B. Botta, A. Vitali, P. Menendez, D. Misiti, G. Delle Monache, *Curr Med Chem* **2005**, *12*, 717–739.
- [80] H. Li, Z. Ban, H. Qin, L. Ma, A. J. King, G. Wang, *Plant physiology* **2015**, *167*, 650–659.
- [81] D. Pockrandt, S. M. Li, *Chembiochem* **2013**, *14*, 2023–2028.
- [82] J. M. Schuller, G. Zocher, M. Liebhold, X. Xie, M. Stahl, S. M. Li, T. Stehle, *J Mol Biol* **2012**, *422*, 87–99.
- [83] M. Anioł, A. Świdarska, M. Stompor, A. K. Żoźnierczyk, *Medicinal Chemistry Research* **2012**, *21*, 4230–4238.
- [84] A. M. Keiler, O. Zierau, G. Kretzschmar, *Planta Medica* **2013**, *79*, 576–579.
- [85] D. Nikolic, Y. Li, L. R. Chadwick, S. Grubjesic, P. Schwab, P. Metz, R. B. van Breemen, *Drug metabolism and disposition: the biological fate of chemicals* **2004**, *32*, 272–279.
- [86] D. G. Panaccione, *FEMS Microbiol Lett* **2005**, *251*, 9–17.
- [87] U. Metzger, C. Schall, G. Zocher, I. Unsold, E. Stec, S. M. Li, L. Heide, T. Stehle, *Proc Natl Acad Sci U S A* **2009**, *106*, 14309–14314.
- [88] S. Sirikantaramas, F. Taura, Y. Tanaka, Y. Ishikawa, S. Morimoto, Y. Shoyama, *Plant and Cell Physiology* **2005**, *46*, 1578–1582.
- [89] B. Scott, C. A. Young, S. Saikia, L. K. McMillan, B. J. Monahan, A. Koulman, J. Astin, C. J. Eaton, A. Bryant, R. E. Wrenn, et al., *Toxins* **2013**, *5*, 1422–1446.
- [90] B. A. Chauder, C. C. Lopes, R. S. C. Lopes, A. J. M. da Silva, V. Snieckus, *Synthesis* **1998**, *1998*, 279–282.
- [91] P. Ballester, M. Capo, X. Garcias, J. M. Saa, *The Journal of Organic Chemistry* **1993**, *58*, 328–334.
- [92] T. Kuzuyama, J. P. Noel, S. B. Richard, *Nature* **2005**, *435*, 983–987.
- [93] T. Kumano, S. B. Richard, J. P. Noel, M. Nishiyama, T. Kuzuyama, *Bioorg Med Chem* **2008**, *16*, 8117–8126.
- [94] P. Koehl, *Nature chemical biology* **2005**, *1*, 71–72.

- [95] S. Rosselli, M. Bruno, A. Maggio, R. A. Raccuglia, M. Safder, C.-Y. Lai, K. F. Bastow, K.-H. Lee, *Phytochemistry* **2011**, *72*, 942–945.
- [96] B. A. Schütz, A. D. Wright, T. Rali, O. Sticher, *Phytochemistry* **1995**, *40*, 1273–1277.
- [97] F. Taura, S. Morimoto, Y. Shoyama, *J Biol Chem* **1996**, *271*, 17411–17416.
- [98] M. Tello, T. Kuzuyama, L. Heide, J. P. Noel, S. B. Richard, *Cell Mol Life Sci* **2008**, *65*, 1459–1463.
- [99] T. Bonitz, V. Alva, O. Saleh, A. N. Lupas, L. Heide, *PLoS ONE* **2011**, *6*, DOI 10.1371/journal.pone.0027336.
- [100] R. Klein, Modellierung von Prenyltransferasen Und Terpensynthasen Und Untersuchungen Zum Molekularen Docking von Reaktionsintermediaten, Martin-Luther-Universität Halle-Wittenberg, **2014**.
- [101] L. A. Wessjohann, B. Sontag, M. A. Dessoy, in (Ed.: ed. H.-G. Schmalz), *Bioorganic Chemistry Highlights And New Aspects*, Wiley-VCH, Weinheim, *Organic Chemistry Highlights IV*, Wiley-VCH, Weinheim, **1999**, pp. 79–88.
- [102] L. Wessjohann, S. Zakharova, D. Schulze, J. Kufka, R. Weber, L. Bräuer, W. Brandt, *Chimia* **2009**, *63*, 340–344.
- [103] M. Liebhold, X. Xie, S. M. Li, *Org Lett* **2012**, *14*, 4882–4885.
- [104] Y. Yang, Y. Miao, B. Wang, G. Cui, K. M. Merz, *Biochemistry* **2012**, *51*, 2606–2618.
- [105] M. E. Tanner, *Natural product reports* **2015**, *32*, 88–101.
- [106] G. Cui, X. Li, K. M. Merz Jr., *Biochemistry* **2007**, *46*, 1303–1311.
- [107] T. Kumano, S. B. Richard, J. P. Noel, M. Nishiyama, T. Kuzuyama, *Bioorganic and Medicinal Chemistry* **2008**, *16*, 8117–8126.
- [108] R. A. Weber, Synthese Und Biokatalytische Umsetzung von Prenyldiphosphaten, Martin-Luther-Universität Halle-Wittenberg, **2011**.
- [109] L. Y. P. Luk, Q. Qian, M. E. Tanner, *Journal of the American Chemical Society* **2011**, *133*, 12342–12345.
- [110] E. Stec, N. Steffan, A. Kremer, H. Zou, X. Zheng, S.-M. Li, *ChemBioChem* **2008**, *9*, 2055–2058.
- [111] D. J. Hosfield, Y. Zhang, D. R. Dougan, A. Broun, L. W. Tari, R. V Swanson, J. Finn, *Journal of Biological Chemistry* **2004**, *279*, 8526–8529.
- [112] U. Metzger, C. Schall, G. Zocher, I. Unsöld, E. Stec, S.-M. Li, L. Heide, T. Stehle, *Proceedings of the National Academy of Sciences of the United States of America* **2009**, *106*, 14309–14314.

- [113] H. L. Ruan, E. Stec, S. M. Li, *Archives of microbiology* **2009**, *191*, 791–795.
- [114] J. H. G. Lebbink, A. Fish, A. Reumer, G. Natrajan, H. H. K. Winterwerp, T. K. Sixma, *Journal of Biological Chemistry* **2010**, *285*, 13131–13141.
- [115] D. N. Brems, H. C. Rilling, *On the Mechanism of the Prenyltransferase Reaction. Metal Ion Dependent Solvolysis of an Allylic Pyrophosphate*, *J Am Chem Soc.* 1977 Dec 7;99(25):8351-2., **n.d.**
- [116] S. Frick, R. Nagel, A. Schmidt, R. R. Bodemann, P. Rahfeld, G. Pauls, W. Brandt, J. Gershenzon, W. Boland, A. Burse, *Proceedings of the National Academy of Sciences of the United States of America* **2013**, *110*, 4194–9.
- [117] S. Ohnuma, T. Koyama, K. Ogura, *Biochem Biophys Res Commun* **1993**, *192*, 407–412.
- [118] R. D. Shannon, *Acta Crystallographica Section A* **1976**, *32*, 751–767.
- [119] R. D. Shannon, C. T. Prewitt, *Journal of Inorganic and Nuclear Chemistry* **1970**, *32*, 1427–1441.
- [120] N. Pace, E. Weerapana, *Biomolecules* **2014**, *4*, 419–434.
- [121] Y. Kharel, Y. W. Zhang, M. Fujihashi, K. Miki, T. Koyama, *The Journal of biological chemistry* **2001**, *276*, 28459–28464.
- [122] W. Cheng, W. Li, *Science (New York, N.Y.)* **2014**, *343*, 878–81.
- [123] L. Song, C. D. Poulter, *Proc Natl Acad Sci U S A* **1994**, *91*, 3044–3048.
- [124] Q. Qian, A. W. Schultz, B. S. Moore, M. E. Tanner, *Biochemistry* **2012**, *51*, 7733–7739.
- [125] F. H. Wallrapp, J.-J. Pan, G. Ramamoorthy, D. E. Almonacid, B. S. Hillerich, R. Seidel, Y. Patskovsky, P. C. Babbitt, S. C. Almo, M. P. Jacobson, et al., *Proceedings of the National Academy of Sciences of the United States of America* **2013**, *110*, E1196–202.
- [126] L. Bräuer, W. Brandt, L. A. Wessjohann, *J Mol Model* **2004**, *10*, 317–327.
- [127] Y. Shoyama, A. Takeuchi, F. Taura, T. Tamada, M. Adachi, R. Kuroki, S. Morimoto, *Acta Crystallogr Sect F Struct Biol Cryst Commun* **2005**, *61*, 799–801.
- [128] D. Baker, G. Pryce, G. Giovannoni, A. J. Thompson, *Lancet Neurol* **2003**, *2*, 291–298.
- [129] R. Mechoulam, *Science* **1970**, *168*, 1159–1165.
- [130] Y. Gaoni, R. Mechoulam, *Journal of the American Chemical Society* **1964**, *86*, 1646–1647.
- [131] F. Taura, *Drug Discov Ther* **2009**, *3*, 83–87.

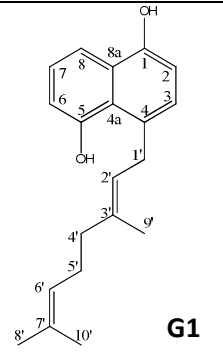
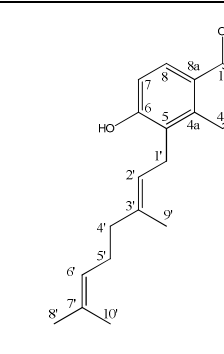
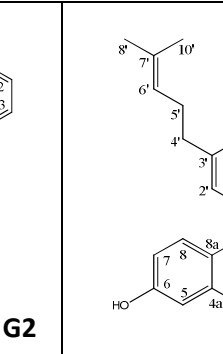
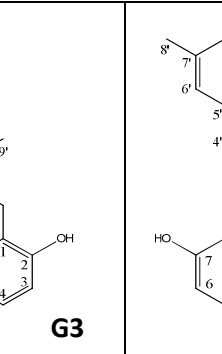
- [132] Y. Shoyama, T. Tamada, K. Kurihara, A. Takeuchi, F. Taura, S. Arai, M. Blaber, S. Morimoto, R. Kuroki, *J Mol Biol* **2012**, *423*, 96–105.
- [133] M. S. Dwiyantri, T. Yamada, M. Sato, J. Abe, K. Kitamura, *BMC Plant Biol* **2011**, *11*, 152.
- [134] D. Jakubczyk, J. Z. Cheng, S. E. O'Connor, *Natural product reports* **2014**, *31*, 1328–38.
- [135] N. Gerhards, L. Neubauer, P. Tudzynski, S.-M. Li, *Toxins* **2014**, *6*, 3281–3295.
- [136] F. Taura, S. Morimoto, Y. Shoyama, R. Mechoulam, *Journal of the American Chemical Society* **1995**, *117*, 9766–9767.
- [137] M. Henze, M. Beyer, H. Klink, J.-A. Verreet, *Plant Disease* **2007**, *91*, 1445–1449.
- [138] M. Nowicki, E. U. Kozik, M. R. Foolad, in *Translational Genomics for Crop Breeding*, John Wiley & Sons Ltd, **2013**, pp. 241–265.
- [139] R. Gonzalez-Fernandez, J. V Jorriin-Novo, *Journal of proteome research* **2012**, *11*, 3–16.
- [140] T. A. Unger, *Pesticide Synthesis Handbook*, Elsevier Science, **1996**.
- [141] M. Liu, G. Wang, L. Xiao, X. Xu, X. Liu, P. Xu, X. Lin, *Marine drugs* **2014**, *12*, 3838–3851.
- [142] E. M. Soylu, S. Kurt, S. Soylu, *International journal of food microbiology* **2010**, *143*, 183–189.
- [143] D.-S. Yang, J.-G. Wei, W.-B. Peng, S.-M. Wang, C. Sun, Y.-P. Yang, K.-C. Liu, X.-L. Li, *Fitoterapia* **2014**, *99*, 261–266.
- [144] S. K. Adla, F. Sasse, G. Kelter, H.-H. Fiebig, T. Lindel, *Organic & biomolecular chemistry* **2013**, *11*, 6119–6130.
- [145] K. Rullah, M. F. F. Mohd Aluwi, B. M. Yamin, M. N. Abdul Bahari, L. S. Wei, S. Ahmad, F. Abas, N. H. Ismail, I. Jantan, L. K. Wai, *Bioorganic & medicinal chemistry letters* **2014**, *24*, 3826–3834.
- [146] K. Y. Khaw, S. B. Choi, S. C. Tan, H. A. Wahab, K. L. Chan, V. Murugaiyah, *Phytomedicine : international journal of phytotherapy and phytopharmacology* **2014**, *21*, 1303–1309.
- [147] H. A. Jung, T. Yokozawa, B.-W. Kim, J. H. Jung, J. S. Choi, *The American journal of Chinese medicine* **2010**, *38*, 415–429.
- [148] H. Yu, J. C. Sutton, *Canadian Journal of Plant Pathology* **1997**, *19*, 237–246.
- [149] G. Van der Auwera, R. De Baere, Y. Van de Peer, P. De Rijk, I. Van den Broeck, R. De Wachter, *Molecular biology and evolution* **1995**, *12*, 671–678.

- [150] S. M. Bowman, S. J. Free, *BioEssays : news and reviews in molecular, cellular and developmental biology* **2006**, 28, 799–808.
- [151] G. Qin, Y. Zong, Q. Chen, D. Hua, S. Tian, *International journal of food microbiology* **2010**, 138, 145–150.
- [152] S. Gong, J. Hao, Y. Xia, X. Liu, J. Li, *Pest management science* **2009**, 65, 1337–1343.
- [153] D. P. Hollis, *Analytical Chemistry* **1963**, 35, 1682–1684.
- [154] U. H. W. B. T.-N. M. R. S. in P. A. Diehl, Ed. , **2008**, 493–501.
- [155] C. Simmler, J. G. Napolitano, J. B. McAlpine, S.-N. Chen, G. F. Pauli, *Current opinion in biotechnology* **2014**, 25, 51–59.
- [156] S. Akoka, L. Barantin, M. Trierweiler, *Analytical chemistry* **1999**, 71, 2554–2557.
- [157] K. I. Marro, D. Lee, E. G. Shankland, C. M. Mathis, C. E. Hayes, C. E. Amara, M. J. Kushmerick, *Journal of magnetic resonance (San Diego, Calif. : 1997)* **2008**, 194, 67–75.
- [158] K. Mehr, B. John, D. Russell, D. Avizonis, *Analytical chemistry* **2008**, 80, 8320–8323.
- [159] I. W. Burton, M. A. Quilliam, J. A. Walter, *Analytical chemistry* **2005**, 77, 3123–3131.
- [160] M. Farag, A. Porzel, J. Schmidt, L. Wessjohann, *Metabolomics* **2012**, 8, 492–507.
- [161] D. J. Cookson, B. E. Smith, *Analytical Chemistry* **1982**, 54, 2591–2593.
- [162] R. Crouch, D. Russell, I. Agilent Technologies, S. C. C. 95051, USA, *Easy, Precise and Accurate Quantitative NMR Application Note*, **2011**.
- [163] V. Silvestre, S. Goupry, M. Trierweiler, R. Robins, S. Akoka, *Analytical chemistry* **2001**, 73, 1862–1868.
- [164] Dimitar Vasilev, Synthesis of Isoprenyl Diphosphate Surrogates as Potential Inhibitors of Prenyl Converting Enzymes, Halle, Univ., Naturwissenschaftliche Fakultät II., **2015**.
- [165] L. A. Wessjohann, H. F. Schreckenbach, G. N. Kaluđerović, in *Science of Synthesis*, **2015**, pp. 177–211.
- [166] L. A. Wessjohann, J. Keim, B. Weigel, M. Dippe, *Curr Opin Chem Biol* **2013**, 17, 229–235.
- [167] M. L. Nickerson, A. D. Bosley, J. S. Weiss, B. N. Kostiha, Y. Hirota, W. Brandt, D. Esposito, S. Kinoshita, L. Wessjohann, S. G. Morham, et al., *Human Mutation* **2013**, 34, 317–329.
- [168] M. L. Nickersen, B. N. Kostiha, W. Brandt, W. Fredericks, K.-P. Xu, F.-S. Yu, B. Gold, J. Chodosh, M. Goldberg, D. W. Lu, et al., *PLoS One* **2010**, 5, e10760.

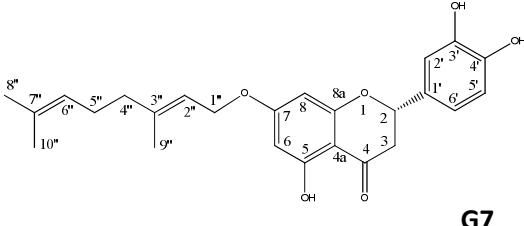
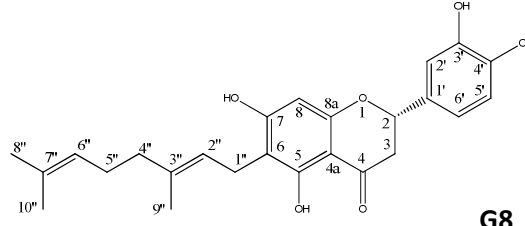
- [169] K. Nakagawa, Y. Hirota, N. Sawada, N. Yuge, M. Watanabe, Y. Uchino, N. Okuda, Y. Shimomura, Y. Suhara, T. Okano, *Nature* **2010**, *468*, 117–121.
- [170] L. A. Wessjohann, B. Sonntag, *Angew. Chem. Int. Ed. Engl* **1996**, *35*, 1697–1699.
- [171] L. Bräuer, W. Brandt, D. Schulze, S. Zakharova, L. Wessjohann, *ChemBiochem* **2008**, *9*, 982–992.
- [172] D. H. Bishop, K. P. Pandya, H. K. King, *Biochem J* **1962**, *83*, 606–614.
- [173] B. A. Haddock, C. W. Jones, *Bacteriol Rev* **1977**, *41*, 47–99.
- [174] K. Andries, P. Verhasselt, J. Guillemont, H. W. Gohlmann, J. M. Neefs, H. Winkler, J. Van Gestel, P. Timmerman, M. Zhu, E. Lee, et al., *Science* **2005**, *307*, 223–227.
- [175] M. Kurosu, E. Begari, *Molecules* **2010**, *15*, 1531–1553.
- [176] S. Zakharova, M. Fulhorst, L. Luczak, L. A. Wessjohann, *Arkivoc* **2004**, 79–96.
- [177] W. Brandt, L. Bräuer, N. Gunnewich, J. Kufka, F. Rausch, D. Schulze, E. Schulze, R. Weber, S. Zakharova, L. Wessjohann, *Phytochemistry* **2009**, *70*, 1758–1775.
- [178] K. Suvarna, D. Stevenson, R. Meganathan, M. E. Hudspeth, *Journal of bacteriology* **1998**, *180*, 2782–2787.
- [179] J. Debnath, S. Siricilla, B. Wan, D. C. Crick, A. J. Lenaerts, S. G. Franzblau, M. Kurosu, *Journal of medicinal chemistry* **2012**, *55*, 3739–3755.
- [180] M. Melzer, L. Heide, *Biochimica et Biophysica Acta (BBA) - Lipids and Lipid Metabolism* **1994**, *1212*, 93–102.
- [181] L. C. Tarshis, P. J. Proteau, B. A. Kellogg, J. C. Sacchettini, C. D. Poulter, *Proc Natl Acad Sci U S A* **1996**, *93*, 15018–15023.
- [182] R. M. Phan, C. D. Poulter, *Org Lett* **2000**, *2*, 2287–2289.
- [183] M. Fulhorst, Prenyltransferases as Potential Biocatalysts., Martin-Luther-Universität Halle-Wittenberg: Halle (Saale), **2003**.
- [184] M. M. Bradford, *Anal Biochem* **1976**, *72*, 248–254.
- [185] L. V Lee, B. Granda, K. Dean, J. Tao, E. Liu, R. Zhang, S. Peukert, S. Wattanasin, X. Xie, N. S. Ryder, et al., *Biochemistry* **2010**, *49*, 5366–5376.
- [186] X. Yu, X. Xie, S. M. Li, *Appl Microbiol Biotechnol* **2011**, *92*, 737–748.
- [187] J.K. Cho, Y.B. Ryu, M. J. Curtis-Long, H. W. Ryu, H. J. Yuk, D. W. Kim, H. J. Kim, W. S. Lee, K. H. Park, *Bioorg. Med. Chem.* **2012**, *20*, 2595-602

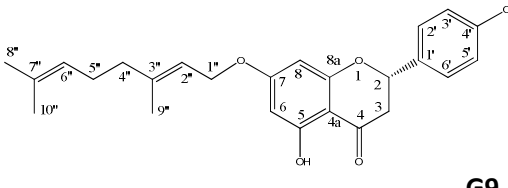
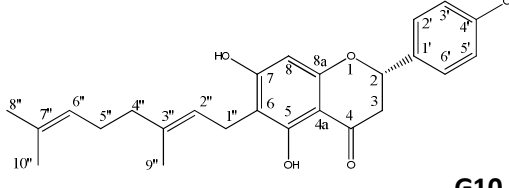
10. Appendix

10.1. ¹H-NMR-Data of aromatic prenylated products mediated by NphB.

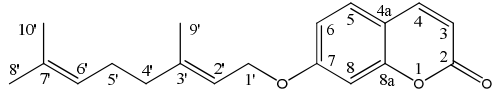
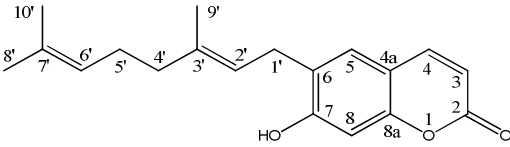
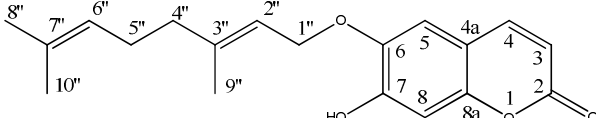
| Compd. |  |  |  |  |
|--------|---|---|---|--|
| | G1 | G2 | G3 | G4 |
| | 4-geranyl-1,5-DHN | 5-geranyl-1,6-DHN | 1-geranyl-2,6-DHN | 1-geranyl-2,7-DHN |
| Pos. | δ_H , multi., J | δ_H , multi., J | δ_H , multi., J | δ_H , multi., J |
| 1 | / | / | / | / |
| 2 | 6.94, d, 7.6 Hz | 6.60, dd, 7.4, 0.8, Hz | / | / |
| 3 | 7.25, d, 7.6 Hz | 7.17, dd, 8.6, 7.4 Hz | 6.90, d, 9.0 Hz | 6.87, d, 8.8 Hz |
| 4 | / | 7.29, dt, 8.6, 0.8, 0.6 Hz | 7.01, d, 9.0 Hz | 7.44, d, 8.8 Hz |
| 5 | / | / | 7.12, d, 2.5 Hz | 7.56, d, 8.8 Hz |
| 6 | 6.87, dd, 7.6, 0.9 Hz | / | / | 6.83, dd, 8.8, 2.4 Hz |
| 7 | 7.31, dd, 8.5, 7.6 Hz | 7.01, d, 9.0 Hz | 6.79, dd, 9.1, 2.5 Hz | / |
| 8 | 7.67, d, 8.5 Hz | 7.94, dd, 0.6, 9.0 Hz | 7.58, d, 9.1 Hz | 6.89, d, 2.3 Hz |
| 1' | 4.70, d, 6.4 Hz | 3.69, d, 6.2 Hz | 3.70, d, 6.3 Hz | 3.69, d, 6.2 Hz |
| 2' | 5.12 - 5.03, m | 5.17, m | 5.17, m | 5.17, m, 12.0 Hz |
| 3' | / | / | / | / |
| 4' | 2.20 - 2.00, m | 1.96, m | 1.96, m | 1.96, m, 15.5 Hz |
| 5' | 2.20 - 2.00, m | 2.04, m | 2.05, m | 2.04, m, 15.0 Hz |
| 6' | 5.09, m | 5.03, m | 5.01, m | 5.03, m, 14.0 Hz |
| 7' | / | / | / | / |
| 8' | 1.63, s | 1.56, d, 1.0 Hz | 1.55, d, 1.1 Hz | 1.56, d, 1.0 Hz |
| 9' | 1.74, s | 1.86, d, 1.0 Hz | 1.85, d, 1.1 Hz | 1.86, d, 1.0 Hz |
| 10' | 1.57, s | 1.52, d, 0.7 Hz | 1.51, d, 0.5 Hz | 1.52, d, 0.7 Hz |
| HRMS | calc. mass [C ₂₀ H ₂₄ O ₂ -H] : 295,17035 | | | |
| found: | 295.1702 | 295.1700 | 295.1701 | 295.1703 |
| | Solvent: DMSO [d6] | Solvent: CD ₃ OD | | |
| | | | | Confirmed in literature ^[186] (data not shown) |

| | | |
|-----------|---|---|
| | <p style="text-align: right;">G5</p> | <p style="text-align: right;">G6</p> |
| Positions | 3-geranyl-2,4,6-trihydroxyacetophenone | 1-geranyl-2-naphthalene |
| | δ_H , multi., <i>J</i> | δ_H , multi., <i>J</i> |
| 1 | / | / |
| 2 | / | / |
| 3 | / | 7.09, d, 8.8 Hz |
| 4 | / | 7.56, d, 8.8 Hz |
| 5 | 5.89, s | 7.71, d, 8.0 Hz |
| 6 | / | 7.23, ddd, 8.0, 6.9, 1.2 Hz |
| 7 | | 7.38, ddd, 8.5, 6.9, 1.2 Hz |
| 8 | | 7.82, d, 8.5 Hz |
| 1' | 3.17, d, 7.1 Hz | 3.74, d, 6.6 Hz |
| 2' | 5.16, m | 5.17, m |
| 3' | / | / |
| 4' | 2.04, dd, 14.6, 7.2 Hz | 2.09 – 1.93, m |
| 5' | 1.93, dd, 8.6, 6.3 Hz | 2.09 – 1.93, m |
| 6' | 5.05, m | 5.01, ddd, 7.0, 5.7, 1.3 Hz |
| 7' | / | / |
| 8' | 1.61, s | 1.54, s |
| 9' | 1.73, s | 1.87, s |
| 10' | 1.55, s | 1.51, s |
| 1'' | 2.59, s | |
| | [C ₁₈ H ₂₄ O ₄ -H] ⁻ Exact Mass: 303.1602 Found: 303.1605 | [C ₂₀ H ₂₄ O-H] ⁻ Exact Mass: . 280.1827 Found |

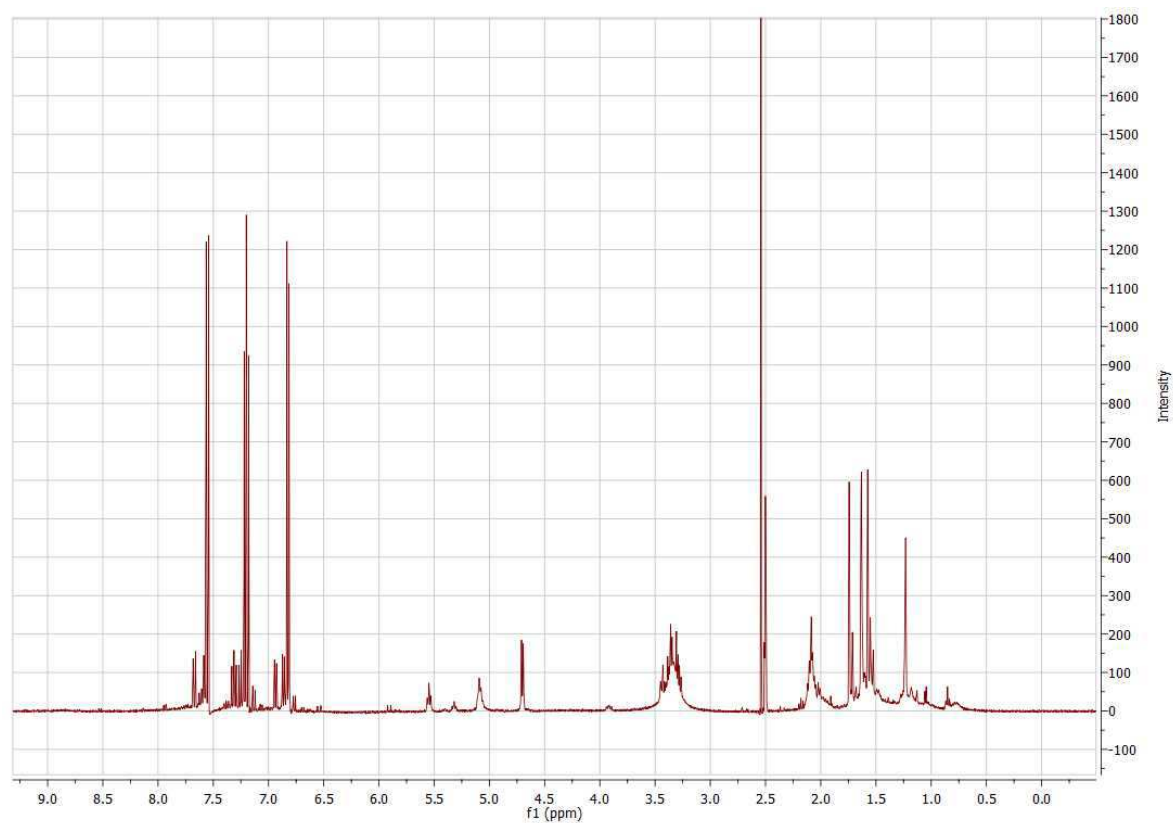
| |  G7 | |  G8 | |
|------|--|---------------------|---|---------------------|
| Pos. | 7-O-geranyl-eriodictyol | | 6-geranyl-eriodictyol | |
| | δ_{H} , multi., <i>J</i> | δ_{C} | δ_{H} , multi., <i>J</i> | δ_{C} |
| 1 | / | / | / | / |
| 2 | 5.31, dd, 12.7, 3.0 Hz | 80.7 | 5.25, dd, 12.8, 3.0 Hz | 80.4 |
| 3 | 3a: 2.72, dd, 17.2, 3.0 Hz 3b: 3.09, dd, 17.2, 12.7 Hz | 44.1 | 3a: 2.68, dd, 17.1, 3.0 Hz 3b: 3.05, dd, 17.1, 12.8 Hz | 44.2 |
| 4 | / | / | / | / |
| 5 | / | / | / | / |
| 6 | 6.03, d, 2.3 Hz | 95.3 | / | / |
| 7 | / | / | / | / |
| 8 | 6.01, d, 2.3 Hz | 96.1 | 5.94, s | 95.3 |
| 1'' | 4.58, d, 6.5 Hz | 66.4 | 3.21, d, 7.2 Hz | 21.7 |
| 2'' | 5.41, m | 120.3 | 5.19, m | 123.9 |
| 3'' | / | / | / | / |
| 4'' | 2.13, dd, 13.7, 7.2 Hz | 27.2 | 1.94, dd, 8.7, 6.1 Hz | 27.7 |
| 5'' | 2.07, dd, 10.7, 4.7 Hz | 40.4 | 2.05, dd, 14.6, 7.2 Hz | 40.9 |
| 6'' | 5.08, m | 124.9 | 5.06, m | 125.4 |
| 7'' | / | / | / | / |
| 8'' | 1.64, s | 26.2 | 1.61, s | 25.8 |
| 9'' | 1.74, s | 16.6 | 1.74, s | 16.2 |
| 10'' | 1.59, s | 18.1 | 1.56, s | 17.7 |
| 2' | 6.92, s | 114.8 | 6.91, s | 114.6 |
| 5' | 6.79, s | 116.3 | 6.80, s | 116.2 |
| 6' | 6.79, s | 119.3 | 6.78, s | 119.2 |
| | Determined by HSQC, HMBC and COESY Exact Mass: 423,18131 [C ₂₅ H ₂₈ O ₆ -H] | | Determined by HSQC, HMBC and COESY and confirmed by literature ^[187] [C ₂₅ H ₂₈ O ₆ -H] | |
| HRMS | 423.1813 | | 423.1825 | |

| |  G9 | |  G10 | |
|--|---|---------------|---|---------------|
| Positions | 7O-geranyl-naringenin | | 6-geranyl-naringenin | |
| | δ_H , multi., <i>J</i> | δ_C | δ_H , multi., <i>J</i> | |
| 1 | / | / | / | |
| 2 | 5.37 (dd, <i>J</i> =12.9, 2.9, 1H) | 80.45 | 5.31 (dd, <i>J</i> =12.9, 3.0, 1H) | 80.61 |
| 3 | 3a: 2.73 (dd, <i>J</i> =17.2, 2.9, 1H) 3b: 3.14 (dd, <i>J</i> =17.2, 12.9, 1H), | 44.20 | 3a: 2.68 (dd, <i>J</i> =17.1, 3.0, 1H), 3b: 3.10 (dd, <i>J</i> =17.1, 12.9, 1H) | 44.08 |
| 4 | / | 197.85 | / | 198.14 |
| 4a | | 103.22 | | 103.99 |
| 5 | / | 162.55 | / | 165.16 |
| 6 | 6.04 (d, <i>J</i> =2.2, 1H) | 109.71 | 5.93 (s, 1H) | 96.41 |
| 7 | / | 165.94 | / | 168.75 |
| 8 | 6.02, d, 2.2 Hz | 95.40 | / | 95.57 |
| 8a | | 162.46 | | 164.65 |
| 1' | 4.58 (d, <i>J</i> =6.5, 1H) | 21.79 | 3.21 (d, <i>J</i> =7.2, 1H) | 66.38 |
| 2' | 5.41, td, 6.5, 1.0 Hz | 128.98 | 5.19, m | 120.27 |
| 3' | / | 135.23 | / | 142.81 |
| 4' | 2.10, m | 40.90 | 2.05, dd, 14.4, 7.2 Hz | 40.53 |
| 5' | 2.10, m | 27.73 | 1.91-1.98 m | 27.29 |
| 6' | 5.08 (d, <i>J</i> =6.9, 1H) | 128.98 | 5.06, m | 124.85 |
| 7' | / | 131.26 | / | 132.67 |
| 8' | 1.64, s | 25.84 | 1.61, s | 25.83 |
| 9' | 1.74, s | 16.19 | 1.75, s | 16.66 |
| 10' | 1.59, s | 17.69 | 1.56, s | 17.74 |
| 1''/4'' | | 130.97/158.99 | | 130.97/159.08 |
| 2''/6'' | 7.32 (d, <i>J</i> =8.5, 1H) | 123.96/125.46 | 7.31 (d, <i>J</i> =8.5, 1H) | 129.06/129.06 |
| 3''/5'' | 6.81 (d, <i>J</i> =8.6, 1H) | 116.30/116.30 | 6.81 (d, <i>J</i> =8.6, 1H) | 116.32/116.32 |
| Confirmed by literature: ^{[92][94]} | | | | |
| HRMS | Exact Mass: [C ₂₅ H ₂₈ O ₅ - H] ⁺ calc. 407,1860 found. 407.1874 | | Exact Mass: [C ₂₅ H ₂₈ O ₅ - H] ⁺ calc. 407,1860 found. 407.1873 | |

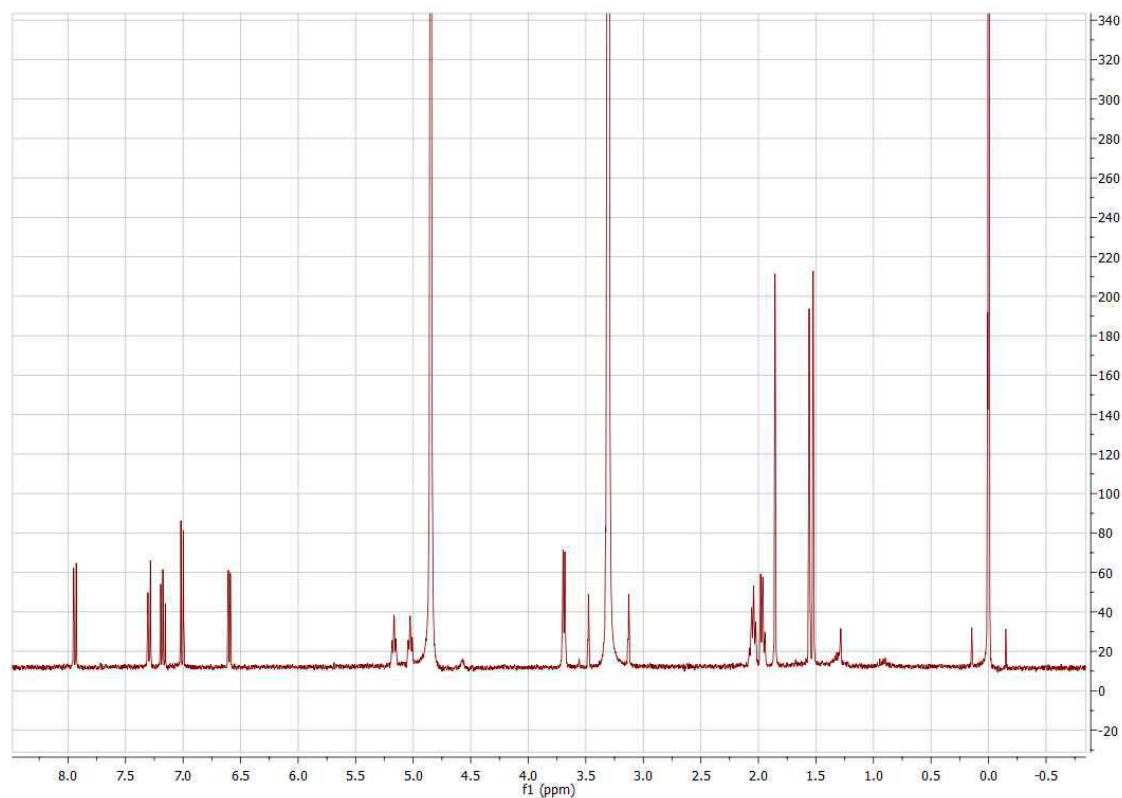
| | G11 | G12 | | |
|------|--|---|--|------------|
| Pos. | 7O-Geranyl-(2S)-2-(3',4'-(4''-ethoxy)-dihydroxyphenyl)-5,7-dihydroxy-4-chromanone | 6O-Geranyl-3-(3',4'-dimethoxyphenyl)-6,7-dihydroxycoumarin | | |
| | δ_H , multi., <i>J</i> | δ_C | δ_H , multi., <i>J</i> | δ_C |
| 1 | / | | / | / |
| 2 | 5.37, dd, 12.9, 3.0 Hz | 80.7 | / | 129.5 |
| 3 | 3a: 2.74, dd, 17.2, 3.0 Hz 3b: 3.16, dd, 17.1, 12.8 Hz | 44.1 | / | / |
| 4 | / | / | 7.93, s | 142.1 |
| 5 | / | / | 7.05, s | 113.0 |
| 6 | 6.05, d, 2.3 Hz | 95.5 | / | / |
| 7 | / | / | / | / |
| 8 | 6.02, d, 2.3 Hz | 96.4 | 6.94, s | 101.5 |
| 1'' | 4.59, d, 6.5 Hz | 66.3 | 4.76, d, Hz | 67.2 |
| 2'' | 5.41, m | 120.2 | 5.51, m | 120.4 |
| 3'' | / | / | / | / |
| 4'' | 2.13, dd, 13.7, 7.2 Hz | 27.2 | 2.13, m | 27.2 |
| 5'' | 2.07, dd, 9.4, 5.7 Hz | 40.4 | 2.13, m | 40.5 |
| 6'' | 5.09, m | 124.7 | 5.08, m | 124.8 |
| 7'' | / | / | / | / |
| 8'' | 1.64, s | 25.8 | 1.61, s | 24.9 |
| 9'' | 1.74, s | 15.9 | 1.81, s | 16.7 |
| 10'' | 1.60, s | 17.4 | 1.59, s | 17.7 |
| 1' | / | / | / | / |
| 2' | 7.06, d, 1.8 Hz | 112.5 | 7.34, d, <i>J</i> = 2.0 Hz | 113.5 |
| 5' | 6.82, d, 8.1 Hz | 116.1 | 7.00, d, <i>J</i> = 8.4 Hz | 112.6 |
| 6' | 6.92, dd, 8.2, 1.8 Hz | 120.5 | 7.28, dd, 8.4, 2.0 Hz | 122.5 |
| 1''' | 4.11, q, 7.0 Hz | 65.6 | 3.87, s | 150.7 |
| 2''' | 1.42, t, 7.0 Hz | 15.1 | 3.88, s | 150.7 |
| | Determined by HSQC, HMBC and COESY | | Determined by HSQC, HMBC and COESY | |
| | [C ₂₇ H ₃₂ O ₆ -H] ⁻ Exact Mass: 451,2126 | | [C ₂₇ H ₃₀ O ₆ -H] ⁻ Exact Mass: 449,1969 | |
| HRMS | 451.2131 | | 449.1971 | |

| |  G13 |  G14 |  G15 |
|------|---|--|--|
| Pos. | 7O-geranyl-umbelliferone | 6-geranyl-umbelliferone | 6O-geranyl-aesculetine |
| | δ_H , multi., J | δ_H , multi., J | δ_H , multi., J |
| 1 | / | / | / |
| 2 | / | / | / |
| 3 | 7.88, d, 9.5 Hz | 7.81, d, 9.4 Hz | 7.81, d, 9.4 Hz |
| 4 | 6.23, d, 9.5 Hz | 6.16, d, 9.4 Hz | 6.23, d, 9.4 Hz |
| 5 | 7.52, d, 8.6 Hz | 7.28, s | 6.91, s |
| 6 | 6.91, dd, 8.6, 2.4 Hz | / | / |
| 7 | / | / | / |
| 8 | 6.88, d, 2.4 Hz | 6.71, s | 6.97, s |
| 1' | 4.66, d, 6.5 Hz | 4.80 overlap | 4.75, d, 6.5 Hz |
| 2' | 5.45, m | 5.34, m | 5.49, m |
| 3' | / | / | / |
| 4' | 2.12, m | 2.13, dd, 14.0, 6.7 Hz | 2.12, m |
| 5' | 2.12, m | 2.05, dd, 12.9, 6.1 Hz | 2.14, m |
| 6' | 5.08, m | 5.10, m | 5.07, m |
| 7' | / | / | / |
| 8' | 1.62, s | 1.65, s | 1.60, s |
| 9' | 1.77, s | 1.71, s | 1.79, s |
| 10' | 1.59, s | 1.59, s | 1.58, s |
| | [C ₁₉ H ₂₂ O ₃ -H] ⁻ Exact Mass: 297,1496 | | Determined by HSQC, HMBC and COESY [C ₁₉ H ₂₂ O ₄ -H] ⁻ Exact Mass: 313,1445 |
| HRMS | 297.1502 | 297.1503 | 313.1450 |

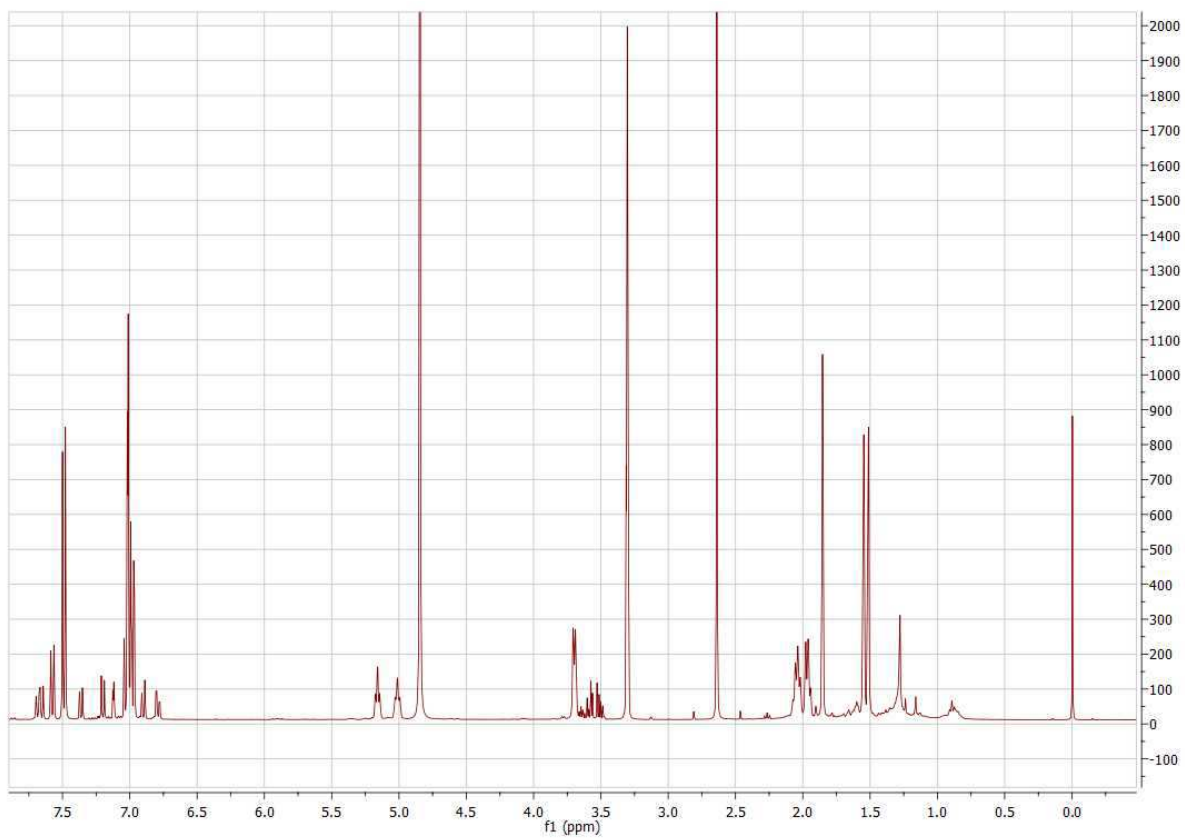
10.2. ^1H -NMR-spectra of geranylated NphB-enzyme-products



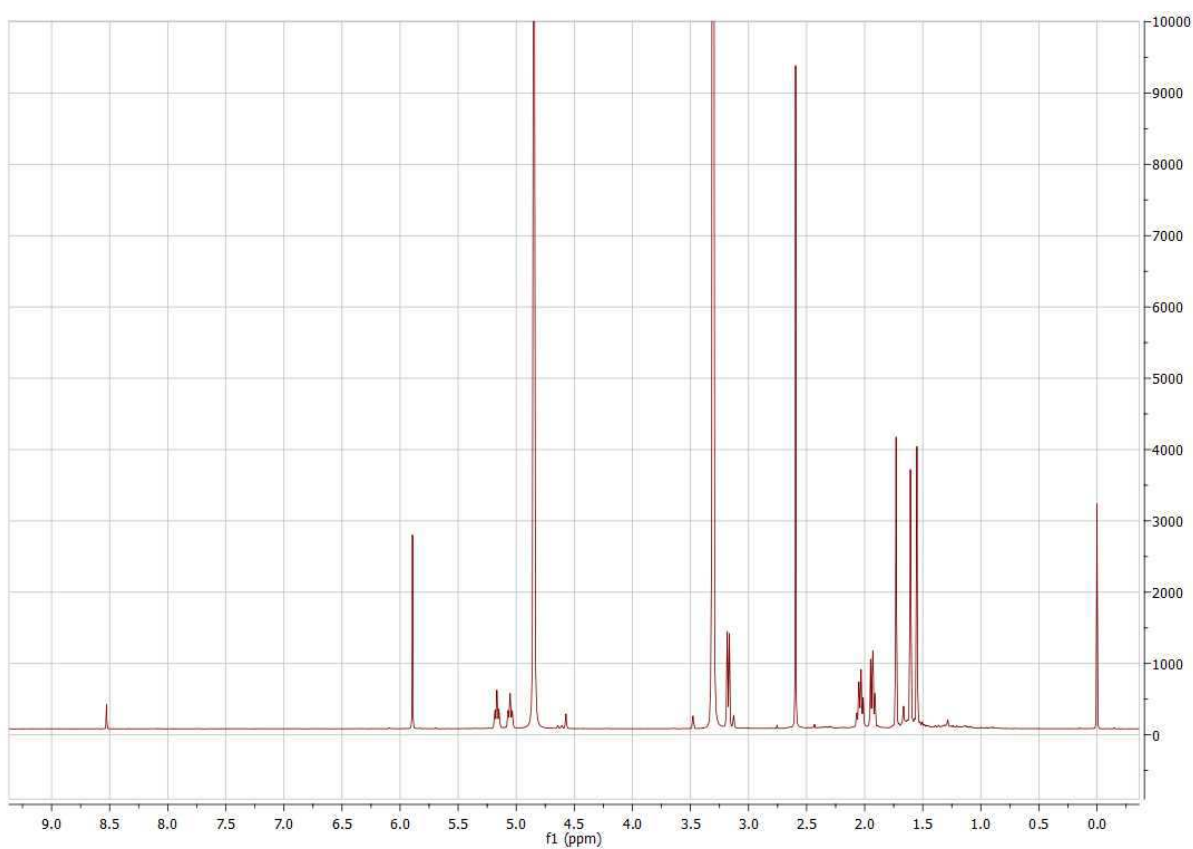
^1H -NMR-Spectra of 4-geranyl-1,5-dihydroxynaphthalene in DMSO-D_6 (**G1**)



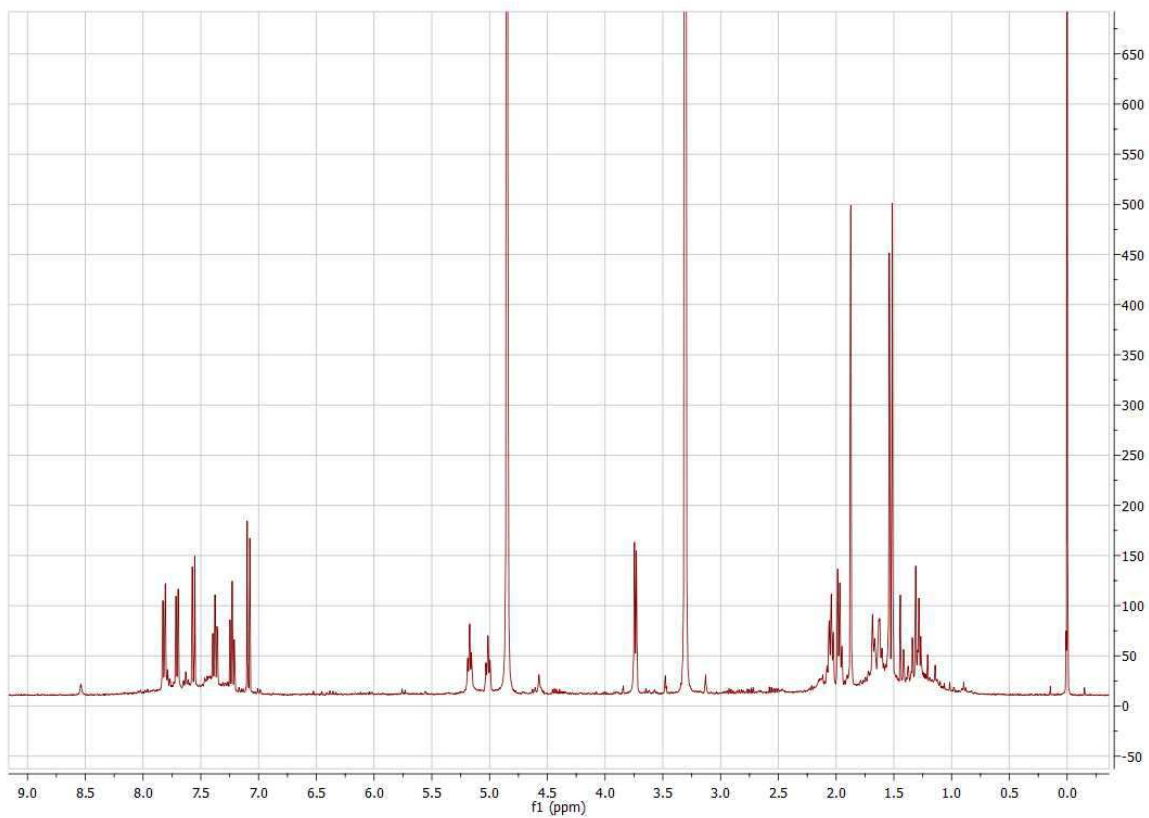
^1H -NMR-Spectra of 5-geranyl-1,6-dihydroxynaphthalene in CD_3OD (**G2**)



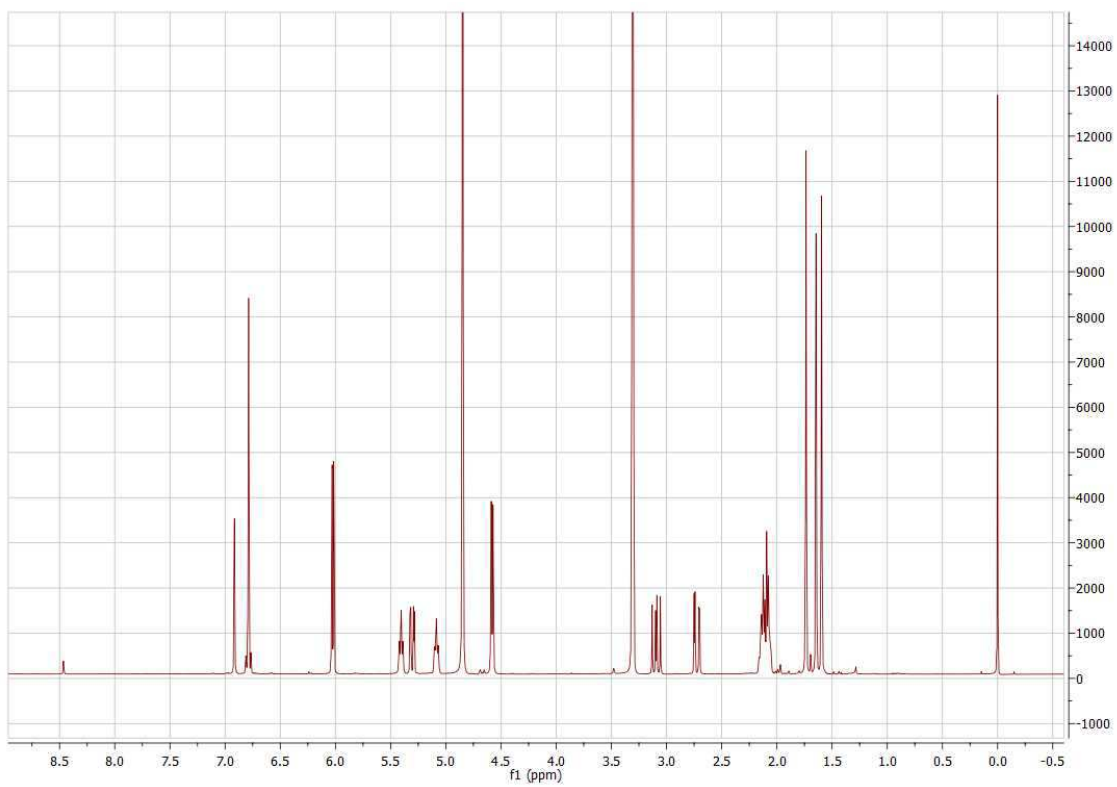
¹H-NMR-Spectra of 1-geranyl-2,6-dihydroxynaphthalene in CD₃OD (**G3**)



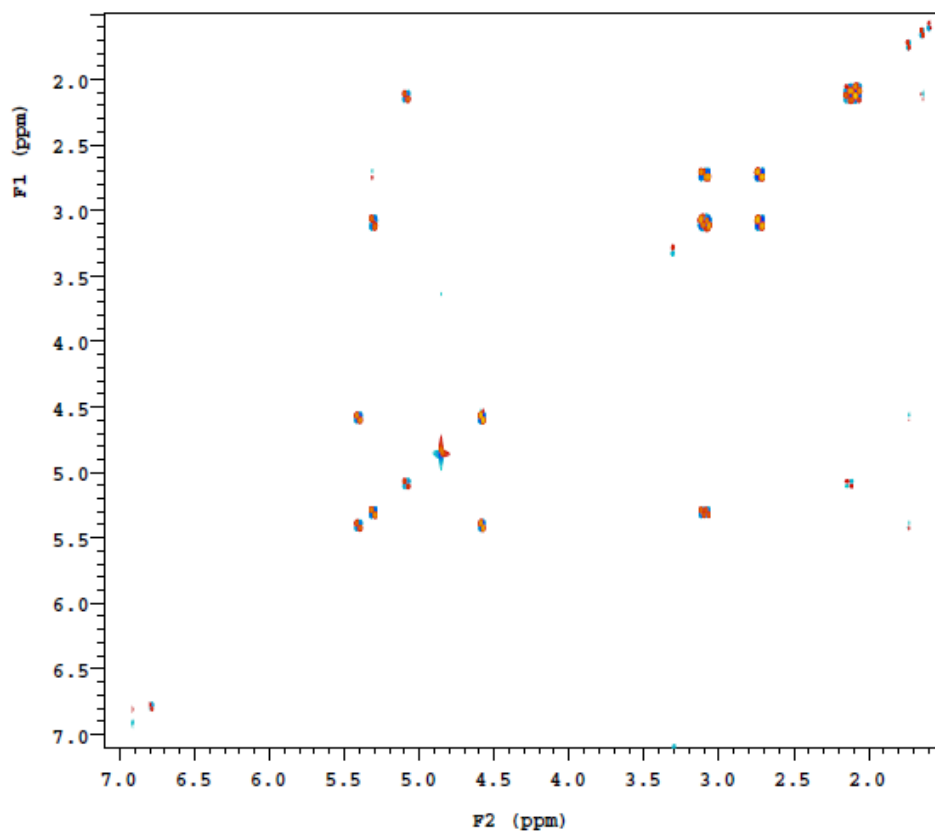
¹H-NMR-Spectra of 3-geranyl-2,4,6-trihydroxyacetophenone in CD₃OD (**G5**)



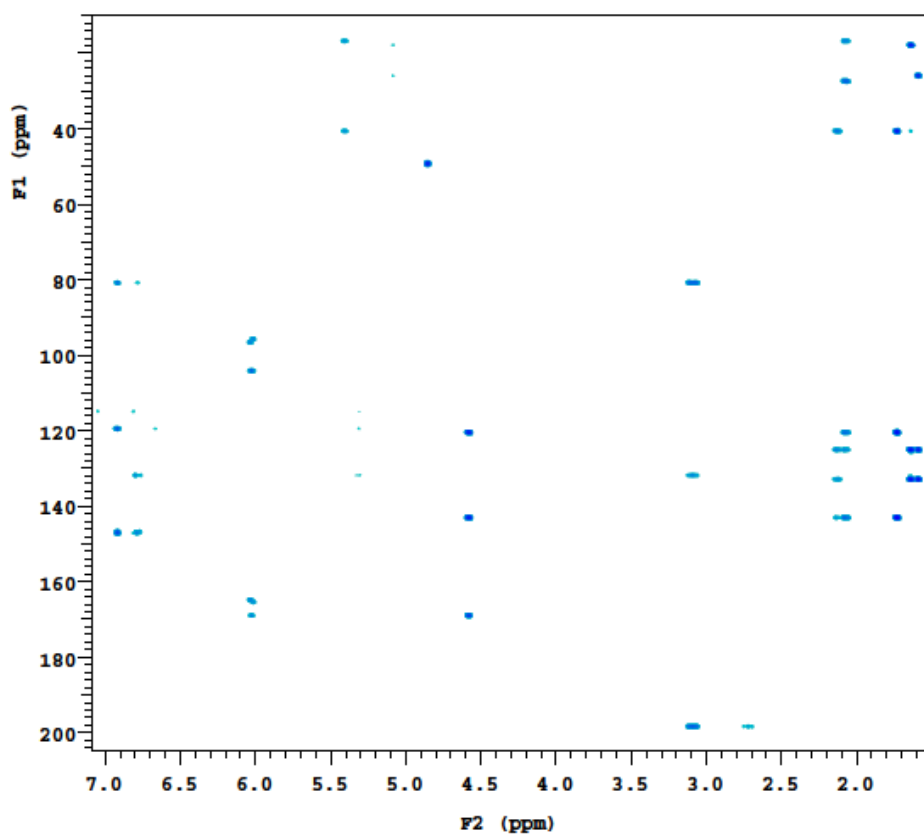
$^1\text{H-NMR}$ -Spectra of 1-geranyl-2-naphthalene in CD_3OD (G6)



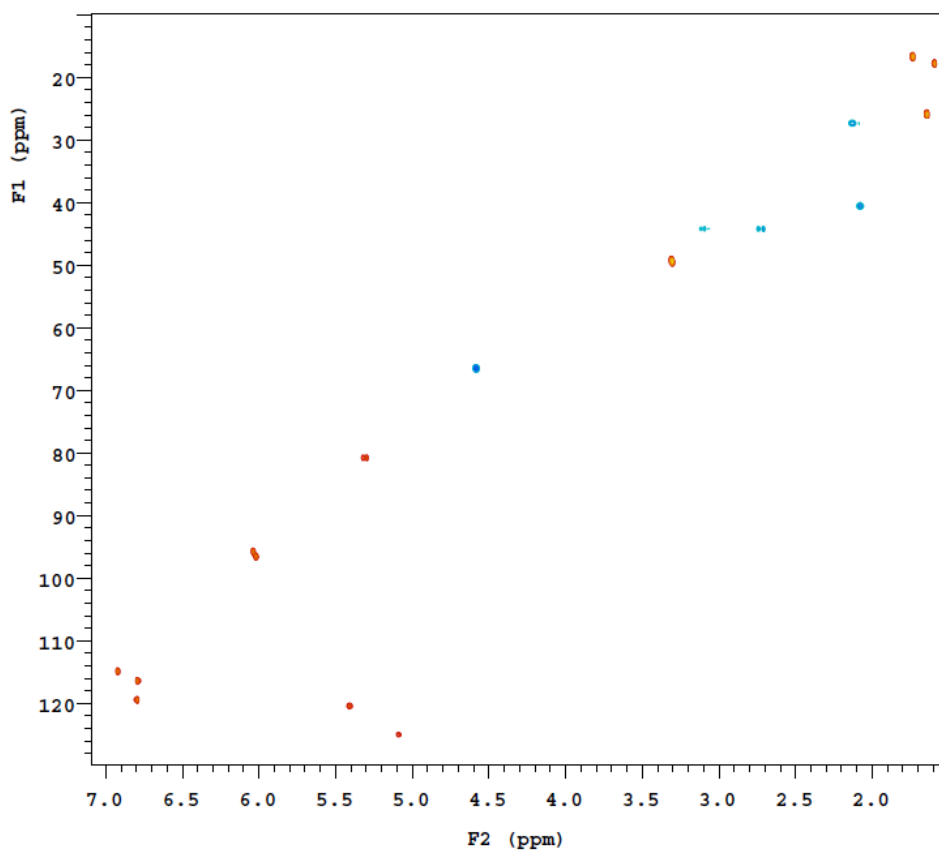
$^1\text{H-NMR}$ -Spectra of 7*O*-geranyl-eriodictyol in CD_3OD (G7)



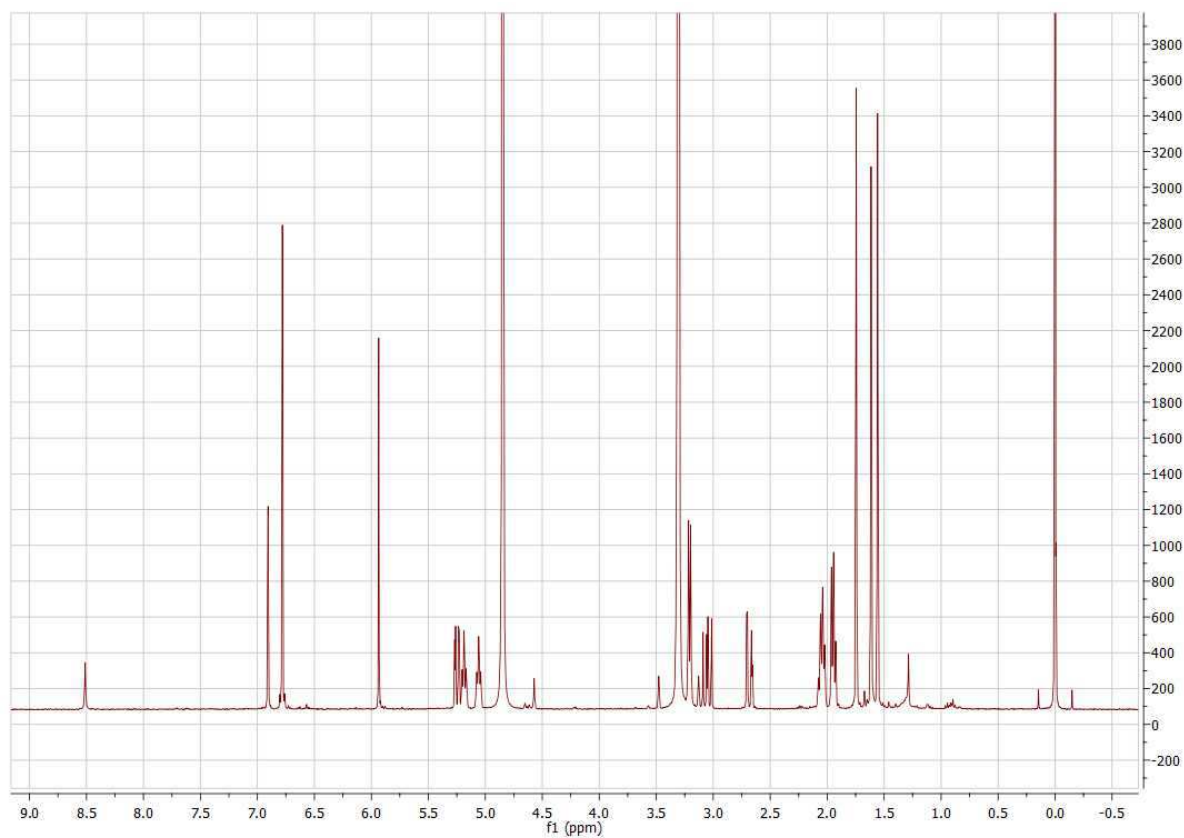
2D-NMR COSY spectra of 7*O*-geranyl-eriodictyol recorded in CD₃OD (G7)



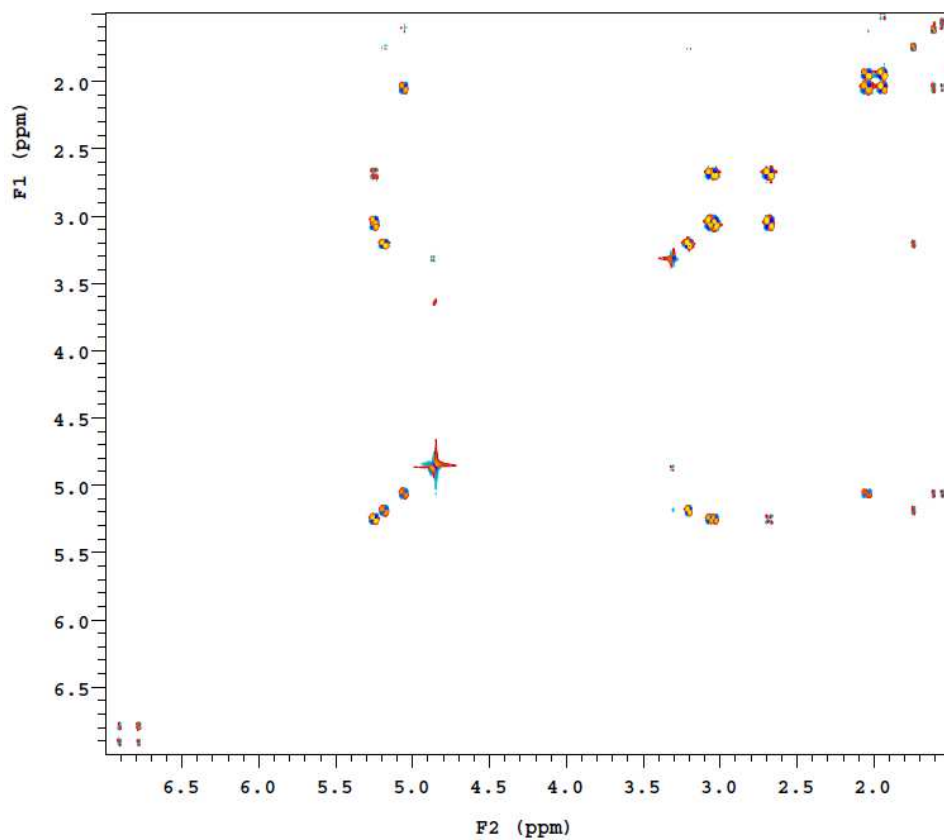
2D-NMR HMBC spectra of 7*O*-geranyl-eriodictyol recorded in CD₃OD(G7)



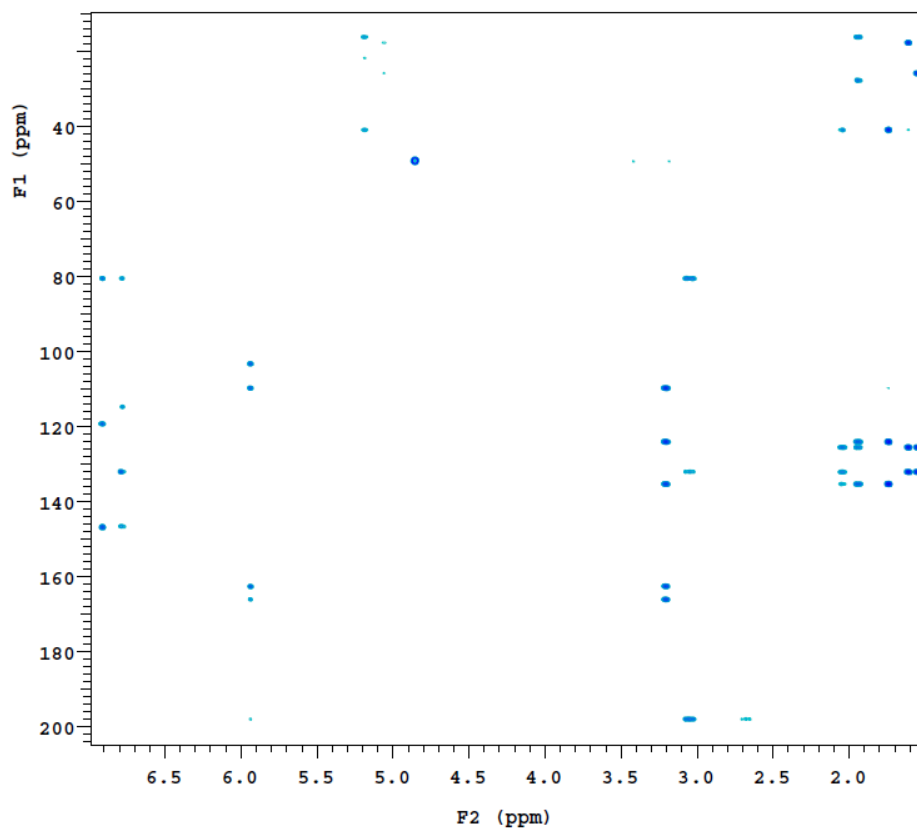
2D-NMR HSQC spectra of 7*O*-geranyl-eriodictyol recorded in CD₃OD (**G7**)



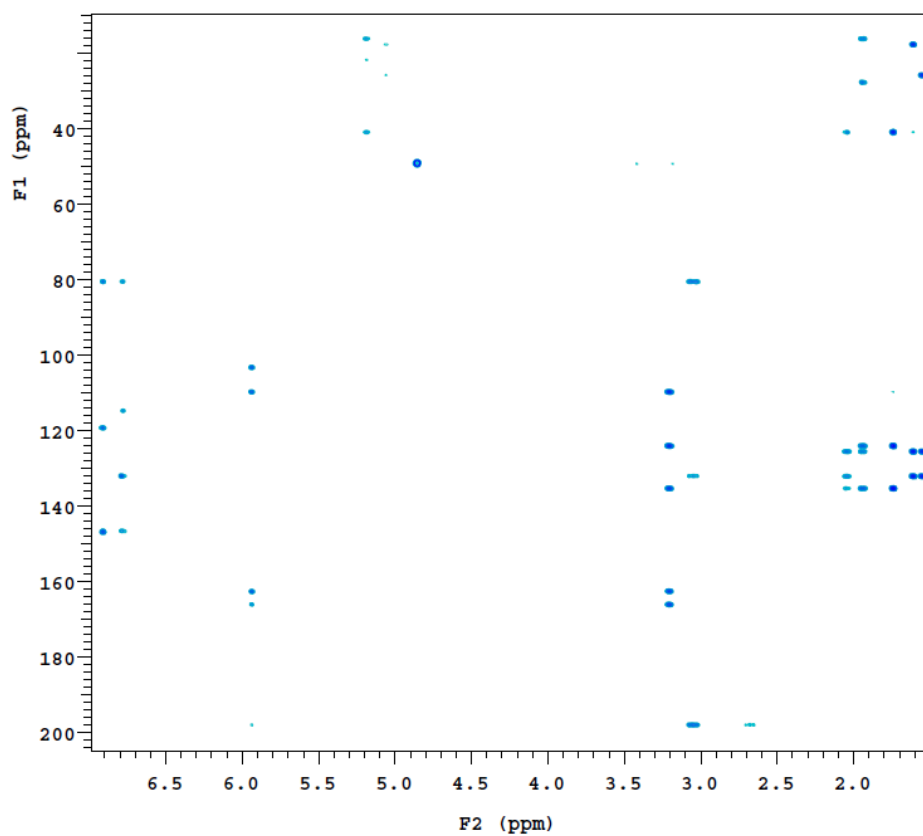
¹H-NMR-Spectra of 6-geranyl-eriodictyol in CD₃OD (**G8**)



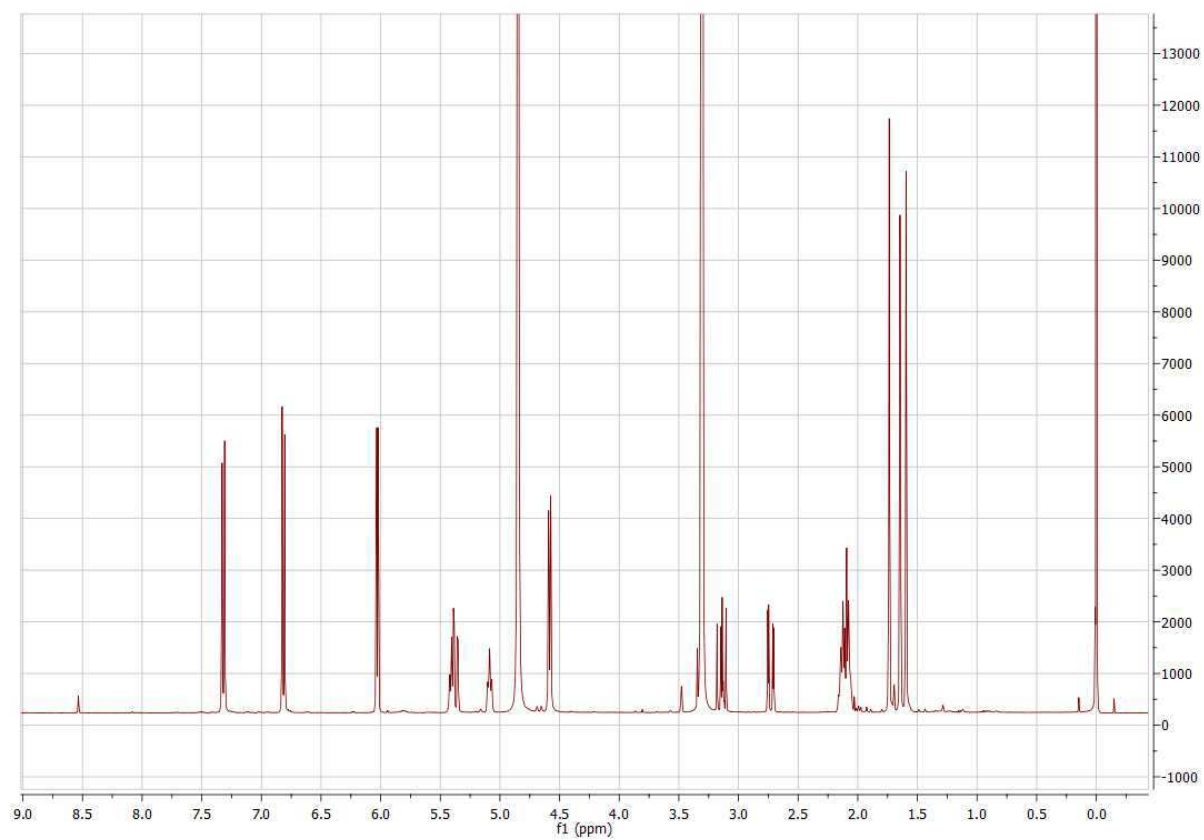
2D-NMR COSY spectra of 6-geranyl-eriodictyol recorded in CD₃OD (**G8**)



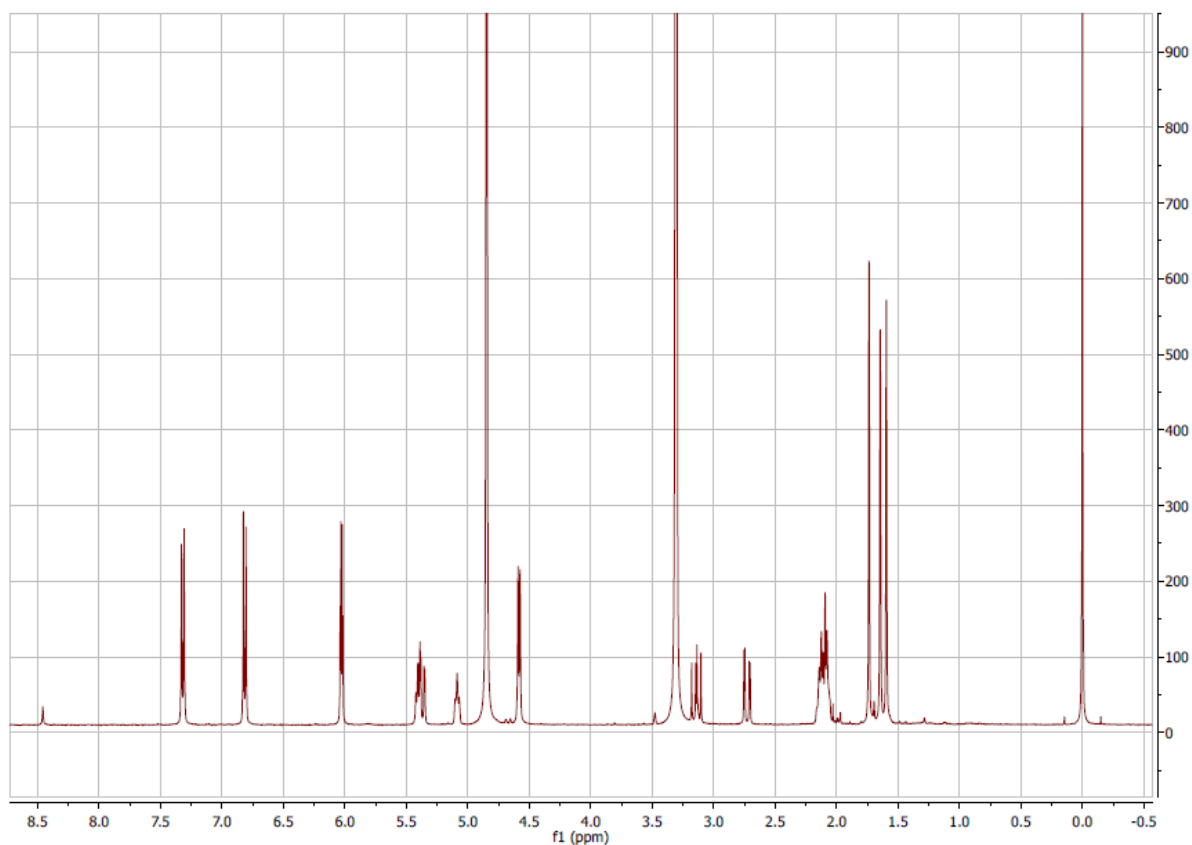
2D-NMR HMBC spectra of 6-geranyl-eriodictyol recorded in CD₃OD (**G8**)



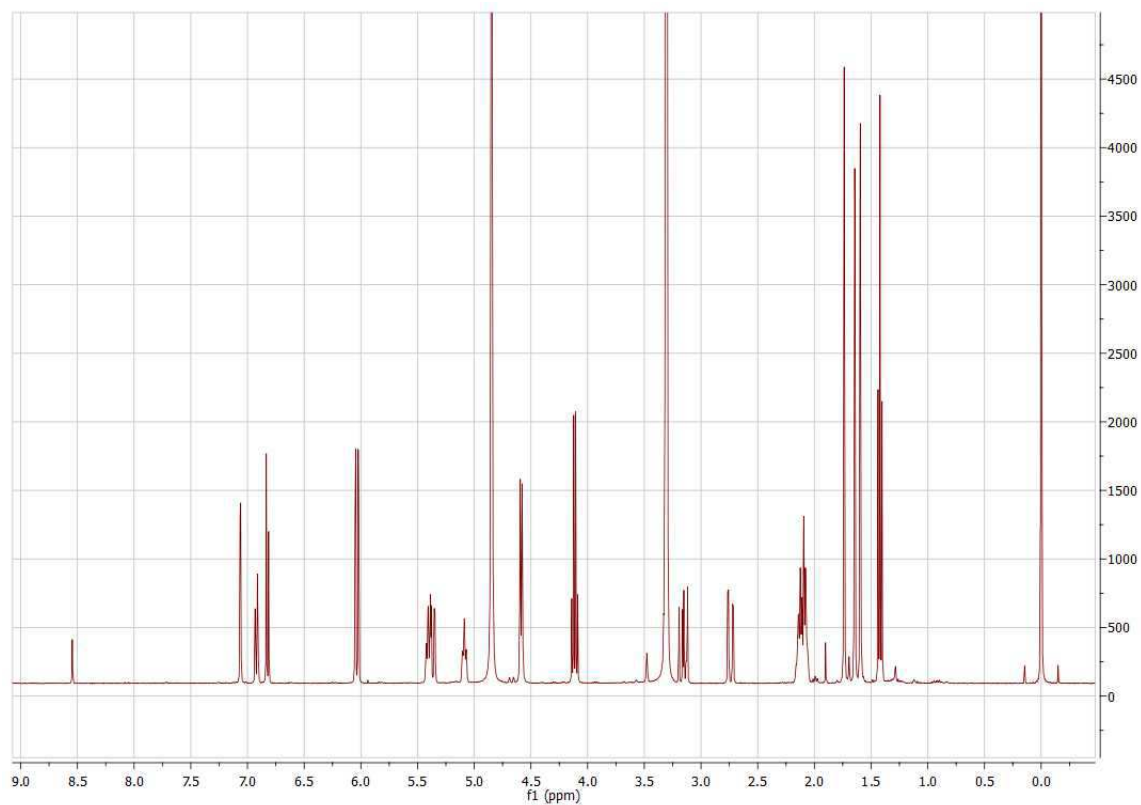
2D-NMR HSQC spectra of 6-geranyl-eriodictyol recorded in CD₃OD (**G8**)



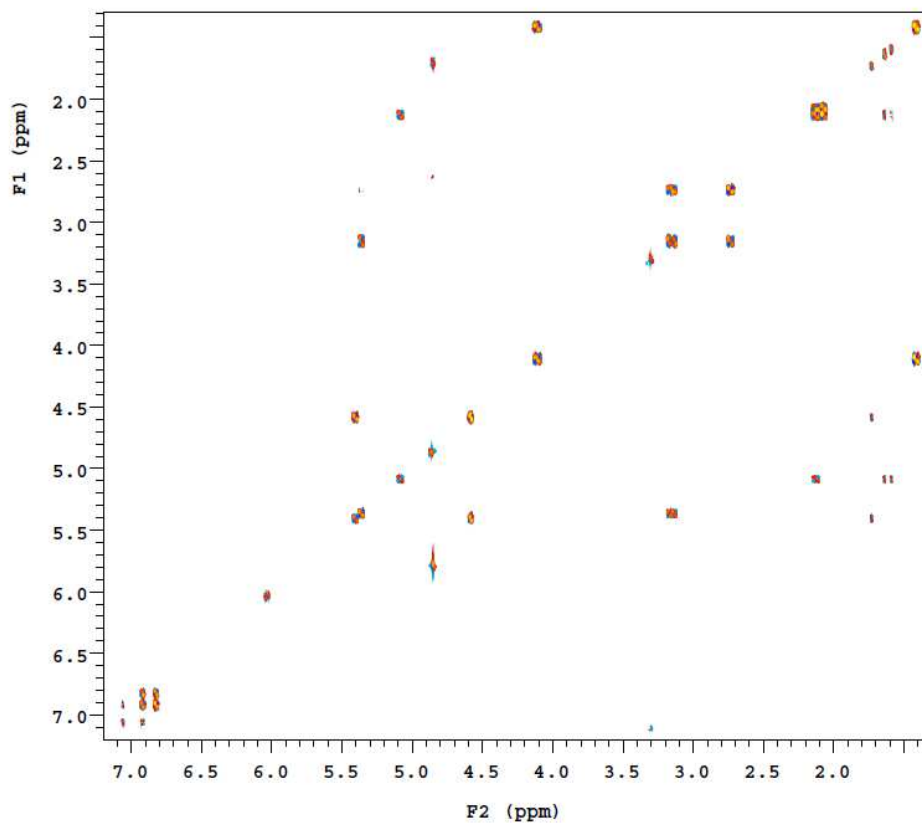
¹H-NMR-Spectra of 7O-geranyl-naringenin in CD₃OD (**G9**)



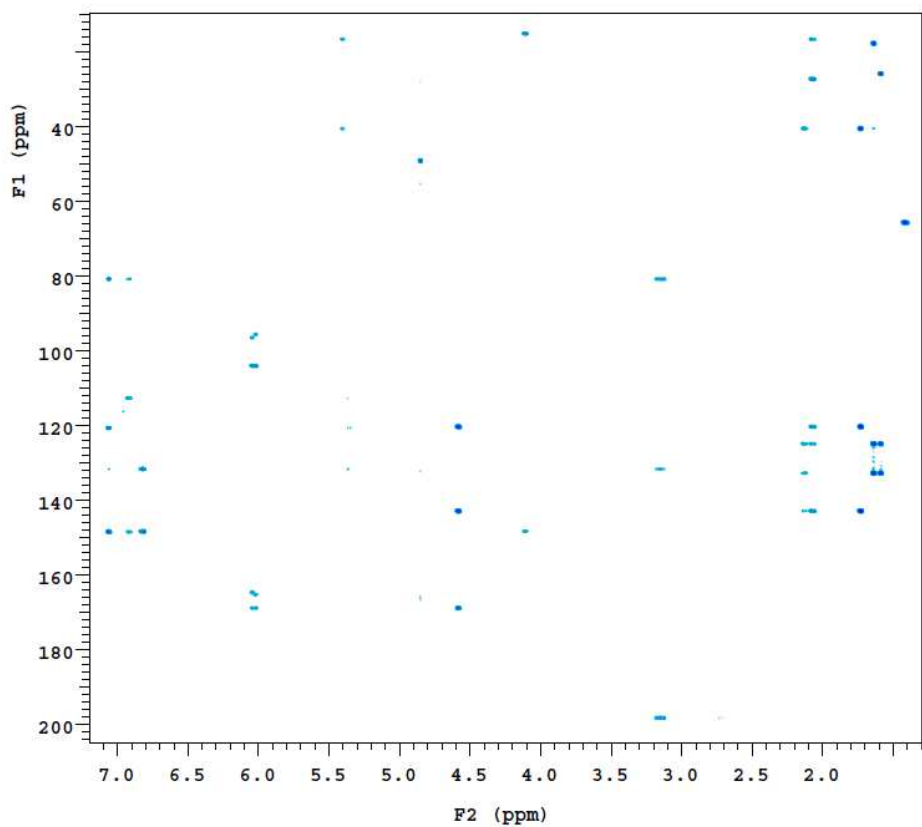
¹H-NMR-Spectra of 6-geranyl-naringenin in CD₃OD (**G10**)



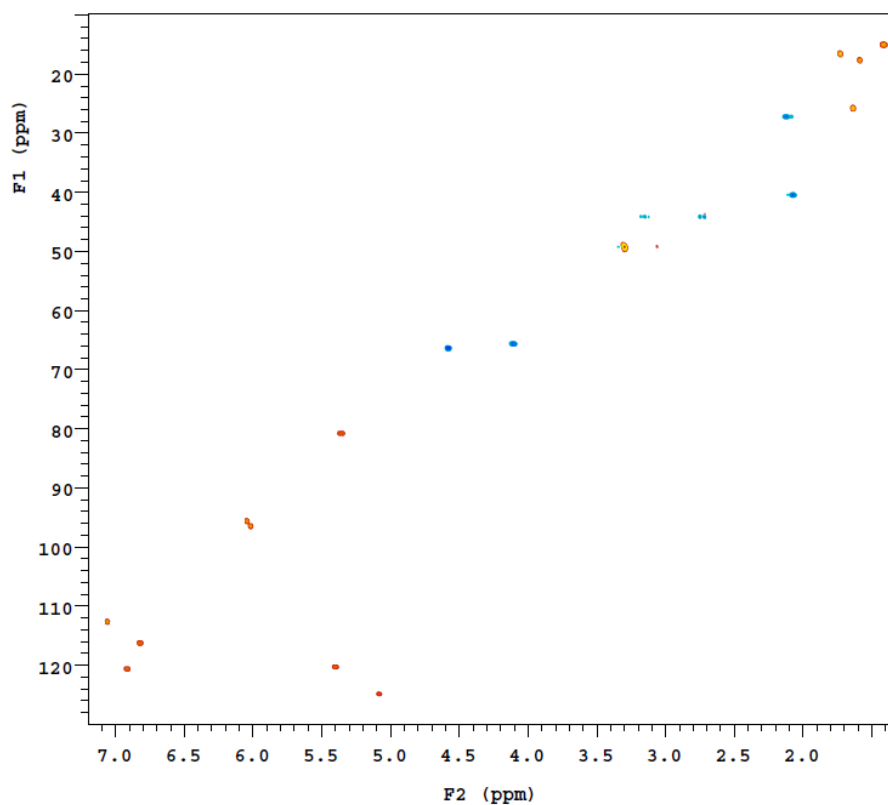
¹H-NMR-Spectra of 7*O*-geranyl-(2*S*)-2-(3',4'-(4'-ethoxy)-dihydroxyphenyl)-5,7-dihydroxy-4-chromanone in CD₃OD (**G11**)



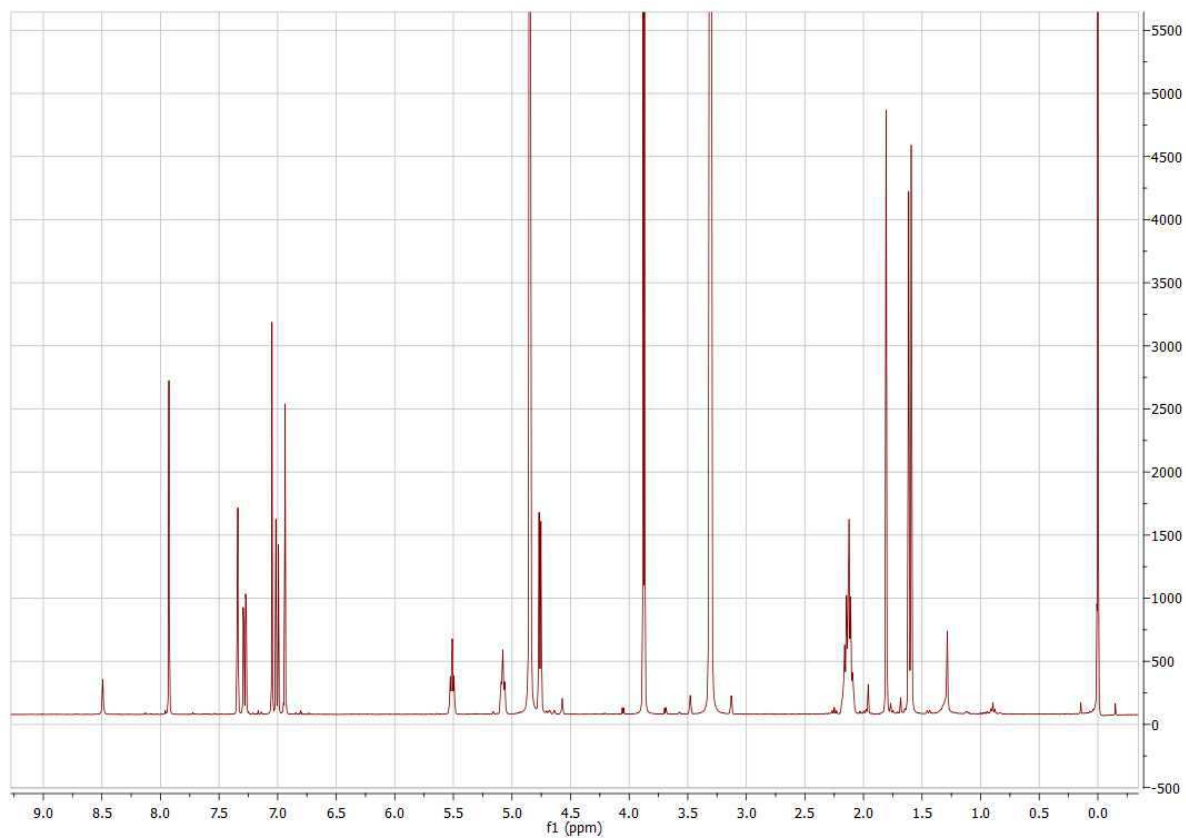
2D-NMR COSY spectra of 7*O*-geranyl-(2*S*)-2-(3',4'-(4'-ethoxy)-dihydroxyphenyl)-5,7-dihydroxy-4-chromanone recorded in CD₃OD (**G11**)



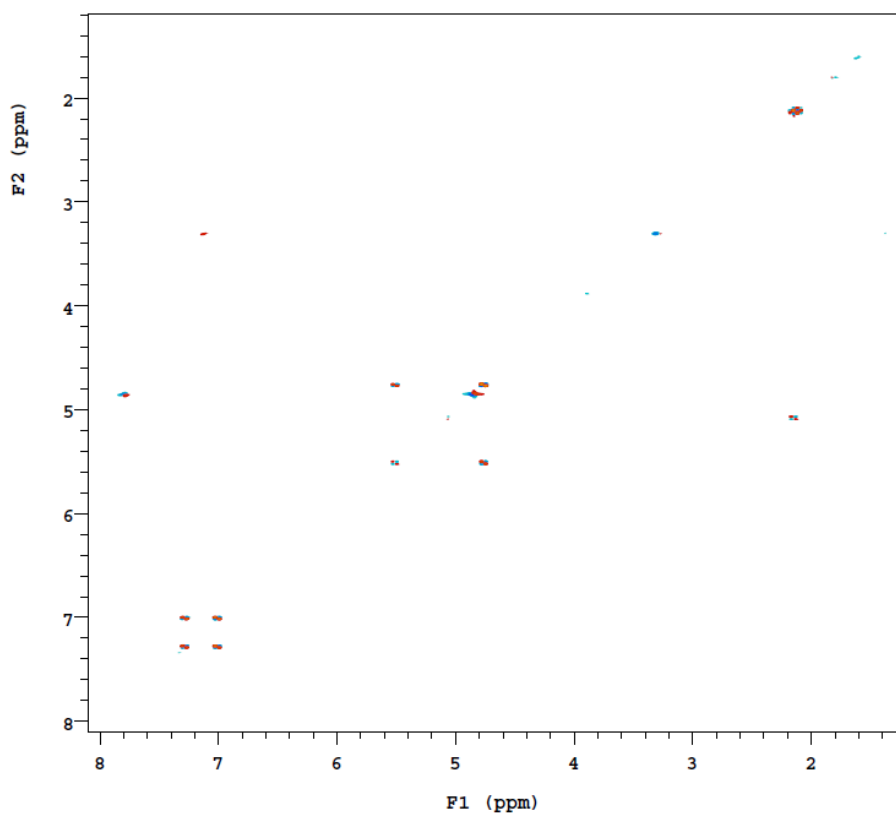
2D-NMR HMBC spectra of 7*O*-geranyl-(2*S*)-2-(3',4'-(4'-ethoxy)-dihydroxyphenyl)-5,7-dihydroxy-4-chromanone recorded in CD₃OD (**G11**)



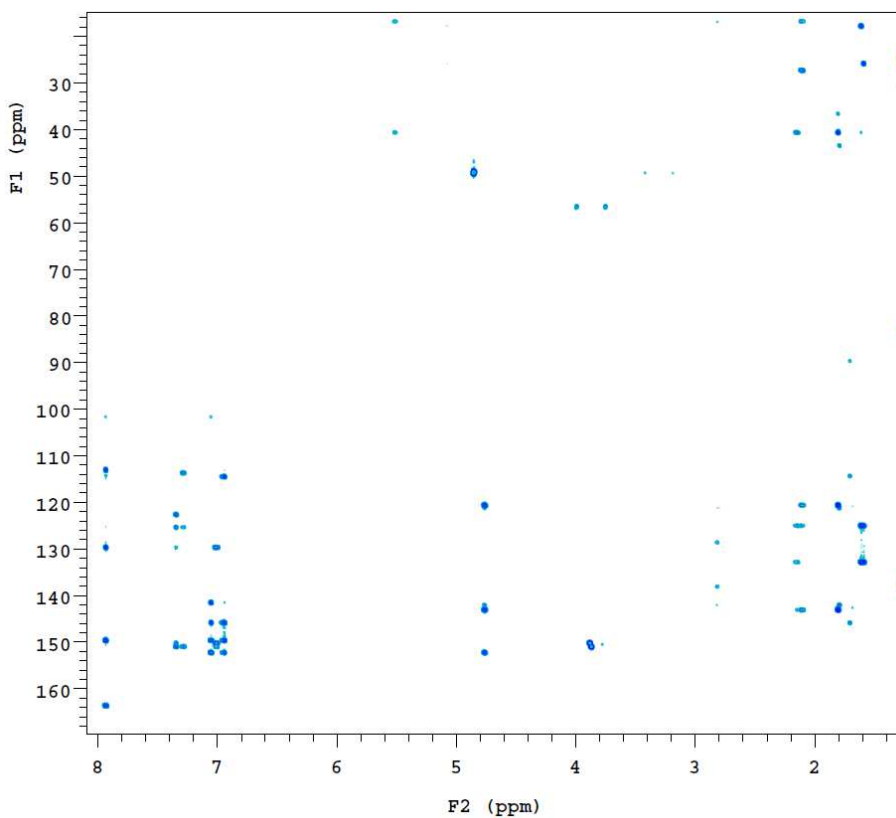
2D-NMR HSQC spectra of 7*O*-geranyl-(2*S*)-2-(3',4'- (4'-ethoxy)-dihydroxyphenyl)-5,7-dihydroxy-4-chromanone recorded in CD₃OD (**G11**)



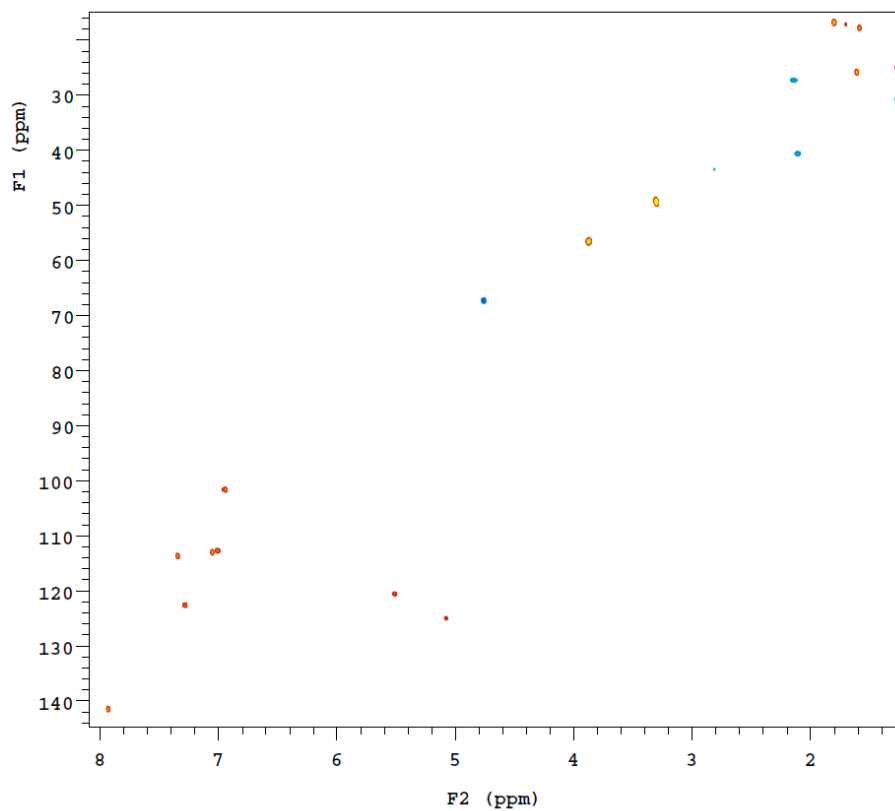
¹H-NMR-Spectra of 6*O*-geranyl-3-(3',4'-dimethoxyphenyl)-6,7-dihydroxycoumarin in CD₃OD (**G12**)



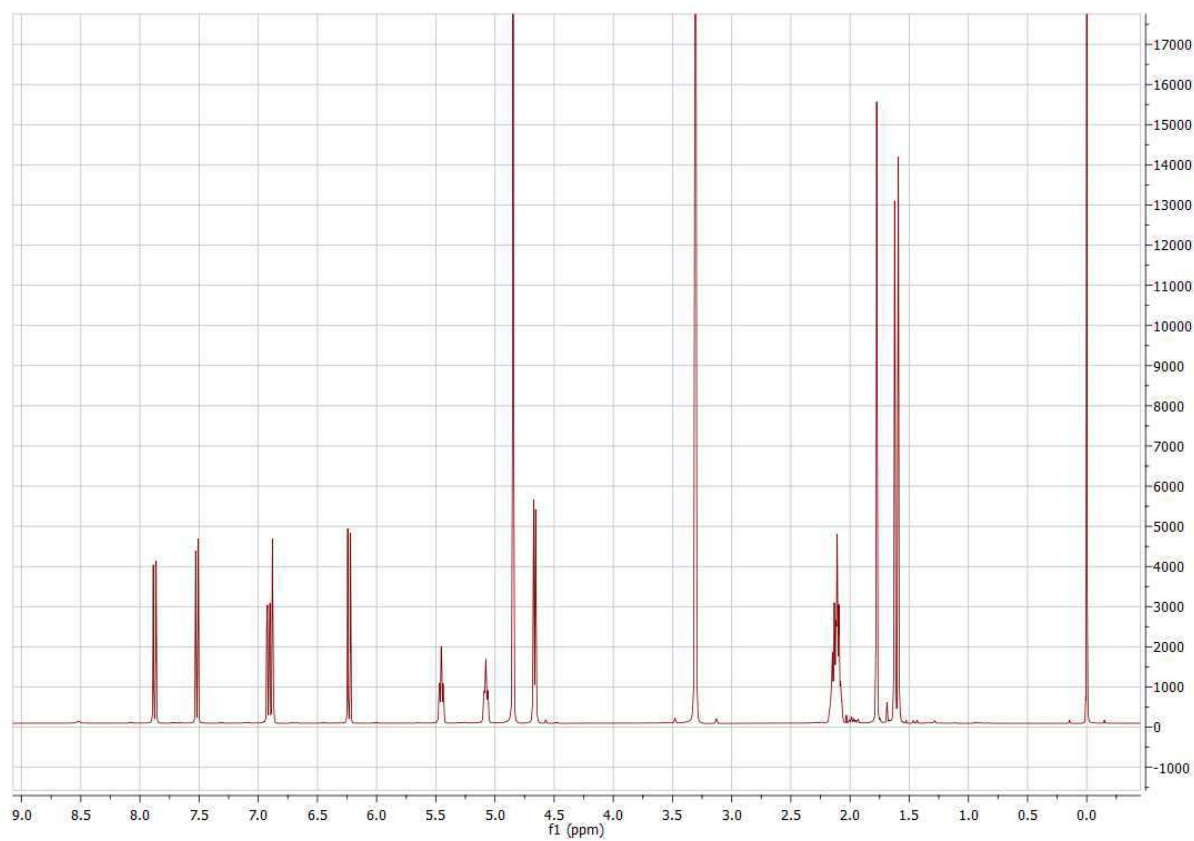
2D-NMR COSY spectra of 6*O*-geranyl-3-(3',4'-dimethoxyphenyl)-6,7-dihydroxycoumarin recorded in CD₃OD (**G12**)



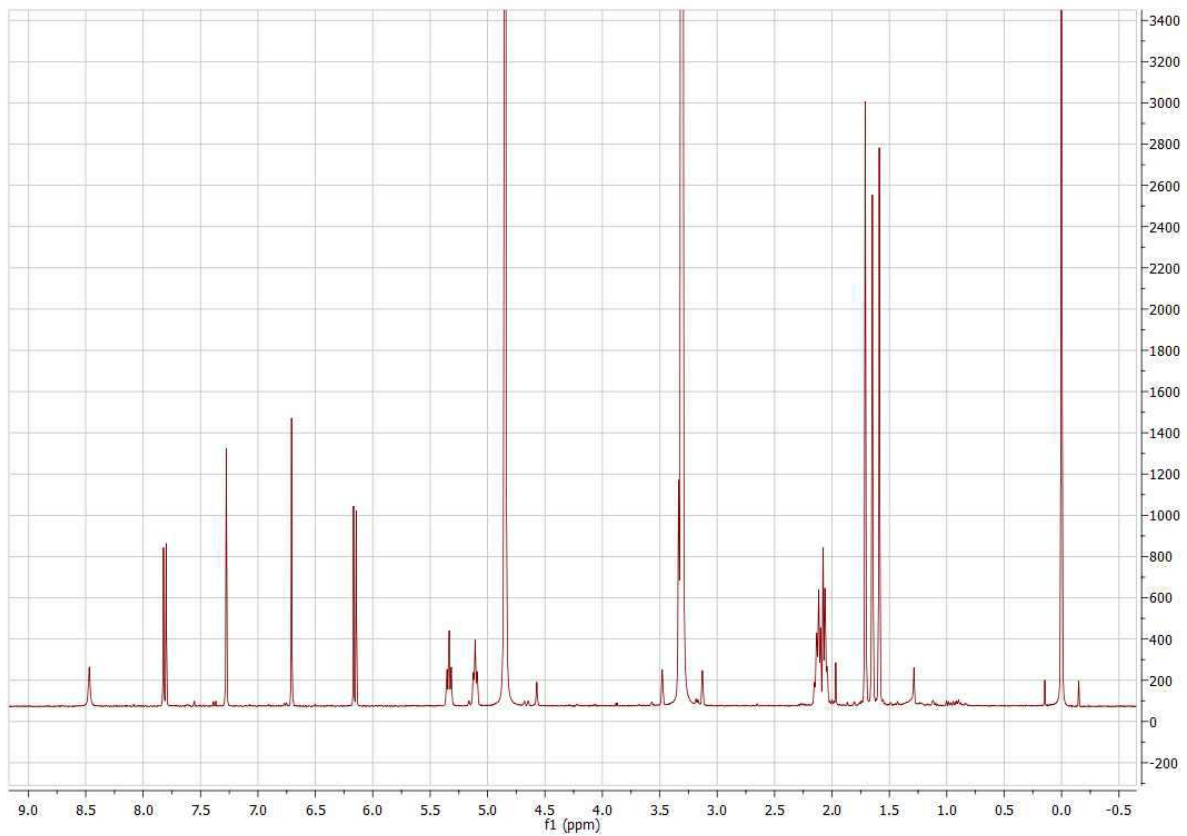
2D-NMR HMBC spectra of 6*O*-geranyl-3-(3',4'-dimethoxyphenyl)-6,7-dihydroxycoumarin recorded in CD₃OD (**G12**)



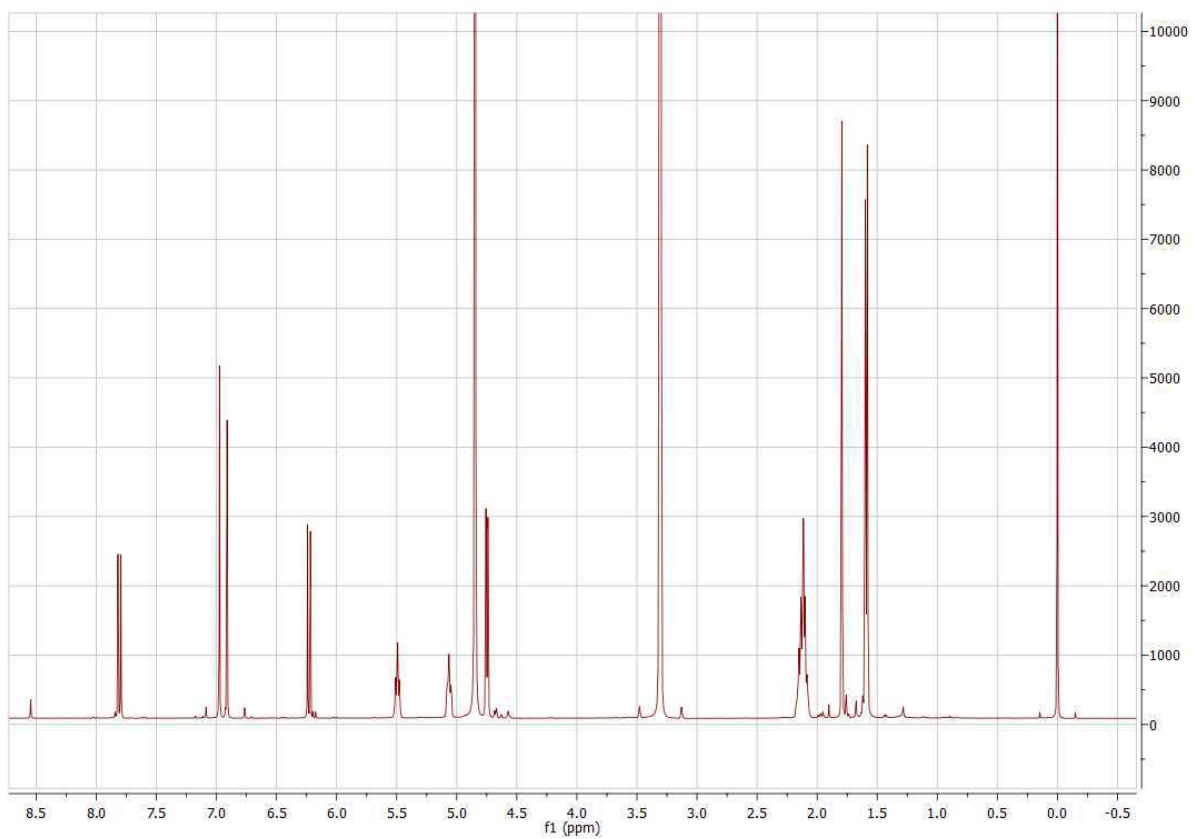
2D-NMR HSQC spectra of 6*O*-geranyl-3-(3',4'-dimethoxyphenyl)-6,7-dihydrocoumarin recorded in CD₃OD (**G12**)



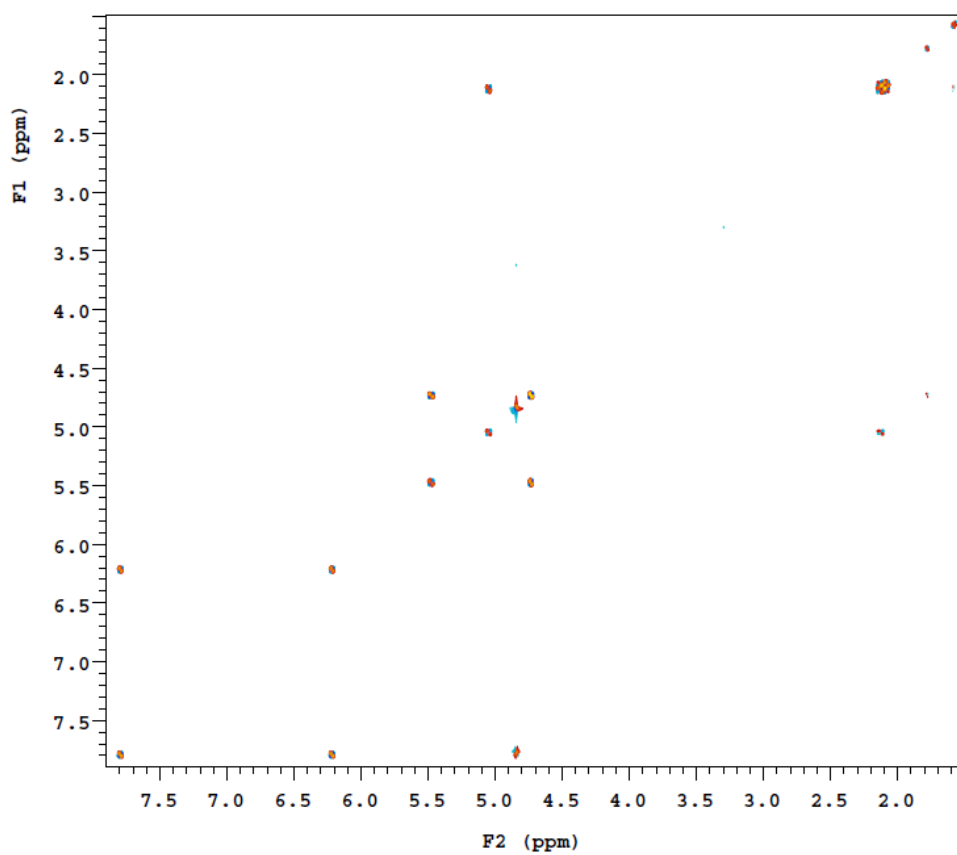
¹H-NMR-spectra of 7*O*-geranyl-umbelliferone in CD₃OD (**G13**)



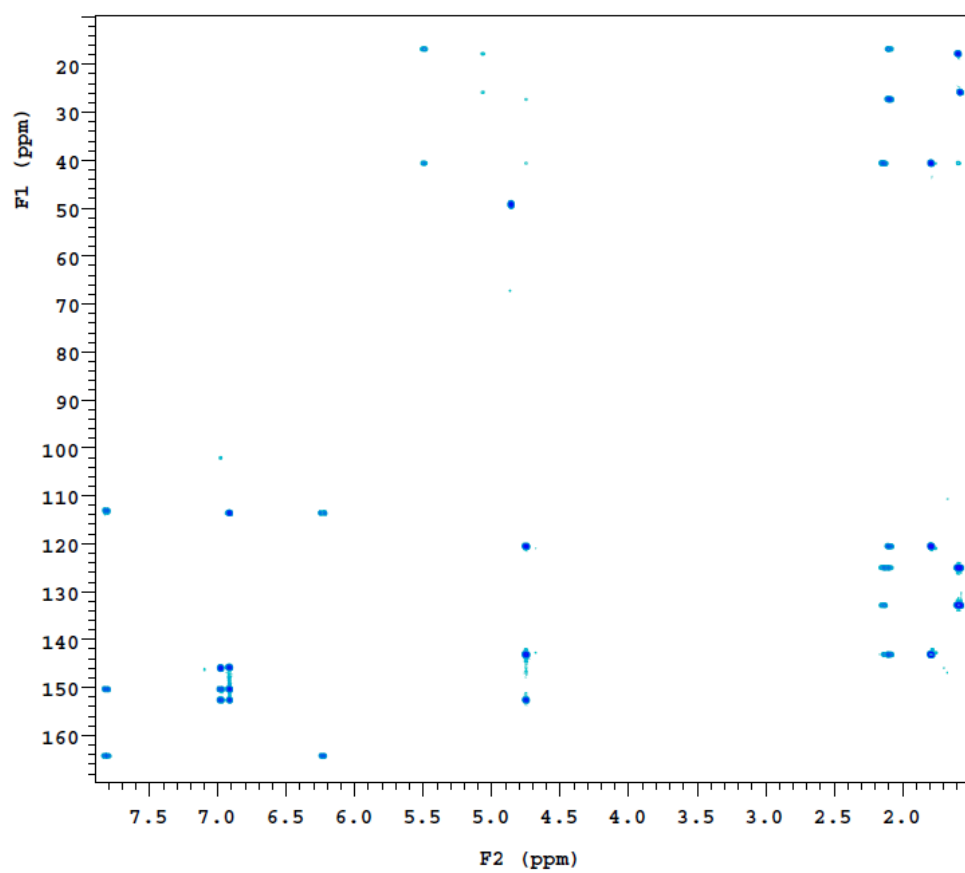
¹H-NMR-Spectra of 6-geranyl-umbelliferone in CD₃OD (G14)



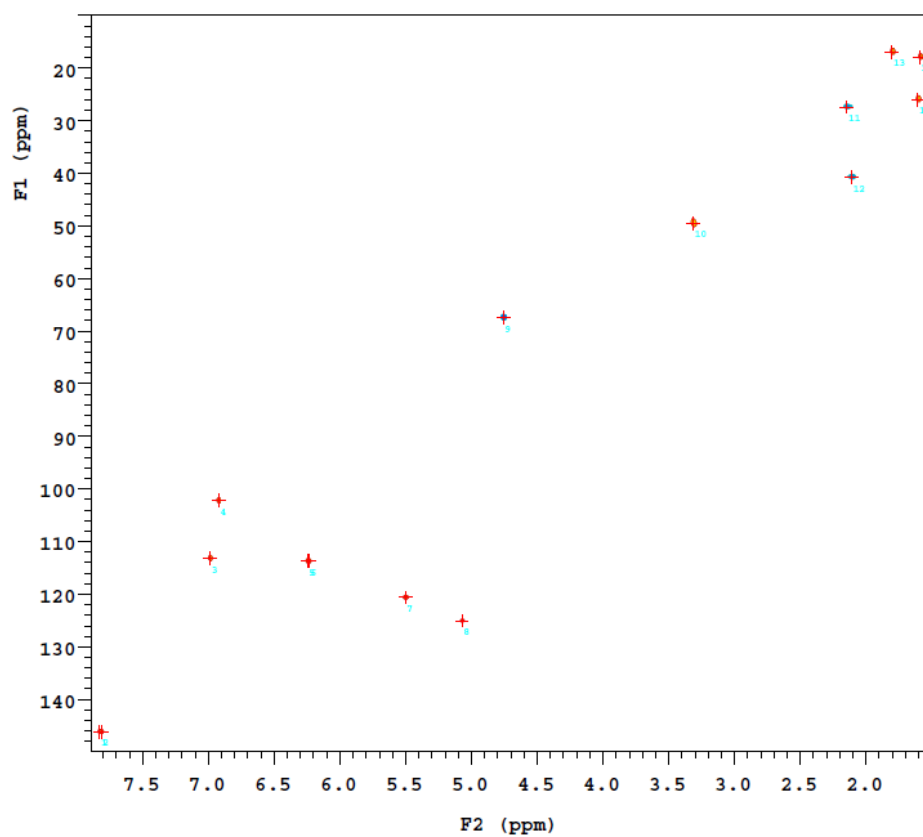
¹H-NMR-Spectra of 6*O*-geranyl-aesculetin in CD₃OD (G15)



2D-NMR COSY spectra of 6*O*-geranyl-aesculetin recorded in CD₃OD (**G15**)



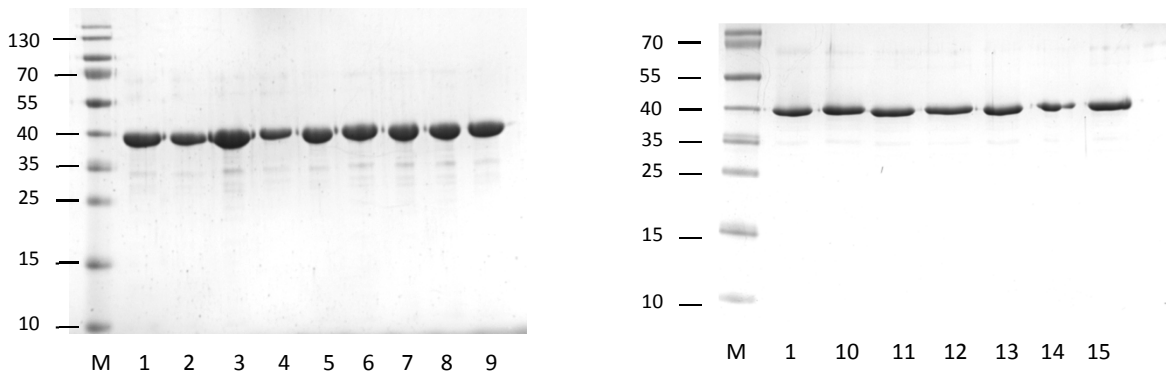
2D-NMR HMBC spectra of 6*O*-geranyl-aesculetin recorded in CD₃OD(**G15**)



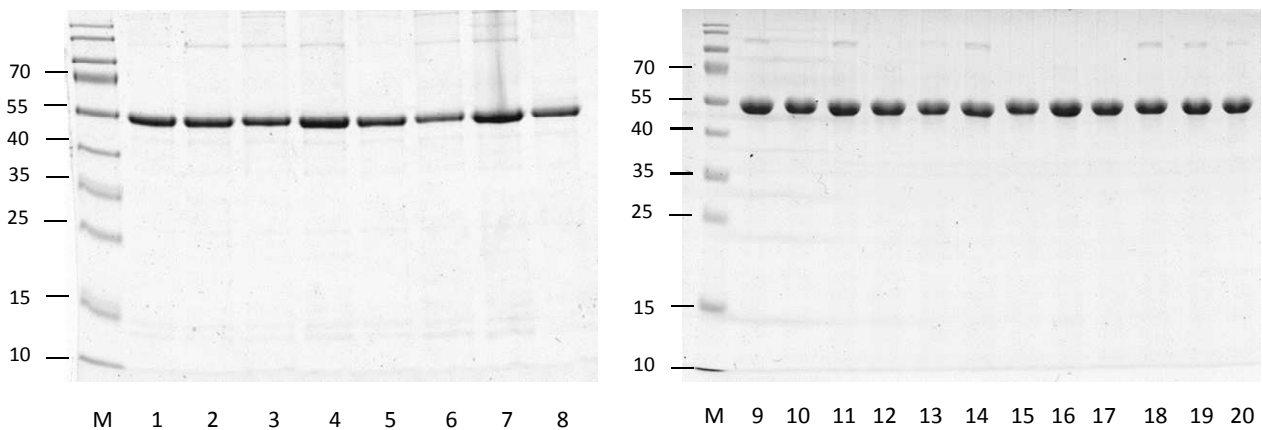
2D-NMR HSQC spectra of 6*O*-geranyl-aesculetin recorded in CD₃OD (**G15**)

10.3. Supplementary figures

10.3.1. Protein expression and purification of the NphB mutants

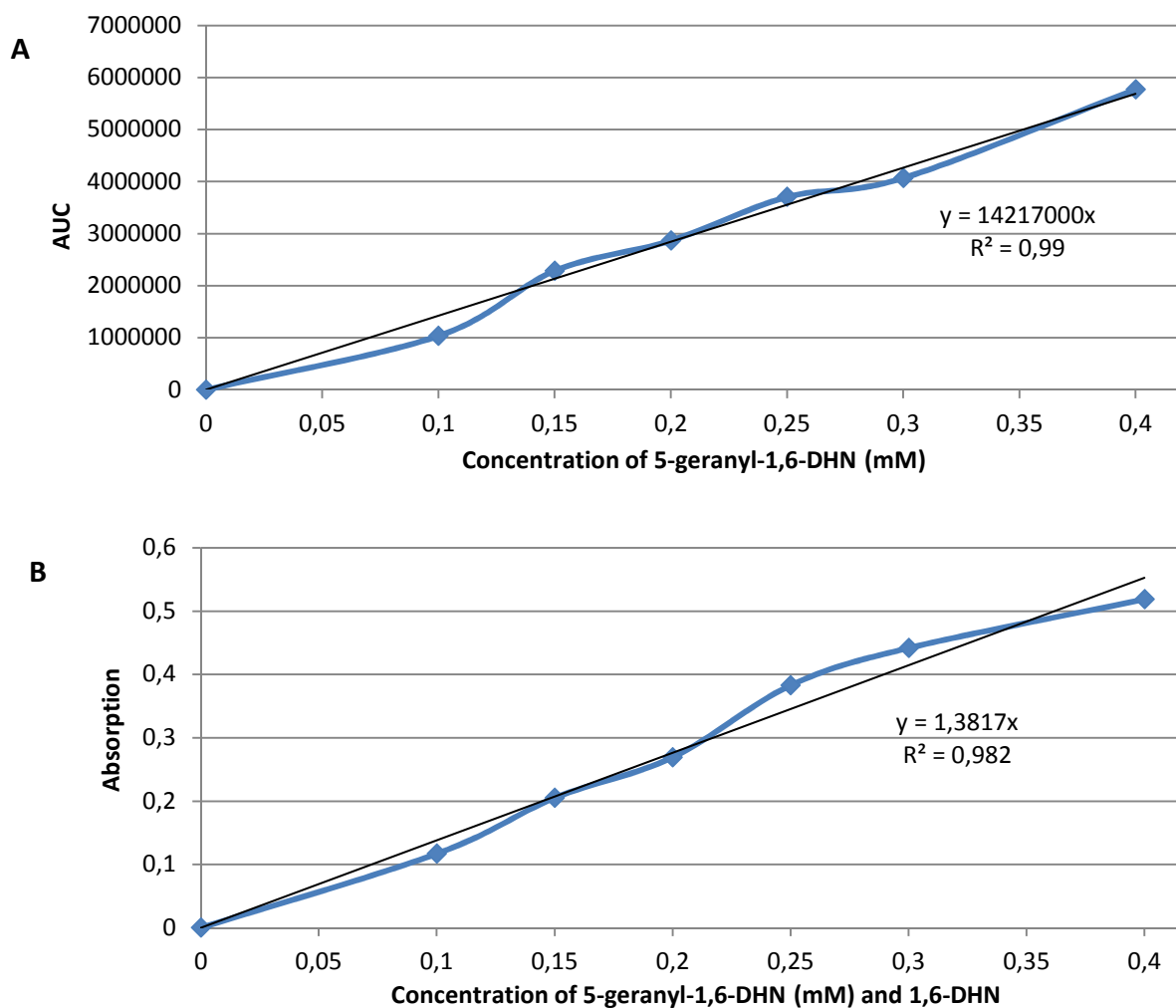


Supplementary Figure 1. Purification of the NphB and representative mutations. The protein is shown in the gel without Trx-Tag. Lanes of the SDS-PAGE (14 % crosslinking) represent the molecular markers (M), the wild-type NphB (1), S51A (2), S64A (3), S64R (4), M106A (5), D110N (6), D110A (7), Y121F (8), Y121W (9), M162A (10), M162C (11), M162F (12), M162L (13), M162W (14), D100A/Y121F (15).



Supplementary Figure 2. Purification of the NphB with Trx-tag. The protein is shown in the gel with Trx-Tag. Lanes of the SDS-PAGE (14 % crosslinking) represent the molecular markers (M), the wild-type NphB (1), V47A (2), V49E (3), S51E (4), F213A (5), F213V (6), F213L (7), S214A (8), Y216A (9), Y216E (10), V271D (11), V271E (12), Y288D (13), Y288E (14), V294A (15), Q295A (16), L298A (17), M106A/Q295A (18), M106A/Q295A/V294A (19) and wild-type NphB (20)

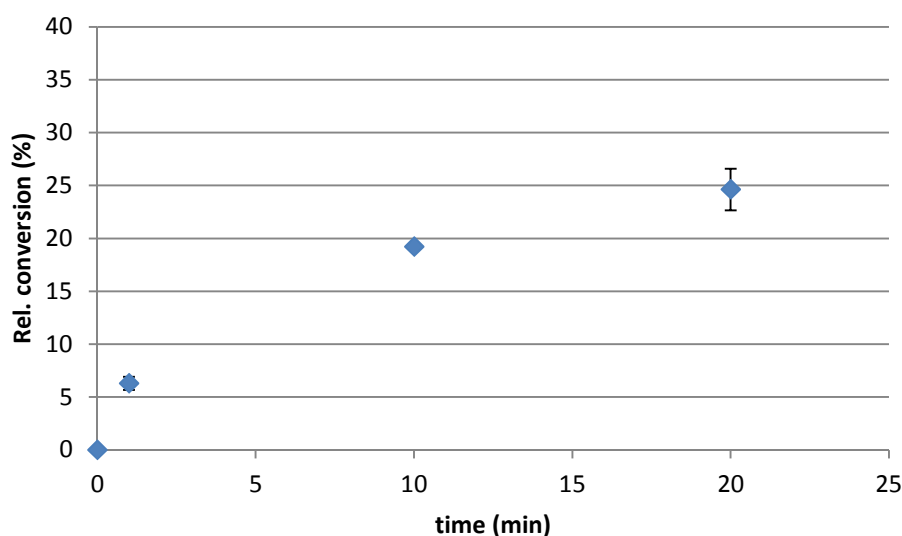
10.3.2. NphB UV/Vis-assay validation



Supplementary Figure 3. The calibration curves of the UV/Vis-method are shown. (A) The quantitative HPLC measurements of 5-geranyl-1,6-DHN at 340 nm. 1 mg of the main product is equal to absorption of 14.217.000 AUC. **(B)** Quantitative UV/Vis measurements of 5-geranyl-1,6-DHN at 340 nm. 1 mg of the main product is equal to absorption of 1.38 AU.

10.3.3. MenA – assay conditions

The chosen combinations of concentrations were 5 mM GPP, 5 mM MgCl₂ and 5 mM 1,4-DHN-2A in the presences of 12% DMSO (v/v) which was previously used in the inhibitor screening of NphB. To establish the conditions for MenA, the same composition were chosen to simplify the conclusion and to identify the most potent inhibitors among the diphosphate mimics. In order to determine the linear product formation range, 25 µl MenA was incubated for 0, 1, 10, 20, 30, 40, 60 and 180 min at 37 °C.



Supplementary Figure 4. Product conversion of MenA. The product formation range of 25 µL (v/v) MenA using 5 mM GPP, 5 mM MgCl₂ and 5 mM 1,4 DHN-2A in the presences of 12% DMSO (v/v).

The reaction mixtures resulted in a completely saturated progress curve after incubation for 40 min using 25 µl MenA. Therefore, the enzyme amount was reduced to 5 µl and the reaction mixture was incubated for 10 min. The progress curve for 5 µl MenA was observed to be linear between 1-20 min. The impact of the inhibitor could be well identified under following conditions using 5 mM of GPP, 1,4-DHN-2A and MgCl₂ in the presences of 12% (v/v) DMSO and 5 µl MenA incubated at 37°C under 350 rpm for 10 min.

10.4. Material and equipment

Table 8. Labor Equipment (in Germany)

| | |
|--|--|
| Autoklav | H+P Varioklav Thermo Scientific, Bonn |
| BiopharmaLynx 1.3.2 | Waters Corporation, Eschborn |
| Biologische Sicherheitswerkbank | Thermo Scientific Hera Safe, Langenselbold |
| Circulardichroismus Spektrometer | Jasco J-815, Easton; USA |
| Elektrophoresekammer (horizontal) | Biometra Compact XS/S, Göttingen |
| Elektrophoresekammer (vertikal) | Biometra Compact M, Göttingen |
| Biometra Minigel-Twin | |
| Entsalzungssäule PD-10 (14,5 × 50 mm, Säulenvolumen 13,5 mL, Sephadex G-25, Partikelgröße 85-260 µm) | GE Healthcare Life Sciences, Freiburg |
| Flockeneisbereiter | Scotsman AF 100, Vernon Hills; USA |
| FPLC (Äkta) | ÄKTApurifier, GE Healthcare Life Sciences, Freiburg |
| | Schaltventileinheit: BOX-900 |
| | pH-Detektor: pH/C-900 |
| | UV-VIS-Detektor: UV-900 |
| | Pumpe: P-900 |
| | Fraktionssammler: Frac-950 |
| | Kühlschrank: Unichromat 1500, UniEquip, München |
| Geldokumentationsanlage | Biodocanalyze Biometra, Göttingen |
| Hig-pressure dispersion | Constant Systems Ltd., Northants, England |
| HPLC | Merck HITACHI D-7000 |
| | UV-VIS Detektor: Merck HITACHI L-7420 |
| | Fluoreszenzdetektor: Merck HITACHI L-7480 |
| | Autosampler: Merck HITACHI L-7250 |
| HPLC Säule (UPPS Versuche) | YMC-ODS AQ 150 x 4 mm, 5 µm, YMC Europe GmbH, Dinslaken |
| | YMC-Pack, R-ODS-5-A, 250 x 4.6 mm I.D., S-5 µm, 120 A, YMC Co., Ltd., Kyoto, Japan |
| HPLC Säule (NphB Verusche) | Infors HT Multitron, Bottmingen; Schweiz |
| Inkubationsschüttler | Infors HT Unitron, Bottmingen; Schweiz |
| | Infors HT Ecotron, Bottmingen; Schweiz |
| Kulturröhrchen | Röhre 13 mL, 100x16 mm, PP, Sarstedt, Nümbrecht |
| Kryoröhrchen | Nalgene® cryogenic vials, 2.0 mL, steril, Nalgene Nunc International, New York; USA |
| LC/ESI-Massenspektrometer | HPLC-Anlage: Agilent Technologies der 1200er Serie, Böblingen |
| | LC/MS/MS-Massenspektrometer: API 3200™, AB SCIEX, Darmstadt |
| MALDI-TOF Mass Spectrometry | Ultraflex-II TOF/TOF mass spectrometer |
| | MALDI source |
| | Nitrogen laser |
| | LIFT cell for fragment ion postacceleration |
| | Gridless ion reflector |
| | Software: Flex Analysis 3.0 |
| | Biotoools 3.0 |

| | |
|---|---|
| Magnetrührer | FlexControl software |
| Microliter pickup | Bruker Daltonik, Bremen |
| C18 180 µm × 20 mm pre-column with RP column 1.7µm BEH 130 C18 | MR 3001 K, Heidolph, Schwabach |
| Mikrotiterplatte | Waters Corporation, Massachusetts, USA |
| Mikrotiterplattenspektrophotometer | 96 <i>MicroWell plate</i> , Nunc, flacher Boden, ohne Deckel, VWR, Poole; England |
| Mischer/Vortexer | SpectraMax M5, Molecular Devices, Biberach Vortex Genie® 2 G560E, Scientific Industries, Inc., New York; USA |
| NMR | VARIAN UNITY 400, Agilent Technologies, Böblingen VARIAN VNMRS 600, Agilent Technologies, Böblingen |
| Petrischale | Schale 94/16 L.Mg.ON steril, Greiner Bio-One, Frickenhausen |
| pH-Meter | FiveGoTM FG2, Mettler Toledo, Gießen |
| Photometer | Eppendorf Bio Photometer Plus, Hamburg |
| Pipetten | Eppendorf Research, Hamburg |
| Pipettenspitzen | Sarstedt, Nümbrecht |
| Reaktionsgefäße | Röhre 50mL, 114x28mm, PP, Sarstedt, Nümbrecht Röhre 15mL, 120x17mm, PP, Sarstedt, Nümbrecht Reagiergefäß 1,5mL, Sarstedt, Nümbrecht SafeSeal Reagiergefäß 2mL, PP, Sarstedt, Nümbrecht Multiply®-Pro Gefäß 0,2mL, PP, Sarstedt, Nümbrecht |
| Spannungsquelle | Biometra Standard Power Pack P25, Göttingen |
| SYNAPT G2 HDMS | Waters Corporation, Massachusetts, USA |
| Taumler | Heidolph Polymax 1040, Schwabach |
| Thermoblock | Biometra TSc ThermoShaker, Göttingen |
| Thermocycler | Biometra T Professional Basic Gradient, Göttingen |
| UV/VIS Spektrometer | Jasco V-560, Easton; USA |
| Wasseraufbereitungsanlage | MilliQ-biocal, Millipore, Billerica; USA |
| Wasserbad | Lauda A100, Lauda-Königshofen |
| Zentrifugen | Eppendorf 5424, Hamburg Hettich Mikro 120, Kirchlingern Beckman AvantiTM J-E, Rotoren: JA-10, JA- 16.250, JS-5.3, Krefeld |

Table 9. Used Chemicals

| | |
|---|---------------------------------|
| 1-Hydroxynaphthalene | Sigma-Aldrich, Taufkirchen |
| 2-Hydroxynaphthalene | |
| 1,3-Dihydroxynaphthalene | |
| 1,4-Dihydroxynaphthalene | |
| 1,5-Dihydroxynaphthalene | |
| 1,6-Dihydroxynaphthalene | |
| 1,7-Dihydroxynaphthalene | |
| 2,3-Dihydroxynaphthalene | |
| 2,6-Dihydroxynaphthalene | |
| 2,7-Dihydroxynaphthalene | |
| 2,4,6-trihydroxyacetophenone | |
| 10x <i>Pfu</i> Puffer mit 20 mM MgSO ₄ | Thermo Scientific, Darmstadt |
| 10x <i>FastDigest</i> ® Puffer | Thermo Scientific, Darmstadt |
| 10x <i>DreamTaq</i> ™ Puffer | Thermo Scientific, Darmstadt |
| 6x DNA <i>Loading Dye</i> | Thermo Scientific, Darmstadt |
| AccuPrime Pfx Supermix | Invitrogen AG, Kalifornien, USA |
| Acetonitril | Merck, Darmstadt |
| Acrylamid/Bisacrylamid (40 %) | Merck, Darmstadt |
| Agar | Carl Roth, Karlsruhe |
| Agarose | Carl Roth, Karlsruhe |
| Ammoniumperoxodisulfat | Carl Roth, Karlsruhe |
| Ampicillin, Natriumsalz | Carl Roth, Karlsruhe |
| β-Mercaptoethanol | Carl Roth, Karlsruhe |
| BIOMOL®-Reagenz | ENZO Life Sciences, Lörrach |
| Bradford-Reagenz Roti□-Quant | Carl Roth, Karlsruhe |
| 1-Butanol | Sigma-Aldrich, Taufkirchen |
| Chloramphenicol | Carl Roth, Karlsruhe |
| <i>Coomassie</i> Brilliantblau G-250 | Carl Roth, Karlsruhe |
| Dithiothreitol (DTT) | Sigma-Aldrich, Taufkirchen |
| dNTP-Mix (10 mM pro dNTP) | Thermo Scientific, Darmstadt |
| Eriodictyol | Sigma-Aldrich, Taufkirchen |
| Esculetin | Sigma-Aldrich, Taufkirchen |
| Essigsäure, Rotipuran® 100 % | Carl Roth, Karlsruhe |
| Ethanol | Merck, Darmstadt |
| Ethidiumbromid (10 mg mL ⁻¹) | VWR, Poole; England |
| <i>Gene-Ruler</i> ™ 1 kb DNA Ladder | Thermo Scientific, Darmstadt |
| Glycerin | Carl Roth, Karlsruhe |
| Hefeextrakt | Carl Roth, Karlsruhe |
| HisTrap IMAC-Säule | Qiagen, Hilden |
| 2-(4-(2-Hydroxyethyl)-piperazinyl)-ethansulfonsäure (Hepes) | Carl Roth, Karlsruhe |
| Iodoacetamide | Sigma-Aldrich, Taufkirchen |
| Imidazol | Carl Roth, Karlsruhe |
| Isopropanol | Merck, Darmstadt |
| Isopropyl-β-D-thiogalactopyranosid (IPTG) | Carl Roth, Karlsruhe |
| Kanamycinsulfat | Carl Roth, Karlsruhe |
| K ₂ HPO ₄ | Merck, Darmstadt |
| KH ₂ PO ₄ | Merck, Darmstadt |
| MgCl ₂ · 6 H ₂ O | Carl Roth, Karlsruhe |
| N ₂ | Air Liquide, Düsseldorf |
| NaCl | Carl Roth, Karlsruhe |
| NaOH | Carl Roth, Karlsruhe |
| Naphthalen | Sigma-Aldrich, Taufkirchen |
| Naringenin | Sigma-Aldrich, Taufkirchen |
| Natriumlaurylsulfat (SDS) | Carl Roth, Karlsruhe |
| <i>n</i> -Heptan, HPLC <i>Grade</i> | Carl Roth, Karlsruhe |
| <i>n</i> -Hexan, GC <i>Ultra Grade</i> | Carl Roth, Karlsruhe |
| <i>PageRuler</i> ™ <i>Plus Prestained Protein</i> | Thermo Scientific, Darmstadt |

| | |
|---|------------------------------|
| <i>Ladder</i> | |
| <i>Roti®-Quant (Bradford-Reagenz)</i> | Carl Roth, Karlsruhe |
| <i>Salzsäure (37 %), rauchend</i> | Carl Roth, Karlsruhe |
| <i>TALON® Metallaffinitätsmatrix</i> | Clontech, Mountain View; USA |
| <i>Tetramethylethylendiamin (TEMED)</i> | Carl Roth, Karlsruhe |
| <i>Tris(hydroxymethyl)-aminomethan (Tris)</i> | Carl Roth, Karlsruhe |
| <i>Tris-Hydrochlorid</i> | Carl Roth, Karlsruhe |
| <i>Triton X-100, reinst</i> | Carl Roth, Karlsruhe |
| <i>Trysin</i> | Promega, Madison, WI, USA |
| <i>Trypton/Pepton</i> | Carl Roth, Karlsruhe |
| <i>Tween® 20</i> | Sigma-Aldrich, Taufkirchen |
| <i>Umbelliferon</i> | Sigma-Aldrich, Taufkirchen |
| <i>Vektor</i> | Merck KGaA, Darmstadt |
| <i>pET28a(+)</i> | |
| <i>pET32a(+)</i> | |

10.5. Nucleotide sequence of the use enzymes (5'-3')

10.5.1. Ec_UPPS

GTGATGTTGTCTGCTACTCAACCACTTAGCGAAAAATTGCCAGCGCATGGCTGCCGTCATGTTGCGATCATTAT
GGACGGCAATGGCCGCTGGGCAAAAAAGCAAGGGAAGATTTCGTGCCTTTGGGCATAAAGCCGGGGCAAAAT
CCGTCCGCCGGGCTGTCTCTTTTTCGGCCAACAACGGTATTGAGGCGTTAACGCTGTATGCCTTTAGTAGTGAA
AACTGGAACCGACCAGCGCAGGAAGTCAGTGCCTTAATGGAAGTGTGGTGGGCGCTCGATAGCGAAGTA
AAAAGTCTGCACCGACATAACGTGCGTCTGCGTATTATTGGCGATACCAGTCGCTTTAACTCGCGTTTGCAAGA
ACGTATTCGTAATCTGAAGCGCTAACAGCCGGGAATACCGGTCTGACGCTGAATATTGCGGCGAACTACGGT
GGACGTTGGGATATAGTCCAGGGAGTCAGGCAACTGGCTGAAAAGGTGCAGCAAGGAAACCTGCAACCAGA
TCAGATAGATGAAGAGATGCTAAACCAGCATGTCTGTATGCATGAACTGGCCCCTGTAGATTTAGTAATTAGG
ACTGGGGGGGAGCATCGCATTAGTAACTTTTTGCTTTGGCAAATTGCCTATGCCGAACTTTACTTTACAGATGT
TCTCTGGCCCCGATTTTCGATGAACAAGACTTTGAAGGGGCGTTAAATGCCTTTGCTAATCGAGAGCGTCGTTTTCG
GCGGCACCGAGCCCGGTGATGAAACAGCCTGA

10.5.2. Hb_UPPS

CATATGGAATTCATGGAAGTGTATAACGGAGAACGTCAGGTGTCTTTTCGTCTGCTCGGTAAATACATGCGCA
AAGGTCTGACTCTATTCTGACGCAAGGGCCGATTCCCACTCACATTGCCTTCATTTTAGACGGGAATGGCCGC
TTTGCGAAGAAACACAAACTGCCAGAAGGTGGTGGACATAAGGCTGGCTTTCTTGCAATTGCTGAACGTGCTTA
CGTACTGCTATGAACTGGGCGTCAAATATGCCACCATCTATGCCTTCTCCATTGACAATTTCCGTGCGAAACCGC
ATGAAGTGCAGTATGTGATGAACCTGATGCTGGAGAAAATTGAGGGTATGATCATGGAGGAGTCGATTATCA
ACGCGTATGACATTTGTGTTTCGCTTTGTTGGCAATCTCAAAGTCTGATGAACCGCTGAAAACAGCTGCGGAC
AAAATTATGCGCGCTACCGCGAAGAATAGCAAGTTTGTCTGTTGTTGGCAGTATGCTATACTCTACGGATGA
AATTGTGCACGCAGTAGAGGAAAGCTCGAAAGATAAACTCAAATCCGATGAAATCTGCAATGATGGCAATGG
CGATTGTGATCAAAATCGAAGAAATGGAACCACTCAGAAATCAAGCTGGTTGAATTAGAACGGAATACC
TACATCAACCCTTATCCTGATGTCCTGATTCGTACAAGTGGCGAAACTCGCCTGAGCAACTACTTGTTATGGCA
GACCACCAACTGCATTCTGACTCACCAGCATGCGTTATGGCCGAAATTGGTCTGCGTCATGTGGTTTTGGGCCG
TAATCAACTGTCAGCGCCATTACAGCTATCTTGAGAAACACAAAGAGTATCTGAAAGGATCCCTCGAG

10.5.3. Hp_UPPS

CATATGGAATTCATGGACAATACCCTGAAACATCTCGCGATCATTATGGATGGCAATGGTCGCTGGGCCAAAC
TGAAGAACAAAGCTCGTGCGTATGGGCATAAGAAAGGCGTGAAAACACTTAAGGACATCACTATCTGGTGTG
CAAACCACAAATTAGAATGCCTTACCCTGTATGCGTTTAGCACCGAAAATTGGAAACGGCCGAAATCAGAAGT
CGACTTCCTGATGAAAATGCTGAAGAAATACCTCAAAGATGAACGCTCTACCTACCTGAACAACAATATCCGGT
TTCGTGCCATTGGAGATCTGGAAGGGTTTTCGAAAGAGTTACGCGATACCATTCTCCAACCTGGAGAATGACAC
ACGCCACTTCAAAGACTTTACCAGGTTCTGGCTCTCAATTATGGCTCCAAGAACGAGTTATCACGTGCCTTCA
AATCTCTGCTGGAAAGTCTCCATCCCACATCAACTTGCTGGAAAGCCTGGAGAACGAGATTAGCAATCGCTTG
GATACGCATGATCTGCCGGAAGTGGATTTGCTGCTGCGTACTGGTGGCGAAATGCGCTTGAGTAACTTCTGT
TATGGCAGTCGAGCTATGCAGAACTGTTCTTTACGCCGATTCTTTGGCCCGACTTTACGCCGAAAGATCTTGAA
AACATTATTTTCGGATTTCTACAAACGCGTACGTAAATTTGGTGAACCTGAAATGCGGATCCCTCGAG

10.5.4. MI_UPPS

CATATGGAATTCATGTTCCCGATTAAGAAACGCAAAGCGATCAAAAACAACAATATCAACGCAGCTCAGATTCC
GAAACACATTGCGATTATTATGGATGGCAATGGTCGCTGGGCCAAAACAGAAGAAAATGCCGCGTATCAAAGG
CCATTATGAGGGCATGCAAACGGTCAAGAAAATTACTCGTTATGCGTCTGATTTGGGTGTGAAATACCTGACC
CTGTATGCCTTTAGCACCGAAAACCTGGAGTCTCCGAAAGATGAAGTCAACTACCTGATGAAACTTCCAGGCG
ATTTCTGAATACCTTTCTTCCCGAACTGATTGAGAAAAACGTGAAAGTTGAAACCATTGGGTTTCATTGACGAT
TTACCGGATCATACCAAGAAGGCTGTACTGGAAGCCAAAGAGAAAACCAAACACAACACAGGTCTGACACTG
GTATTTGCGTTAAACTATGGTGGGCGCAAAGAGATTATCTCTGCCGTTGAGTTGATTGCAGAACGCTATAAATC
GGGAGAGATCAGCTTGGACGAAATTAGCGAAACGCACTTCAATGAGTACCTGTTTACGGCCAATATGCCTGAT
CCTGAGCTCCTGATTGCACTTCAGGCGAAGAACGTTTATCCAATTTCTGATCTGGCAATGCAGTTACTCCGA
ATTTGTGTTTATCGACGAATTTTGGCCAGACTTCAACGAAGAATCGCTGGCGCAGTGTATCAGCATCTATCAGA
ATCGCCATCGTCGTTTTGGTGGACTCGGATCCCTCGAG

10.5.5. Mt_UPPS

CATATGGAATTCATGGCGCGTGATGCGCGGAAACGCACGTATCCAACCTTCCGCAGTTGCCTCCGGCACCCG
ATGACTATCCGACCTTTCTGACACTAGCACCTGGCCGGTAGTATCCCCGAATTACCGGCTGCACCGTATGGT
GGCCCATGTCCGCCACCGCAGCATAACGAGTAAAGCTGCGGCTCCACGTATCCGGCGGATCGCTTGCCGAATC
ATGTCGCGATTGTGATGGACGGCAATGGCCGTTGGGCAACTCAACGCGGTCTGGCCCGCACAGAAGGTCACA
AAATGGGCGAAGCCGTCGTGATTGACATCGCGTGTGGTGCCATTGAGCTCGGGATCAAATGGCTGAGTCTTTA
CGCCTTTTCGACCGAAAACCTGGAAACGTTCCCCAGAAGAAGTACGCTTTCTGATGGGCTTCAACCGCGATGTG
GTTCCGCGTGTGCGGATACGCTGAAGAAGCTGGGAGTCCGCATTGTTGGGTTGGCTCTCGCCCGCGCTTAT
GGCGCTCTGTGATCAACGAACCTGGCCGTTGCGGAAGAGATGACGAAAAGCAACGATGTGATTACCATCAATT
ACTGCGTTAACTACGGCGGTCTACCGAGATCACGGAAGCCACACGGGAGATTGCCCGTGAAGTGGCCGCGAG
GACGGCTCAATCCGGAACGCATCACCGAATCGACCATTGCACGTCACTTACAGCGCCCCGATATCCGGATGTC
GATCTGTTTCTGCGCACCGCGGTGAACAGCGCAGCTCGAATTTTCATGCTTTGGCAAGCAGCGTATGCTGAGT
ACATCTCCAGGACAAACTGTGGCCTGACTATGATCGTGCAGATCTGTGGGCCGCTTGCGAAGAGTATGCGTC
ACGTAATCGTCGCTTTGGGAGCGCGGGATCCCTCGAG

10.5.6. NphB with Trx-Tag

ATGAGCGATAAAATTATTCACCTGACTGACGACAGTTTTGACACGGATGTA CTCAAAGCGGACGGGGCGATCC
TCGTCGATTTCTGGGCAGAGTGGTGCGGTCCGTGCAAAATGATCGCCCCGATTCTGGATGAAATCGCTGACGA
ATATCAGGGCAAAGTACCGTTGCAAACTGAACATCGATCAAAACCCTGGCACTGCGCCGAAATATGGCATC
CGTGGTATCCCGACTCTGCTGCTGTTCAAAAACGGTGAAGTGGCGGCAACCAAAGTGGGTGCACTGTCTAAAG
GTCAGTTGAAAGAGTTCCTCGACGCTAACCTGGCCGGTCTGGTCTGGCCATATGCACCATCATCATCATCAT
TCTTCTGGTCTGGTGCCACGCGTTCTGGTATGAAAGAAACCGCTGCTGCTAAATTCGAACGCCAGCACATGG
ACAGCCCAGATCTGGGTACCGACGACGACGACAAGGCCATGGCTGATATCGGATCCATGAGCGAAGCTGCGG
ATGTTGAACGCGTGTATGCGGCAATGGAAGAGGCAGCAGGCCCTTAGGTGTGGCTTGTGCGCGTGATAAAA
TCTACCCGTTACTGAGCACCTTTCAGGATACGCTGGTGGAAAGGTGGTTCCTGGTAGTGTCTCAATGGCATCC
GGTCGTCACAGTACCGAACTGGACTTCAGCATTTAGTCCCAGACATCGCATGGAGATCCGTATGCGACCGTAG
TCGAGAAAGGCTGTTTCCGGCCACTGGCCATCCTGTGGATGACCTGTTGGCCGATACCCAGAAACATCTCCCA
GTAAGCATGTTTGCCATTGACGGCGAAGTGAAGTGGCGGCTTCAAGAAAACCTACGCGTTCTTCCGACAGATA
ACATGCCAGGAGTTGCGGAACTGAGCGCGATTCCGTCCATGCCGCTGCTGTTGCAGAGAATGCCGAACTCTT
TGCCCGTTATGGGCTGGACAAAGTCCAGATGACGAGTATGGACTATAAGAAACGCCAGGTCAACCTGTACTTC
AGTGAAGTGAAGTGCACAACTTGGAAAGCTGAATCGGTGCTGGCCCTTGTTCGTGAGCTGGGTCTGCATGTT
CAAACGAATTGGGTCTGAAATTTGCAAACGGAGCTTTTCGGTGTATCCACGCTGAATTGGGAAACAGGCAA
GATCGATCGCTTGTGCTTTGCCGTTATCTCGAATGATCCTACCCCTGTACCCTCTTCAGACGAAGGGGATATTGA
GAAATTCACAACACTATGCAACTAAAGCGCCGATGCTTATGTTGGCGAAAAGCGCACGTTAGTGTACGGCCTT
ACGCTCTCTCCGAAAGAAGAGTACTACAACTGGGTGCGTATTACCACATTACCGATGTCCAACGCGGGTACT
GAAAGCCTTTGACTCTCTGGAGGATTAATGAGAGCTCCGTCGACAAGCTTGGCGCCGCACTCGAGCACCACCA
CCACCACCACTGAGATCCGGCTGCTAACAAAGCCCCGAAAGGAAGCTGAGTTGGCTGCTGCCACCGCTGAGCAA
TAACTAGCATAACCCCTTGGGGCCTCTAACGGGTCTTGAGGGGTTTTTTG

11. Tables

11.1. Table of figures

| | |
|--|----|
| FIGURE 1. SELECTED ISOPRENOIDS, THE ISOPRENE-SCAFFOLD IS MARKED IN RED. | 1 |
| FIGURE 2. PRENYLTRANSFERASES DISCUSSED IN THE TEXT INCLUDING THEIR BIOSYNTHETIC PRODUCTS, THE NATURAL ISOPRENOIDS. | 4 |
| FIGURE 3. COMPARISON OF TERTIARY STRUCTURES OF <i>CIS</i> - AND <i>TRANS</i> - PRENYLTRANSFERASE. VIEW OF STRUCTURAL ELEMENTS WITHOUT SUBSTRATE. THE A-HELICES OR THE LOOPS ARE IN DARKER GREY AND THE B-SHEETS ARE IN NAVY BLUE COLORED. | 7 |
| FIGURE 4. TWO ALTERNATIVE MECHANISMS OF FPP OR INTERMEDIATE SUBSTRATE CONDENSATE WITH IPP FORMING THE FINAL PRODUCT UPP CATALYZED BY UPPS. (R = C ₅ -UNIT; PP = DIPHOSPHATE)..... | 8 |
| FIGURE 5. BIOCATALYTIC CONVERTED NON-NATURAL IPP ANALOGS BY UPPS..... | 11 |
| FIGURE 6. CLADOGRAM OF THE PROTEIN SEQUENCE OF CPTASES FROM THE LINEAR TYPE DESCRIBED IN LITERATURE. THE INVESTIGATED ENZYMES ARE MARKED IN GREEN; PTASES MARKED WITH (C) ARE CRYSTALLIZED AND AVAILABLE AS PDB-FILE. SRT1, <i>C. JEJUNI</i> UPPS AND RER2 ARE INCLUDED TO THE LIST OF KNOWN CPTASE. (ACCESSION FILES: <i>SACCHAROMYCES CEREVISIAE</i> (SRT1): Q03175; MT_UPPS: P60479; <i>ARABIDOPSIS LYRATA</i> CPT: D7LFB0; <i>LYCOPERSICON HIRSUTUM</i> (Z,Z-FPS): B8XA40; ML_UPPS: O82827; EC_UPPS: P60472; HP_UPPS: P55984; <i>CAMPYLOBACTER JEJUNI</i> UPPS: Q9PP99; <i>PERIPLOCA SEPIUM</i> (Ps_PT): Q8H984; HB_PPS: Q8W3U4; <i>TARAXACUM KOK-SAGHYS</i> : (TKCPT1) ^[68] ; <i>S. CEREVISIAE</i> (RER2): P35196; Hs_DHDDS: Q86SQ9; <i>THERMOCOCCUS KODAKARAENSIS</i> UPPS: Q5JGE1) | 12 |
| FIGURE 7. EXPRESSION AND PURIFICATION OF ML_UPPS (A), MT_UPPS (B), HP_UPPS (C) AND HB_UPPS (D). CE = CRUDE EXTRACT AFTER PROTEIN EXPRESSION, PE = PURIFIED PROTEIN AFTER SEPARATION BY IMAC AND DESALTING, M = MOLECULAR MARKER, RE = REFERENCE ENZYME (IN COMPARISON MT_UPPS WITH A CONCENTRATION OF 27.2 MG ML ⁻¹ DETERMINED BY BRADFORD) AND BE = BEFORE INDUCTION WITH IPTG. * = PURIFIED ENZYME, ** = <i>E. COLI</i> CHAPERON. ^[69] | 13 |
| FIGURE 8. PRINCIPLE OF THE P _i -ASSAY. ^{[70][71]} CPTASES CONJUGATES ONE PRENYL UNIT (I.E. IPP) TO THE ALLYLIC SUBSTRATE (I.E. FPP)..... | 14 |
| FIGURE 9. PRINCIPLE OF THE HPLC ASSAY. MIXTURES WERE INCUBATED WITH THE FLUORESCENCE LABELED ALLYLIC STARTER UNIT (MANT-O-GPP) AND THE ELONGATION SUBSTRATES (R = H: BPP; R = CL: CL-BPP; R = CH ₃ : IPP) WITH RECOMBINANT ML_UPPS AND MT_UPPS AT RT FOR 16 H. DETECTION WAS CARRIED OUT WITH A FLUORESCENCE DETECTOR (λ _{EX} = 352 NM / λ _{EM} = 420 NM). | 15 |
| FIGURE 10. BIOCATALYTIC ACTIVITY OF CPTASES WITH ALLYLIC PROLONGATION UNIT. MEASURED WITH THE PI-ASSAY, (A) SHOWS THE SUMMARY TABLE. <i>E,E</i> -FPP IS THE STARTER UNIT WITH IPP (B), BPP (C) AND CL-BPP (D) AS PROLONGATION UNIT. | 16 |
| FIGURE 11. HPLC CHROMATOGRAM OF THE ML_UPPS AND MT_UPPS PRODUCT FORMATION. MT_UPPS (A) AND ML_UPPS (B) INCUBATED WITH MANT-O-GPP AND IPP AT RT FOR 16 H. THE FLUORESCENCE WAS DETECTED AT λ _{EX} = 352 NM AND λ _{EM} = 420 NM. | 17 |
| FIGURE 12. HPLC CHROMATOGRAMS OF ARTIFICIAL SUBSTRATES. (A) ML_UPPS WITH BPP AND (B) CL-BPP OR (C) MT_UPPS WITH BPP AND (D) CL-BPP INCUBATED AT RT FOR 16 H WITH MANT-O-GPP AS STARTER UNIT. DETECTION WAS CARRIED WITH A FLUORESCENCE DETECTOR (λ _{EX} = 352 NM / λ _{EM} = 420 NM)..... | 18 |
| FIGURE 13. REPRESENTATIVE STRUCTURES OF PRENYLATED AROMATIC RING SYSTEMS. | 22 |
| FIGURE 14. THE BIOSYNTHESIS OF NAPHTERPIN INVOLVES PRENYLATION OF FLAVIOLIN (A). THE GERANYL MOIETY IS DEPICTED IN RED (B). | 22 |
| FIGURE 15. STRUCTURE OF THE AROMATIC PRENYLTRANSFERASE NPHB (PDB-CODE 1ZB6). (A) TOP VIEW OF STRUCTURAL ELEMENTS AND (B) SURFACE REPRESENTATION OF THE PROTEIN WITH BOUND AROMATIC SUBSTRATE 1,6-DHN (GREEN), THE CO-SUBSTRATE ANALOGUE GERANYL-S-THIOLODIPHOSPHATE (ORANGE = THIOLODIPHOSPHATE; GREY = ALLYLIC RESIDUE) AND THE CATALYTIC Mg ²⁺ ION (VIOLET SPHERICAL DOTS). THE A-HELICES AND LOOPS ARE DEPICTURED IN DARKER GREY AND THE B-SHEETS ARE IN NAVY BLUE. | 23 |
| FIGURE 16. GENERAL STEPS OF THE “REGULAR” PRENYLATION OF AROMATIC COMPOUNDS. (A) S _N 1 – LIKE PATHWAY AND (B) S _N 2 – LIKE PATHWAY PROPOSED MECHANISMS FOR THE REACTION MEDIATED BY NPHB . PP REPRESENTS A DIPHOSPHATE RESIDUE. | 24 |

| | |
|--|----|
| FIGURE 17. EXPRESSION OF DIFFERENT NPHB CONSTRUCTS. LANES OF THE SDS-PAGE (10 % CROSSLINKING) REPRESENT THE MOLECULAR MARKERS (M), BEFORE AND AFTER INDUCTION OF GENE EXPRESSION IN DIFFERENT MEDIUM, UNDER DIFFERENT CONDITIONS AND IN DIFFERENT VECTOR CONSTRUCTS. | 26 |
| FIGURE 18. PURIFICATION OF NPHB. LANES OF THE SDS-PAGE (16 % CROSSLINKING) REPRESENT THE MOLECULAR MARKERS (M), THE CRUDE EXTRACTS OF CELLS BEFORE (1) AND AFTER (2) INDUCTION OF GENE EXPRESSION, FLOW THROUGH OF THE IMAC (3), TRX-NPHB PURIFIED BY METAL ION AFFINITY CHROMATOGRAPHY (4), A SAMPLE AFTER PROTEOLYTIC CLEAVAGE OF TRX-NPHB (5), AND NPHB (6) AND TRX (7) AFTER SEPARATION BY METAL ION AFFINITY CHROMATOGRAPHY..... | 26 |
| FIGURE 19. HPLC-CHROMATOGRAM. UV-VIS-SPECTRA COUPLED WITH ESI-MS SPECTRA TO CONFIRM THE CONVERSION OF 1,6-DHN AND GPP BY NPHB. PEAK 1: 1,6-DHN (MW 159,04); PEAK 2: 4-GERANYL-1,6-DHN; PEAK 3: 5-GERANYL-1,6-DHN, PEAK 4: 2-GERANYL-1,6-DHN (FOR ALL PRODUCTS: MW 295,17). ... | 27 |
| FIGURE 20. PRENYLATION REACTION OF DIFFERENT NAPHTHOLS CATALYZED BY NPHB. THE STRUCTURAL SCAFFOLD IS DISPLACED IN THE CENTER AND IN BRACES THE YIELD. (G = GERANYL MOIETY)..... | 29 |
| FIGURE 21. PHARMACOPHORE MODEL OF 1,6-DHN. THE PROPERTIES INCLUDE: HYDROGEN BOND DONORS/ACCEPTORS, π -ORBITALS, LIPOPHILICITY, SIZE, POSITIVITY/NEGATIVITY CHARGE(S)..... | 30 |
| FIGURE 22. BIOCATALYTIC GERANYLATION OF FLAVONES AND POLYPHENOLS BY NPHB. SAMPLES WERE INCUBATED FOR 16 H, ANALYZED BY HPLC AND STRUCTURALLY ELUCIDATED BY NMR. (N.D. = NOT DETECTIBLE OR PRODUCT YIELD $\leq 0.1\%$; * = MULTI-GERANYLATED PRODUCTS (ONLY OBTAINED BY MS); BLUE = C-PRENYLATION; RED = O-PRENYLATION AND IN VIOLET GERANYLATED PRODUCTS OF UNKNOWN CONSTITUTION ARE PRESENTED. | 31 |
| FIGURE 23. PHARMACOPHORE MODEL OF THE FLAVONE NARINGENIN. THE PROPERTIES INCLUDE: HYDROGEN BOND DONORS/ACCEPTORS, sp^2 HYBRIDIZATION, LIPOPHILICITY, SIZE, ELECTRO POSITIVITY/NEGATIVITY AND CHARGE(S). | 33 |
| FIGURE 24. NATURAL AND ARTIFICIAL PRENYL-DONORS FOR NPHB. THE OUTCOME IS DIVIDED IN CONVERTED (GREEN), CONVERSION ONLY LC-MS CONFIRMED (YELLOW) AND NON-CONVERTED SUBSTRATES (RED). KINETICS WERE ANALYZED DURING THE FIRST HOUR IN THE PRESENCES OF 5 mM 1,6-DHN AND 5 mM GPP OR ITS ANALOGUES. | 37 |
| FIGURE 25. BINDING MODE OF THE Mg^{2+} -ION (YELLOW SPHERICAL ARRANGED DOTS) COORDINATED BY THE AMINO ACIDS SER51, ASP62, ASP110 AND LYS118 AND WATER MOLECULES (BORDEAUX RED SPHERICAL ARRANGED DOTS) IN THE COMMONLY FOUND OCTAHEDRAL MAGNESIUM CLUSTER IN THE ACTIVE SITE. 1,6 DHN IS COLORED IN GREEN, THE DIPHOSPHATE MOTIF IS HELD IN ORANGE (PHOSPHATE)/LIGHT RED (OXYGEN) AND THE ALLYLIC CARBONS ARE GREY. (PDB-CODE: 1ZB6)..... | 41 |
| FIGURE 26. HPLC ANALYSIS OF THE REACTION MIXTURE CONTAINING DIFFERENT METAL IONS. THE MOST ACTIVE ONE WAS Mg^{2+} FOLLOWED BY Mn^{2+} , Ca^{2+} , Co^{2+} , Ba^{2+} AND Ni^{2+} WITH RESPECTIVELY DECREASES. LESS ACTIVITY COULD BE OBSERVED IN THE PRESENCES OF Zn^{2+} . (RIGHT) PART SHOWS THE DISTRIBUTION OF THE PRODUCTS (N. D. = NOT DETECTED; BLUE = 2-GERANYL-1,6-DHN; RED = 4-GERANYL-1,6-DHN; GREEN = 5-GERANYL-1,6-DHN) AND (LEFT) PART SHOWS THE ACTIVITY AMONG THE DIFFERENT METAL-IONS RELATIVE TO THE WT-ENZYME ($9.50 \text{ PKAT } Mg^{-1}$) DETERMINED BY UV-VIS ASSAY..... | 42 |
| FIGURE 27. BINDING OF THE AROMATIC SUBSTRATE 1,6-DHN IN THE ACTIVE SIDE WITH THE AMINO ACIDS INVOLVED (LABELED). 1,6 DHN IS COLORED IN GREEN AND THE DIPHOSPHATE MOTIF IS HELD IN ORANGE (PHOSPHATE)/LIGHT RED (OXYGEN); THE ALLYLIC CARBONS ARE GREY. Mg^{2+} -ION (SHOWN AS PINK SPHERICALLY ARRANGED DOTS) AND BLUE REPRESENTS THE B-SHEETS..... | 43 |
| FIGURE 28. FS-MOTIF WITH INTERACTION TO THE AROMATIC SUBSTRATE. ELIMINATING THE SERINE HYDROXY GROUP (SER214ALA) LEADS TO A SLIGHT DECREASE ACTIVITY OF 13.0%. IN CONTRAST, ALTERATION OF THE PHE213 MOIETY TO LIPOPHILIC SIDE CHAIN GOES ALONG WITH THE BIOACTIVITY OF THE CHAIN LENGTH: LEU > VAL > ALA WITH 82.7%, 15.9% AND 0.1% REMAINING ACTIVITY, RESPECTIVELY. | 44 |
| FIGURE 29. MUTAGENESIS OF THE 1,6-DHN BINDING POCKETS. (TOP) TURNOVER NUMBER OF THE MUTANTS RELATIVE TO THE WT-ENZYME ($9.50 \text{ PKAT } Mg^{-1}$) DETERMINED BY UV-VIS ASSAY. (BOTTOM) PRODUCT RATIO AFTER ADDITIONAL INCUBATION OF 16 H ANALYZED BY HPLC. (N. D. = NOT DETECTED; BLUE = 2-GERANYL-1,6-DHN; RED = 4-GERANYL-1,6-DHN; GREEN = 5-GERANYL-1,6-DHN)..... | 44 |
| FIGURE 30. THE BINDING SITE OF GPP (DIPHOSPHATE MOTIF IN ORANGE, THE SULFIDE GROUP IN YELLOW AND THE ALLYLIC RESIDUE IN GREY) IS SHOWN WITH THE KEY AMINO ACIDS RESIDUES IN THE CENTER. IN GREEN THE AROMATIC SUBSTRATE 1,6-DHN, IN MAGENTA THE Mg^{2+} -ION AND THE WATER MOLECULES ARE IN RED DOTS. 46 | 46 |

| | |
|---|----|
| FIGURE 31. MUTAGENESIS OF THE GPP BINDING POCKETS. (TOP) TURNOVER NUMBER OF THE MUTANTS RELATIVE TO THE WILD-TYPE (WT)-ENZYME (9.50 pKAT MG-1) DETERMINED BY UV-VIS ASSAY. (BOTTOM) PRODUCT RATIO AFTER ADDITIONAL INCUBATION OF 16 H ANALYZED BY HPLC. (N. D. = NOT DETECTED; VIOLATE = PRODUCT PROPORTION NOT DETERMINED; BLUE = 2-GERANYL-1,6-DHN; RED = 4-GERANYL-1,6-DHN; GREEN = 5-GERANYL-1,6-DHN)..... | 47 |
| FIGURE 32. STABILIZATION OF THE INTERMEDIATE BY THREE TYROSINES. (LEFT)ACTIVE CENTER OF NPHB (PDB-CODE 1ZB6) WITH AROMATIC SUBSTRATE 1,6-DHN (GREEN) AND GSPP IN COMPARISON (RIGHT) TO FGAPT2 WITH TRYPTOPHAN AND DIMETHYLALLYL-S-THIOLODIPHOSPHATE IN THE CENTER (PDB-CODE 3I4X). TRYPTOPHAN SIDE CHAINS STABILIZE THE ALLYLIC CATION BY CATION-D-INTERACTIONS WITH THE AROMATIC RING. | 48 |
| FIGURE 33. MUTATION OF VAL 49 INTO GLUTAMIC ACID. (LEFT) THE TORSION ANGLE IS DRAWN THE CRYSTAL STRUCTURE. (RIGHT) THE TORSION ANGLE (A) OF THE ALLYLIC SUBSTRATE IS A = 80° IN THE ORIGINAL ENZYME AND A = 89° IN THE V49E MUTANT (CALCULATION MOE VERSION 2014.9). THE π-BOND INTERACTS WITH THE D _{SP2} -C-O ORBITAL AND FORMS THE DELOCALIZATION OF THE ALLYLIC CATION. THUS, THE ENERGY EFFORT IS REDUCED FOR THE CLEAVAGE OF THE C-O-BOND AND THE CATION FORMATION. | 50 |
| FIGURE 34. A S _N 2- OR FRIEDEL-CRAFTS-ALKYLATION-LIKE REACTION MECHANISM. ^[92] (LEFT) PRESENTATION OF THE CATALYTIC SEQUENCE IN NPHB WITH THE PUTATIVE ROLES OF ASP 110 AND TYR 121. (RIGHT) THE POSITION OF THE AMINO ACIDS IN THE ACTIVE SITE. TYR 121 APPEARS TO BE IN THE PERFECT PLACE TO DEPROTONATE THE Σ-COMPLEX. | 51 |
| FIGURE 35. H-BOND FORMATION WITH THE AROMATIC SUBSTRATE AND THE SURROUNDED RESIDUES. IN GREEN 1,6-DHN IS SHOWN, THE BLUE DASHED LINE INDICATES THE DISTANCE TO THE SECOND SUBSTRATE GPP, AND RED THE CORRESPONDING WATER MOLECULES. | 53 |
| FIGURE 36. PROPOSED BIOCATALYTIC GERANYLATION OF 1,6-DHN CATALYZED BY THE AROMATIC PTASE NPHB. 1,6 DHN IS COLORED IN GREEN AND THE DIPHOSPHATE MOTIF IS HELD IN ORANGE (PHOSPHATE)/LIGHT RED (OXYGEN); THE ALLYLIC CARBONS ARE GREY. Mg ²⁺ -ION (PINK SPHERICAL ARRANGED DOTS) AND BLUE REPRESENTS THE B-SHEETS. | 55 |
| FIGURE 37. BIOSYNTHETIC PATHWAY OF Δ ¹ -TETRAHYDROCANNABINOLIC STARTS WITH CANNABIGEROLIC ACID (CBGA) AND GERANYL DIPHOSPHATE (GPP). THE DECARBOXYLATION IS A NON-ENZYMATIC REACTION DURING THE STORAGE OR INDUCED BY HEAT. | 56 |
| FIGURE 38. PROPOSED CATALYTIC CASCADE OF THCA SYNTHESIS BEGINNING WITH CBGA TO THCA. FAD IS COLORED IN BLACK, SUBSTRATES IN RED AND THE ENZYMATIC INVOLVED KEY AMINO ACIDS IN BLUE. FIGURE MODIFIED ACCORDING TO YOSHINARI SHOYAMA ET. AL. ^[132] | 57 |
| FIGURE 39. POSSIBLE NON-NATURAL SUBSTRATES FOR THCAS AND THEIR ASSUMED PRODUCTS: (A) 6-GERANYL NARINGENIN, (B) 2-GERANYL-1,6-DHN AND (C) 5-GERANYL 1,6-DHN..... | 59 |
| FIGURE 40. HPLC CHROMATOGRAPH OF THE ENZYME-CONVERSION. ASSAY WITH (A) 2-GERANYL-1,6-DIHYDROXYPHTHALENE AND THCA-SYNTHASE (R _{T-EDUCT} = 7.1 MIN); (B) 5-GERANYL-1,6-DIHYDROXYPHTHALENE (R _{T-EDUCT} = 5.7 MIN) AND (C) 6-GERANYL-NARINGENIN (R _{T-EDUCT} = 6.5 MIN) IN THE PRESENCES OF THCA-SYNTHASE. NO SIGNALS OR CORRESPONDING M/Z OF THE CYCLIC PRODUCT COULD BE OBSERVED WHICH LEAD TO THE ASSUMPTION THAT THIS PRODUCT WAS NOT FORMED. | 60 |
| FIGURE 41. VIEW INTO THE ACTIVE CENTER OF THCA SYNTHASE. THE NATURAL SUBSTRATE CBGA (GREY) AND THE PROPOSED ALTERNATIVE SUBSTRATE 2-GERANYL-1,6-DHN (GREEN) ARE DOCKED IN THE ACTIVE CENTER WITH THE CO-SUBSTRATE FAD (VIOLET). THE DOCKING WAS PERFORMED BY PD DR. WOLFGANG BRANDT WITH MOE (2014)..... | 61 |
| FIGURE 42. GROWTH INHIBITION ACTION ON FUNGI. (A) <i>PHYTOPHTHORA INFESTANS</i> (B) <i>SEPTORIA TRITICI</i> (C) <i>BOTRYTIS CINEREA</i> WERE MEASURED IN THE PRESENCES OF 42 (BLUE), 14 (RED), 4.7 (GREEN), 1.6 (PURPLE), AND 0.52 μG ML ⁻¹ (LIGHT BLUE) OF 1,6-DHN (LEFT) AND 5-GERANYL-1,6-DHN (RIGHT). DMSO SERVED AS CONTROL AND AS POSITIVE CONTROL PYRACLOSTROBIN (DATA NOT SHOWN). FURTHERMORE, EVERY VALUE WAS CORRECTED WITH THE NEGATIVE CONTROL AND THE DIFFERENCE WAS REPRESENTED IN [%]. | 63 |
| FIGURE 43. ESTIMATION OF T1 OF THE EXTERNAL STANDARD 1,6 DHN BY AN INVERSION RECOVERY..... | 68 |
| FIGURE 44. CALIBRATION CURVE FOR QNMR USING 1,6-DHN AS STANDARD (BLACK-SQUARES). THE METHOD WAS VALIDATED WITH THE DIHYDROXYPHTHALENE ANALOGUES 1,7-DHN (±0.01 MM) AND 2,3-DHN (±0.05 MM) MARKED AS BLUE-CIRCLES AND RED-TRIANGLE, RESPECTIVELY. THE TECHNICAL REPLICATE 1,6-DHN (±0.01 MM) CONFIRMS THE ACCURACY AND IS COLOURED AS GREEN-DIAMOND. | 69 |

FIGURE 45. SPECTRA OF THE NON- AND GERANYLATED 1,6-DHNS TO ILLUSTRATE THE WAVELENGTH SHIFT. (LEFT) SPECTRA OF THE THREE GERANYLATED 1,6-DHN SEPARATED BY CHROMATOGRAPHY AND MEASURED BY UV/VIS SPECTROMETRY. THE LOCAL MAXIMA OF ALL THREE GERANYLATED PRODUCTS IS AT 336 NM (BLUE = MAIN PRODUCT 5-GERANYL-1,6-DHN; GREY = 4-GERANYL-1,6-DHN; GREEN = 2-GERANYL-1,6-DHN). (RIGHT) SPECTRA OF 1,6-DHN AND 5-GERANYLATED-1,6-DHN. UV/VIS SPECTRA SHOWS THE LOCAL MAXIMA SHIFT OF THE SUBSTRATE (1,6-DHN) AND THE PRODUCT (EXEMPLARILY 5-GERANYLATED 1,6-DHN) (BLACK = 1,6-DHN; BLUE = 5-GERANYLATED-1,6-DHN; RED = DIFFERENTIAL SPECTRA BETWEEN THE GERANYLATED AND NON-GERANYLATED 1,6-DHN). 72

FIGURE 46. UV/VIS SPECTRA INDICATE THE TIME DEPENDENT PRODUCT FORMATION OF GERANYLATED 1,6-DHN AT 340 NM (DARK BLUE) AND 345 NM (BORDEAUX RED). SAMPLES OF THE ENZYMATIC REACTION WERE INCUBATED FOR 0-2 H AT 28°C, MEASURING THE UV/VIS ABSORPTION AT 340 NM ($R^2=0.997$) AND 345 NM ($R^2=0.996$). THE ENZYME REACTION WITHOUT GPP IS REPRESENTED IN BLACK. NO PRODUCT FORMATION IS OBSERVED DURING THIS TIME. 73

FIGURE 47. RATIO BETWEEN THE BIOCATALYTIC CONVERSIONS OF 1,6-DHN WITH GPP BY NPHB. (BLUE = 5-GERANYL-1,6-DHN; GREY = 4-GERANYL-1,6-DHN; GREEN = 2-GERANYL-1,6-DHN). 74

FIGURE 48. COMPARISON OF ENZYME ACTIVITY USING THE TWO DIFFERENT APPROACHES. SAMPLES OF THE ENZYMATIC REACTION WERE INCUBATED FOR 2 H AND AFTERWARDS ANALYZED BY HPLC (BLUE LINE; $Y = 0.0075$; $R^2=0.99$) AND BY UV/VIS (RED LINE; $Y = 0.0069$; $R^2=0.99$). THE SPECIFIC ENZYME ACTIVITY BASED ON HPLC-DATA WAS CALCULATED TO BE $8.60 \text{ PKAT MG}^{-1}$ AND BASED ON UV/VIS, $7.95 \text{ PKAT MG}^{-1}$ WHICH IS AN ACCURACY OF 92.6%. 75

FIGURE 49. PRENYLATION OF 1,4-DIHYDROXY-2-NAPHTHOIC ACID AND GERANYL DIPHOSPHATE CATALYZED BY MENA TO MENAQUINONE AND THEIR ROLE IN THE ELECTRON FLOW SYSTEM MEDIATE THE ENERGY PATHWAY. 78

FIGURE 50. THE MOST POTENT INHIBITORS FOR THE UBI A-TRANSFERASES. (LEFT) B-KETO CARBOXYLIC ACIDS WITH AN IC_{50} VALUE OF 0.36 mM AND THE (RIGHT) B-HYDROXY CARBOXYLIC ACIDS WITH A IC_{50} VALUE OF 0.58 mM.^[176] 79

FIGURE 51. OVERVIEW OF THE DIFFERENT HEAD GROUPS DESIGNED FOR MIMICKING THE DIPHOSPHATE GROUP (R = GERANYL RESIDUE; 4 AND 5: R = DIMETHYLALLYL (4A, 5A), GERANYL (4B, 5B), FARNESYL (4C, 5C); 3: R = GERANYL (3B), FARNESYL (3C); 7: R = DIMETHYLALLYL (7A), GERANYL (7B)). 80

FIGURE 52. INHIBITION OF THE THREE PRENYLTRANSFERASES: MENA (GREEN COLUMN), NPHB (BLUE COLUMN) AND UBI A (RED COLUMN). POS. CONT. = POSITIVE CONTROL WITHOUT ANY INHIBITOR. E = WITH THE METHYL-ESTER PROTECTION GROUP. 82

FIGURE 53. IC_{50} -VALUES OF THE COMPOUND 3C AND 4C FOR UBI A. (LEFT) 3C SHOWED AN IC_{50} -VALUE OF 0.69 ± 0.03 mM AND (RIGHT) 4C WITH ON VALUE OF 0.75 ± 0.02 mM (DATA OUT OF MSONGA PHD THESIS). 85

FIGURE 54. BIOCATALYTIC CONVERSION TO 2-GERANYL-NAPHTHALENE-1,4-DIONE STARTING WITH 1,4-DIHYDROXY-2-NAPHTHOIC ACID (1,4-DHN-2A) AND GPP IN THE PRESENCE OF PURIFIED *E. COLI* MENA. THIS PRODUCT GETS AUTO-DECARBOXYLATION AND OXIDATION TO 2-GERANYL-NAPHTHALENE-1,4-DIONE UNDER THIS CONDITION. THE STRUCTURE WAS CONFIRMED BY $^1\text{H-NMR}$, IR AND HRMS. 100

11.2. Table of tables

TABLE 1. OVERVIEW ABOUT THE SELECTED CPTASES. 11

TABLE 2. BIOCATALYTIC ACTIVITY DURING THE PURIFICATION OF NPHB. LANES PRESENT THE CRUDE EXTRACTS OF CELLS AFTER INDUCTION OF GENE EXPRESSION IN *E. COLI*, Trx-NPHB PURIFIED BY METAL ION AFFINITY CHROMATOGRAPHY AND AFTER PROTEOLYTIC CLEAVAGE OF Trx-NPHB AND SEPARATION BY METAL ION AFFINITY CHROMATOGRAPHY. SAMPLES WERE INCUBATED FOR 24 H AT 25 °C AND ANALYZED BY HPLC. 27

TABLE 3. NPHB CATALYZED GERANYLATION OF FLAVONES AND POLYPHENOLS. THE YIELD WAS CALCULATED FROM THE AUC OF THE PRODUCT DIVIDED BY THE OVERALL YIELD (SUBSTRATE PLUS PRODUCT) MEASURED BY HPLC AFTER 16 H INCUBATION AT ROOM TEMPERATUR. 34

TABLE 4. GERANYLATED COUMARIN DERIVATIVES BY NPHB. THE YIELD WAS CALCULATED FROM THE AUC OF THE PRODUCT DIVIDED BY THE OVERALL YIELD (SUBSTRATE PLUS PRODUCT) MEASURED BY HPLC AFTER 16 H INCUBATION AT ROOM TEMPERATURE. 35

| | |
|---|-----|
| TABLE 5. COMPARISON OF THE AROMATIC PTASES NPHB AND FGAPT2 REGARDING THE ALLYLIC DONOR..... | 39 |
| TABLE 6. INHIBITION IN PERCENT (IN COMPARISON TO THE POSITIVE CONTROL WITHOUT INHIBITION) FOR THE COMPOUND 4 AND 5 WITH FOCUS ON THE CHAIN LENGTH DEPENDENCY AT 1 MM CONCENTRATION..... | 83 |
| TABLE 7. OLIGONUCLEOTIDES FOR SITE-DIRECTED MUTAGENESIS. | 91 |
| TABLE 8. LABOR EQUIPMENT (IN GERMANY) | 138 |
| TABLE 9. USED CHEMICALS..... | 140 |

11.3. Table of equations

| | |
|---|----|
| EQUATION 1. EQUATION FOR ACCURATE DETERMINATION OF UNKNOWN SAMPLE CONCENTRATION. ^[126] | 66 |
| EQUATION 2. T1 CALCULATION TO CORRECTLY SETUP THE QUANTITATIVE EXPERIMENT..... | 67 |
| EQUATION 3. DIFFERENTIAL SPECTRA OF $\lambda=345$ NM AND $\lambda=600$ NM | 72 |

11.4. Table of supplementary figures

| | |
|--|-----|
| SUPPLEMENTARY FIGURE 1. PURIFICATION OF THE NPHB AND REPRESENTATIVE MUTATIONS. THE PROTEIN IS SHOWN IN THE GEL WITHOUT TRX-TAG. LANES OF THE SDS-PAGE (14 % CROSSLINKING) REPRESENT THE MOLECULAR MARKERS (M), THE WILD-TYPE NPHB (1), S51A (2), S64A (3), S64R (4), M106A (5), D110N (6), D110A (7), Y121F (8), Y121W (9), M162A (10), M162C (11), M162F (12), M162L (13), M162W (14), D100A/Y121F (15)..... | 135 |
| SUPPLEMENTARY FIGURE 2. PURIFICATION OF THE NPHB WITH TRX-TAG. THE PROTEIN IS SHOWN IN THE GEL WITH TRX-TAG. LANES OF THE SDS-PAGE (14 % CROSSLINKING) REPRESENT THE MOLECULAR MARKERS (M), THE WILD-TYPE NPHB (1), V47A (2), V49E (3), S51E (4), F213A (5), F213V (6), F213L (7), S214A (8), Y216A (9), Y216E (10), V271D (11), V271E (12), Y288D (13), Y288E (14), V294A (15), Q295A (16), L298A (17), M106A/Q295A (18), M106A/Q295A/V294A (19) AND WILD-TYPE NPHB (20)..... | 135 |
| SUPPLEMENTARY FIGURE 3. THE CALIBRATION CURVES OF THE UV/VIS-METHOD ARE SHOWN. (A) THE QUANTITATIVE HPLC MEASUREMENTS OF 5-GERANYL-1,6-DHN AT 340 NM. 1 MG OF THE MAIN PRODUCT IS EQUAL TO ABSORPTION OF 14.217.000 AUC. (B) QUANTITATIVE UV/VIS MEASUREMENTS OF 5-GERANYL-1,6-DHN AT 340 NM. 1 MG OF THE MAIN PRODUCT IS EQUAL TO ABSORPTION OF 1.38 AU. | 136 |
| SUPPLEMENTARY FIGURE 4. PRODUCT CONVERSION OF MENA. THE PRODUCT FORMATION RANGE OF 25 μ L (v/v) MENA USING 5 MM GPP, 5 MM $MgCl_2$ AND 5 MM 1,4 DHN-2A IN THE PRESENCES OF 12% DMSO (v/v). | 137 |

Eidesstattliche Erklärung

Hiermit erkläre ich, Hans Felix Schreckenbach, dass ich die vorliegende Arbeit selbstständig und ohne fremde Hilfe verfasst habe. Andere als die von mir angegebenen Quellen und Hilfsmittel habe ich nicht benutzt und die den benutzten Werken wörtlich oder inhaltlich entnommenen Stellen habe ich als solche kenntlich gemacht. Außerdem erkläre ich, dass ich mich mit der vorliegenden wissenschaftlichen Arbeit erstmals um die Erlangung des Doktorgrades bewerbe.

Ort, Datum

Lebenslauf

Werdegang

- 04.2016- Selbstständigkeit als Apotheker
- 07.2015-03.2016 Angestellter Apotheker in den Apotheken von Herrn Schwedler
- 04.2011-07.2015 Promotion am Leibniz-Institut in Halle/Saale
- 10.2005-02.2011 Pharmaziestudium an der Universität des Saarlandes
Abschluss: Approbation
Diplom Pharmazeut
- 07.2004-04.2005 Grundwehrdienst im 7.Gebirgssanitärerregiment, Kempten und
Sanitätszentrum Amberg als Sanitäter
- 08.1992-07.2004 Grundschule und Gymnasium
Physikpreis der Deutschen Physikalischen Gesellschaft

Auslandsaufenthalte

- 04.2011-11.2011 Universität von Uppsala, Schweden
Diplomarbeit mit Auslandsaufenthalt bei Prof. Dr. Per Artursson
(Diplomvater: Prof. Dr. C.-M. Lehr - Universität des Saarlandes)
- 02.2008-05.2008 Universität von Exeter, England
Forschungspraktikant bei Prof. Jennifer A. Littlechild
(Biocatalysis Centre School of Biosciences)

Publikationen

- Patent J. Keim, S. Ludwig, H.F. Schreckenbach, A.L. Wessjohann, C. Dreisbach, T. Früh,
Europäische Patentanmeldung
(Veröffentlichungsnr.: WO2015036335 A1 und EP2848693A1)
- Buchkapitel L. A. Wessjohann, H. F. Schreckenbach, G. N. Kaluđerović, in K. Faber, W.-D.
Fessner, N. J. Turner (Eds.): "Enzymatic C-Alkylation of Aromatic Compounds",
Georg Thieme Verlag KG, Stuttgart, Science of Synthesis, Biocatalysis in
Organic Synthesis 2 (2014), pp 177–211